Folding and Stability Studies on Amyotrophic Lateral Sclerosis-Associated apo Cu, Zn Superoxide dismutases

by

Kenrick Allistair Vassall

A thesis

presented to the University of Waterloo

in fulfillment of the

thesis requirement for the degree of

Doctor of Philosophy

in

Chemistry

Waterloo, Ontario, Canada, 2009

AUTHOR'S DECLARATION

I hereby declare that I am the sole author of this thesis. This is a true copy of the thesis, including any required final revisions, as accepted by my examiners.

I understand that my thesis may be made electronically available to the public

Abstract

Amyotrophic lateral sclerosis (ALS) is a debilitating, incurable, neurodegenerative disease characterized by degradation of motor neurons leading to paralysis and ultimately death in ~3-5 years. Approximately 10% of ALS cases have a dominant inheritance pattern, termed familial ALS (fALS). Mutations in the gene encoding the dimeric superoxide scavenger Cu, Zn superoxide dismutase (SOD), were found to be associated with ~20% of fALS cases. Over 110 predominantly missense SOD mutations lead to fALS by an unknown mechanism; however, it is thought that mutant SOD acquires a toxic gain of function. Mice as well as human post mortem studies have identified mutant SOD-rich aggregates in affected neurons, leading to the hypothesis that mutations in SOD increase the tendency of the protein to form toxic aggregates.

SOD has a complex maturation process whereby the protein is synthesized in an apo or demetalated state, followed by formation of an intramolecular disulfide bond and binding of Zn^{2+} and Cu^{2+}. Each of these post-translational modifications increases the stability of the protein. SOD has been shown to aggregate more readily from destabilized immature states, including the apo state both with and without the disulfide bond, highlighting the importance of these states.

Thermal unfolding monitored by differential scanning calorimetry (DSC) and chemical denaturation monitored by optical spectroscopy were used to elucidate the folding mechanism and stability of both the apo SOD disulfide-intact and disulfide-reduced states. Chemically and structurally diverse fALS-associated mutants were investigated to gain insights into why mutant SODs may be more prone to misfold and ultimately aggregate. The mutations were introduced into a pseudo wild-type (PWT) background lacking free cysteines, resulting in highly reversible unfolding amenable to accurate thermodynamic analysis.

Similarly to what was previously described for fully metallated (holo) SODs, chemical denaturation of the apo disulfide-intact SODs is well described by a 3-state dimer mechanism

with native dimer, monomeric intermediate and unfolded monomer populated at equilibrium. Although removal of metals has a relatively small effect on the stability of the dimer interface, the stability of the monomer intermediate is dramatically reduced. Thermal unfolding of some disulfide-intact apo SOD mutants as well as PWT is well described by a 2-state dimer mechanism, while others unfold via a 3-state mechanism similar to chemical denaturation. All but one of the studied disulfide-intact apo mutations are destabilizing as evidenced by reductions in ΔG of unfolding. Additionally, several mutants show an increased tendency to aggregate in thermal unfolding studies through increased ratios of van't Hoff to calorimetric enthalpy (H_{vH}/ H_{cal}). The effects of the mutations on dimer interface stability in the apo disulfide-intact form were further investigated by isothermal titration calorimetry (ITC) which provided a quantitative measure of the dissociation constant of the dimer (K_d). ITC results revealed that disulfide-intact apo SOD mutants generally have increased K_d values and hence favor dimer dissociation to the less stable monomer which has been proposed to be a precursor to toxic aggregate formation.

Reduction of the disulfide bond in apo SOD leads to marked destabilization of the dimer interface, and both thermal unfolding and chemical denaturation of PWT and mutants are well described by a 2-state monomer unfolding mechanism. Most mutations destabilize the disulfide-reduced apo SOD to such an extent that the population of unfolded monomer under physiological conditions exceeds 50%. The disulfide-reduced apo mutants show increased tendency to aggregate relative to PWT in DSC experiments through increased H_{vH} /H_{cal}, low or negative change in heat capacity of unfolding and/or decreased unfolding reversibility. Further evidence of enhanced aggregation tendency of disulfide-reduced apo mutants was derived from analytical ultracentrifugation sedimentation equilibrium experiments that revealed the presence of weakly associated aggregates. Overall, the results presented here provide novel insights into SOD maturation and the possible impact of stability on aggregation.

Acknowledgements

I wish to thank everyone in the Meiering group, past and present, of the University of Waterloo who have been a part of this sometimes pleasurable, sometimes difficult, but ultimately rewarding journey. Special thanks to Peter Stathopulos and Jessica Rumfeldt who made me feel so welcomed when I first started.

My deepest gratitude to Professor Elizabeth Meiering who was always available to inspire and to guide. Thank you for giving me the opportunity to work on this project and to grow as a scientist. I would also like to thank Professors, Michael Palmer, Janet Wood and John Heikkila who as members of my advisory committee offered very helpful suggestions.

My love and thanks to my always supportive parents Mareen and Kenrick to whom no sacrifice was too great. Thank you to my sister Kareena for always being there for me during the difficult times. To my loving wife Kamar, thank you for your understanding during the long nights of working. You inspire me to become a better man and I am lucky to have your love and support.

Dedication

To my parents Kenrick and Mareen, my sister Kareena and my wife Kamar

Table of Contents

List of Figures

Chapter 1

Chapter 2

Chapter 3

Chapter 4

Chapter 5

List of Tables

Chapter 2

Chapter 3

Chapter 4

List of Abbreviations

ALS……..amyotrophic lateral sclerosis
apo SOD……...fully demetallated human Cu, Zn SOD
a.u……..……..arbitrary units
CCS…….copper chaperone for SOD
C_{mid}……..midpoint of the equilibrium curve
$C_{p\ ex}$…….. excess heat capacity
$C_{p,tot}$……total specific heat of the system
C_p…….… excess specific heat absorption
DSC……...differential scanning calorimetry
DTT……...dithiothreitol
EDTA……. ethylenediaminetetraacetic acid
fALS……...familial amyotrophic lateral sclerosis
f_m……..fraction of protein that exists as free monomer
f_N…….fraction of native protein
f_U……fraction of unfolded protein
GdmCl……guanidinium chloride
GSH……reduced glutathione
HEPES……..…….hydroxyethyl piperazine N'-2-ethane sulfonic acid
H_n.....enthalpy of the natively folded protein
holo SOD…...……fully metallated human Cu, Zn SOD
H_{tot}.....total molar enthalpy
I……. monomeric intermediate
I_2……dimeric intermediate
IA……iodoacetamide
ITC……...isothermal titration calorimetry
$K(T)$…….. ……..equilibrium constant at any temperature T
K……..……..equilibrium constant
K_d……. ……dissociation constant
K_U…….equilibrium constant of unfolding
m……dependence of ΔG of unfolding on denaturant concentration
MW……molecular weight
$[M]_o$ ……..……concentration in the ITC syringe expressed as total concentration of monomer
$[M]_{T,i}$ ……..……total monomer concentration of protein in the cell after each ITC injection
$[M]_{T,i}$ ……. total monomer concentration of protein in the ITC cell after each injection
$[M]_o$ ……..concentration in the syringe expressed as total concentration of monomer
N_2……..……native dimer
NMR……..nuclear magnetic resonance
pdb……protein data bank
P_{dim}…….. total concentrations of dimer
P_{mon}……total concentrations of monomer
PWT…….…...pseudoWT, pseudo wild-type (C6A/C111S) SOD
Q……..heat
q_{dil}…….....heat associated with sample dilution that is unrelated to dissociation

q_i ……heat evolved upon dimer dissociation after each ITC injection
sALS……..sporadic amyotrophic lateral sclerosis
SE……sedimentation equilibrium
S_N…….....dependence of the native signal with urea
SOD.....human Cu,Zn superoxide dismutase
S_U……dependence of the unfolded signal with urea
T……is the temperature in Kelvin
t……..temperature in °C
$T_{0.5}$ ($t_{0.5}$)…….……...temperature in K (˚C) where the fraction unfolded is 0.5
$T_{1,\,0.5}$ ($t_{1,0.5}$)...……..…temperature of half unfolding for 1st transition in 3 state unfolding in K, (°C)
T_1',(t_1')……...…..temperature of the first transition in 3-state unfolding where $K_1(T)$=1 in K, (°C)
T_2', (t_2')…….... temperature of the first transition in 3-state unfolding where $K_1(T)$=1 in K, (°C)
$T_{2,\,0.5}$ ($t_{1,0.5}$).....……temperature of half unfolding for 2nd transition in 3 state unfolding in K, (°C)
t_{avg}……...……average $t_{0.5}$ in °C
TCEP…….……tris(2-carboxyethyl)phosphine
TTR……..……transthyretin
U…….……unfolded monomer
V……..…volume of the ITC reaction cell
v…….……injection volume
Y_{obs}……observed optical signal
Y_N^0 ……...…….……optical signal of the native protein in the absence of urea
Y_U^0 ……...……optical signal of the unfolded protein in the absence of urea
α……extent of a temperature induced unfolding reaction
β……$\Delta H_{vH}/\Delta H_{cal}$ × molecular weight of the SOD homodimer
ΔC_p……...……change in heat capacity of unfolding
ΔC_{p1}…….……change in heat capacity between native protein and intermediate
ΔC_{p2}……change in heat capacity between intermediate and unfolded monomer
$\Delta C_{p,unf}$…total change in heat capacity of unfolding between folded dimer and unfolded monomer
ΔG……...….change in Gibbs free energy of a reaction
$\Delta G_{1,}$ ΔG_d…….....….change in Gibbs free energy of dimer dissociation
$\Delta G_{2,}$…….....….change in Gibbs free energy of monomer intermediate unfolding
ΔG_{mon}……change in free energy change associated with monomer unfolding
ΔG_U…….…..change in free energy of unfolding at a given denaturant concentration
ΔG_{tot}…….....……total change in free energy for the unfolding of a dimer
$\Delta G_U^{H_2O}$ ……..……free energy of unfolding reaction in the absence of denaturant
ΔH……...change in enthalpy of unfolding
ΔH_{cal} ……...calorimetric enthalpy of unfolding
Δh_{cal}…….…….. specific change in enthalpy
ΔH_d……..enthalpy change associated with dimer dissociation
$\Delta H_{vH}/\Delta H_{cal}$ …….....……van't Hoff to Calorimetric enthalpy ratio
ΔH_{vH}……..……van't Hoff enthalpy of unfolding
ΔS…….……change in entropy of unfolding
ΔS_d ……entropy change associated with dimer dissociation
$\Delta\Delta G$…….....ΔG_{mutant} - ΔG_{PWT}
$\Delta\Delta H$……ΔH_{mutant} - ΔH_{PWT}
$\Delta\Delta S$……..……ΔS_{mutant} - ΔS_{PWT}

Chapter 1: General Introduction

1.1 Protein folding

Protein folding can be defined as the process by which the amino acids of a linear polypeptide chain interact and congregate together forming a specific stable motif, known as the native structure, suitable to the function of the protein. Many years ago, Anfinsen demonstrated that proteins fold spontaneously, indicating that all the information required for proteins to attain their 3-dimensional structure is contained within their primary sequence (Anfinsen, 1973). Despite much study, however, we cannot as yet fully decipher the blueprint for protein folding from the amino acid sequence which would enable us to predict structure and eventually function (Englander et al., 2007). It has been shown that a random sampling of all available conformations in search of the conformation of lowest energy cannot occur as this would take a length of time longer than the age of the universe for a typical protein (Leventhal, 1969). In contrast to this time scale, many proteins fold in a matter of seconds (Dill et al., 2007).

The high rate of folding suggests that there must exist pathways which simplify the folding mechanism, possibly by breaking down folding into a series of sequential steps which serve to guide the protein more quickly to its native state (Daggett and Fersht, 2003). Consistent with this, a theory of protein folding has been proposed whereby the protein is broken down into smaller nucleation motifs (Wetlaufer, 1973). These nucleation motifs are sometimes referred to as foldons, each forming native contacts independently with the final protein fold being determined by sequential addition of different foldons (Englander et al., 2007; Lindberg and Oliveberg, 2007). If a protein has multiple overlapping foldons, folding of one foldon influences or initiates folding of another, resulting in global cooperativity and 2-state folding with only

transiently populated metastable intermediates. However, if a protein has fully separated foldons, stable intermediates can accumulate along the protein folding pathway (Lindberg and Oliveberg, 2007).

Intermediates that form along the folding pathway can be productive or "off pathway" or kinetically trapped partially folded states which can accumulate, possibly leading to aggregation (Rumfeldt et al., 2008). Characterizing all species along a reaction pathway, including unfolded states, intermediates and transition states is key to interpreting reaction mechanisms (Travaglini-Allocatelli et al., 2009). This characterization involves not only investigating conformation or structure of the various species along the folding pathway but also understanding the thermodynamic driving forces that govern the transitions between the various conformations.

1.1.1 Thermodynamic driving forces behind protein folding

The current view of protein folding can be effectively visualized energetically and conformationally as a funnel in which the unfolded protein initially can access many high energy conformations. The number of conformations become lessened as more favorable native contacts are made until finally reaching a well defined structure close to or at the lowest energy (Figure 1.1). A larger protein will tend to have a more rugged funnel in which population of intermediate states is more likely (Jahn and Radford, 2008). It is instructive to consider the thermodynamic driving forces behind the spontaneous transformation of the initially unfolded protein to a fully functional folded one.

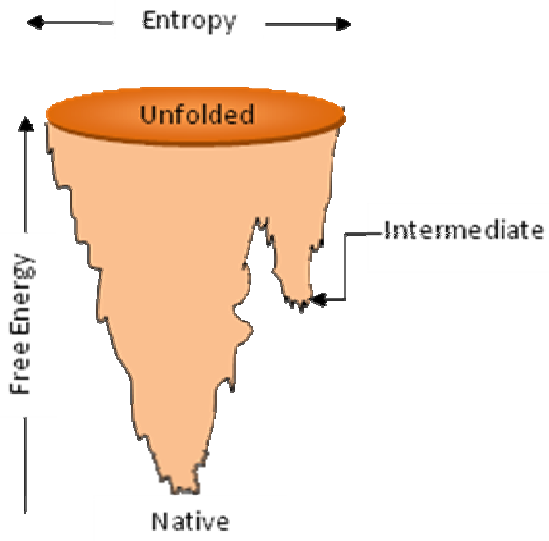

Figure 1.1. Schematic of a protein folding funnel. The funnel represents the conformational and energy landscape of a protein. Unfolded protein at the top of the funnel has both maximum entropy and free energy. At the bottom of the funnel the protein has its smallest entropy but this is more than compensated by an increase in enthalpy due to increased contacts in the native state, resulting in a lower overall free energy. Some proteins, particularly large multi-domain proteins can populate folding intermediates. These intermediates can sometimes constitute kinetic traps to folding.

The free energy change (ΔG) of any reaction is related to the change in enthalpy (ΔH) and entropy (ΔS) by the Gibbs-Helmholtz Equation: $\Delta G = \Delta H - T\Delta S$. Any reaction, including protein folding, will proceed spontaneously so long as ΔG is negative. The key factor driving protein folding is the hydrophobic effect, whereby hydrophobic residues exposed to solvent in the unfolded conformation congregate together forming a compact core which excludes water. The hydrophobic effect is almost entirely entropic at temperatures close to room temperature, motivated by the freeing of water molecules from forming cage-like structures known as clathrates around non-polar molecules (Dill et al., 2005; Frank, 1945; Makhatadze, 1995). Non-polar amino acids will coalesce inward and away from the bulk aqueous solvent in order to liberate water molecules from these constrictive cage-like structures, enabling increased water-water interactions and greater disorder. Additionally, packed hydrophobic cores enable enthalpically favorable van der Waals interactions between amino acid side chains. The positive driving force of the hydrophobic effect is greatly counteracted by a loss of entropy of the unfolded polypeptide chain due to a reduction in conformational freedom once the protein folds (Baldwin, 2007). The result of this is a very delicate balance between the protein remaining unfolded or spontaneously folding. Due to this delicate balance, other stabilizing forces such as hydrogen bonding between backbone atoms and/or sidechain atoms as well as salt-bridges between oppositely charged amino acids side-chains can be very important in defining the final protein fold and stabilizing it (Lins and Brasseur, 1995; Pace et al., 1996). Despite these stabilizing forces, the overall ΔG of folding (defined as the difference in free energy between the unfolded and folded conformations) of globular proteins is quite small, typically between -5 and -15 kcal/mol, which is equivalent to only 1-3 hydrogen bonds (Kumar et al., 2006; Rose et al., 2006). The relatively low stability of the folded state can be important for protein function, which may require increased flexibility and hence limited stability; additionally it may enable

faster turnover of the protein (Williams et al., 2006). Low stability also makes incorrect folding and/or aggregation possible, however, which can have significant negative implications as discussed in the succeeding section.

1.2 Protein aggregation and disease

The association of protein aggregation with incurable disease states has injected new urgency into the study of protein folding. Examples of such diseases are numerous and include familial hypophyseal diabetes insipidus, amyotrophic lateral sclerosis (ALS), Alzheimer's, Parkinson's, Huntington's, congenital myopathies, sickle cell anemia and prion encephalopathies (Chiti and Dobson, 2006; Gregersen, 2006). These diseases are characterized by the deposition of protein aggregates in affected cells and are sometimes referred to as protein conformational diseases (Carrell and Lomas, 1997). The aggregates can have a range of morphologies ranging from amorphous to higher ordered elongated fibrils (Ecroyd and Carver, 2008). Given that the protein molecules trapped in these aggregates can differ profoundly in conformation from their native states, it is thought that many of the proteins involved in protein conformational diseases undergo either local or global unfolding to a misfolded conformation prior to aggregation (Figure 1.2) (Chiti and Dobson, 2006). Additionally, partially folded or misfolded conformations generally have exposed hydrophobic groups which can serve as interfaces for the interaction of proteins in an aggregate (Agorogiannis et al., 2004).

Organisms possess very elaborate mechanisms for handling misfolded proteins. Highly conserved cellular proteins known as chaperones can "rescue" an improperly folded protein, allowing it to refold to its proper conformation without aggregating with itself or other proteins

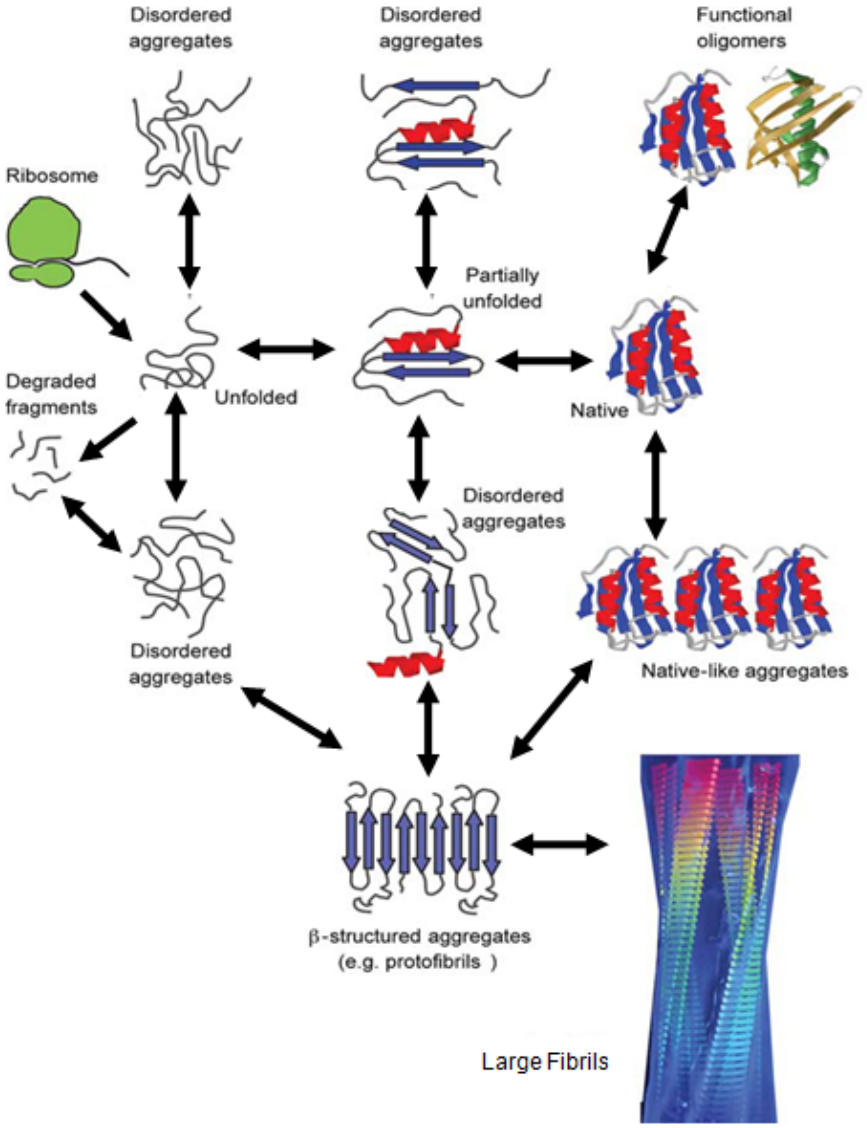

Figure 1.2. Pathways to protein misfolding and aggregation. Protein misfolding or unfolding can be a precursor to aggregation. More ordered fibrilar aggregates tend to form from partially unfolded conformations while fully unfolded conformations tend to give rise to amorphous aggregates. Adapted and modified from (Murphy and Kendrick, 2007).

(Liberek et al., 2008). Improperly folded proteins, which cannot be corrected by chaperones, are marked for degradation, often through the ubiquitin proteasome pathway (Schwartz and Ciechanover, 2009). One of the hallmarks of conformational diseases is that misfolding and subsequent aggregation of the relevant protein either cannot be corrected or overwhelms cellular chaperones and the aggregates are seemingly resistant to degradation even when ubiquinated (Stefani and Dobson, 2003). In fact, chaperones and other cellular proteins involved in degradation pathways often co-precipitate with the associated proteins (Gregersen, 2006).

In addition to occurring sporadically, conformational diseases are often associated with protein mutations. These mutations might increase the tendency of the protein to adopt partially folded forms that are precursors to aggregation. For example, folding and stability studies on mutants of tetrameric transthyretin (TTR), implicated in the disease famililial amyloid polyneurophathy, suggest that the mutations result in destabilization and/or increases in the rate of dissociation or unfolding (Hammarstrom et al., 2002). Similarly, mutations in lysozyme, which cause the disease hereditary non-neuropathic systemic amyloidosis, have been shown to enhance both global and local unfolding of the structure (Canet et al., 2002). Additionally, mutations implicated in familial prion disease have been shown to significantly increase the population of a marginally stable partially folded intermediate along the unfolding pathway (Apetri et al., 2004). Mutations can also change physicochemical properties of proteins such as net charge, hydrophobicity and secondary structure propensity that can be as or even more important in increasing aggregation tendency than global or local destabilization (Chiti et al., 2003).

It is striking that some of the more common neurodegenerative diseases such as Alzheimer's, Parkinson's, Huntington's, and ALS are characterized as protein conformational diseases (Chiti and Dobson, 2006). The post-mitotic nature of neurons might make efficient

protein degradation and clearance more important due to the long lifespan of these cells, hence making them more susceptible to insults resulting from protein misfolding and aggregation (Tai and Schuman, 2008). It has been proposed that there may be common mechanisms underlying all the neurological protein conformational diseases and hence insights gained in the study of one of these diseases could be applicable to the others (Soto, 2003). The next section will describe some clinical features of one of these neurological diseases, amyotrophic lateral sclerosis which is of particular interest in this thesis.

1.3 Amyotrophic lateral sclerosis

First described by the French neurobiologist and physician Jean-Martin Charcot in 1869, ALS is the most common adult onset motor neuron disease (Eisen, 2009). It is primarily characterized by selective death of both upper and lower motor neurons with typical symptoms being weakness initiating in the hand or legs, slurred speech and dysphagia (Cleveland, 1999; Rowland and Shneider, 2001). The average age of onset of the disease is between 50-60 years old, inevitably resulting in paralysis and it is invariably fatal usually within ~ 3-5 years after first symptoms (Eisen, 2009). The disease has an incidence of 1.5-2 per 100,000 people, giving it a prevalence of ~6 per 100,000 (Mitchell and Borasio, 2007). Overall, the disease is more prevalent in men by a ratio of 1.5:1 worldwide and prevalence for both sexes increases with age, reaching 33 per 100,000 for men and 14 per 100, 000 in women in the 60-75 year age group (Majoor-Krakauer et al., 2003). Despite much study, the pathogenic mechanism of ALS is unknown and there are limited treatment options with only the drug riluzole, a glutamate release inhibitor, known to slow progression but only by 3-6 months (Eisen, 2009).

A pathological hallmark of the disease is the presence of specific intraneural aggregates, namely: ubiquitinated inclusions; neurafilament-rich, hyaline conglomerate inclusions[1] and Bunina bodies[2] (Strong et al., 2005). However, as is the case for many protein conformational diseases, it is not clear what role these aggregates play in disease pathology; there is ongoing debate as to whether the aggregates are themselves toxic, harmful byproducts of cellular degeneration or instead protective by sequestering harmful proteins (Bruijn et al., 2004; Goodall and Morrison, 2006).

In 90-95% of cases ALS appears as a sporadic disease (sALS), however 5-10% of the cases follow familial patterns and are referred to as fALS (Rothstein, 2009). Except for subtle differences, sALS and fALS are clinically indistinguishable (Hand and Rouleau, 2002). In 1993, Rosen *et al.* found that mutations in the gene for Cu, Zn superoxide dismutase, SOD1, were implicated in the etiology of ALS (Rosen et al., 1993). Overall, ~ 20% of fALS cases are attributed to mutations in the SOD1 gene (Rothstein, 2009). The link established between SOD1 and some cases of ALS was met with great excitement as it provided novel ideas on the mechanism of this elusive disease and it has enabled murine models to be established that have provided invaluable insights into the progression of the disease (Julien and Kriz, 2006).

1.4 Superoxide Dismutase (SOD)

The superoxide dismutases are metalloenzymes which appear to be ubiquitous among all oxygen consuming species. They provide protection against the reactive superoxide radical $\cdot O_2^-$ which can cause severe oxidative damage if allowed to accumulate in the cell (Fridovich, 1986;

[1] Hyaline conglomerate inclusions are large aggregates containing neurofilaments and other proteins in the soma of motor neurons (Goodall, E. F. and Morrison, K. E. (2006) Amyotrophic lateral sclerosis (motor neuron disease): proposed mechanisms and pathways to treatment. *Expert Rev Mol Med* **8,** 1-22.
[2] Bunina bodies are eosinophilic bodies located in the soma of anterior horn cells that are unique to ALS. (Ibid.)

McCord et al., 1971; Weisiger and Fridovich, 1973). There are four distinct SODs, which differ in structure, evolutionary relationships and metals found in the active site. The first two, manganese (III) SOD, found in bacteria and mitochondria, and iron (III) SOD, found in some bacteria and some plants, come from the same evolutionary line and exist either as homotetramers or homodimers (Fridovich, 1986; Miller, 2004). The third, a nickel (III) containing enzyme, has been found in *Streptomyces* species. Ni SOD exists as a tetramer and is evolutionarily distinct from all other SODs (Youn et al., 1996). The fourth, Cu, Zn SOD, which is the subject of this research is also evolutionarily unique and is found in the cytoplasm and chloroplasts of eukaryotes as well as some bacteria (Fridovich, 1986).

Eukaryotic intracellular Cu Zn SODs are homodimeric enzymes, with each ~16 kDa subunit containing 151-158 amino acid residues, one bound Zn(II) and one bound Cu(II) (Bordo et al., 1994). The enzyme is negatively charged at physiological pH with a typical pI of 4-5 (pI = 4.7 in humans) (Fridovich, 1986). The Cu, Zn SODs are highly conserved enzymes with ~50 % sequence similarity between species (Fridovich, 1986). Indeed, human Cu, Zn SOD has approximately 82% sequence similarity with SOD of other mammals and comparison of the structure of bovine Cu, Zn SOD with human Cu, Zn SOD demonstrates that all the main structural features are identical (Getzoff et al., 1989; Parge et al., 1992).

1.4.1 Structure of Cu Zn Superoxide Dismutase

As its main structural unit, each 153 amino acid human SOD monomer contains eight antiparallel β-strands connected by turns and three long external loops, which combine to form a flattened cylinder (Richardson et al., 1975; Strange et al., 2003; Tainer et al., 1982) (Figure 1.3).

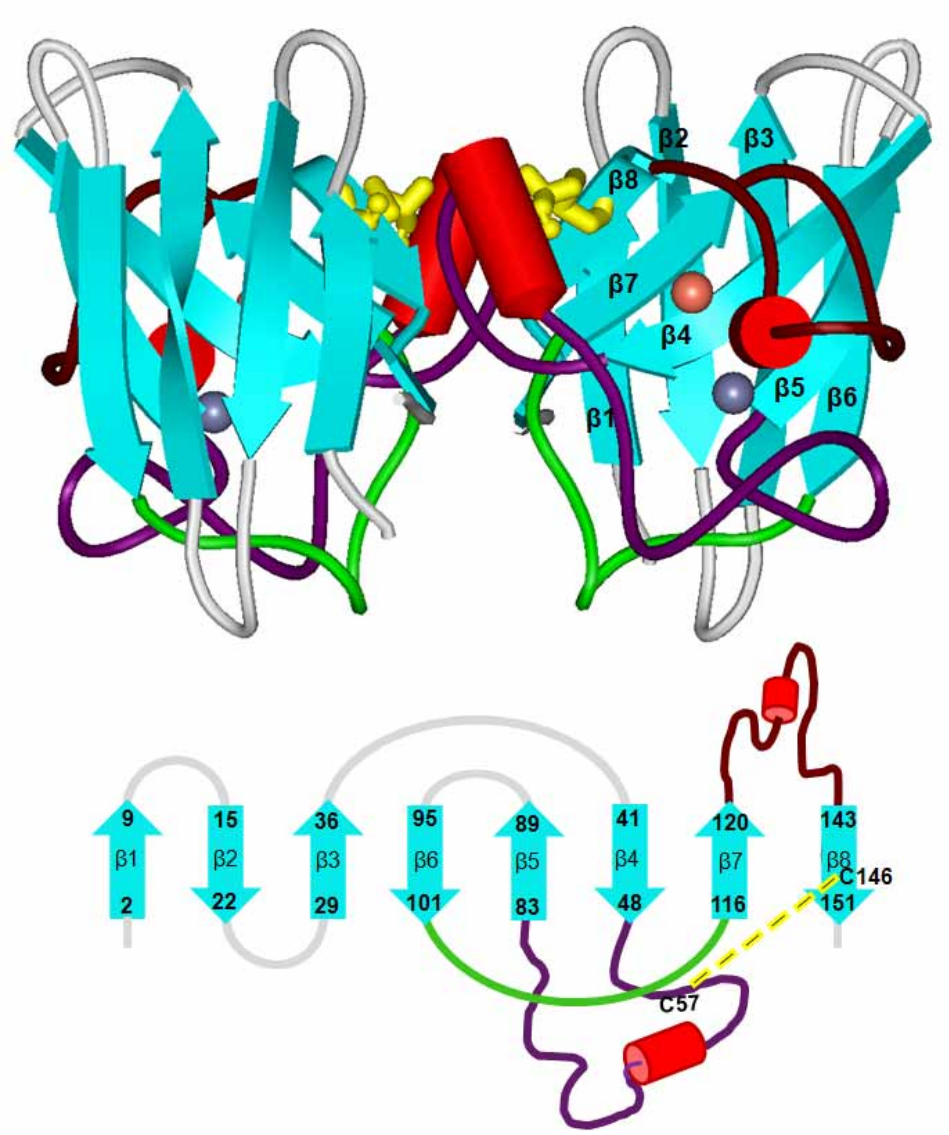

Figure 1.3. Structure and topology of Cu, Zn Superoxide dismutase. (A) Ribbon representation of the three dimensional structure of dimeric Cu, Zn SOD, showing the main structural features. Cu^{2+} and Zn^{2+} are shown as orange and blue spheres, respectively. β-strands are coloured cyan, turns are coloured grey and α-helices are depicted as red cylinders. The three long external loops: loop 4 (the zinc binding loop), loop 6 (forming the Greek key connection) and loop 7 (the electrostatic loop) are coloured purple, green, and brown respectively. The lone disulfide bond in each SOD monomer is represented in yellow stick representation. (B) The topology of Cu, Zn SOD, demonstrating the Greek key motif. The topology diagram is coloured in accordance with the three dimensional structure in (A). The residue numbers corresponding to the beginning and the end of each β-strand are shown and the intramolecular disulfide bond between C57 and C146 is represented as a yellow broken line. The figure was generated from pdb code 1HL5 (Strange et al., 2003) and rendered in Viewer Lite Pro.

There are two strands across the top of the cylinder and a further two strands across the bottom with remaining connections occurring between adjacent strands, creating a Greek key β barrel topology (Getzoff et al., 1989) (Figure 1.3). The active site is located on the outside of the β-barrel and is flanked by the two longest external loops: loop 4 and loop 7, forming an active site channel; the third and shortest loop, loop 6, forms a Greek key connection across the β barrel (Richardson et al., 1975; Strange et al., 2003; Tainer et al., 1982). Each monomer contains a disulfide bond between loop 4 and the beginning of β-stand 8. This disulfide bond helps to ensure that loop 4 and loop 7 remain adjacent to each other (Tainer et al., 1982). The protein also contains two short helical regions: a 3/10 helix in loop 4 and an α-helix in loop 7.

The Cu^{2+} and Zn^{2+} ion in each SOD monomer are 6.3 Å apart and sit at the bottom of the active site channel (Strange et al., 2003; Tainer et al., 1982). The solvent exposed copper ion is five coordinate with a distorted square pyramidal geometry (Tainer et al., 1982). In human Cu, Zn SOD, four of these these coordinate bonds to copper are formed by His 63, His 48, His 120 and His 46 (Figure 1.4) with bond lengths of approximately 2.1 Å, with the fifth coordination bond being formed with one of four highly conserved water molecules (Parge et al., 1992; Strange et al., 2003). With the exception of His 63, all Cu ligands are located in the β barrel (Tainer et al., 1982). The Zn ion is four coordinate, forming a tetrahedral geometry with a trigonal planar distortion and is not exposed to solvent (Richardson et al., 1975; Tainer et al., 1982). The Zn binding ligands are located in loop 4 of SOD and hence this loop is also known as the zinc binding loop (Figure 1.3). In human Cu Zn SOD Zinc is coordinated at ~ 1.9 Å by Asp 83 and at ~ 2.0 Å by His 71 and His 80; the fourth coordinate bond is with His 63 forming a Cu-His63-Zn imidazole bridge (Figure 1.4) (Parge et al., 1992; Richardson et al., 1975; Strange et al., 2003; Tainer et al., 1982).

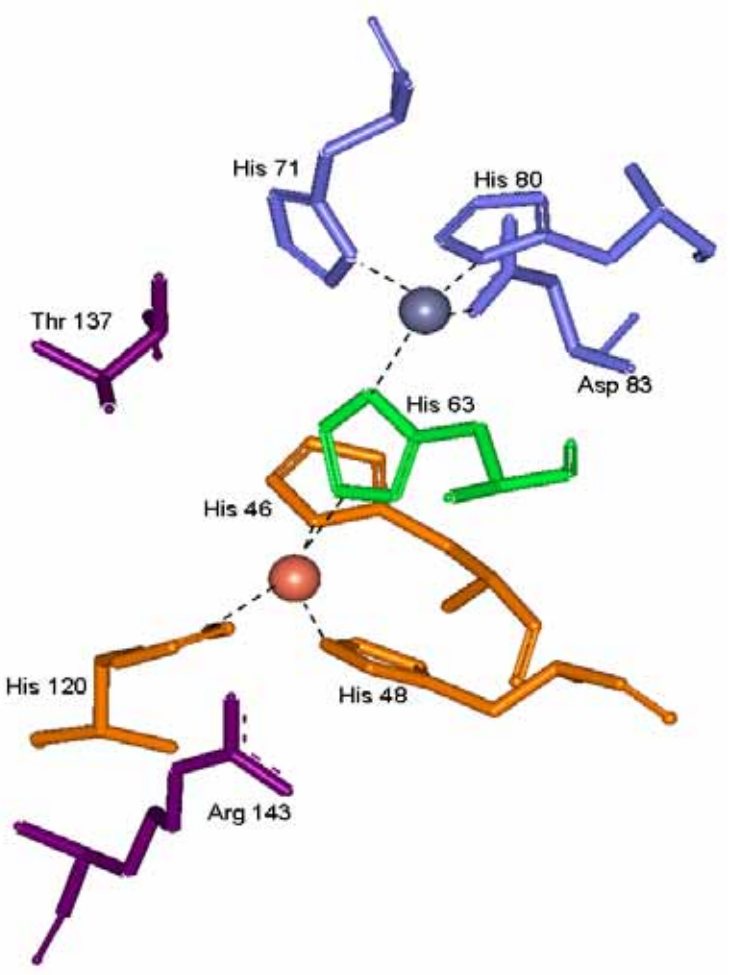

Figure 1.4. The active site configuration of human Cu, Zn superoxide dismutase. Cu^{2+} and Zn^{2+} are represented as orange and blue spheres, respectively. Key amino acids are shown in stick representation and are labelled. Cu and Zn binding amino acid residues are coloured orange and blue, respectively. His 63 forms an imidazole bridge, coordinating both Cu and Zn atoms is coloured green. The residues Arg 143 and Thr 137, which provide steric hindrance for large substrates thereby increasing the specificity of SOD, are shown in purple. Additionally, Arg 143 helps to position the superoxide radical above the catalytic copper. The figure was generated from pdb code 1SOS (Parge et al., 1992) and rendered in Viewer Lite Pro. Dashed lines represent coordination bonds between the residues and the metal.

The two monomers of the SOD dimer have a 2-fold symmetry with the monomers oriented such that the two catalytic coppers are facing away from each other ~ 34 Å apart (Tainer et al., 1982). The dimer interface of the enzyme is very tight with no gaps bigger than the size of a water molecule (Getzoff et al., 1986). The dimer contact of SOD consists of many hydrophobic and water mediated interactions and is stabilized by 4 main chain hydrogen bonds; the most important residues in the dimer interface are 50-53, 114, 148 and the C-terminal residues 150-153 (Hough et al., 2004) (Figure 1.5). The H-bonds across the interface are formed between G51 and G114 of one monomer and I151 of the other (Getzoff et al., 1989). The disulfide bond between C57 and C146 plays an indirect but important role in maintaining the dimer interface by properly positioning the residues at the C-terminus (residues 150-153) so that they can participate in crucial interface contacts (Tainer et al., 1982). Dimerization buries ~ 550 Å of surface area per monomer, or ~8 % of the total monomer surface (Getzoff et al., 1986; Tainer et al., 1982). Although most of the interactions between residues in the interface are hydrophobic in nature, ~ 30 % of the buried residues are hydrophilic and directly interact with hydrophilic residues of the opposing monomer (Getzoff et al., 1986; Richardson et al., 1975).

1.4.1.1 Role of metals in SOD structure

Structural studies on demetallated or apo SOD revealed that this state of the protein contains the same secondary and most of the tertiary structure of fully metallated SOD (holo SOD) and is also a symmetrical homodimer (Strange et al., 2003). There is, however, significant disorder in the Zn binding loop and the electrostatic loop in apo SOD (Strange et al., 2003). There are more significant differences between the apo SOD and holo SOD free monomer. In apo and holo SOD engineered monomer variants, Phe 50 and Gly 51 in the dimer interface are

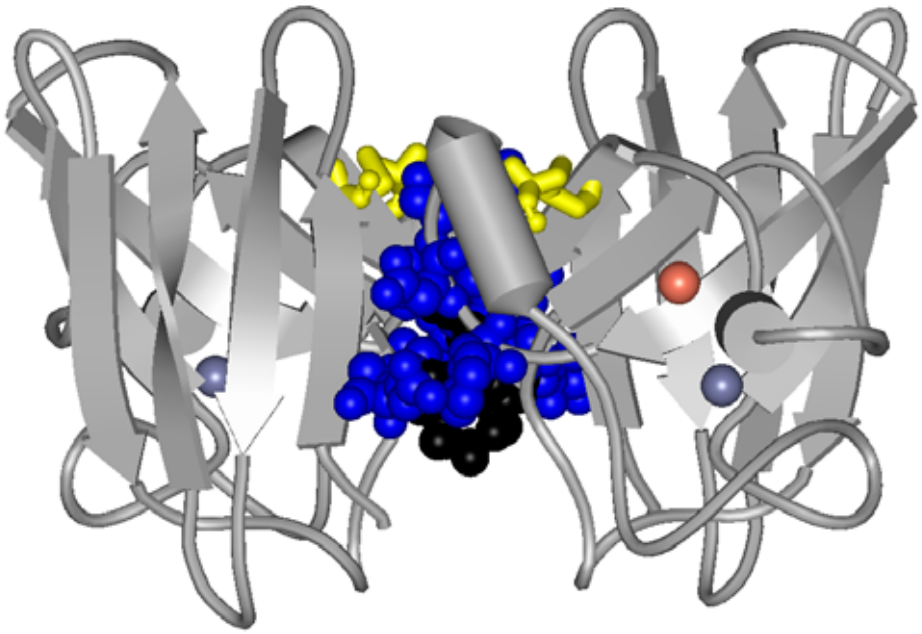

Figure 1.5. The dimer interface of Cu Zn SOD. The metals Cu and Zn are shown as orange and blue spheres respectively. The most important residues in the dimer interface of SOD: F50, G51, D52, N53, G114, V148, G150, I151, A152, Q153 are shown in CPK representation. The residues G51, G114 and I151 which are involved in hydrogen bonding are shown in black while all other residues are shown in blue. The 2 cysteines in each monomer involved in the formation of the lone intramolecular disulfide, C57 and C146, are shown in yellow stick representation. This disulfide bond which joins loop 4 to beta strand 8 helps to orient the residues 150-153 allowing them to form important contacts in the dimer interface. The figure was generated from pdb code 1HL5 (Strange et al., 2003) and rendered using the program Viewer Lite Pro.

both replaced by glutamic acid to prevent dimerization. Solution structures of these proteins reveal notable perturbation in the β-barrel of the apo protein (Banci et al., 1998; Banci et al., 2003) (Figure 1.6). There is increased disorder in β-strands 4, 5 and 7; particularly in strand 4, where there is a significant shortening of the strand, which results in the copper binding ligands, H46 and H48, moving from β-strand 4 to loop 4. Overall, the β-barrel in apo SOD is slightly more open when compared to holo SOD (Figure 1.6).

1.4.2 Stability of SOD

The Cu, Zn SODs are very stable proteins with thermal denaturation occurring at temperatures greater than 80°C as measured by differential scanning calorimetry (Lepock et al., 1990). Studies on bovine Cu, Zn SOD indicate that the enzyme retains most of its activity in the presence of 10M urea and retains full activity after treatment for one hour with 4% sodium dodecyl sulfate (Forman and Fridovich, 1973). The extremely high stability of the SOD enzyme is thought to arise from widespread hydrophobic interactions within the dimer interface and between residues in the β barrel as well as from extensive electrostatic interactions (Getzoff et al., 1989; Parge et al., 1992). Additionally, the stability of the protein is heavily dependent on the presence of post-translational modifications, namely: formation of the lone covalent intramolecular disulfide and addition of both Cu and Zn (see below).

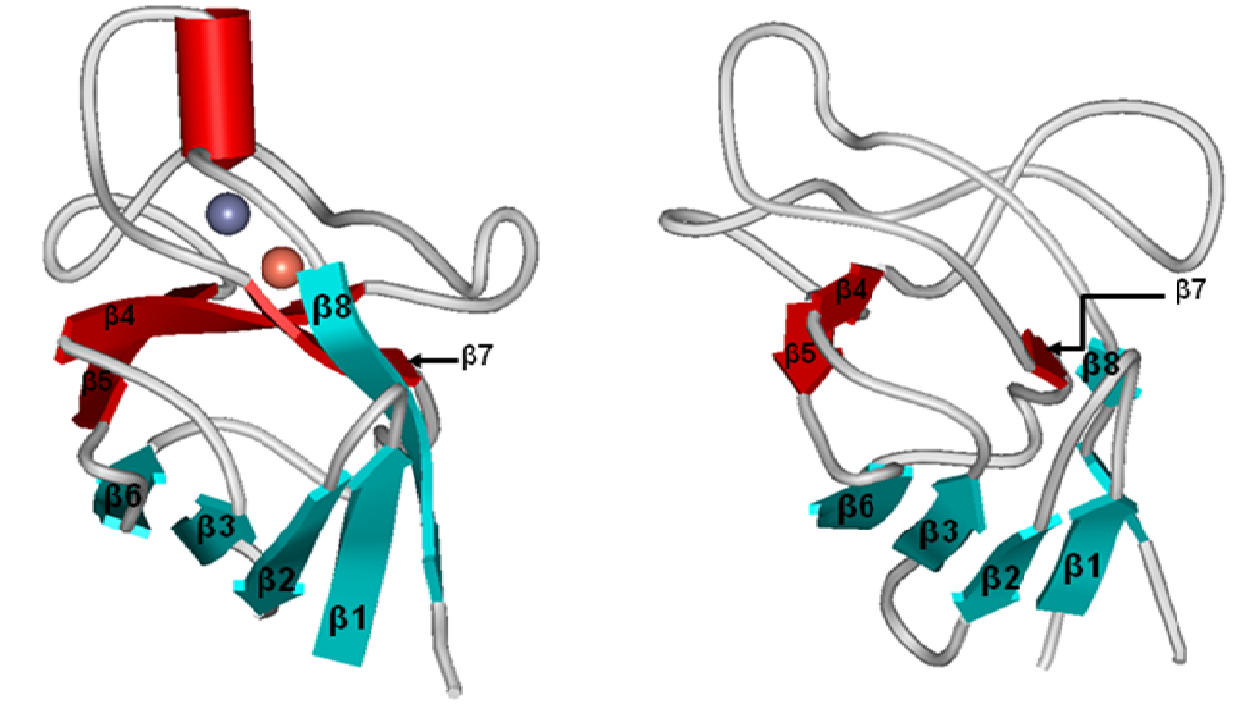

Figure 1.6. Structural differences between monomeric apo and holo Cu, Zn superoxide dismutase. The dimer interface of SOD was disrupted by substituting the hydrophobic residues Phe 50 and Gly 51 in the dimer interface with the charged residue Glu. Cu and Zn bound to the holo protein are depicted as orange and blue spheres, respectively. (A) The holo SOD monomer has a very well defined β-barrel. (B) The apo monomer has a more open β-barrel due to significant shortening of β-strands 4, 5, and 7 depicted in red and labelled. In particular, β-strand 4, which contains copper binding residues, is severely destabilized and is shortened from 8 residues in the holo protein to only 3 residues in the apo protein. Both holo and apo SOD images were rendered using view lite pro from pdp files 1RK7 (apo) and 1BA9 (holo) (Banci et al., 1998; Banci et al., 2003).

1.4.2.1 Role of post-translational modifications

SOD is first synthesized on the ribosome in an immature state that lacks both Cu and Zn as well as the native disulfide bond between C57 and C146 (disulfide-reduced apo SOD). This disulfide-reduced apo SOD has significantly weakened dimerization propensity (Doucette et al., 2004; Lindberg, 2004) and significantly reduced stability with temperature of unfolding less than 50 °C (Chapter 4). Formation of the disulfide-bond in apo SOD markedly increases its stability (with temperature of unfolding increasing by ~ 10 degrees) and dramatically increases dimerization propensity (Doucette et al., 2004; Stathopulos et al., 2006).

The full mechanism of maturation of SOD is yet to be deciphered. However, it has been shown that the copper chaperone for SOD (CCS) accelerates formation of the disulfide bond (though the disulfide can form spontaneously), while Zn binds by an unknown mechanism perhaps prior to the interaction of CCS with SOD (Furukawa et al., 2004). CCS has also been shown to catalyze the addition of Cu to SOD; in addition there is a CCS independent mechanism for Cu addition that involves reduced glutathione (GSH) (Carroll et al., 2004; Culotta et al., 1997; Rae et al., 1999).

1.4.3 Catalytic mechanism of SOD

Cu Zn SOD catalyses the dismutation of O_2^- through successive reversible encounters with the catalytic Cu to yield O_2 and H_2O_2 according to the following reaction scheme (Klug et al., 1972; Tainer et al., 1983):

$$\text{SOD-Cu}^{2+} + {}^{\cdot}\text{O}_2^- \leftrightarrow \text{SOD-Cu}^{1+} + \text{O}_2$$

$$\text{SOD-Cu}^{1+} + {}^{\cdot}\text{O}_2^- + 2\text{H}^+ \leftrightarrow \text{SOD-Cu}^{2+} + \text{H}_2\text{O}_2$$

Overall: $2 \cdot O_2^- + 2H^+ \leftrightarrow O_2 + H_2O_2$

Cu, Zn SOD catalyses the dismutation of O_2^- with a rate constant of 2.3 x 10^9 $M^{-1}s^{-1}$ between 20 and 25^0C at pH 7.0 (Klug et al., 1972). Despite the fact that the catalytic copper of Cu Zn SOD accounts for only ~ 0.1% of the enzyme's molecular surface, this rate of catalysis is ~ 10% of the maximum diffusion-controlled limit as determined by collision theory (Getzoff et al., 1983; Margerum, 1978). This exceptionally high catalytic efficiency of SOD was explained through analysis of electrostatic field vectors of the protein (Getzoff et al., 1983). There are long range electropositive attractions exerted mainly by conserved lysine residues within the active site channel for the negatively charged O_2^- substrate (Getzoff et al., 1983). These residues are found in loop 7 of the SOD monomer and hence this loop is also referred to as the electrostatic loop (Figure 1.3). There is also a conserved arginine residue ~ 5 Å from the catalytic copper (Arg 143 in humans) which is thought to position the substrate above the copper (Figure 1.4) (Cudd and Fridovich, 1982; Getzoff et al., 1983). It appears that the overall negatively charged SOD enzyme pushes the O_2^- substrate into the positive active site channel, where it is guided to the conserved positive arginine and finally to the positively charged copper (Getzoff et al., 1983). Specificity for small negatively charged substrates is imposed by the narrowing of the active site channel from 24 Å to 10 Å and finally to 4 Å just above the copper. Additionally, Thr 137 as well as the guanidinium group of Arg 143 provide steric hindrance to large species, which further enhances specificity (Figure 1.4) (Bertini, 1998; Hart et al., 1999).

1.5 fALS and SOD

The *sod 1* gene which codes for human Cu, Zn SOD spans 11 kb of DNA and is located on chromosome 21q22.1 (Hand and Rouleau, 2002). To date, over 110, mostly missense *sod 1*

mutations linked to ALS have been identified, and they occur in all 5 coding exons of the gene and hence span the entirety of the SOD structure (Figure 1.7) (see *http://alsod.iop.kcl.ac.uk* for a continually updated list of SOD mutations linked to ALS). The mutations have a wide variety of chemical and structural contexts. All of the fALS-associated SOD mutations are dominant except D90A, which can be recessive (Andersen et al., 1995). A4V is the most common mutation in North America accounting for 50% of all cases, followed by I113T at 11.7% (Hand and Rouleau, 2002).

The first ALS-associated SOD mutations that were discovered occurred primarily in three regions: in loops joining the β barrel, in the dimeric interface region and at the base of the active site loop (Deng et al., 1993). Due to the importance of these areas for SOD structure and mechanism, the hypothesis was formulated that ALS-linked SOD mutations destabilize the protein leading to a loss of function which causes the disease (Deng et al., 1993; Siddique and Deng, 1996). In fact, early measurements of SOD activity levels in the blood of ALS patients indicated that these levels were lower than normal for some SOD fALS patients (Deng et al., 1993; Orrell et al., 1995). This loss of function hypothesis, however, was challenged by results of mice studies in which mice expressing mutations in the *sod1* gene were shown to develop symptoms of ALS while retaining normal SOD activity levels (Ripps et al., 1995). Additionally, mice with a deleted *sod1* gene do not develop ALS symptoms and are relatively normal (Borchelt et al., 1994; Reaume et al., 1996). These results, and others, that contradict the loss of function mechanism have spawned the idea that mutant SOD is somehow toxic to the cell. It is this gain of function hypothesis that has prevailed in the literature.

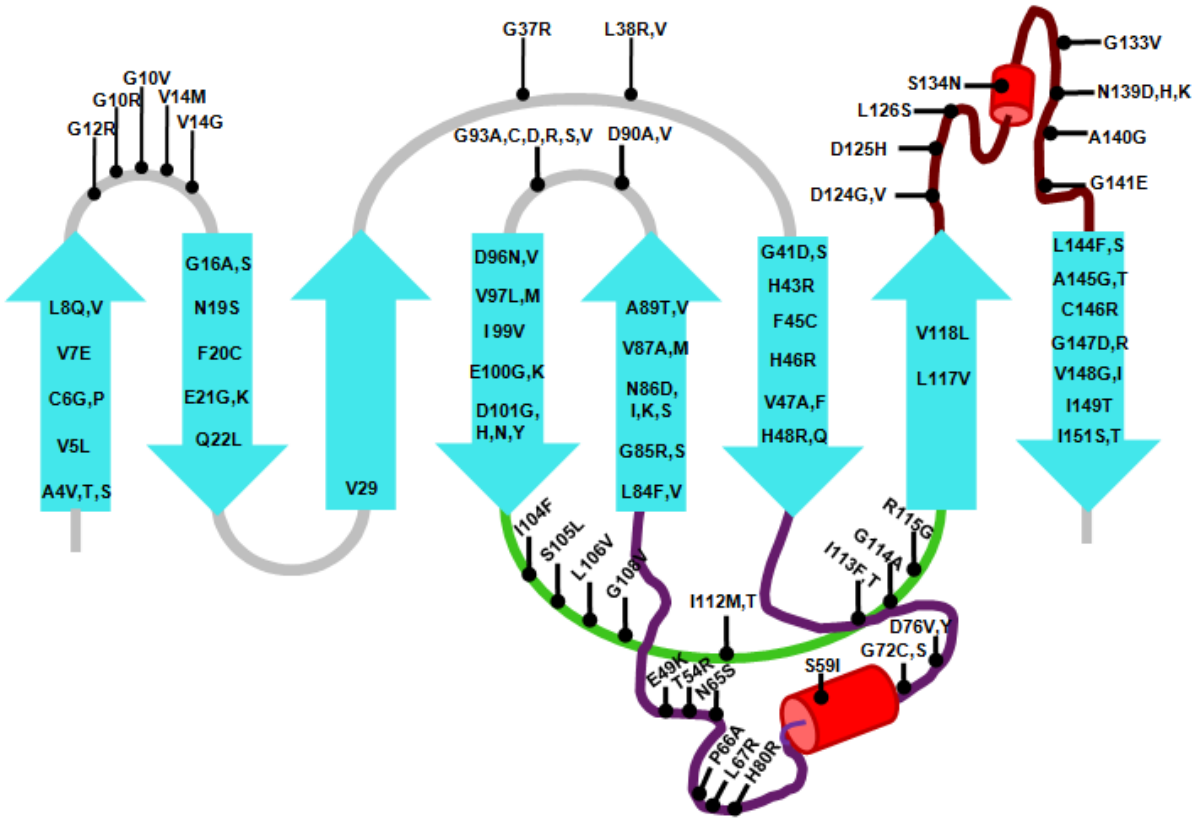

Figure 1.7. Location of fALS-associated missense SOD mutations. The mutations are indicated on the SOD topology diagram which has the same colour scheme as in Figure 1.3. Mutations in SOD that are associated with familial ALS are distributed throughout the SOD structure. Mutations are particularly concentrated in the 3 major loops (loop 4, 6 and 7) as well as β-strands 4, 5, 6 and 8. Additionally, there are many glycine mutations in the turns (data from *http://alsod.iop.kcl.ac.uk*).

1.5.1 Mechanisms for Cu, Zn SOD mediated fALS

Amazingly, almost all of the more than 110 SOD mutations share the same clinical phenotype, although the age of onset and the duration of disease differs between them and between the individual patients (Guegan and Przedborski, 2003). Presently, it is still unclear how all the different SOD mutations result in the same clinical phenotype. Two potential gain of function hypotheses, which are not mutually exclusive, have been proposed and are described below.

1.5.1.1 Oxidative damage hypothesis

The first hypothesis is called the oxidative damage hypothesis. It maintains that mutant SOD is less tightly folded and that as a result, the catalytic Cu^{2+} is more accessible to aberrant substrates, thus performing harmful redox chemistry (Barber et al., 2006). One such substrate is peroxynitrite, which is formed spontaneously from the combination of nitric oxide and the superoxide radical. When this substrate is acted upon by SOD, the highly reactive nitronium species is produced that can damage proteins through tyrosine nitration (Beckman et al., 1993). This is supported by the finding of elevated levels of 3-nitrotyrosine in the spinal cord of ALS patients (Beal et al., 1997). There are, however, lines of evidence against this hypothesis. Firstly, toxicity is not reduced by eliminating the enzyme copper chaperone for SOD (CCS), which leads to a reduction of Cu incorporation into the enzyme (Subramaniam et al., 2002); secondly, there are conflicting results regarding evidence for oxidative damage in SOD-mediated ALS in human and mice studies (Barber et al., 2006). Additionally, transgenic mice harboring two known ALS-linked SOD mutations in metal binding regions (H48Q and H46R) still developed the disease despite being deficient in catalytic copper (Wang et al., 2002). These results indicate that

oxidative damage is likely not a general mechanism for SOD-mediated fALS, however, it may still play a role for some mutants.

1.5.1.2 Aggregation hypothesis

The second hypothesis, called the aggregation hypothesis, maintains that mutant SOD has a stronger propensity to misfold and form proteinaceous aggregates that are toxic to the cell. An extension of this hypothesis is that SOD aggregates bind other proteins that are essential to the viability of the cell. This model is supported by *in vivo* studies, in which mutant SOD-rich aggregates were formed in affected neurons but not in normal ones; in some cases forming prior to disease symptoms (Durham et al., 1997; Johnston et al., 2000; Koide et al., 1998). In addition, proteinaceous inclusions rich in Cu, Zn SOD have been identified in affected cells of ALS patients (Matsumoto et al., 1996; Shibata et al., 1996; Shibata et al., 1994). There is evidence suggesting that smaller SOD protein complexes or oligomers are responsible for SOD toxicity and not the much larger visible cytoplasmic inclusions (Johnston et al., 2000). This is due to the fact that in mice studies, these smaller aggregates form before the onset of disease symptoms while larger SOD inclusions form much later in the disease (Johnston et al., 2000). This result shows commonality to other protein conformational neurodegenerative diseases such as Alzheimer's, where increasingly, smaller soluble protein oligomers are being implicated in the disease instead of larger fibrils (Valentine and Hart, 2003). Considering the strong evidence for this aggregation hypothesis for SOD mediated fALS, there is a great need for protein folding studies that could help to elucidate how mutations mediate changes in the folding mechanism and stability of SOD that will lead to aggregate formation.

1.6 Probing the stability and folding mechanism of SOD

Studies conducted over the last several years have sought to compare the stabilities of fALS-associated SOD mutants and WT. These studies include thermal and chemical denaturation experiments and have mostly focused on the demetallated or apo protein (Lindberg et al., 2002; Rodriguez et al., 2005; Valentine et al., 2005). It has been shown *in vitro* that metal loss is a necessary precondition for aggregation (Khare et al., 2004) and that aggregation of the apo protein can be enhanced by fALS mutations (DiDonato et al., 2003; Stathopulos et al., 2003). Furthermore, aggregates formed by apo SOD *in vitro* have been found to have a similar morphology to those seen *in vivo* (Stathopulos et al., 2003). It is thought that the reduced stability of apo SOD makes it more amenable to the structural changes required for aggregation. While these previous studies have indicated a general but not universal tendency of mutations to destabilize apo SOD, the analysis has been hampered by the irreversibility of SOD unfolding which greatly limits the information that can be extracted. Investigating reversible unfolding creates the opportunity to conduct a more reliable comparison of thermodynamic stability between mutants and WT. Additionally, reversible folding is required to deduce the mechanism of unfolding that is vital to identifying species along the folding pathway which may be pre-disposed to potentially toxic aggregation. A major reason for previously observed irreversibility in WT and mutant unfolding is adventitious disulfide cross-linking by the free cysteines C6 and C111 that occurs as the protein unfolds. This problem is not easily alleviated by the addition of reducing agents, as this may result in the reduction of the lone native disulfide-bond in SOD (Lindberg et al., 2002).

1.6.1 The Pseudo wild-type construct

Due to experimental difficulties associated with studying reversible unfolding of SOD, many studies have utilized a variant, in which the problematic free cysteines, C6 and C111, are mutated to alanine and serine, respectively. Importantly, these mutations are not associated with ALS, and this construct has been found to have virtually identical activity, structure and stability to WT SOD (Hallewell et al., 1991; Lepock et al., 1990; McRee et al., 1990; Parge et al., 1992; Stathopulos et al., 2003). Due to the close similarities with WT, this construct is commonly referred to as pseudo wild-type (PWT). It has been shown to unfold with high reversibility both in thermal and chemical denaturation studies in both apo and holo forms (see Chapter 2 and 3) (Lindberg et al., 2005; Rumfeldt et al., 2009; Rumfeldt, 2006; Stathopulos et al., 2006; Stathopulos et al., 2003; Svensson et al., 2006; Vassall et al., 2006).

1.7 Research goals and objectives

This dissertation is centered on investigations of the folding mechanisms and thermodynamic stabilities of apo SODs (both with and without the native disulfide bond). Calorimetric techniques, namely differential scanning calorimetry (DSC) and isothermal titration calorimetry (ITC), which measure the heat associated with protein unfolding reactions (section 2.1.1) were utilized. In addition, changes in the circular dichroism and fluorescence signal were used to monitor equilibrium unfolding (Section 3.1.1 and 3.1.2). Several fALS-associated SOD mutants were investigated (Figure 1.8) and results were rationalized by considering the structural contexts of these mutants. This enabled the identification of common properties that may result in an increased tendency of apo SOD mutants to aggregate.

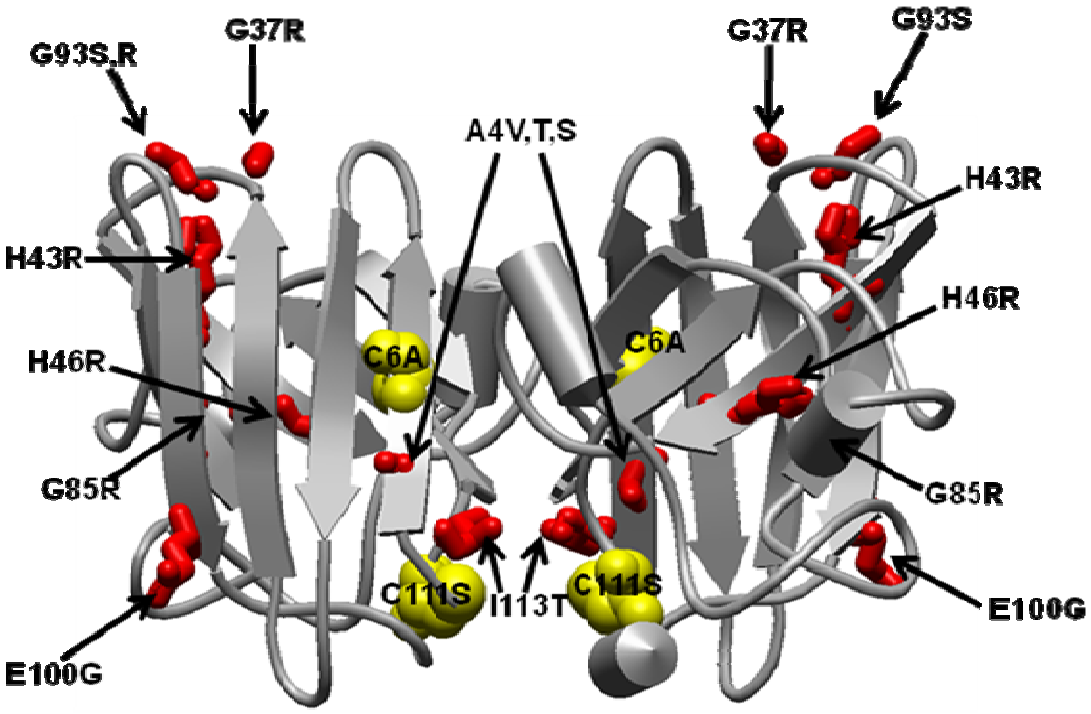

Figure 1.8. Ribbon representation of apo SOD showing the location of the mutations studied in this thesis. The heavy atoms of the fALS-associated mutations: H46, G85, G93, H43, G37, A4 and I113 are shown in red and labelled according to the corresponding mutations. The fALS mutations span the entire structure of SOD and have a variety of structural contexts. H46R and G85R alter metal binding in the protein, A4V, T, S and I113T are located at the dimer interface, G93S, R and G37R are in tight turns, H43R disrupts packing in the β-barrel and E100G removes a salt bridge with K30 (see Section 2.4.1 for full description of structural contexts). Shown in yellow space filling representation are the residues C6 and C111 that are mutated to A and S, respectively, in the PWT construct; all mutations were studied against this background. The figure was rendered from pdb code 1HL4 (Strange et al., 2003) using Viewer Lite Pro.

In order to guarantee folding reversibility, the PWT construct (section 1.6.1) was used and mutations were studied in this background.

Chapter 2 describes thermal unfolding studies of fALS-associated SOD mutants with an intact disulfide bond using DSC and highlights key changes in folding mechanism, entropy, enthalpy and overall free energy. Additionally, the effects of the mutations on dimer interface stability were probed using ITC.

In chapter 3, as a complement to thermal unfolding studies presented in Chapter 2, the mechanism of disulfide-intact apo PWT and mutants is probed using equilibrium chemical denaturation monitored by optical spectroscopy. New methodology is presented enabling us to better characterize an elusive folding intermediate that might be an important precursor to toxic aggregation in ALS.

Finally in chapter 4, using a combination of thermal and chemical denaturation techniques, investigations into the role of the lone native intramolecular disulfide bond in SOD are presented through analysis of folding mechanism and thermodynamic stability of disulfide-reduced apo SOD. In addition, the effects of several mutations on stability in this background are described and data illustrating enhanced aggregation tendency of fALS-associated mutants are presented. Overall, these studies complement work done by others in the Meiering research group that defined the stability and folding mechanism of holo PWT and mutants and has provided valuable insights into the role of post-translational modifications in SOD.

Chapter 2: Thermodynamic analysis of fALS-associated disulfide-intact mutant apo SOD dimer dissociation and unfolding by calorimetry

Acknowledgements

I would like to thank Jessica Rumfedlt and Julia Maeve Bonner for performing some of the DSC scans for apo A4V. I would also like to thank Mingsze Tong for performing some scans on apo A4T as well as Ryan Sobering and Kristin Dimmick for protein preparation and purification and Peter Stathopulos for his assistance in methodology of DSC and ITC experiments. Additionally, I am indebted to Kristin Dimmick, Mingsze Tong and Peter Stathopulos for making mutations in the *sod1* gene. I am also grateful to R. William Lewis for help with Matlab.

2.1 Introduction

Despite the purported importance of metal loss as a precursor step for SOD aggregation (Khare et al., 2004), there have been relatively few quantitative thermodynamic studies on the effects of mutations on the stability of apo SOD. Most published folding and stability studies on apo SOD mutants have provided only estimates of stability through apparent melting temperatures of unfolding or through kinetics of unfolding (Lindberg et al., 2005; Rodriguez et al., 2005). Others within the Meiering group have used equilibrium techniques to characterize the thermal unfolding mechanism and stability of the PWT control as well as mutants at position G93 (G93A,D,R,S,V) and E100G (Rumfeldt, 2006; Stathopulos, 2005; Stathopulos et al., 2006). Here, differential scanning calorimetry (DSC) was used to investigate the thermal unfolding

mechanism and stability of several additional fALS-associated mutants located in diverse regions of the SOD structure (Figure 1.8). These include mutations within the dimer interface of SOD (A4V, A4S, A4T, and I113T), mutations that occur close to or at the metal binding site of SOD (H46R and G85R) and mutations located in the beta barrel, away from the metal binding sites and dimer interface (H43R and G37R)[3]. As a complement to the DSC studies, isothermal titration calorimetry (ITC) was used to determine the thermodynamics of dimer dissociation of the mutants H46R, G93S, H43R, A4T, A4V, A4S and I113T.

2.1.1 Protein thermal unfolding studies using differential scanning calorimetry

DSC is a very effective and accurate tool for measuring the thermodynamics of thermal denaturation of proteins (Freire, 1995). In this technique, a sample cell containing protein and a reference cell containing buffer are heated at a constant rate. The instrument measures the power required to maintain a constant temperature between the two cells. This power is proportional to the difference in heat capacity between the two cells. By subtracting a buffer *versus* buffer scan from a sample *versus* buffer scan, the heat capacity of the sample is determined. Figure 2.1 illustrates the typical features of a DSC unfolding thermogram; the native or pre-transition baseline as well as the unfolded or post-transition baseline is indicated along with the peak associated with the endothermic unfolding transition. The difference between the post-transition and pre-transition baselines represents the change in heat capacity for protein unfolding, ΔC_p, while the area under the endothermic unfolding transition peak represents the

[3] Some of the DSC data have been published for G85R and I113T: Vassall, K. A., Stathopulos, P. B., Rumfeldt, J. A., Lepock, J. R. and Meiering, E. M. (2006) Equilibrium thermodynamic analysis of amyotrophic lateral sclerosis-associated mutant apo Cu,Zn superoxide dismutases. *Biochemistry* **45,** 7366-79.

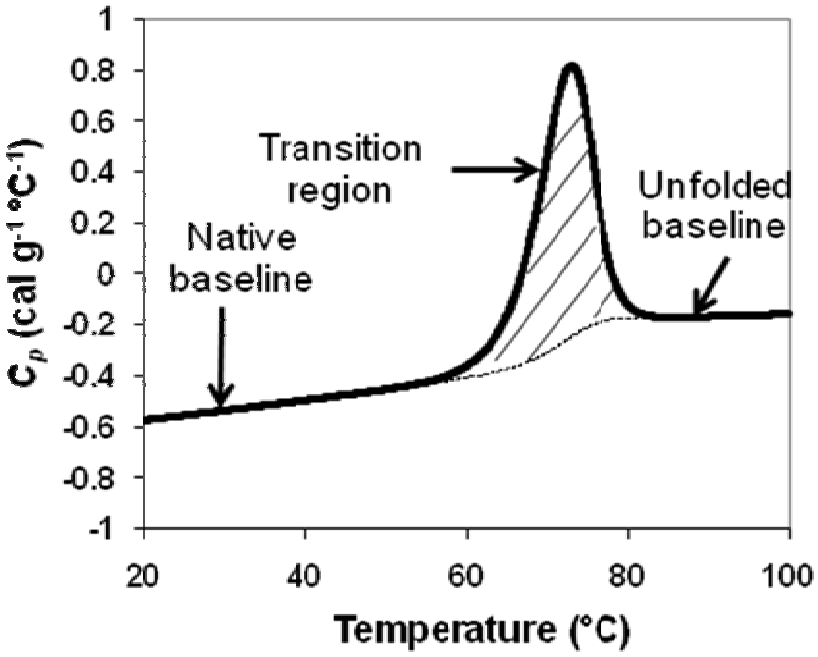

Figure 2.1. The typical features of a protein unfolding thermogram measured by differential scanning calorimetry. The unfolding endotherm (solid line) is shown as well as the baseline progressed into the unfolding transition region (hashed area). The difference between the unfolded (post-transition) baseline and the native (pre-transition) baseline is the $\Delta C_{p,\ tot}$ of unfolding while the area under the unfolding thermogram or transition region (hashed area) is the ΔH_{cal}. Due to the asymmetry of the transitions, the temperature of half unfolding ($t_{0.5}$) is usually close to but not necessarily identical to the temperature at C_p maximum.

calorimetric enthalpy of unfolding, ΔH_{cal}. Fitting of the DSC thermogram to the appropriate model yields the equilibrium constant of unfolding at each temperature as well as the van't Hoff enthalpy of unfolding, ΔH_{vH}. The ratio of ΔH_{vH} to ΔH_{cal} ($\Delta H_{vH}/\Delta H_{cal}$) will be unity if the model used for fitting is correct; however, if the fitting model used is incorrect due to unaccounted for population of intermediates, this ratio will be less than 1 (Sturtevant, 1987). Additionally, aggregation of the protein as it unfolds can result in $\Delta H_{vH}/\Delta H_{cal}$ being greater than 1 (Stathopulos et al., 2006). This capability to report on possible aggregation through comparison of ΔH_{vH} and ΔH_{cal} is an advantage of this technique and can be particularly useful in determining whether mutant forms of SOD have an increased tendency to aggregate.

In considering the possible unfolding mechanisms of dimeric apo SOD, the 3 simplest models are: 2-state dimer unfolding ($N_2 \leftrightarrow 2U$, Model 1), and 3-state dimer unfolding with monomeric intermediate ($N_2 \leftrightarrow 2I \leftrightarrow 2U$, Model 2) or dimeric intermediate ($N_2 \leftrightarrow I_2 \leftrightarrow 2U$, Model 3). In these models, N_2 is the native dimer, I and I_2 are the monomeric and dimeric intermediate, respectively and U is the unfolded monomer. In Model 1, the protein unfolds *via* a single transition, however, in the latter two unfolding occurs over two transitions. These mechanisms may be distinguished from each other based on the protein concentration dependence of the shape of the unfolding thermograms (Figure 2.2) (Burgos et al., 2008). In 2-state dimer unfolding, only a single peak is observed at all concentrations; the shape of the peak is the same across the entire protein concentration range, however, the temperature of unfolding increases as protein concentration increases. In the case of the 3-state models, a leading shoulder corresponding to the first of the two transitions can sometimes be seen. The shoulder will be more prominent if the enthalpy change associated with the first transition is large and if the first transition occurs at significantly lower temperature than the second. In 3-state unfolding with a

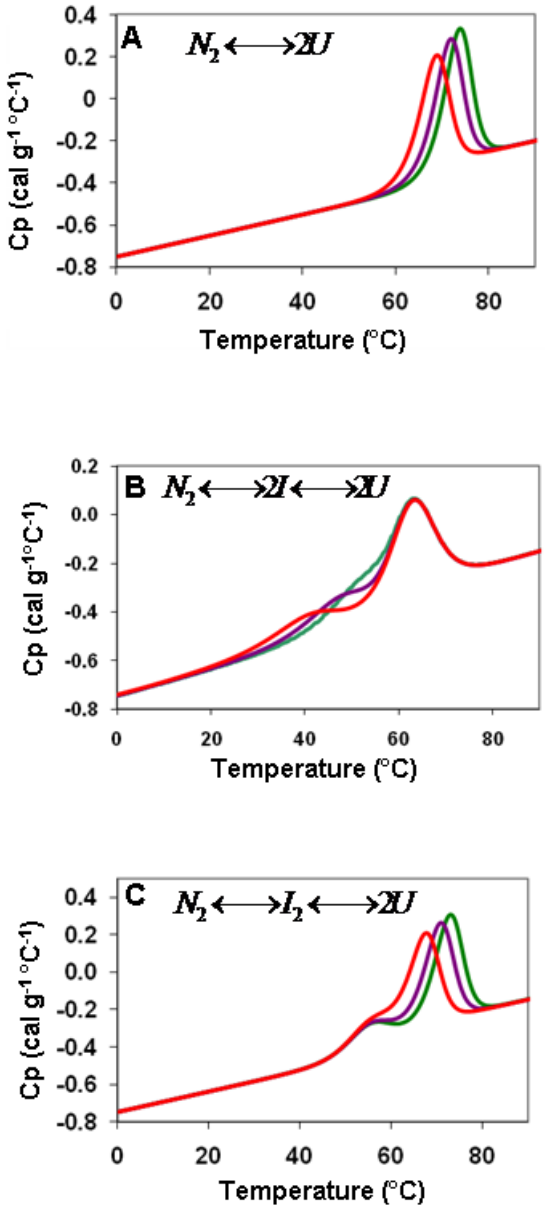

Figure 2.2. Simulations of the simplest models for the thermal unfolding of a dimer. Simulations are shown for: (A) 2-state dimer model, (B) 3-state model with a monomeric intermediate and (C) 3-state model with dimeric intermediate. All parameters in each of the simulations are identical except for the protein concentration. Three protein concentrations, 0.05 mg/mL (red), 0.4 mg/mL (violet) and 1.6 mg/mL (green), are compared. For the 2-state dimer unfolding model, there is an increase in temperature of unfolding with increasing concentration. For the 3-state model with a monomeric intermediate, the shoulder which represents the first unfolding transition (dimer dissociation) shifts to high temperature at increased protein concentration while the peak associated with monomer unfolding is relatively constant. The opposite is true for a 3-state model with a dimeric intermediate; the shoulder, corresponding to dimer intermediate formation does not shift with protein concentration, however the peak associated with dimeric intermediate unfolding shifts to higher temperatures.

monomeric intermediate, the shoulder corresponding to dimer dissociation will shift to higher temperatures as protein concentration increases while the peak associated with the second monomer unfolding transition will be concentration independent. This occurs because the first transition involves a change in molecularity, while the second is unimolecular. The opposite is true for 3-state unfolding with a dimeric intermediate, where the location of the shoulder is independent of protein concentration, while the peak associated with dimeric intermediate unfolding shifts to higher temperatures as protein concentration increases.

2.1.2 Dimer interface stability studies using isothermal titration calorimetry

In addition to DSC studies, isothermal titration calorimetry (ITC) was employed to investigate the specific effects of mutations on SOD dimerization. It has been proposed before that monomerization is required to initiate SOD aggregation (Chattopadhyay et al., 2008; Khare et al., 2004; Rakhit et al., 2007). Nevertheless, this is the first quantitative analysis of dimerization propensity of mutants that has been presented. ITC is a widely used technique, capable of simultaneously determining ΔS, ΔH and ΔG for protein binding reactions (Bjelic and Jelesarov, 2008; Leavitt and Freire, 2001; Okhrimenko and Jelesarov, 2008). In a typical ITC experiment, a ligand or a protein is titrated into a cell containing another protein. The heat absorbed or released upon binding in the sample cell upon titration is determined from the power required to maintain thermal equilibrium between sample and reference cells. Although the vast majority of ITC applications to date have involved the thermodynamic characterization of ligand/protein interactions or hetero-protein subunit binding, an additional application involves measuring subunit interactions in homo-oligomeric proteins (Bello et al., 2008; Lovatt et al., 1996; Luke et al., 2005; Velazquez-Campoy et al., 2004). Given that the individual subunits of

the homo-oligomer of interest often cannot be prepared in pure monomeric form, dissociation is measured rather than association. In these dissociation experiments, a high concentration of oligomer is titrated into buffer *via* a series of sequential small volume injections. With each injection, the total concentration of protein increases in the cell and the extent of dissociation is determined by this concentration and the dissociation constant K_d. The heat of dissociation will be typically positive and decrease with each injection as protein concentration in the cell increases (Figure 2.3). The data can be fit to an oligomer dissociation model to obtain the thermodynamic parameters governing the dissociation reaction. There are some limitations to this technique, however, in that there is the requirement that a sufficiently large change in enthalpy occur upon dissociation, which is not the case for all proteins. Additionally, if the K_d is too small (K_d<10^{-7} M), there will be little dissociation and it will not be measurable; conversely, if K_d is too high (K_d>10^{-3} M) then there will only be a small concentration of oligomer in the syringe and hence very little dissociation upon dilution (Velazquez-Campoy et al., 2004). These practical limitations can often be overcome by altering the reaction conditions such as pH or temperature in order to get the K_d into the useful range.

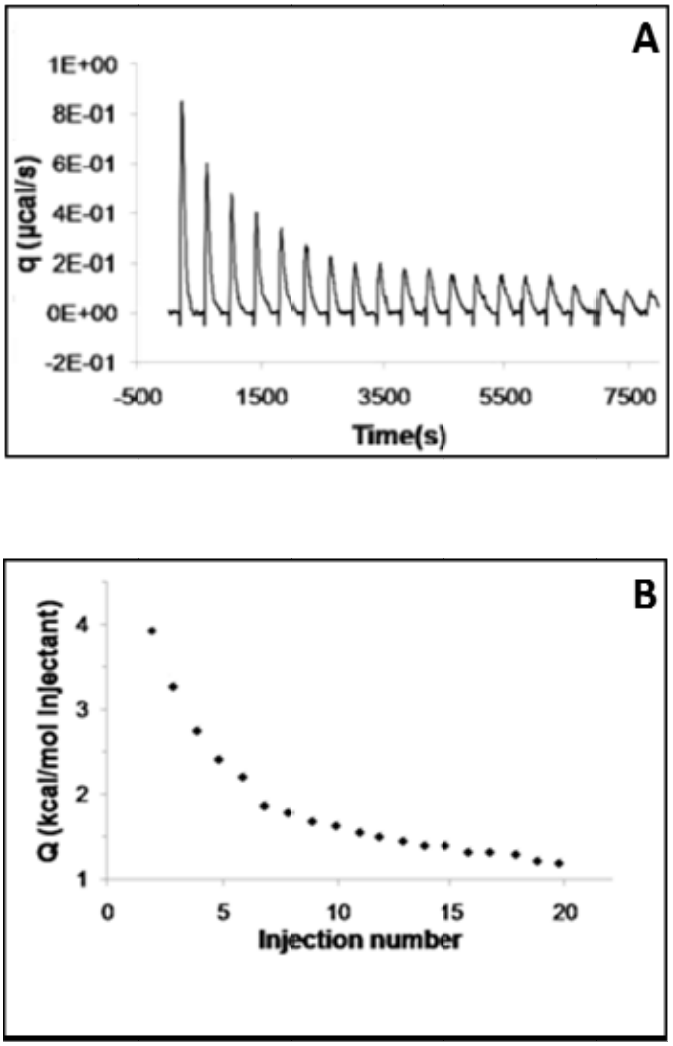

Figure 2.3. ITC dimer dissociation data for a typical globular protein. (A) Injections of protein into buffer results in endothermic dimer dissociation requiring an input of power to maintain the sample and reference cell at equal temperature. Each peak represents a single injection, with the instrument returning to baseline prior to the next injection. The power required to maintain equal temperature successively decreases with additional injections since dissociation decreases as the protein concentration increases in the cell. (B) The heat associated with each injection, *q*, obtained from integrating the raw data in (A) is plotted against injection number. This data can be fit to a dimer dissociation model to obtain the thermodynamic parameters associated with monomer formation. The figure was adapted from (Galvagnion et al., 2009).

2.2 Materials and Methods

2.2.1 Chemicals and reagents

Unless otherwise specified, all chemicals and reagents referred to in this thesis were purchased from Bioshop Canada Inc., Burlington ON.

2.2.2 Human SOD recombinant expression and purification

Human Cu,Zn SOD1 was expressed using the plasmid vector pHSOD1ASLacI^q (Getzoff et al., 1992). In addition to the human *sod1* gene containing the appropriate mutations used in this study, this plasmid (which is a pBR322 derivative) contains the tac1 promoter and lac repressor as well as the ampicillin resistance gene (*amp^r*). It should be noted that in this bacterial expression system, the SOD protein will lack the native N-terminal acetylation. This is unlikely to have a significant effect on folding owing to the unstructured nature of the SOD N-terminus and its location on the surface of the molecule away from the dimer interface. This is further supported by close similarities in the stability of the acetylated and the non-acetylated SOD (Furukawa and O'Halloran, 2005; Rodriguez et al., 2005). The human *sod1* gene is joined to a leader sequence from *Photobacterium leiognathi* that encodes a signal peptide that directs the export of the translated protein to the periplasmic space. The plasmid was transformed into the *Escherichia coli* strain QC779 (F-, Δ(argF-lac)169, LAM-, φ(sodB-kan)1(-Δ2), IN(rrnD-rrnE)1, rpsL179(strR), sodA25::MudPR13) (Carlioz and Touati, 1986). This cell strain is ideal because it is deficient in both bacterial SOD genes (iron SOD and manganese SOD) due to mutations made by Mu transposons (Natvig et al., 1987), and hence does not interfere with enzyme assays. Additionally, this bacterial strain is resistant to the antibiotics kanamycin and chloramphenicol. The *E. coli* cells were made electrocompetent as previously described (Miller and Nickoloff,

1995). Briefly, 5 mL volume of fresh overnight *E. coli* cells was inoculated into 500 mL of LB broth. The cells were grown to mid log phase at 37°C with shaking at 300 RPM before being harvested by centrifuging at 4000 x g for 15 mins. The supernatant was discarded and the cells were then resuspended in 500 mL of ice-cold 10% glycerol. Three additional successive centrifugation and resuspension steps were carried out with cells being resuspended in 250 mL, 20 mL and 2 mL of ice cold 10% glycerol respectively. These cells were transformed using an electroporation procedure as described previously (Miller, 1994). Briefly, 40 µL of the electrocompetent cells, stored in 10% glycerol was mixed with 1 µg of plasmid in a 0.1 cm electroporation cuvette (BioRad Laboratories, Inc., Hercules, CA). A high strength electric field of 1.8 kV was then applied to the mixture for 1 second to effect the transformation (BioRad *E. coli* Pulser, BioRad Laboratories, Inc.). The electroporated cells were subsequently combined with 1 mL of a mixture containing: 0.4% (w/v) glucose, 20.0 g tryptone, 5.0 g yeast extract, 0.5 g NaCl, 0.01 M $MgSO_4$ per litre and incubated at constant temperature of 37 °C for 1 hour. After incubation, the cells were concentrated by centrifugation and resuspension in 0.1 mL and plated on LB agar plates containing the antibiotics ampicillin (100 µg/mL), kanamycin (30 µg/mL) and chloramphenicol (30 µg/mL) and grown overnight at 37 °C. Individual colonies were picked from the plates and transferred to LB medium containing ampicillin (100 µg/mL), kanamycin (30 µg/mL) and chloramphenicol (30 µg/mL) and grown overnight. The overnight LB broth cultures were diluted 1 in 100 into 1 x 6 L of a standard rich 2TY mixture (yeast extract (10 g/L), bacto-tryptone (16 g/L) and NaCl (5 g/L) containing the same concentrations of antibiotics. The cells were grown in 2TY media at 37 °C with constant shaking of 200 rpm until an optical density of 0.6-0.8 absorbance units at 600 nm was reached. The protein was induced at this optical density with 0.25 mM isopropylthiogalactoside. In addition, to ensure proper metalation of the protein, $CuSO_4$ and $ZnSO_4$ were added to final concentrations of 0.5 mM and 0.1 mM, respectively. The

cells were grown for a further 8 hours at 37 °C before being harvested by centrifugation at 4500 g for 15 minutes.

Cu Zn SOD was released from the periplasm of harvested cells through osmotic shock as previously described (Koshland and Botstein, 1980). Briefly, pelleted cells from 1 L of culture were combined and resuspended in 50 mL of an ice cold solution containing 10 mM Tris-HCl buffer, pH 7.5, 20% (w/v) sucrose solution and 15 mM ethylenediaminetetraacetic acid (EDTA). The cells were then gently agitated on ice for 20 mins, after which the cells were pelleted by centrifugation at 4000 g for 30 minutes. Lysis of the periplasm was then induced through the addition of 20 mL of ice cold milli Q water (Millipore Ltd. Bedford, MA) and agitation on ice for 20 minutes. This mixture was then centrifuged at 4500 g for 40 minutes and the soluble periplasmic fraction was collected.

The SOD protein in the soluble periplasmic fraction was purified via a 2-step process. Firstly, the soluble fraction was diluted to a final total protein concentration of ~0.8 mg/mL with 20 mM Tris-HCl buffer, pH 7.5 and 1.4 mM (final concentration) of $CuSO_4$. This mixture was heated at 70 °C for 20 minutes, resulting in the precipitation of less thermostable protein contaminants which were subsequently removed by centrifugation for 10 minutes at 4000 g. $(NH_4)_2SO_4$ was then added to the supernatant to a final concentration of 3 M to increase the salt concentration prior to the final purification step which utilized hydrophobic interaction chromatography. This high salt protein solution and all buffers used in the chromatography experiment were filtered through 0.45 μm low protein binding filters followed by degassing for ~ 20 minutes before loading onto the column (Waters, Corporation, Mississauga, ON). The column used has dimensions of 2.2 cm diameter x 10 cm length and contained the Poros 20 micron HP2 (polystyrene-divinylbenzene) hydrophobic interaction chromatography resin (PerSeptive Biosystems, Foster City, CA). The protein high salt solution was loaded onto the column and

eluted over 4 column volumes using the elution buffers: 20mM Tris-HCl pH 8, 3 M $(NH_4)_2SO_4$ and 20 mM Tris-HCl pH 8 mixed in a gradient (65% to 35% 3M $(NH_4)_2SO_4$). The collected fractions were assayed for SOD activity as described previously (Marklund and Marklund, 1974). This SOD activity assay is based on the ability of the protein to inhibit the auto-oxidation of pyrogallol. Briefly, 10 μL of the collected protein fractions were mixed with 3 mL of a solution containing 1 mM diethylenetriaminepentaacetic acid, 0.1 μM bovine catalase (Sigma, St Louis, MO), and 50 mM tris-HCl, pH 8.2 in a 4 mL polystyrene cuvette. This mixture was allowed to equilibrate at 25 °C. 70μL of a solution containing 8 mM Pyrogallol (Sigma, St Louis, MO) and 10 mM HCl was then added to this equilibrated mixture and the rate of auto-oxidation of pyrogallol was quantified as the rate of change of absorbance at 420 nm. This rate was compared to a reference assay which was conducted as described above with the exception that protein collected from the purification was left out. The fractions containing the highest levels of SOD activity were collected, pooled, and subsequently dialyzed extensively against Milli-Q water to remove salt using Spectra/Por regenerated cellulose 3000 Da cutoff tubing (Spectrum Laboratories Inc., Rancho-Dominguez, CA). After dialysis was complete, the protein was concentrated using an amicon filtration system with a 3000 Da molecular weight cutoff low protein binding filter (YM3 Amicon ultrafiltration regenerated cellulose membrane; Millipore Ltd., Bedford, MA). Protein concentration was determined using the method of Lowry and/or UV absorbance at 280 nm using a monomer molar extinction coefficient of 5400 $M^{-1}cm^{-1}$ (Lowry et al., 1951; Lyons et al., 1996). Finally, protein purity, typically >90%, was assessed by Sodium Dodecyl Sulphate Polyacrylamide Gel Electrophoresis (SDS-PAGE) as previously described (Laemmli, 1970) with a 4% acrylamide stacking gel and a 12% acrylamide resolving gel.

2.2.3 Preparation of Apo SOD

Demetallated or apo SOD was prepared by dialysing the purified metallated protein against metal chelator (McCord and Fridovich, 1969). Briefly, 100 mL of metallated or holo SOD at a protein concentration of 0.5-1 mg/mL was placed in a 3000 Da cutoff regenerated cellulose dialysis tubing (Spectrum Laboratories, Inc.) and dialyzed against 4 L of 50 mM sodium acetate, 100 mM EDTA, pH 3.8 at 4°C with 3 exchanges of buffer over a 24 hour period. This was followed by further dialysis against 4 L of a solution containing 50 mM sodium acetate, 100 mM NaCl, pH 3.8 with 3 exchanges over 24 hours. Finally, salt was removed by dialyzing the protein against 4 L of MQ water (Millipore Ltd. Bedford, MA) at 4°C also with 3 exchanges over 24 hours. At the end of dialysis the apo protein was then concentrated using the amicon concentration system with a YM3, low protein binding regenerated cellulose 3000 Da cutoff filter (Millipore Ltd., Bedford, MA). Protein concentration was re-determined using the method of Lowry and by absorbance at 280 nm using an extinction coefficient of 5400 $M^{-1}cm^{-1}$ (Lowry et al., 1951; Lyons et al., 1996). In order to verify that the metals were successfully removed differential scanning calorimetry (DSC) thermograms using the Microcal LLP VP (Microcal Inc, Northampton, MA, USA) were collected on ~ 0.5 mg/mL apo protein samples at pH 7.8 (20mM, HEPES) to verify the presence of only one species with a melting temperature characteristic of apo SOD. Additionally, for some samples metal content was assessed by inductively coupled plasma atomic emission spectroscopy (In-house analytical service in the Department of Earth Science, University of Waterloo, ON).

2.2.4 Differential scanning calorimetry

Excess specific heat as a function of temperature for apo SOD thermal unfolding was measured using a Microcal LLP VP differential scanning calorimetry machine (Microcal Inc, Northampton, MA, USA). Protein concentrations ranged from ~0.05 to ~2 mg/mL and samples were buffered with 20 mM HEPES, pH 7.8. The scan rate employed in all experiments was 1°C per minute; it has been found previously that no scan rate dependence is observed for apo SOD when scanning between 0.25 and 1.5 °C per minute (Stathopulos et al., 2006). Buffer *versus* buffer scans were collected prior to the acquisition of protein *versus* buffer scans. The buffer *versus* buffer thermograms were subtracted from protein *versus* buffer thermograms. Data were then normalized to units of cal g^{-1} °C before fitting to 2-state and 3-state unfolding models, described below.

2.2.4.1 Analysis of DSC thermal unfolding data

Using the formalism of Sturtevant (Sturtevant, 1987; Tamura et al., 1995; Tamura and Sturtevant, 1995), DSC data were fit to 2-state models describing monomer and/or dimer unfolding as well as more complex 3-state dimer unfolding models involving the formation of a monomeric or dimeric intermediate, as outlined below.

2.2.4.1.1 2-State unfolding

For a 2-state unfolding process involving either monomer or dimer, equilibria can be expressed respectively, as:

$$\underset{P_{mon}(1-\alpha)}{N} \xleftrightarrow{K\,(T)} \underset{P_{mon}(\alpha)}{U} \tag{2.1}$$

and,

$$\underset{P_{\dim}(1-\alpha)}{N_2} \xleftrightarrow{K(T)} \underset{2P_{\dim}(\alpha)}{2U} \tag{2.2}$$

where P_{mon} and P_{dim} are the total concentrations of monomer and dimer, respectively, in mol/L and α is the extent of the reaction and $K(T)$ is the equilibrium constant at any temperature T. The enthalpy of the unfolding for any 2-state process is given by:

$$H_{tot} = H_n + \alpha\Delta H \tag{2.3}$$

where H_n is the enthalpy of the natively folded protein and is the reference state and ΔH is the change in enthalpy associated with the unfolding reaction. The calorimeter measures the excess total specific heat of the system ($C_{p,tot}$) which is the temperature derivative of the total molar enthalpy (H_{tot}):

$$C_{p\,tot} = \frac{dH_{tot}}{dT} = C_{p_{(N)}} + \alpha\Delta C_{p_{unf}} + \Delta H\frac{d\alpha}{dT} \tag{2.4}$$

$$\Delta C_{p_{unf}} = C_{p(U)} - C_{p(N)} \tag{2.5}$$

$$\therefore C_{p_{tot}} = C_{p(N)} + \alpha\left(C_{p(U)} - C_{p(N)}\right) + \Delta H\frac{d\alpha}{dT} \tag{2.6}$$

$$= C_{p(N)} + \alpha C_{p(U)} - \alpha C_{p(N)} + \Delta H\frac{d\alpha}{dT}$$

$$= C_{p(N)}(1-\alpha) + \alpha C_{p(U)} + \Delta H\frac{d\alpha}{dT}$$

$C_{p(N)}$ and $C_{p(U)}$ can be defined as the native and unfolding baselines, respectively:

$$C_{p(N)} = A + BT \tag{2.7}$$

$$C_{p(U)} = C + DT \tag{2.8}$$

where A and C are the Y-intercepts of the folded and unfolded baselines and B and D are their slopes and T is the temperature in Kelvin. Substituting Equations 2.7 and 2.8 into Equation 2.6 we obtain:

$$C_{p,tot} = (A + BT)(1 - \alpha) + (C + DT)\alpha + \Delta H \frac{d\alpha}{dT} \tag{2.9}$$

In the fitting procedure, α must be calculated at different temperatures and an expression for $\frac{d\alpha}{dT}$ needs to be evaluated. α can be defined from $K(T)$ for a monomer unfolding reaction from:

$$K(T) = \frac{\alpha}{(1 - \alpha)} \tag{2.10}$$

Equation 2.10 can be rearranged as:

$$\alpha = \frac{K(T)}{1 + K(T)} \tag{2.11}$$

Similarly for a dimer unfolding reaction:

$$K(T) = \frac{4P_{\text{dim}}\alpha^2}{1 - \alpha} \tag{2.12}$$

and

$$\alpha = \frac{-K(T) + \sqrt{K(T)(K(T) + 4P_{\text{dim}})}}{8P_{\text{dim}}} \tag{2.13}$$

In determining equilibrium constants (and hence α) at any given temperature, $K(T)$ is initially set to its value at the temperature of half completion ($T_{0.5}$), which can be defined by setting α=0.5 in Equations 2.11 and 2.12 such that for monomer unfolding, $K(T_{0.5}) = 1$, and for dimer unfolding, $K(T_{0.5}) = 2P_{dim}$. In this approach, data fitting returns parameters calculated at the $T_{0.5}$. In order to calculate $K(T)$ at different temperatures, we utilize the van't Hoff relationship:

$$\frac{d \ln K(T)}{dT} = \frac{\Delta H_{vH}(T)}{RT^2} \tag{2.14}$$

Knowing both $T_{0.5}$ from fitting and $K(T_{0.5})$ by definition, $K(T)$ can be found at any temperature T from integrating Equation 2.14:

$$\int_{T_{0.5}}^{T} \frac{d \ln K(T)}{dT} = \frac{1}{R} \int_{T_{0.5}}^{T} \frac{\Delta H_{vH}(T)}{T^2} dT \tag{2.15}$$

where ΔH_{vH} is the van't Hoff enthalpy and R is the universal gas constant. Fitted data are normalized per gram of protein. Hence, ΔH_{vH} can be defined in terms of specific change in enthalpy, Δh_{cal} (cal/g) as:

$$\Delta H_{vH} = \beta^* \Delta h_{cal} = \Delta H_{cal} \tag{2.16}$$

where ΔH_{cal} is the calorimetric enthalpy. If β is left as a floating parameter in fitting it converges to the apparent molecular weight of the cooperative unfolding unit such that:

$$\beta = \frac{\Delta H_{vH}}{\Delta H_{cal}} \bullet M_w \tag{2.17}$$

where M_w is the true molecular weight of the cooperative unfolding unit.

Substituting Eq. 2.16 into 2.15, one obtains:

$$\int_{T_{0.5}}^{T} \frac{d \ln K(T)}{dT} = \frac{\beta}{R} \int_{T_{0.5}}^{T} \frac{\Delta h_{cal}(T)}{T^2} dT \tag{2.18}$$

By definition:

$$\Delta h_{cal}(T) = \int_{T_{0.5}}^{T} \Delta C_{p\,unf} dT \tag{2.19}$$

Substituting Equations 2.7 and 2.8 into Equation 2.5 and integrating from T to $T_{0.5}$ gives:

$$\int_{T_{0.5}}^{T} \Delta C_{p\,unf} dT = \Delta h_{cal}\left(T_{0.5}\right) + (C - A)(T - T_{0.5}) + \frac{1}{2}(D - B)\left(T^2 - {T_{0.5}}^2\right) \tag{2.20}$$

Equation 2.20 can be substituted into Equation 2.19 and 2.18 to give:

$$\int_{T0.5}^{T} \frac{d\ln K(T)}{dT} = \ln\frac{K(T)}{K(T_{0.5})} = \frac{\beta}{R}\int_{T0.5}^{T} \frac{\Delta h_{cal}(T_{0.5}) + (C-A)(T-T_{0.5}) + \frac{1}{2}(D-B)(T^2 - {T_{0.5}}^2)}{T^2}$$

(2.21)

Integrating Eq. 2.21 and rearranging gives:

$$\frac{R}{\beta}\frac{K(T)}{K(T_{0.5})} = \Delta h_{cal}(T_{0.5})\left(\frac{1}{T} - \frac{1}{T_{0.5}}\right) - (C-A)T_{0.5} + (C-A)\ln\frac{T}{T_{0.5}} - \frac{1}{2}(D-B){T_{0.5}}^2 + \frac{1}{2}(D-B)(T-T_{0.5})$$

$$\therefore K(T) = \frac{\beta}{R}\left(\Delta h_{cal}(T_{0.5})\left(\frac{1}{T} - \frac{1}{T_{0.5}}\right) - (C-A)T_{0.5} + (C-A)\ln\frac{T}{T_{0.5}} - \frac{1}{2}(D-B){T_{0.5}}^2 + \frac{1}{2}(D-B)(T-T_{0.5})\right)K(T_{0.5})$$

(2.22)

$\frac{d\alpha}{dT}$ can be expressed with respect to α and $\Delta H_{vH}(T)$ for 2-state monomer and dimer unfolding by differentiation Equations 2.10 and 2.12 respectively, with respect to T and substituting into the van't Hoff equation (Equation 2.14) as follows.

For monomer unfolding:

$$\frac{d\ln K(T)}{dT} = \frac{\Delta H_{vH}(T)}{RT} = \frac{\beta\Delta h_{cal}(T)}{RT^2} = \frac{1}{\alpha}\frac{d\alpha}{dT} + \frac{1}{1-\alpha}\frac{d\alpha}{dT} \tag{2.23}$$

Rearranging gives:

$$\frac{d\alpha}{dT} = \frac{\beta\Delta h_{cal}(T)\alpha(1-\alpha)}{RT^2} \tag{2.24}$$

For dimer unfolding:

$$\frac{d\ln K_{eq}}{dT} = \frac{\Delta \mathrm{H}_{VH}(T)}{RT} = \frac{\beta\Delta h(T)}{RT^2} = \frac{2}{\alpha}\frac{d\alpha}{dT} + \frac{1}{1-\alpha}\frac{d\alpha}{dT} \tag{2.25}$$

and rearranging gives:

$$\frac{d\alpha}{dT} = \frac{\beta\Delta h(T)}{RT^2}\frac{\alpha(1-fu)}{2-\alpha} \tag{2.26}$$

Substituting Equations 2.24 and 2.26 into Equation 2.6 one obtains the final fitting equations for the 2-state monomer unfolding model:

$$C_p = (A + BT)(1-\alpha) + (C + DT)\alpha + \frac{\beta \Delta h_{cal}{}^2 (T_{0.5})\alpha(1-\alpha)}{RT^2} \quad (2.27)$$

and,

2-state dimer unfolding model:

$$C_p = (A + BT)(1-\alpha) + (C + DT)\alpha + \frac{\beta \Delta h_{cal}{}^2 (T_{0.5})}{RT^2} \frac{\alpha(1-\alpha)}{2-\alpha} \quad (2.28)$$

Datasets at each protein concentration were fit individually with *A, B, C, D,* β, $T_{0.5}$, $\Delta h_{cal}(T_{0.5})$ as floating parameters. Fitting was performed using the Microcal Origin version 5.0 (Microcal Inc., Northampton, MA, USA).

2.2.4.1.2 3-State dimer thermal unfolding with a dimeric or monomeric intermediate

Due to the increased complexity and the additional parameters inherent in fitting to a 3-state model, fitting of individual datasets can lead to great inaccuracies. Hence, in contrast to the 2-state fits, multiple datasets obtained for different protein concentrations were only fit globally to the 3-state models. In the process of global fitting, data are fit simultaneously for all protein concentrations with some of the more ill defined parameters shared across all datasets, thereby increasing the accuracy of their determination. The formulation for data fitting to 3-state dimer unfolding models involving a monomeric or dimeric intermediate is similar to that of a 2-state unfolding model, except that 2 transitions need to be considered. These transitions are defined by $K_1(T)$ and $K_2(T)$, which are the equilibrium constants describing the first and second transitions, respectively. The following equations follow the logic described above for the 2-state transitions, incorporating the two equilibria.

For 3-state dimer unfolding with a monomer intermediate the following scheme and equations apply:

$$\begin{array}{ccccc} N_2 & \xleftarrow{K_1(T)} & 2M & \xleftarrow{K_2(T)} & 2U \\ P_{\dim}(1-\alpha) & & 2P_{\dim}(1-\alpha_2) & & 2P_{\dim}(\alpha_1\alpha_2) \end{array} \tag{2.29}$$

$$K_1(T) = \frac{[M]^2}{[N_2]} = 4P_{\dim}\frac{{\alpha_1}^2(1-\alpha_2)^2}{1-\alpha_1} \tag{2.30}$$

$$K_2(T) = \frac{[U]^2}{[M]^2} = \frac{{\alpha_2}^2}{(1-\alpha_2)^2} \tag{2.31}$$

$$\alpha_1 = \frac{2}{1+\sqrt{1+\dfrac{16P_{\dim}}{K_1(T)\left(1+\sqrt{K_2}(T)\right)^2}}} \tag{2.32}$$

$$\alpha_2 = \frac{\sqrt{K_2(T)}}{1+\sqrt{K_2(T)}} \tag{2.33}$$

and for 3-state dimer unfolding with dimeric intermediate:

$$\begin{array}{ccccc} N_2 & \xleftarrow{K_1(T)} & I_2 & \xleftarrow{K_2(T)} & 2D \\ P_{\dim}(1-\alpha_1) & & P_{\dim\,\alpha_1}(1-\alpha_2) & & 2P_{\dim}(\alpha_1\alpha_2) \end{array} \tag{2.34}$$

$$K_1(T) = \frac{[I_2]}{[N_2]} = \frac{\alpha_1(1-\alpha_2)}{(1-\alpha_1)} \tag{2.35}$$

$$K_2(T) = \frac{[D]^2}{[I_2]} = \frac{4P_{\dim}\alpha_1{\alpha_2}^2}{1-\alpha_2} \tag{2.36}$$

$$\alpha_1 = \frac{K_1(T)}{1+K_1(T)-\alpha_2} \tag{2.37}$$

$$\alpha_2 = \frac{2K_2(T)(1+K_1(T))}{K_2(T)(2+K_1(T)) + \sqrt{K_2(T)^2(2+K_1(T))^2 + 4K_2(T)(4P_{\text{dim}}K_1(T) - K_2(T))(1+K_1(T))}}$$

(2.38)

Note that Equation 2.31 is cast to give thermodynamic values in dimer units. Equilibrium constants at half completion for each transition can be found by substituting α_1=0.5 in Equations 2.30 and 2.35 and α_2=0.5 into Equations 2.31 and 2.36 such that for a 3-state model with monomeric intermediate one obtains:

$$K_1(T_{1,0.5}) = 2P_{\text{dim}}\left(\frac{1}{1+\sqrt{K_2(T_{1,0.5})}}\right)^2 \tag{2.39}$$

and

$$K_2(T_{2,\,0.5}) = 1 \tag{2.40}$$

and for a 3-state model with dimeric intermediate,

$$K_1(T_{1,0.5}) = 1 + \frac{2}{1+\sqrt{1+\frac{8P_{\text{dim}}}{K_2(T_{2,0.5})}}} \tag{2.41}$$

and

$$K_2(T_{2,0.5}) = \frac{4P_{\text{dim}}K_1(T_{2,0.5})}{1+2K_1(T_{2,0.5})} \tag{2.42}$$

where $T_{1,\,0.5}$ is the temperature of half unfolding for the first transition and $T_{2,\,0.5}$ is the temperature of half unfolding for the second transition. Similar to Equation 2.3, for both 3-state models:

$$H_{tot} = H_n + \alpha_1\Delta H_1 + 2\alpha_1\alpha_2\Delta H_2 \text{ x } 0.5 \tag{2.43}$$

0.5 is a factor added to normalize to per mole of dimer. Analogous to the derivation of Equation 2.6 from 2.3, an Equation for $C_{p,\,tot}$ here can be obtained from the derivative of Equation 2.43:

$$C_{p\,tot} = \frac{dH}{dT} = \Delta h_{cal1}\frac{d\alpha_1}{dT} + \Delta h_{cal2}\left(\alpha_2\frac{d\alpha_1}{dT} + \alpha_1\frac{d\alpha_2}{dT}\right) + (1-\alpha_1)C_{pN} + \alpha_1(1-\alpha_2)C_{pI} + \alpha_1\alpha_2 C_{pU} \tag{2.44}$$

Similarly to what was described in Section 2.2.3.1.1 for 2-state fitting, $K_1(T)$ and $K_2(T)$ (and hence α_1 and α_2) can be determined using the van't Hoff equation (Equation 2.14). In the process of determining $K(T)$ at any given temperature, initial values of $K_1(T)$ and $K_2(T)$ were both set to 1. This is in contrast to the 2-state fits were $K(T)$ was initially set to its value of at half completion. This change is necessary for 2 reasons. Firstly, as can be seen in Equations 2.39, 2.41 and 2.42, the equilibrium constant at half completion is not as conveniently defined as it is for the 2-state models where it is 1 for the 2-state monomer unfolding model and $2P_{dim}$ for the dimer unfolding model. Secondly, it is necessary to select initial values for $K_1(T)$ and $K_2(T)$ that are independent of protein concentration in order to be able to share parameters across the entire protein concentration range in global fitting. It should be noted, however, that in the case of the 3-state dimer unfolding with monomer intermediate, $K_2(T)$ is in fact 1 at half completion (Equation 2.40). Given that our initial $K(T)$ values are set to 1, the van't Hoff relationship can be integrated, similarly to Equation 2.18 to determine $K_1(T)$ and $K_2(T)$ at any temperature:

$$\int_{T_1'}^{T}\frac{d\ln K_1(T)}{dT} = \frac{\beta_1}{R}\int_{T_1'}^{T}\frac{\Delta h_{cal1}(T)}{T^2}dT \tag{2.45}$$

and

$$\int_{T_2'}^{T}\frac{d\ln K_2(T)}{dT} = \frac{\beta_2}{R}\int_{T_2'}^{T}\frac{\Delta h_{cal2}(T)}{T^2}dT \tag{2.46}$$

In Equations 2.45 and 2.46, T_1' is the temperature at which $K_1(T) = 1$ and T_2' is the temperature at which $K_2(T) = 1$. We can describe the van't Hoff expression similarly to Equation 2.22 if we first define the native, intermediate and unfolding baselines respectively as $C_{p(N)}$, $C_{p(I)}$ and $C_{p(U)}$ such that:

$$C_{p(N)} = A + BT \tag{2.47}$$

$$C_{p(I)} = C + DT \tag{2.48}$$

$$C_{p(U)} = E + FT \tag{2.49}$$

where A, C, E are the intercepts of the native, intermediate and unfolded baselines respectively and B, D, F are their slopes. Hence, considering that our fitted parameters are described at $K(T)$=1, we can solve for both $K_1(T)$ and $K_2(T)$ at any temperature from:

$$K_1(T) = \begin{pmatrix} \Delta h_{cal1}(T_1')\left(\frac{1}{T} - \frac{1}{T_1'}\right) - (C-A)T_1' + (C-A)\ln\frac{T}{T_1'} \\ -\tfrac{1}{2}(D-B)T_1'^2 + \tfrac{1}{2}(D-B)(T-T_1') \end{pmatrix} \frac{\beta_1}{R} \tag{2.50}$$

and

$$K_2(T) = \begin{pmatrix} \Delta h_{cal2}(T_2')\left(\frac{1}{T} - \frac{1}{T_2'}\right) - (E-C)T_2' + (E-C)\ln\frac{T}{T_2'} \\ -\tfrac{1}{2}(F-D)T_2'^2 + \tfrac{1}{2}(F-D)(T-T_2') \end{pmatrix} \frac{\beta_2}{R} \tag{2.51}$$

Analogous to Equations 2.24 and 2.26, $\frac{d\alpha_1}{dT}$ and $\frac{d\alpha_2}{dT}$ are determined for 3-state models by differentiating Equations 2.30,2.31, 2.35 and 2.36 with respect to T and substituting into the van't Hoff equation (Equation 2.14). Hence, for 3-state dimer unfolding with monomeric intermediate:

$$\frac{d\alpha_1}{dT} = \left(\frac{\beta_1 \Delta h_1}{RT^2} + \frac{\alpha_2 \beta_2 \Delta h_1}{RT}\right)\left(\frac{\alpha_1(1-\alpha_1)}{2-\alpha_1}\right) \tag{2.52}$$

and,

$$\frac{d\alpha_2}{dT} = \frac{\beta_2 \Delta h_2}{2RT^2}\alpha_2(1-\alpha_1) \tag{2.53}$$

while for 3-state dimer unfolding with dimeric intermediate:

$$\frac{d\alpha_1}{dT} = \left(\frac{\beta_1 \Delta h_{cal1}(T)}{RT^2}\left(\frac{2-\alpha_2}{\alpha_2}\right) + \frac{\beta_2 \Delta h_{cal2}(T)}{RT^2}\right)\left(\frac{\alpha_1\alpha_2(1-\alpha_1)}{2-\alpha_1\alpha_2}\right) \tag{2.54}$$

$$\frac{d\alpha_2}{dT} = \left(\frac{\beta_2 \Delta h_{cal2}(T)}{RT^2} - \frac{1}{\alpha_1} \frac{d\alpha_1}{dT} \right) \left(\frac{\alpha_2 (1-\alpha_2)}{2-\alpha_2} \right) \tag{2.55}$$

Substituting Equations 2.16, 2.45-2.49 and 2.52-2.55 into Equation 2.43 yields the Equations used for fitting to the two 3 state models:

for 3-state dimer unfolding with monomeric intermediate,

$$C_{p\,tot} = \left(\frac{\beta_1 \Delta h_{cal1}(T)^2}{RT^2} + \frac{\alpha_2 \beta_2 \Delta h_{cal1}(T)^2}{RT} \right) \frac{\alpha_1 (1-\alpha_1)}{2-\alpha_1} +$$
$$\left(\left(\frac{\beta_1 \Delta h_{cal1}(T)}{RT^2} + \frac{\alpha_2 \beta_2 \Delta h_{cal1}(T)}{RT} \right) \frac{\alpha_1 \alpha_2 (1-\alpha_1)}{2-\alpha_1} + \frac{\beta_2 \Delta h_{cal2}(T)}{2RT^2} \alpha_2 \alpha_1 (1-\alpha_1) \right) \Delta h_{cal2}(T) +$$
$$(1-\alpha_1)(A+BT) + \alpha_1 (1-\alpha_2)(C+DT) + \alpha_1 \alpha_2 (E+FT) \tag{2.56}$$

and

for 3-state dimer with dimeric intermediate,

$$C_{p\,tot} = \Delta h_1 \left(\frac{\beta_1 \Delta h_{cal1}(T)}{RT^2} \left(\frac{2-\alpha_2}{\alpha_2} \right) + \frac{\beta_2 \Delta h_{cal2}(T)}{RT^2} \right) \left(\frac{\alpha_1 \alpha_2 (1-\alpha_1)}{2-\alpha_1 \alpha_2} \right)$$
$$+ \Delta h_2 \left(\begin{array}{l} \alpha_2 \left(\dfrac{\beta_1 \Delta h_{cal1}(T)}{RT^2} \left(\dfrac{2-\alpha_2}{\alpha_2} \right) + \dfrac{\beta_2 \Delta h_{cal2}(T)}{RT^2} \right) \left(\dfrac{\alpha_1 \alpha_2 (1-\alpha_1)}{2-\alpha_1 \alpha_2} \right) \\ + \alpha_1 \left(\dfrac{\beta_2 \Delta h_{cal2}(T)}{RT^2} - \dfrac{1}{\alpha_1} \dfrac{d\alpha_1}{dT} \right) \left(\dfrac{\alpha_2 (1-\alpha_2)}{2-\alpha_2} \right) \end{array} \right) \tag{2.57}$$
$$+ (1-\alpha_1)(A+BT) + \alpha_1 (1-\alpha_2)(C+DT) + \alpha_1 \alpha_2 (E+FT)$$

It is usually impossible to determine the slope and intercept of the intermediate; additionally, the unfolded baseline can be ill-defined due to exothermic aggregation at high temperatures. Hence Equations 2.56 and 2.57 were simplified slightly by setting the slope of both the intermediate and unfolded baselines as equal to the native baseline (i.e $B=D=F$). This simplification is reasonable

because it is based on the assumption that ΔC_p of unfolding is independent of temperature which has been found to be generally true for proteins over small temperature ranges (Prabhu and Sharp, 2005). In using this approach the intercepts of both the intermediate and unfolded baselines can be defined relative to the native baseline using temperature interpendent ΔC_{p1} and ΔC_{p2}:

$$C=\Delta C_{p1}+A \tag{2.58}$$

and

$$E=\Delta C_{p1}+\Delta C_{p2}+A=C+\Delta C_{p2} \tag{2.59}$$

Hence, Equations 2.56 and 2.57 can be re-written as:

$$\begin{aligned} C_{p\,tot} &= \left(\frac{\beta_1 \Delta h_{cal1}(T)^2}{RT^2}+\frac{\alpha_2\beta_2\Delta h_{cal1}(T)^2}{RT}\right)\frac{\alpha_1(1-\alpha_1)}{2-\alpha_1}+ \\ &\left(\left(\frac{\beta_1\Delta h_{cal1}(T)}{RT^2}+\frac{\alpha_2\beta_2\Delta h_{cal1}(T)}{RT}\right)\frac{\alpha_1\alpha_2(1-\alpha_1)}{2-\alpha_1}+\frac{\beta_2\Delta h_{cal2}(T)}{2RT^2}\alpha_2\alpha_1(1-\alpha_1)\right)\Delta h_{cal2}(T) \\ &+A+BT+\alpha_1\Delta C_{p1}\ +\alpha_1\alpha_2\Delta C_{p2} \end{aligned} \tag{2.60}$$

and,

$$\begin{aligned} C_{p\,tot} &= \Delta h_1\left(\frac{\beta_1\Delta h_{cal1}(T)}{RT^2}\left(\frac{2-\alpha_2}{\alpha_2}\right)+\frac{\beta_2\Delta h_{cal2}(T)}{RT^2}\right)\left(\frac{\alpha_1\alpha_2(1-\alpha_1)}{2-\alpha_1\alpha_2}\right) \\ &+\Delta h_2\left(\begin{array}{l}\alpha_2\left(\dfrac{\beta_1\Delta h_{cal1}(T)}{RT^2}\left(\dfrac{2-\alpha_2}{\alpha_2}\right)+\dfrac{\beta_2\Delta h_{cal2}(T)}{RT^2}\right)\left(\dfrac{\alpha_1\alpha_2(1-\alpha_1)}{2-\alpha_1\alpha_2}\right) \\ +\alpha_1\left(\dfrac{\beta_2\Delta h_{cal2}(T)}{RT^2}-\dfrac{1}{\alpha_1}\dfrac{d\alpha_1}{dT}\right)\left(\dfrac{\alpha_2(1-\alpha_2)}{2-\alpha_2}\right)\end{array}\right) \\ &+A+BT+\alpha_1\Delta C_{p1}+\alpha_1\alpha_2\Delta C_{p2} \end{aligned} \tag{2.61}$$

For fitting to 3-state models with monomeric and dimeric intermediate, β_1, β_2, ΔC_{p1} and ΔC_{p2}, T_1', T_2', along with the corresponding enthalpies at these temperatures $\Delta h_{cal1}(T_1')$ *and*

$\Delta h_{cal2}(T_2')$, respectively, were set as globally shared parameters between all datasets. β_1, β_2, ΔC_{p1} and ΔC_{p2} were generally ill-defined by the data and hence were fixed during fitting. Both β_1 and β_2 were fixed to 31,500 which is the molecular weight of the SOD dimer. In 3-state fitting with a monomeric intermediate, ΔC_{p1}, which is related to the change in solvent accessible surface area upon dimer dissociation of apo SOD (Myers et al., 1995), was set to 1.6 kcal mol^{-1} $°C^{-1}$. This value was estimated from a Kirchoff plot derived from ITC experiments on apo A4V SOD where enthalpy of dimer dissociation was determined as a function of temperature (see Section 2.3.4.1). Since $\Delta C_{p1}+\Delta C_{p2} = \Delta C_{p\ unf}$ (total ΔC_p upon unfolding of apo SOD from fully folded dimer to unfolded monomers), the value of ΔC_{p2} was set by subtracting ΔC_{p1} from a $\Delta C_{p\ unf}$ of 3.3 kcal mol^{-1} $°C^{-1}$ which gives a value of 1.7 kcal $mol^{-1}°C^{-1}$ (note that in this case ΔC_{p2} is expressed as per mole dimer). $\Delta C_{p\ unf}$ of 3.3 kcal $mol^{-1}°C^{-1}$ was previously determined by others in this laboratory for thermal unfolding of apo SOD (Stathopulos et al., 2006). This value is an average of $\Delta C_{p\ unf}$ derived from several approaches: from a Kirchoff plot (ΔH vs $T_{0.5}$, where ΔC_p = slope of the plot), the mean ΔC_p from fits of several apo SOD datasets, and theoretical ΔC_p calculated from the 3-D structure of apo SOD and the primary sequence.

For 3-state fitting with a dimer intermediate, ΔC_{p1} was initially set to 0 and ΔC_{p2} to 3.3 kcal $mol^{-1}°C^{-1}$. The best values of ΔC_{p1} and ΔC_{p2} were determined by systematically changing the fixed values, increasing ΔC_{p1} by 10% of the $\Delta C_{p\ unf}$ of 3.3 kcal $mol^{-1}K^{-1}$ while simultaneously decreasing ΔC_{p2} by the same amount and selecting the fit with lowest chi^2. All global fitting was performed using Matlab version 7.8 (The MathWorks Inc., Natick, MA, USA).

2.2.4.1.3 Calculation of thermodynamic parameters from DSC fitting

The thermodynamic quantities ΔG, ΔH and ΔS were calculated from the fitted parameters obtained from fitting the apo SOD mutants to the 2-state dimer unfolding model as well as the 3-state model with monomeric intermediate. Given that fitting of DSC data returned values only at a single temperature for each transition, thermodynamic values at other temperatures have to be extrapolated. These thermodynamic values were calculated for each unfolding transition using the following Equations:

$$\Delta G(T) = \Delta \mathrm{H}(T) - T\Delta S(T) \tag{2.62}$$

where $\Delta H(T) = \Delta H(T_{ref}) + \Delta C_p (T - T_{ref})$ (2.63)

$$\Delta S(T) = \Delta S(T_{ref}) + \Delta C_p \ln \frac{T}{T_{ref}} \tag{2.64}$$

and $\Delta S(T_{ref}) = \dfrac{\Delta \mathrm{H}(T_{ref}) - \Delta G(T_{ref})}{T_{ref}}$ (2.65)

In Equations 2.62-2.65, T_{ref} is the temperature at which thermodynamic paramters are known and $\Delta H(T_{ref})$, $\Delta \mathrm{S}T_{ref}$) and $\Delta G(T_{ref})$ are the corresponding enthalpy, entropy and free energy at this temperature respectively. $\Delta G(T_{ref})$ can be calculated from :

$$\Delta G(T_{ref}) = -RT_{ref} \ln K(T_{ref}) \tag{2.66}$$

For both transitions in 3-state dimer unfolding with monomeric intermediate, $K(T_{ref}) = 1$, while in 2-state dimer unfolding $K(T_{ref}) = 2P_{dim}$. Due to the inherent large uncertainties in determining ΔC_p from the differences in baselines, $\Delta C_{p\ unf}$ for 2-state dimer unfolding was taken to be 3.3 kcal $\mathrm{mol}^{-1} {}^{\circ}\mathrm{C}^{-1}$. This value for apo SOD unfolding was obtained previously (Stathopulos

et al., 2006) as described in the preceding section. For 3-state dimer unfolding with monomeric intermediate, ΔC_p for each step was set to the same fixed values used in fitting; i.e., 1.6 and 1.7 kcal mol^{-1} $°C^{-1}$ for the two transitions respectively.

2.2.5 Isothermal titration calorimetry

ITC experiments were carried out using a Microcal Isothermal Titration Calorimetry 200 instrument (Microcal Inc, Northampton, MA, USA). Initially, high concentrations (0.55-1.3 mM total monomer) of apo SOD buffered in 20 mM HEPES, pH 7.8, were loaded into the syringe. This high concentration protein solution was diluted into the 205.3 μL ITC reaction cell, which at the start of the experiment contained 20 mM HEPES, pH 7.8. Successive small injections of between 0.2 and 0.7 μL were performed, resulting in a gradual increase in the protein concentration in the ITC reaction cell. Typically, a total of 15-50 total injections were carried out, with time intervals between injections greater than 180 seconds and continuous stirring of 500-750 rpm. The power required to maintain a constant temperature between sample and reference cell upon each injection was recorded by the instrument and the heat associated with each injection was found by manually integrating this power with respect to time. Blank experiments were performed in which 20 mM HEPES buffer, pH 7.8, in the syringe was injected into the sample cell containing the same buffer under identical conditions to assess mechanical heat effects unrelated to protein dilution. These heat values from the blank experiment were subtracted from the heats of the protein dilution experiments before data fitting. The data were fit according to a dimer dissociation model as outlined in section 2.2.4.1 using previously derived formalism (Burrows et al., 1994; Velazquez-Campoy et al., 2004).

2.2.5.1 Isothermal titration calorimetry data analysis

Dilutions of protein into the ITC cell result in the dissociation of dimer (N_2), producing monomer (M), as governed by the dissociation constant, K_d

$$N_2 \xleftrightarrow{K_d} 2M \tag{2.67}$$

$$\text{where } K_d = \frac{[M]^2}{[N_2]} \tag{2.68}$$

The actual concentration of monomer formed after injection i can be analytically solved using the following Equation:

$$[M]_i = \frac{K_d}{4}\left(\sqrt{1+\frac{8[M]_{T,i}}{K_d}}-1\right) \tag{2.69}$$

where $[M]_{T,i}$ is the total protein concentration in the cell in mol/L after each injection (expressed as total concentration of monomer subunits contained in both monomer and dimer), which is defined mathematically as:

$$[M]_{T,i} = [M]_0\left[1-\left(1-\frac{v}{V}\right)^i\right] \tag{2.70}$$

where $[M]_o$ is the concentration in the syringe expressed as total concentration of monomer, V is the volume of the ITC reaction cell, v is the injection volume and the term $1-\frac{v}{V}$ is used to correct for dilution of ITC cell contents with each injection. The heat evolved upon dimer dissociation after each injection (q_i) is proportional to the increase in monomer concentration after each injection and can be expressed as:

$$q_i = V\Delta H_d\left[[M]_i - [M]_{i-1}\left(1-\frac{v}{V}\right) - f_m[M]_o\frac{v}{V}\right] + q_{dil} \tag{2.71}$$

where ΔH_d is the enthalpy change of dissociation in per mole monomer, q_{dil} is a correction factor that accounts for the heat associated with sample dilution that is unrelated to dissociation, f_m is the fraction of protein in the syringe that exists as free monomer, which can be expressed as:

$$f_m = \frac{1}{4[M]_o}\left(-K_d + \sqrt{K_d{}^2 + 8K_d[M]_o}\right), \tag{2.72}$$

and the term $f_m[M]_o \frac{v}{V}$ in Eq. 2.71 thus accounts for the addition of pre-existing monomers injected into the cell from the syringe.

The raw data (power *versus* time) was integrated and subsequently fit to Equation 2.71 with ΔH_d, K_d and q_{dil} as floating parameters using Microcal Origin version 7.0 (Microcal Inc, Northampton, MA, USA).

2.3 Results

2.3.1 Reversible thermal unfolding of fALS-associated apo SOD mutants

Previous DSC thermal unfolding studies on the fALS-associated apo SOD mutant E100G as well as the G93 mutants: G93A,D,S,R,V, found that the mutants unfold with high reversibility, comparable to or greater than apo PWT SOD (Rumfeldt, 2006; Stathopulos et al., 2006; Vassall et al., 2006). Reversibility is typically greater than 95% when scanning to the end of the unfolding endotherm and decreases when scanning beyond. This is higher than for the holo forms of PWT and mutants, which typically exhibit ~70% reversibility when scanned through 75% of the transition (Stathopulos et al., 2006). Similarly, the reversibility of unfolding for the apo SOD mutants studied here: G37R, H43R, H46R, A4T, A4S, A4V, I113T and G85R, scanned in 20 mM HEPES, pH 7.8 was assessed by heating the sample to the end of the transition with immediate cooling and subsequent re-scanning (Figure 2.4). The reversibility was quantitatively evaluated by calculating the area under the unfolding endotherm for both the 1st scan and the 2nd scan (i.e., the calorimetric enthalpy) after subtraction of the baselines. All mutants have reversibility of 95% or greater when scanned to the end of the unfolding transition with the exception of A4V, which has a somewhat lower reversibility of ~85%. This very high level of reversibility allows analysis of the data in terms of equilibrium thermodynamic parameters.

While apo PWT SOD has an apparent $t_{0.5}$ (temperature at maximum peak height) of ~ 59 °C (Stathopulos et al., 2003), the apo mutants G37R, H43R, A4T, A4S, A4V and I113T all have apparent $t_{0.5}$s ranging from between 8 and 16 °C lower (Figure 2.4). G85R and H46R have

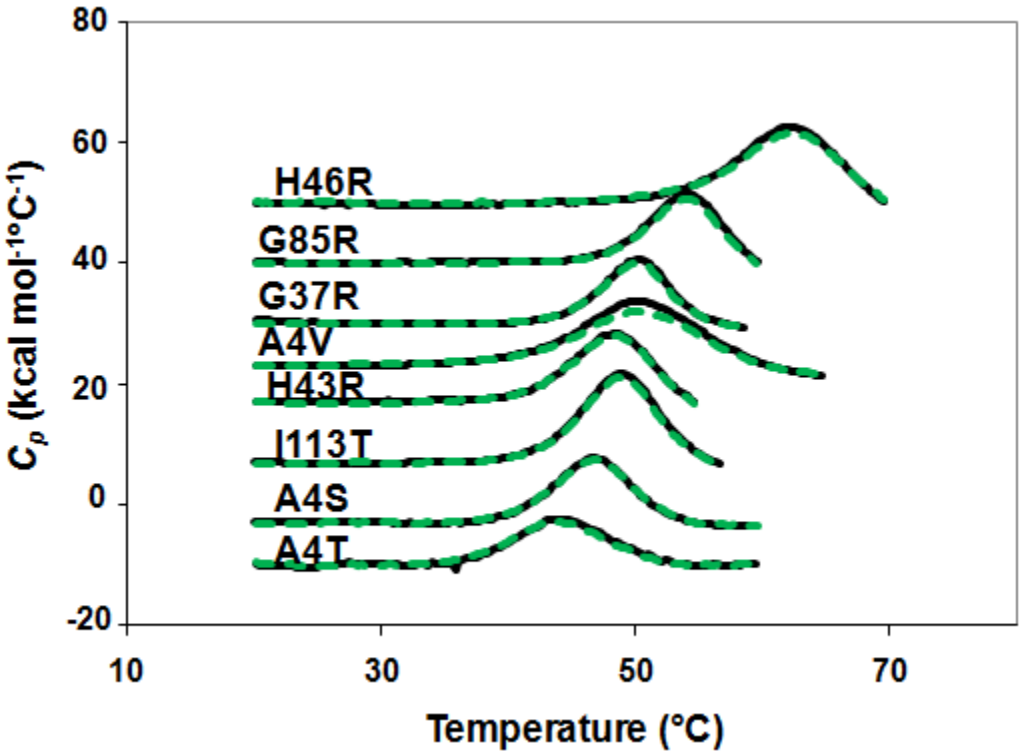

Figure 2.4. Reversibility of thermal denaturation of apo SOD mutants H46R, G85R, H43R, G37R, I113T, A4V, A4S, and A4T determined by DSC. Two consecutive scans were conducted to determine reversibility with the second scan (green broken line) obtained immediately after cooling the sample after completion of the first scan (black solid line). The reversibility, determined by integrating the area under the endotherm (ΔH_{cal}) for the first scan and the rescan after subtraction of the baselines is 95% or greater for all mutants except for A4V where it ~ 85%. Datasets were offset for purposes of comparison.

apparent $t_{0.5}$ values much closer to PWT, with G85R being ~3 °C lower and H46R being ~3 °C higher. Similar changes in apparent t_{05} values were reported previously for the mutants G85R, H46R, G37R and I113T compared to wild-type, however generally the apparent $t_{0.5}$ values reported in that study are ~ 5 °C lower than those presented here (Rodriguez et al., 2005). These lower apparent $t_{0.5}$ values may be related to the demonstrated irreversibility of the previously reported unfolding thermograms (Chrunyk and Wetzel, 1993; Stathopulos et al., 2003) and as well as to the use of phosphate buffer instead of HEPES used here.

2.3.2 Mechanism of folding of fALS-associated apo SOD mutants

Previous thermal unfolding studies on apo SOD found that data for PWT are very well fit by a 2-state dimer unfolding model over a large range of protein concentration, with van't Hoff to calorimetric enthalpy ratios close to 1 (Stathopulos et al., 2006). Additionally, for PWT there is a clear protein concentration dependent increase in the $t_{0.5}$ (temperature of half unfolding in °C) which provides further evidence of dimer unfolding. The protein concentration dependent increase in $t_{0.5}$ fit quite well to what is predicted for 2-state dimer unfolding (Stathopulos et al., 2006).

In light of the previously demonstrated applicability of the 2-state dimer unfolding model for apo PWT SOD thermal unfolding, this model was used as the starting point for analyzing the folding mechanisms for the apo SOD mutants studied here (Figure 2.5). Table 2.1 summarizes the fitted parameters $t_{0.5}$, $\Delta C_{p\ unf}$ ($t_{0.5}$), ΔH_{cal} ($t_{0.5}$) and ΔH_{vH} ($t_{0.5}$) as well as the $\Delta H_{vH}/\Delta H_{cal}$ ratio, obtained for the 2-state dimer model fitting of the mutants. As can be seen from this table, the $\Delta C_{p\ unf}$ ($t_{0.5}$) values for the fits are quite variable, as was noted previously for analyses of other apo SODs (Stathopulos et al., 2006). This is not surprising, as ΔC_p determined from fitting the

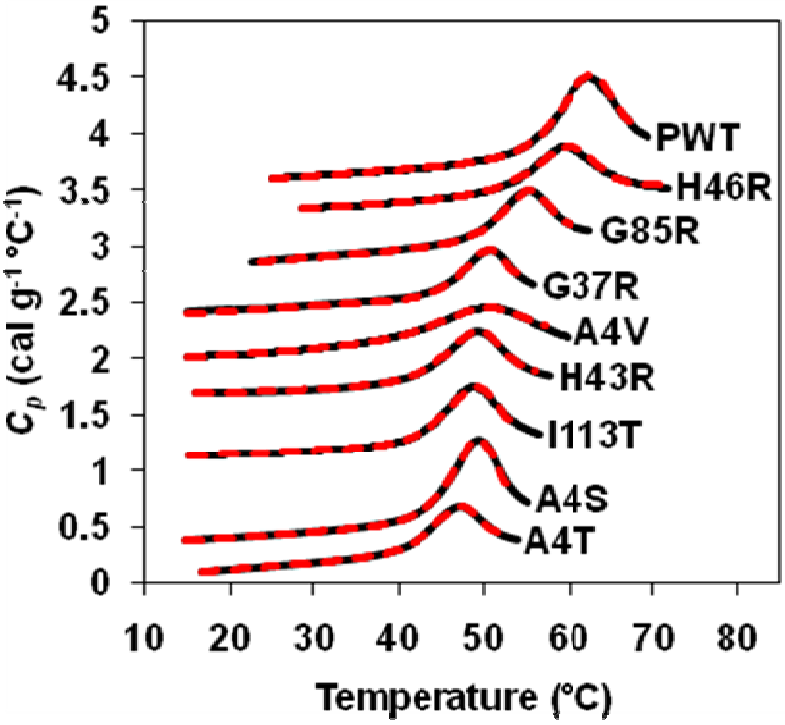

Figure 2.5. Typical DSC thermograms with corresponding dimer 2-state fits for apo PWT SOD and mutants. Data are presented as black solid lines while the corresponding dimer 2-state ($N_2 \leftrightarrow 2U$) fits are presented as red broken lines for apo PWT SOD and the apo SOD mutants H46R G85R, G37R, H43R, A4V, I113T, A4S and A4T. Parameters obtained from the fits are summarized in Table 2.1. Datasets were offset for purposes of comparison.

Table 2.1: DSC Dimer 2-State Fitted Parameters for apo SOD

APO SOD	[APO SOD] mg/mol	$t_{0.5}$[c] °C	$\Delta C_{p\ unf}$[d] (kcal (mol dimer^{-1})°C^{-1})	$\Delta H_{vH}(T_{0.5})$[e] (kcal (mol dimer)$^{-1}$)	$\Delta H_{cal}(T_{0.5})$[e] (kcal (mol dimer)$^{-1}$)	$\frac{\Delta H_{vH}}{\Delta H_{cal}}$
PWT[a]	0.05	57.8 ± 0.6	3.71	106.5 ± 18.9	110.1 ± 15.7	0.97
PWT[a]	0.20	58.3 ± 0.1	2.95	112.8 ± 6.7	111.0 ± 3.6	1.02
PWT[a]	0.21	58.4 ± 0.1	3.74	116.8 ± 9.1	139.5 ± 6.8	0.84
PWT[a]	0.27	57.8 ± 0.0	3.85	115.4 ± 2.7	148.2 ± 1.7	0.78
PWT	0.40	58.6 ± 0.2	2.20	121.7 ± 6.3	120.8 ± 4.0	1.01
PWT[a]	0.44	59.1 ± 0.2	4.25	137.6 ± 9.4	142.6 ± 7.3	0.96
PWT	0.50	59.1 ± 0.0	.3..32	130.0 ± 3.1	151.4 ± 2.0	0.86
PWT	0.50	59.2 ± 0.1	2.73	137.0 ± 6.6	141.2 ± 3.2	0.97
PWT[a]	0.73	58.8 ± 0.0	4.30	144.1 ± 2.5	153.6 ± 1.4	0.94
PWT[a]	1.42	60.0 ± 0.0	4.38	163.6 ± 2.4	170.4 ± 1.7	0.96
PWT[a]	1.50	60.3 ± 0.0	5.11	164.4 ± 4.0	149.8 ± 2.1	1.09
PWT[a]	2.99	61.3 ± 0.0	5.10	178.5 ± 1.4	178.2 ± 0.7	1.00
PWT[a]	3.00	61.9 ± 0.0	3.93	183.3 ± 1.9	127.0 ± 0.7	1.44
AVG + S.D[f]	n/a[g]	n/a	3.85 ± 0.89	n/a	n/a	0.99 ± 0.16
H46R	0.08	60.4 ± 0.3	4.81	90.0 ± 11.4	124.0 ± 9.4	0.73
H46R	0.17	60.9 ± 0.1	2.56	107.8 ± 2.0	153.1 ± 1.6	0.70
H46R	0.32	61.2 ± 0.0	3.31	120.2 ± 2.1	132.0 ± 1.2	0.91
H46R	0.39	61.0 ± 0.0	0.74	128.6 ± 2.1	142.2 ± 1.4	0.90
H46R	0.76	61.1 ± 0.0	5.18	139.2 ± 1.8	170.4 ± 1.6	0.82
AVG + S.D[f]	n/a	n/a	3.32 ± 1.80	n/a	n/a	0.81 ± 0.10
G85R	0.21	53.0 ± 0.2	2.35	148.1 ± 5.4	97.3 ± 3.29	1.52
G85R	0.40	54.2 ± 0.1	2.45	160.4 ± 2.7	92.3 ± 1.4	1.74
G85R	0.50	54.7 ± 0.1	3.82	153.7 ± 5.4	125.2 ± 2.7	1.23
G85R[b]	0.50	55.1 ± 0.0	4.32	160.8 ± 3.6	104.2 ± 2.7	1.54
G85R[b]	0.43	54.9 ± 0.0	2.14	166.5 ± 2.1	87.5 ± 0.6	1.90
G85R[b]	0.17	54.0 ± 0.1	4.12	158.2 ± 6.0	115.6 ± 3.6	1.37
AVG + S.D[f]	n/a	n/a	3.20 ± 0.99	n/a	n/a	1.55±0.24
G37R	0.22	49.1 ± 0.2	2.47	164.1 ± 6.7	69.8 ± 2.7	2.35
G37R	0.27	49.3 ± 0.2	2.12	159.7 ± 4.3	82.9 ± 1.9	1.93
G37R	0.32	49.5 ± 0.0	2.31	165.2 ± 2.0	72.6 ± 0.6	2.28
G37R	0.36	49.8 ± 0.1	1.85	167.5 ± 3.4	79.9 ± 1.2	2.10
AVG + S.D[f]	n/a	n/a	2.19 ± 0.27	n/a	n/a	2.17 ± 0.19
A4V	0.20	48.8 ± 1.6	-0.22	81.5 ± 17.2	107.5 ± 16.3	0.76
A4V	0.30	48.5 ± 0.1	1.73	82.4 ± 1.9	116.2 ± 1.3	0.71
A4V	0.40	49.3 ± 0.1	0.54	86.7 ± 3.5	106.4 ± 2.5	0.81
A4V	0.50	48.4 ± 0.1	2.50	77.5 ± 1.6	100.7 ± 1.2	0.77
A4V	1.00	48.9 ± 0.2	2.21	93.9 ± 3.5	128.0 ± 3.6	0.73
A4V	1.95	50.1 ± 0.0	1.88	120.6 ± 2.2	91.0 ± 0.9	1.33
AVG + S.D[f]	n/a	n/a	1.44 ± 1.05	n/a	n/a	0.85 ± 0.24

H43R	0.21	46.9 ± 0.1	3.60	123.1 ± 2.5	108.0 ± 1.8	1.14
H43R	0.23	47.3 ± 0.0	2.80	120.6 ± 2.0	108.4 ± 1.1	1.11
H43R	0.39	48.1 ± 0.0	3.07	128.8 ± 1.7	108.9 ± 0.7	1.18
AVG + S.D[f]	n/a	n/a	3.16 ± 0.41	n/a	n/a	1.14 ± 0.04
A4S	0.06	44.7 ± 0.1	2.81	132.2 ± 5.8	68.7 ± 2.1	1.92
A4S	0.13	45.8 ± 0.4	1.67	156.3 ± 11.6	70.8 ± 4.9	2.21
A4S	0.19	46.0 ± 0.3	2.85	140.8 ± 8.1	75.0 ± 4.1	1.88
A4S	0.57	47.8 ± 0.0	2.53	155.4 ± 0.9	84.3 ± 0.3	1.84
A4S	0.63	48.3 ± 0.0	4.45	159.0 ± 1.0	143.1 ± 0.5	1.11
AVG + S.D[f]	n/a	n/a	2.86 ± 1.01	n/a	n/a	1.79 ± 0.41
I113T	0.08	43.4 ± 0.5	4.91	68.7 ± 16.8	113.0 ± 15.6	0.61
I113T[b]	0.10	45.3 ± 1.0	1.86	105.3 ± 18.1	88.9 ± 14.1	1.19
I113T	0.15	44.9 ± 0.4	3.03	94.4 ± 9.0	109.3 ± 8.8	0.86
I113T	0.21	45.0 ± 0.2	4.17	110.2 ± 5.8	114.2 ± 4.7	0.96
I113T[b]	0.40	46.0 ± 0.1	2.44	106.2 ± 4.0	122.0 ± 2.2	0.87
I113T[b]	0.50	47.1 ± 0.1	2.79	129.0 ± 4.1	94.3 ± 2.3	1.37
I113T[b]	0.75	46.4 ± 0.1	4.75	118.0 ± 3.9	94.5 ± 1.6	1.25
I113T	1.20	47.8 ± 0.0	3.35	138.5 ± 2.0	11.8 ± 1.0	1.17
AVG + S.D[f]	n/a	n/a	3.41 ± 1.10	n/a	n/a	1.04 ± 0.25
A4T	0.08	40.6 ± 0.2	6.77	76.0 ± 6.0	151.7 ± 7.4	0.50
A4T	0.18	42.9 ± 0.1	3.98	116.3 ± 5.7	116.3 ± 4.0	1.00
A4T	0.20	43.0 ± 0.4	1.20	127.7 ± 18.9	55.2 ± 6.5	2.31
A4T	0.50	44.2 ± 0.3	2.34	133.9 ± 9.4	74.3 ± 5.0	1.80
A4T	1.00	45.9 ± 0.1	2.94	145.7 ± 2.1	81.6 ± 1.0	1.79
AVG + S.D[f]	n/a	n/a	3.45 ± 2.11	n/a	n/a	1.48 ± 0.72

[a]Data taken from (Stathopulos et al., 2006). [b]Data has been published (Vassall et al., 2006). [c]Errors (±) derived from the fitting program. [d]Errors from individual fits could not be reliably determined because they are based on uncertainties in five independent variables. [e]Errors (±) derived using standard procedures (Taylor, 1982) from errors in fitted $\Delta h_{cal}(T_{0.5})$ and β returned by the fitting program. [f]Average and standard deviation. [g] n/a not applicable

baselines is known to be fraught with uncertainty (Liu and Sturtevant, 1996; McCrary et al., 1996; Robinson et al., 1998). The uncertainty in this case is further increased, because the data were fit only to the approximate end of the unfolding transition where thermograms are most reversible, thus, the unfolded baseline is not well defined. There is a lack of equivalence for ΔH_{vH} and ΔH_{cal} values for most of the mutants, reflected in $\Delta H_{vH}/\Delta H_{cal}$ deviating from unity. As has previously been found for apo E100G and the apo G93 mutant SODs (Rumfeldt, 2006; Stathopulos et al., 2006; Vassall et al., 2006), the apo mutants: G37R, G85R, A4T, A4S and H43R, on average have $\Delta H_{vH}/\Delta H_{cal} > 1$, suggesting the formation of aggregates.

Aggregation can cause increases in $\Delta H_{vH}/\Delta H_{cal}$ in various ways. Non-native protein interactions can result in the cooperative unfolding unit being larger than a dimer; this would make the shape of the endotherm more asymmetric, resulting in an increase in ΔH_{vH} (Sturtevant, 1987). Also, mild, reversible, exothermic aggregation occurring during the transition can reduce the size/area of the endotherm leading to lower than expected ΔH_{cal} (Stathopulos et al., 2006). Additionally, low ΔH_{cal} values could result from the presence of misfolded or aggregated protein that may contribute to the measured protein concentration but that does not thermally unfold (Stathopulos, 2005; Stathopulos et al., 2006). In looking at the variations of $\Delta H_{vH}/\Delta H_{cal}$ within mutant apo SOD datasets, it appears that the high ratios are caused by low ΔH_{cal}, as was previously observed for the various G93 apo SOD mutants (Stathopulos, 2005; Stathopulos et al., 2006). Plots of $\Delta H_{vH}/\Delta H_{cal}$ vs. ΔH_{cal} for apo A4S, apo A4T and apo G85R show strong correlations, with R= -0.960, -0.991 and -0.955, respectively, indicating that high ratios are correlated with low calorimetric enthalpies (plots not shown). In contrast, no meaningful correlations were observed for $\Delta H_{vH}/\ \Delta H_{cal}$ vs. ΔH_{vH}. Consistent with this, for the various mutants, the expected increase in enthalpy with $t_{0.5}$ is more uniform for ΔH_{vH} when compared to ΔH_{cal}.

Interestingly, 3 apo SOD mutants studied here: H46R, I113T and A4V, did not exhibit high van't Hoff to calorimetric enthalpy ratios for the 2-state dimer fits (Table 2.1). Apo I113T actually has a ratio that is close to 1 when all datasets are averaged; however, fits to data collected at higher protein concentrations appear to give ratios greater than 1, indicating increased aggregation at higher protein concentrations. All apo H46R datasets and all but the highest concentration dataset for apo A4V SOD have ratios smaller than 1. Low ratios can be indicative of the cooperative unfolding unit being smaller than a dimer (i.e. monomer) or of loss of cooperativity due to intermediate formation (Privalov and Potekhin, 1986; Sturtevant, 1987). These low ratios from dimer 2-state fitting for apo A4V SOD are similar to results described previously for more limited datasets than presented here (Rumfeldt, 2006). Furthermore, for both H46R and A4V apo SODs, the $t_{0.5}$ changes very little with protein concentration, which is contrary to what is expected for dimer unfolding.

One way of evaluating the expected protein concentration dependence of $t_{0.5}$ for a dimer is through plots of ΔG vs. t and $-RT\ln P_{mon}$ vs. t, where R is the universal gas constant, P_{mon} is the total concentration of monomers in mol L^{-1}, T is the temperature in Kelvin and t is the temperature in °C (Tamura et al., 1994). Given that $\Delta G = -RT\ln P_{mon}$ at the $t_{0.5}$, the intersection of these plots is the predicted $t_{0.5}$ at a given protein concentration. Plots of ΔG vs. t generated using the average dimer 2-state fitted parameters of the various datasets and the average fitted $\Delta C_{p\ unf}$, along with the corresponding $-RT\ln P_{mon}$ *versus* t plots are shown in Figure 2.6 for A4V and H46R apo SODs. A plot of the predicted $t_{0.5}$ vs. protein concentration for these two mutants compared to the actual fitted $t_{0.5}$*s* is also displayed in Figure 2.6. It is apparent that the fitted $t_{0.5}$ values for both mutants deviate quite significantly from the predicted. For comparison, the equivalent plots for apo PWT SOD as well as A4T and A4S apo SODs, which did not give low enthalpy ratios, showed significantly better agreement between the predicted $t_{0.5}$ and the fitted $t_{0.5}$

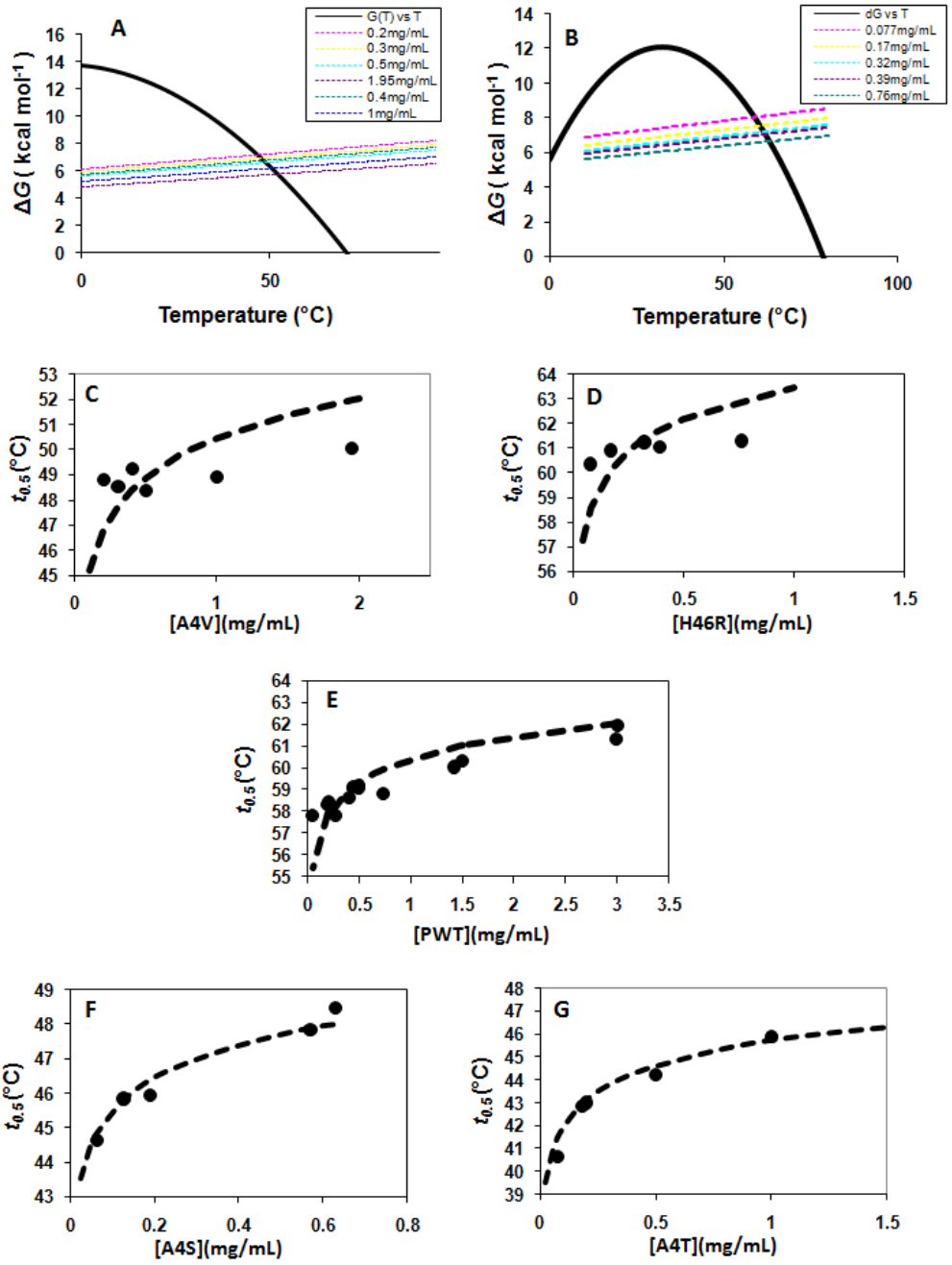

Figure 2.6. Predicted $t_{0.5}$ for thermal unfolding for apo PWT SOD and the apo SOD mutants A4V, H46R, A4T A4S. As illustrated for (A) A4V and (B) H46R, predicted values for $t_{0.5}$ were calculated from the intersection of plots of $-RT\ln P_{mon}$ *versus* t (coloured broken lines) and ΔG *versus* t (black solid line). The ΔG values were calculated using the average fitted parameters for all the 2-state dimer unfolding fits (Table 2.1). Predicted $t_{0.5}$ values (broken black lines) from these plots were then plotted against protein concentration and compared to the actual fitted $t_{0.5}$ values (closed circular data points) from Table 2.1 for (C) A4V and (D) H46R. Similar analysis was carried out for (E) PWT, (F) A4S and (G) A4T for purposes of comparison.

(Figure 2.6). Additionally, the deviations seen for both H46R and A4V apo SODs are systematic in that the fitted $t_{0.5}$ for the lower protein concentrations are above the predicted line, while the fitted $t_{0.5}$ for higher protein concentrations are below the predicted line. This systematic deviation in $t_{0.5}$ indicates a lower than expected dependence of $t_{0.5}$ on protein concentration and indicates that monomer is being formed along the unfolding pathway, suggesting two possible mechanisms (Tamura et al., 1995): 2-state monomer unfolding ($N \longleftrightarrow U$) or 3-state dimer unfolding with a monomeric intermediate ($N_2 \longleftrightarrow 2I \longleftrightarrow 2U$). Hence, both A4V and H46R apo SOD datasets were also fit to these two models (Equations 2.27 and 2.60 respectively). Although fits to a 2-state monomer unfolding model gave van't Hoff to calorimetric ratios fairly close to 1 (Table 2.2) there is a systematic increase in ΔH_{vH} values with protein concentration, which is inconsistent with monomer unfolding (Sturtevant, 1987). Furthermore, ITC dilution experiments demonstrated measurable endothermic heats consistent with dimer dissociating to folded free monomers (see Section 2.3.4), suggesting that the 3-state model with a monomeric intermediate is appropriate. The results of fitting to a 3-state dimer unfolding model with a monomeric intermediate will be considered in the next section.

2.3.2.1 3-State thermal unfolding of H46R and A4V apo SODs

Fitting A4V and H46R apo SOD DSC data to a 3-state model with a monomeric intermediate model (Figure 2.7) allowed the thermodynamics of each step in unfolding (dimer dissociation and subsequent unfolding of monomers) to be quantified. Due to the large number of parameters in this model, the data for all protein concentrations for each mutant were fit simultaneously with the temperatures of unfolding of both transitions as well as the change in enthalpies associated with these transitions as globally shared parameters. Despite the additional constraints caused by

Table 2.2: DSC Monomer 2-State Fitted Parameters for apo SOD Mutants

apo SOD	[apo SOD] (mg/mL)	$t_{(0.5)}$ (°C)	$\Delta C_{p\ unf}$[a] (kcal (mol monomer)$^{-1}$°C^{-1})	$\Delta H_{vH}(t_{0.5})$[b] (kcal (mol monomer)$^{-1}$)	ΔH_{cal} ($t_{0.5}$)[b] kcal (mol monomer)$^{-1}$)	$\frac{\Delta H_{vH}}{\Delta H_{cal}}$
H46R	0.077	61.6 ± 1.3	1.55	72.99 ± 18.0	60.0 ± 11.9	1.22
H46R	0.17	61.9 ± 0.3	0.71	74.6 ± 6.6	72.1 ± 3.9	1.03
H46R	0.32	62.2 ± 0.1	1.01	84.6 ± 2.2	69.1 ± 1.0	1.22
H46R	0.39	62.2 ± 0.2	0.27	86.6 ± 4.7	80.8 ± 2.8	1.07
H46R	0.76	62.2 ± 0.1	1.07	94.9 ± 2.5	97.1 ± 1.5	0.98
A4V	0.2	51.5 ± 1.4	-1.15	45.5 ± 10.6	62.8 ± 8.0	0.72
A4V	0.3	50.3 ± 0.6	-0.02	56.6 ± 7.9	62.6 ± 5.2	0.90
A4V	0.4	50.6 ± 0.3	-0.47	56.9 ± 5.1	56.7 ± 2.8	1.00
A4V	0.5	50.8 ± 0.2	0.29	54.7 ± 2.5	57.7 ± 1.4	0.95
A4V	1	50.3 ± 0.4	0.26	65.9 ± 4.4	66.4 ± 3.2	0.99
A4V	1.95	51.5 ± 0.1	-0.18	79.3 ± 2.6	52.7 ± 1.0	1.50

[a]Errors (±) from individual fits could not be reliably determined because they are based on uncertainties in five independent variables. [b]Errors (±) derived using standard procedures (Taylor, 1982) from errors in fitted $\Delta h_{cal}(t_{0.5})$ and β returned by the fitting program.

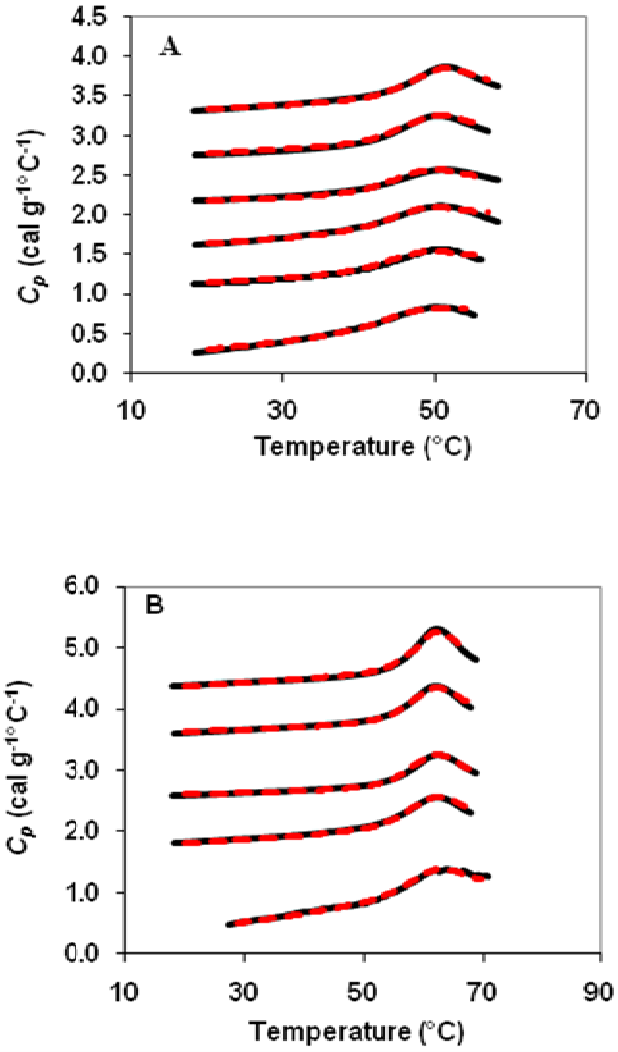

Figure 2.7. DSC thermograms and corresponding global fits to a 3-state model with a monomeric intermediate for A4V and H46R apo SODs. Data are presented as black solid lines while fits are shown as red broken lines for (A) A4V and (B) H46R. The protein concentrations for each scan are (from top to bottom): 0.08, 0.17, 0.32, 0.39, 0.76 mg/mL for H46R and 0.2, 0.3, 0.4, 0.5, 1 and 1.95 mg/mL for A4V. Data were only fit to the approximate end of the unfolding transition due to the presence of downward sloping post-transition baselines (likely resulting from exothermic aggregation). Fitted parameters are summarized in Table 2.3. Datasets were offset for purposes of comparison.

global fitting compared to fitting individual thermograms, the fits were quite good for both proteins across all datasets (Figure 2.7). It should be noted that, for purposes of comparison, data were also fit to a 3-state dimer unfolding model with a dimeric intermediate (fit not shown), but these fits were inferior as judged by an ~ 6-fold increase in the value sum of squares due to error.

The parameters obtained from fitting to the 3-state dimer model with monomeric intermediate for both A4V and H46R apo SODs are summarized in Table 2.3 and plots of $t_{0.5}$ as a function of protein concentration for both transitions are shown in Figure 2.8. As expected for this model, Figure 2.8 shows that the $t_{1,0.5,}$ (temperature in °C of half completion for the first transition, i.e. dimer dissociation,) increases with protein concentration while $t_{2,0.5}$ (temperature of half completion for the second transition, i.e. monomer unfolding) is constant throughout the protein concentration range. This occurs because the first step of unfolding involves a change in molecularity and so is concentration dependent, while the second step involves only monomer unfolding and is therefore concentration independent. For both mutant proteins, the $t_{0.5}$ value for the first transition is in fact significantly lower than that for the second; however, in the protein concentration range studied, it is not sufficiently well separated from $t_{0.5}$ for the second transition for the peaks associated with each step to be clearly resolved.

2.3.3 Thermodynamic stability of fALS-associated apo SOD mutants

The thermodynamic parameters ΔG, ΔH and ΔS were calculated using the values obtained from applying the appropriate unfolding model to the apo SOD mutant data (Table 2.4). Also, the mutation-induced changes in these thermodynamic values are presented as $\Delta\Delta G$ ($\Delta\Delta G = \Delta G_{\text{mutant}} - \Delta G_{PWT}$), $\Delta\Delta H$ ($\Delta\Delta H = \Delta H_{\text{mutant}} - \Delta H_{PWT}$) and $\Delta\Delta S$ ($\Delta\Delta S = \Delta S_{\text{mutant}} - \Delta S_{PWT}$) in Table 2.5. For the apo SOD mutants that could be fit by a 2-state model (G85R, H43R, G37R,

Table 2.3: DSC 3-State dimer with monomeric intermediate fitted parameters for apo SOD

apo SOD	[apo SOD][a] (mg/mL)	t_1' (°C)[b]	t_2' (°C)[b]	ΔH_1 (t_1')[c] (kcal (mol dimer)$^{-1}$)	ΔH_2 (t_2')[c] (kcal (mol monomer)$^{-1}$)
A4V	0.2,0.3,0.4,0.5,1,1.95	80.3 ± 2.0	48.9 ± 0.6	94.6 ± 1.5	42.1 ± 1.1
H46R	0.077,0.17,0.32,0.39, 0.76	87.5 ± 0.9	62.7 ± 0.1	104.4 ± 1.7	73.3 ± 0.9

[a]The concentration of each dataset used in global fitting is indicated. [b] t_1' and t_2' is the temperature in °C at which $K_1(T)=1$ and $K_2(T)=1$. [c]Errors (±) were returned by the fitting program. [c]Errors (±) propagated using standard procedures (Taylor, 1982) from errors in fitted $\Delta h_{cal}(t')$ returned by the fitting program, using a fixed β=31,500.

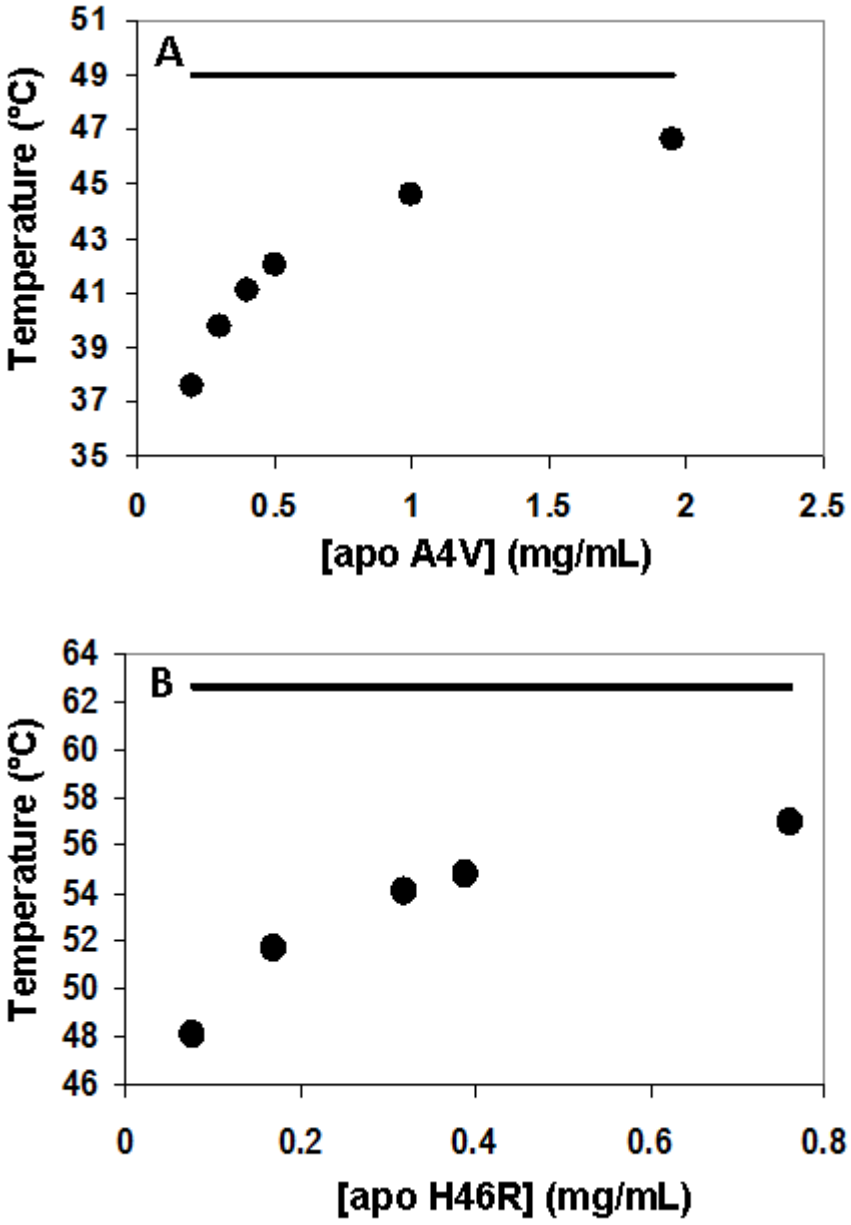

Figure 2.8. Protein concentration dependence of temperatures of half completion for each step of thermal unfolding of A4V and H46R apo SODs. Temperatures of half completion for each step ($t_{1,0.5}$ and $t_{2,0.5}$ respectively) were determined from fits to a 3-state model with a monomeric intermediate for (A) A4V and (B) H46R. The $t_{1,0.5}$ and $t_{2,0.5}$ were calculated as the temperature at which α_1 and α_2 (the extents of dimer dissociation and monomer unfolding respectively) is 0.5 using the fitted parameters in Table 2.3 and solving for T using Equations 2.39, 2.40 and 2.50 and 2.51. The $t_{1,0.5}$ values for the various datasets for each mutant (Table 2.3) is indicated as black circles. The $t_{1,0.5}$ value increases with protein concentration as expected for an unfolding process involving a change in molecularity. The $t_{2,0.5}$ is represented by the solid line and is constant across all concentrations as expected for an unfolding process that does not involve a change in molecularity.

Table 2.4: Summary of thermodynamic parameters for apo SOD mutant thermal unfolding analyzed by DSC

Apo SOD	$t_{0.5}$[a] (°C)	$\Delta t_{0.5}$[b] (°C)	ΔH_1 (37°C)[c] (kcal (mol of dimer)$^{-1}$)	ΔH_2 (37°C)[c] (kcal (mol of monomer)$^{-1}$)	ΔH_{tot} (37°C)[d] (kcal (mol of dimer)$^{-1}$)	ΔS_1 (37°C)[c] (kcal (mol of dimer)$^{-1}$ K^{-1})	ΔS_2 (37°C)[c] (kcal (mol of monomer)$^{-1}$K^{-1})	ΔS_{tot} (37°C)[d] (kcal(mol of dimer)$^{-1}$K^{-1}	ΔG_1 (37°C[c] (kcal (mol of dimer)$^{-1}$)	ΔG_2 (37°C)[c] (kcal(mol of monomer)$^{-1}$)	ΔG_{tot} (37°C)[d] (kcal(mol of dimer)$^{-1}$)
PWT	59.0	n/a[e]	n/a	n/a	65.9 ± 21.8	n/a	n/a	0.170 ± 0.066	n/a	n/a	13.2 ± 1.3
H46R	55.6, 62.7	n/a	23.3 ± 2.2	51.5 ± 0.9	126.2 ± 2.9	0.047 ± 0.006	0.151 ± 0.003	0.348 ± 0.008	8.6 ± 0.2	4.75 ± 0.03	18.1 ± 0.3
G85R	54.5	-4.5	n/a	n/a	100.8 ± 8.5	n/a	n/a	0.282 ± 0.027	n/a	n/a	13.3 ± 0.4
G37R	50.1	-8.9	n/a	n/a	121.6 ± 4.0	n/a	n/a	0.353 ± 0.013	n/a	n/a	12.2 ± 0.2
A4V	42.1, 48.9	n/a	25.0 ± 3.5	31.9 ± 1.3	89.0 ± 4.3	0.057 ± 0.011	0.098 ± 0.004	0.255 ± 0.013	7.1 ± 0.2	1.37 ± 0.03	9.9 ± 0.3
H43R	48.5	-10.5	n/a	n/a	89.7 ± 2.8	n/a	n/a	0.256 ± 0.009	n/a	n/a	10.3 ± 0.1
A4S	47.9	11.1	n/a	n/a	112.0 ± 7.7	n/a	n/a	0.326 ± 0.024	n/a	n/a	10.7 ± 0.3
I113T	47.1	-11.9	n/a	n/a	79.6 ± 16.9	n/a	n/a	0.266 ± 0.053	n/a	n/a	9.4 ± 0.4
A4T	44.5	-14.5	n/a	n/a	99.4 ± 9.3	n/a	n/a	0.291 ± 0.061	n/a	n/a	9.1 ± 0.5

[a] $t_{0.5}$ calculated at 0.5mg/mL for all mutants. Values for PWT, I113T, A4T, A4S, G37R, H43R, G85R calculated from the intersection of $-RT\ln P_{mon}$ and average stability plots (ΔG vs T) (Stathopulos et al., 2006). Two values of $t_{0.5}$ for A4V and H43R are shown and represent the temperature of half completion for the first and second transition respectively, calculated using Equations 2.39, 2.40, 2.50, 2.51. [b]Calculated from $t_{0.5\ \text{mutant}} - t_{0.5\ \text{PWT}}$. [c]Calculated from fitted parameters presented in Table 2.3 using Equations 2.62-2.65 using temperature independent ΔC_{p1} and ΔC_{p2} values of 1.6 kcal mole dimer^{-1} °C^{-1} and 1.7 kcal mole dimer^{-1} °C^{-1} respectively. Note that thermodynamic values in fitting are returned in dimer units but are divided by 2 for the second transition and presented in the table in monomer units as indicated. Errors ($\pm$) in ΔH and ΔS were propagated using standard procedures (Taylor, 1982) from errors returned from fitting program. Errors in ΔG for each transition were determined as follows (McCrary et al., 1996):

$$\sigma_{\Delta G}^2 = \sigma_{\Delta H(T')}^2\left(\frac{\partial \Delta G_u}{\partial \Delta H}\right)^2 + \sigma_{T'}^2\left(\frac{\partial \Delta G_u}{\partial T'}\right)^2 + \sigma_{\Delta C_p}^2\left(\frac{\partial \Delta G_u}{\partial \Delta C_p}\right)^2 \text{ where, } \quad \left(\frac{\partial \Delta G_u}{\partial \Delta H}\right) = \frac{T' - T}{T'}; \quad \left(\frac{\partial \Delta G_u}{\partial T'}\right) = \frac{T\Delta H(T')}{(T')^2} - \Delta C_p \frac{T' - T}{T'} \text{ and}$$

$$\left(\frac{\partial \Delta G_u}{\partial \Delta C_p}\right) = T\ln\left(\frac{T'}{T}\right) - (T' - T).$$ Note that the variance in ΔC_p in this case is zero as it was fixed during fitting see Section 2.2.3.1.2.

[d]Values for PWT, I113T, A4T, A4S, G37R, H43R, G85R calculated for each individual datasets from Equations 2.62-2.65 using a temperature independent ΔC_p value of 3.3 kcal mole dimer^{-1} °C^{-1}. Values shown are averages of the individual datasets from Table 2.1 while errors ($\pm$) are standard deviations. Values for A4V and H46R calculated from $\Delta H_{tot}=\Delta H_1+2\Delta H_2$, $\Delta S_{tot}=\Delta S_1+2\Delta S_2$ and $\Delta G_{tot}=\Delta G_1+2\Delta G_2$ with errors propagated using standard procedures (Taylor, 1982). [e]n/a not applicable.

I113T, A4T, and A4S) only the total thermodynamic quantities, representing unfolding from a native dimer to unfolded monomers could be evaluated, while for the apo SOD mutants that fit a 3-state unfolding model (A4V and H46R), thermodynamic parameters were determined for both steps in the unfolding transition. Given that ΔH_{vH} is typically less prone to experimental error than ΔH_{cal} (Johnson and Fersht, 1995; Liu et al., 2001; Privalov and Potekhin, 1986) and appears to be minimally affected by aggregation (see Section 2.3.2), ΔH_{vH} was used in thermodynamic calculations. Since the fits give values at only a single temperature for each transition (in this study, typically temperatures close to 50 °C), these thermodynamic quantities have to be extrapolated to other temperatures using Equations 2.62-2.65. In extrapolation, it is commonly assumed that $\Delta C_{p\ unf}$ is independent of temperature (Prabhu and Sharp, 2005); however, this is generally true only over short temperature ranges and longer extrapolations can lead to errors in assessing stability (Gomez et al., 1995; Privalov and Makhatadze, 1990). Hence, in addition to presenting thermodynamic values at 37 °C, the effects of mutations on stability ($\Delta\Delta G$) were also calculated at 51.8 °C, which is the average of all the $t_{0.5}$ values in Table 2.1, and are undoubtedly a more accurate reflection of the stability of the mutants relative to PWT.

In interpreting the thermodynamic parameters in Table 2.4 and 2.5, it is evident that the apo SOD mutants have remarkably different stabilities with ΔGs ranging from a low of ~ 9 kcal mol^{-1} for A4T, to a high of ~ 18 kcal mol^{-1} for H46R at 37 °C. Additionally, all the apo SOD mutants except H46R are destabilized relative to PWT with $\Delta\Delta G$s on the order of ~ -5 to -2 kcal mol^{-1} at the t_{avg} while H46R has a $\Delta\Delta G$ of ~ +2. Analysis of the enthalpy and entropy of unfolding gives a more complete picture as to the reasons for these observed effects on stability by the various mutations. All the mutations increase both the enthalpy and entropy of unfolding

Table 2.5: Effects of the mutations on the thermodynamic parameters of apo SOD

Apo SOD	$\Delta\Delta H_{tot}$(37°C)[a] (kcal (mol of dimer)$^{-1}$)	$\Delta\Delta S_{tot}$(37°C)[a] (kcal(mol of dimer)$^{-1}$K^{-1}	$\Delta\Delta G_{tot}$ (37°C)[a] (kcal (mol of dimer)$^{-1}$)	$\Delta\Delta G_{tot}$(*tavg*)[a,b] (kcal (mol of dimer)$^{-1}$)
PWT	n/a	n/a	n/a	n/a
H46R	+60.4	+0.179	+4.9	+2.3
G85R	+35.0	+0.112	+0.1	-1.6
G37R	+55.8	+0.183	-1.1	-3.8
A4V	+23.1	+0.085	-3.3	-4.6
H43R	+23.8	+0.086	-2.9	-4.2
A4S	+46.1	+0.157	-2.5	-4.9
I113T	+13.8	+0.096	-3.8	-4.7
A4T	+33.5	+0.122	-4.2	-6.0

[a] $\Delta\Delta H = \Delta H_{tot\ (mutant)} - \Delta H_{tot\ (PWT)}$, $\Delta\Delta S_{tot} = \Delta S_{tot\ (mutant)} - \Delta S_{tot\ (PWT)}$,, $\Delta\Delta G_{tot} = \Delta G_{tot\ (mutant)} - \Delta G_{tot\ (PWT)}$. [b] Values for $\Delta\Delta G$ calculated at the t_{avg} (51.8 °C) which is the average of $t_{0.5}$ values in Table 2.1.

(+$\Delta\Delta H$ and +$\Delta\Delta S$); however, these stabilizing increases in unfolding enthalpy are sufficient to overcome the destabilization resulting from concomitant increases in entropy only for the mutant H46R. In looking at the thermodynamic parameters associated with both unfolding steps of the apo SOD mutants A4V and H46R, it can be seen that A4V has lower ΔG_1 and ΔG_2 compared to H46R, indicating both markedly reduced dimer interface and monomer stability. The primary reason for decreased dimer stability in A4V compared to H46R is increased entropy, while large decreases in enthalpy are the reason for its lower monomer stability.

2.3.4 Thermodynamic characterization of mutant apo SOD dimer dissociation

While DSC data analysis could be used to determine the thermodynamics of both dimer dissociation and subsequent monomer unfolding for two mutants, only information on the total unfolding process could be obtained for the other mutants. This can occur due to either a strong dimer interface and/or an unstable monomer intermediate, so that the intermediate never becomes significantly populated. In order to further investigate this, the strength of the dimer interface of several of the mutants analyzed by DSC was probed by conducting dilution experiments using ITC. In these experiments, a high concentration of apo SOD protein in 20mM HEPES, pH 7.8 was diluted into the same buffer in the ITC cell. A series of small volume injections results in large dilutions of protein concentration, which induces the dissociation of dimer due to mass action with the absorption of a measurable amount of heat. Apo SOD is a very strong dimer with an estimated K_d $<10^{-8}$ M (at 20 °C pH 5.5) (Doucette et al., 2004). One strategy to decrease the K_d to an experimentally measurable level is to perform ITC titrations at an increased temperature that is still below where the protein unfolds. To facilitate comparison of the thermodynamics of dimer dissociation, datasets were acquired for all mutants at 37°C, 20mM

HEPES, pH 7.8 which were the standard conditions used in this study. This temperature is just below the start of the unfolding transition for the most destabilized apo SOD mutant studied, A4T, as determined by DSC measurements (Figure 2.5). At this temperature, dilution experiments of apo PWT SOD were dominated by exothermic heats of dilution unrelated to dimer dissociation; endothermic peaks associated with dissociation were only measurable for the first ~2 injections where the dilution factor was the greatest (Figure 2.9). All the apo SOD mutants investigated in this study, however, A4V, A4S, A4T, I113T, H46R, H43R, and G93S, produced several measurable heat signals which were integrated and fit to a dimer dissociation model (Equation 2.71), with the results described below (Figure 2.10, 2.12, 2.13, Table 2.6).

2.3.4.1 Dimer dissociation of apo A4V SOD as a function of temperature

Given that DSC analysis of thermal unfolding of apo A4V SOD indicates the presence of a monomeric intermediate, formation of this monomer should be detectable by ITC, providing that dimer dissociation results in sufficient absorption/release of heat. In addition to our standard temperature of 37°C, ITC experiments were performed at lower temperatures with measurable heats of dissociation at temperatures as low as 25°C (Figure 2.10). The data acquired at each temperature were well fit by the dimer dissociation model (Figure 2.10). Tables 2.6 and 2.7 present K_d and ΔH_d (enthalpy change upon dimer dissociation) obtained directly from the fits and the calculated ΔG_d (Gibbs free energy change upon dimer dissociation) and ΔS_d (entropy change upon dimer dissociation) respectively. There are larger errors associated with data acquired at 25°C due to a smaller number of measurable endothermic heats of dilution and overall less signal associated with all injections (Figure 2.10A). As expected for an endothermic process, K_d

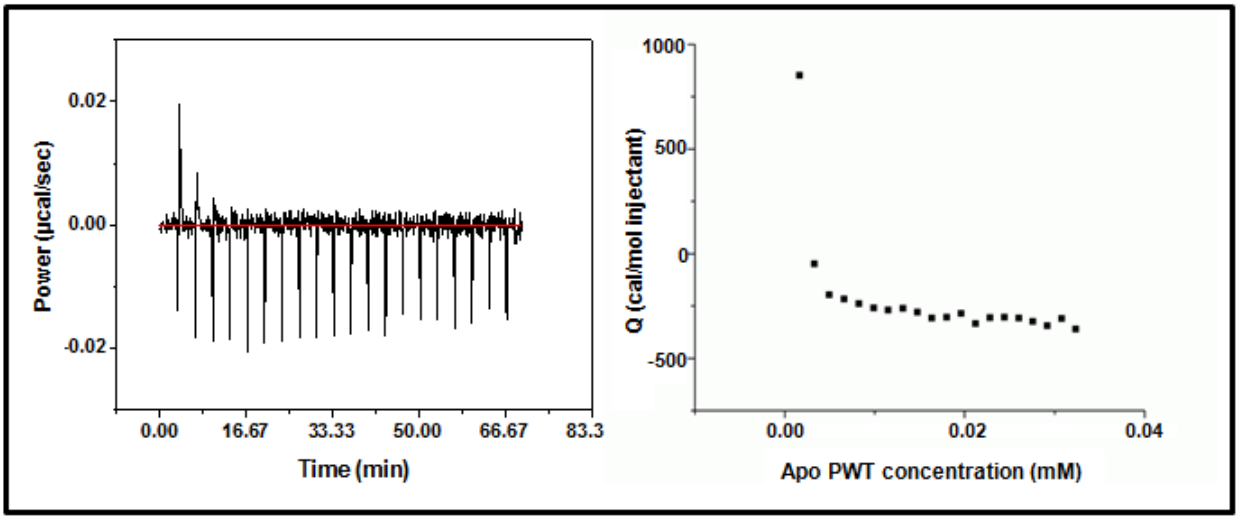

Figure 2.9. Raw ITC trace along with integrated heats for a typical dimer dissociation experiment of apo PWT SOD at 37 °C. Each peak in the power *versus* time trace (left panel) represents a small volume injection (0.5 µM) of protein into the ITC cell. The ITC trace is dominated by negative exothermic peaks (downward peaks) unrelated to dimer dissociation with only a couple of observable small endothermic heats of dissociation (upward peaks), indicating a tight dimer interface. These endothermic heats of dissociation will decrease with each successive injection due to the increase in protein concentration in the cell and the subsequent shifting of equilibria towards native dimer (see Section 2.1.2). The heats obtained from integrating the power *versus* time ITC raw data is shown in the right panel. This data cannot be fit due to too few points defining the curvature of the plot.

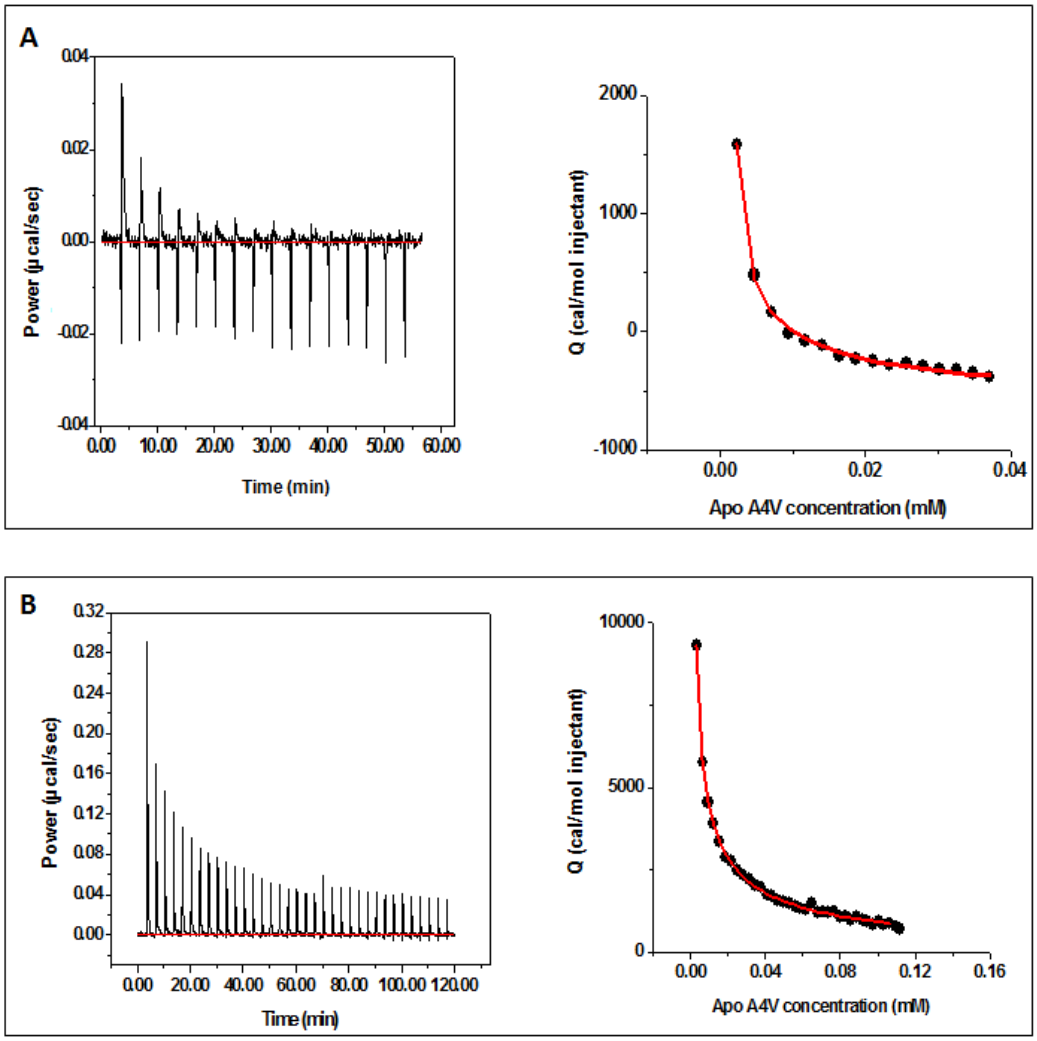

Figure 2.10. Raw apo A4V SOD ITC traces along with integrated heats at 25 and 37 °C. The ITC traces (power *versus* time) are shown in the left panels while the corresponding plots of heat (*Q*) *versus* the total concentration of apo A4V SOD after each injection (black closed circles) are shown in the right panels. Each peak in the raw ITC trace represents a small volume injection (0.5 µM) of protein into the ITC cell. The heats associated with each injection are obtained from integrating each peak in the raw ITC trace. The experiments were performed at (A) 25 °C and (B) 37 °C. The parameters from data fitting (red lines) to a dimer dissociation model (Equation 2.71) at various temperatures are summarized in Table 2.6.

Table 2.6: Summary of ITC fitted values for apo SOD mutants

Apo SOD	t [a] (°C)	K_d [b] (μM)	ΔH_d [b,c] (kcal (mol of dimer)$^{-1}$)
A4V	25	1.0±0.2	13.0±1.1
A4V	28	2.1±0.4	18.8±1.3
A4V	30	7.1±1.9	24.2±2.3
A4V	30	5.2±0.5	24.0±0.6
A4V	37	7.3±0.5	37.9±0.6
A4V	37	13.3±0.6	30.0±0.3
A4V	37	9.5±0.5	29.3±0.4
A4S	37	1.0 ± 0.2	18.6±1.4
A4S	37	2.1 ± 0.2	13.2±0.4
A4S	37	1.8 ± 0.3	13.9±0.9
A4T	37	6.3±1.0	34.5±1.3
A4T	37	4.1±0.3	29.9±0.6
A4T	37	4.8±0.4	28.4±0.6
G93S	37	0.9±0.2	38.1±4.2
G93S	37	1.1±0.2	27.7±0.9
G93S	37	1.6±0.9	26.4±6.06
H43R	37	0.5±0.1	36.5±2.4
H43R	37	0.8±0.2	31.9±3.3
H46R	37	0.6±0.1	14.4±0.9
H46R	37	0.6±0.3	13.9±2.4
H46R	37	0.3±0.2	15.8±3.6
I113T	37	4.6±0.3	23.9±0.4
I113T	37	3.4±0.2	29.8±0.4
I113T	37	3.7±0.3	27.2±0.8

[a] Temperature at which experiments were carried out. [b]Errors (±) as reported by the fitting program. [c]Note that fitting of ITC data to equation 2.71 results in ΔH_d in monomer units, however ΔH_d in the table is expressed in dimer units obtained by multiplying ΔH_d in monomer units by 2.

increases with temperature, from a value of ~1μM at 25 °C to ~10 μM at 37 °C, corresponding to ΔG_d values of 8.2 kcal mol^{-1} and 7.1 kcal mol^{-1}, respectively. The value of 7.1 kcal mol^{-1} for ΔG_d is in almost exact agreement with the value obtained for ΔG_1 from DSC fitting (Table 2.4). There is a considerable increase in the enthalpy of dissociation with temperature, suggesting that dimer dissociation involves a significant change in heat capacity, ($\Delta C_{p,d}$). The magnitude of $\Delta C_{p,d}$ was evaluated by constructing a Kirchoff plot using both the enthalpy (ΔH_d *vs. t*) and the entropy ($T\Delta S_d$ *vs. t*) (Figure 2.11). The $\Delta C_{p,d}$ of 1.56 kcal mol^{-1}°C^{-1}obtained from the slope of the ΔH_d *vs. t* plot agrees very well with the value of 1.64 kcal mol^{-1}°C^{-1}obtained from the corresponding plot obtained with $T\Delta S_d$ with the average of the two being 1.60 kcal mol^{-1}°C^{-1}.

2.3.4.2 Dimer dissociation of H46R, A4S, A4T, I113T, H43R and G93S apo SODs at 37 °C

Similar to A4V, it is not surprising that H46R, the only other apo SOD mutant studied that exhibits 3-state thermal unfolding with the formation of a monomer intermediate, produces measurable ITC dimer dissociation heats (Figure 2.12). However, ITC experiments for apo H46R SOD at 37 °C shows considerably less heat of dissociation than the equivalent experiments for apo A4V SOD. Fitting of the integrated H46R data indicates a significantly smaller K_d and hence stronger dimer interface when compared to A4V; this is consistent with the relative ΔG_1 values obtained by DSC (Tables 2.4, 2.6). The K_d value of ~ 0.5 μM for H46R corresponds to a ΔG_d of 8.9 kcal mol^{-1}, which is quite close to the value of 8.5 for ΔG_1 obtained from 3-state DSC fitting, again providing validation of the 3-state DSC data fitting.

In light of the finding that apo A4V SOD dimer dissociation could be measured at temperatures as low as 25°C, it was speculated that the other A4 apo SOD mutants, A4T and A4S, would perhaps also measurably dissociate at temperatures lower than 37 °C. Unlike what was seen for

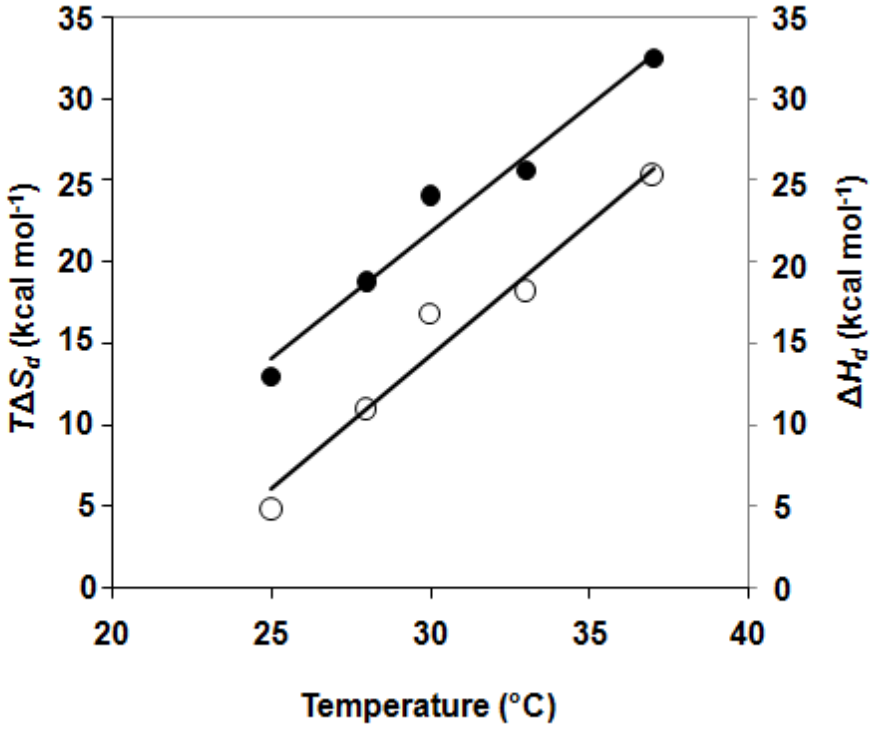

Figure 2.11. The determination of ΔC_p of dimer dissociation of apo A4V SOD from a Kirchoff plot. Data for the plot was obtained by performing ITC dimer dissociation experiments at different temperatures (Table 2.6). Plots of ΔH versus T (black solid circles) as well as corresponding plots of $T\Delta S$ versus T (black open circles) are shown. ΔC_p was determined from the slope of each plot and was found to be 1.56 ± 0.2 kcal $mol^{-1}°C^{-1}$ (r = 0.983) and 1.64 ± 0.2 kcal $mol^{-1}°C^{-1}$ (r = 0.980) for plots of ΔH *versus* T and $T\Delta S$ *versus* T, respectively.

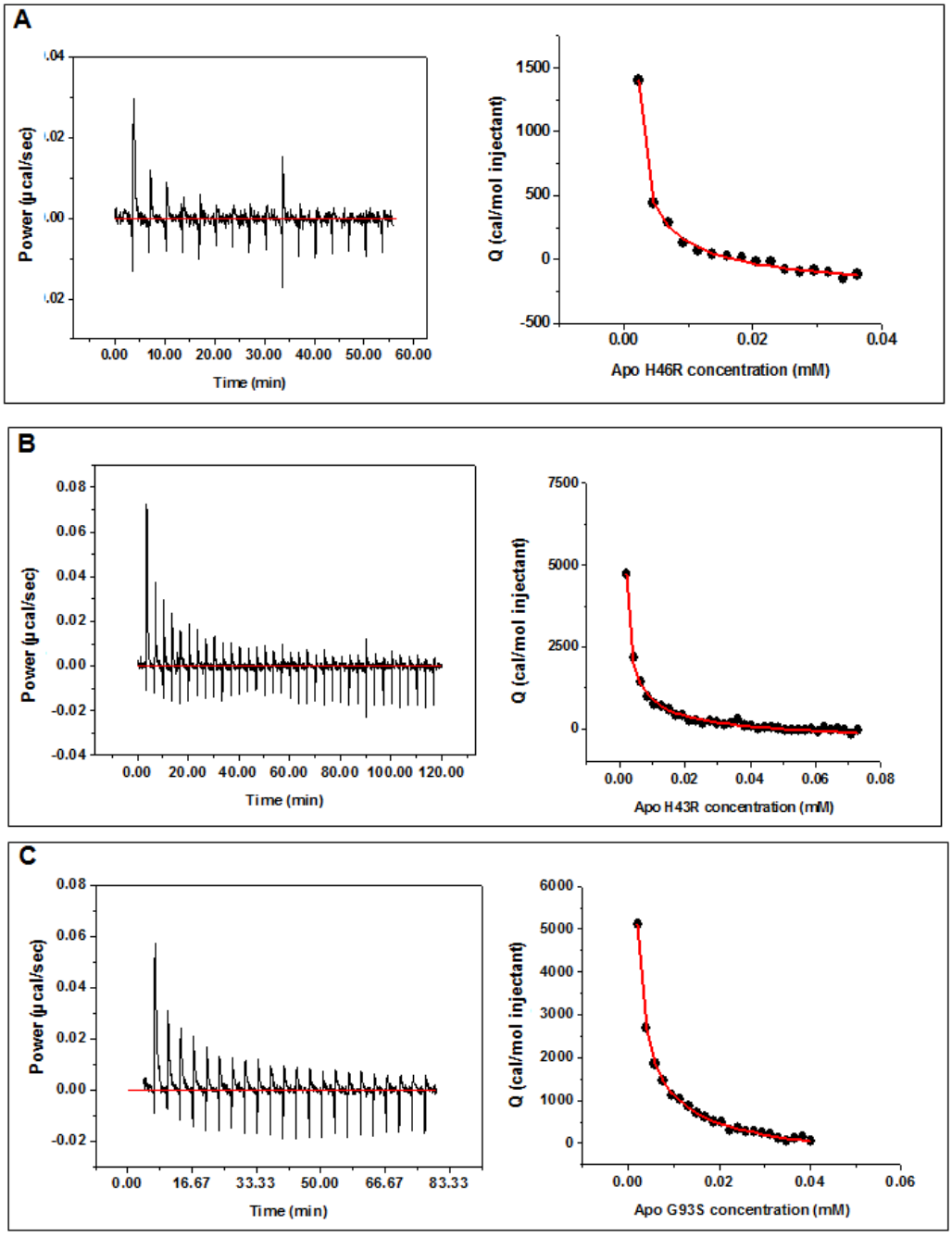

Figure 2.12. Raw ITC traces and integrated heats for H46R, H43R and G93S apo SODs at 37 °C. The ITC traces (power *versus* time) are shown in the left panels while the corresponding plots of heat (*Q*) *versus* concentration of protein (black closed circles) after each injection are shown in the right panels for the mutants (A) H46R, (B) H43R and (C) G93S (black closed circles). The volume of injected protein into the ITC cell was 0.5µM for H43R and G93S and 0.7µM for H46R. Fitting of the data (red solid lines) to a dimer dissociation model (Equation 2.71), yielded parameters presented in Table 2.6.

A4V, however, ITC measurements at 30 °C did not produce sufficient heat for analysis, which provided an immediate qualitative indication that the dimer interface is stronger for these other A4 mutants (data not shown). Fits of the ITC data acquired at 37 °C for A4S and A4T apo SODs provided quantitative conformation of this, with both mutants having smaller K_d values of 1.6 and 5.1 μM, respectively, compared to 10 μM for A4V (Figure 2.13, Table 2.6). Fits of the ITC data for all the other apo SOD mutants, I113T, H43R and G93S, yielded K_d*s* of 3.9, 0.66 and 1.2 μM, respectively (Figure 2.12, 2.13 and Table 2.6). With respect to the enthalpies of dissociation for the various apo SOD mutants, A4T, I113T, G93S and H43R all have enthalpies close to 30 kcal mol^{-1}, which is similar to those for A4V. A4S and H46R, however, have enthalpies almost half of this value (Table 2.7). The trends in the ΔS_d for the various mutants mirror the trends in enthalpy in that A4V, A4S, I113T, H43R and G93S all have similar entropy changes for dissociation that are close to 0.075 kcal $mol^{-1}K^{-1}$ while A4S and H46R have entropies closer to 0.020 kcal $mol^{-1}K^{-1}$ (Table 2.7).

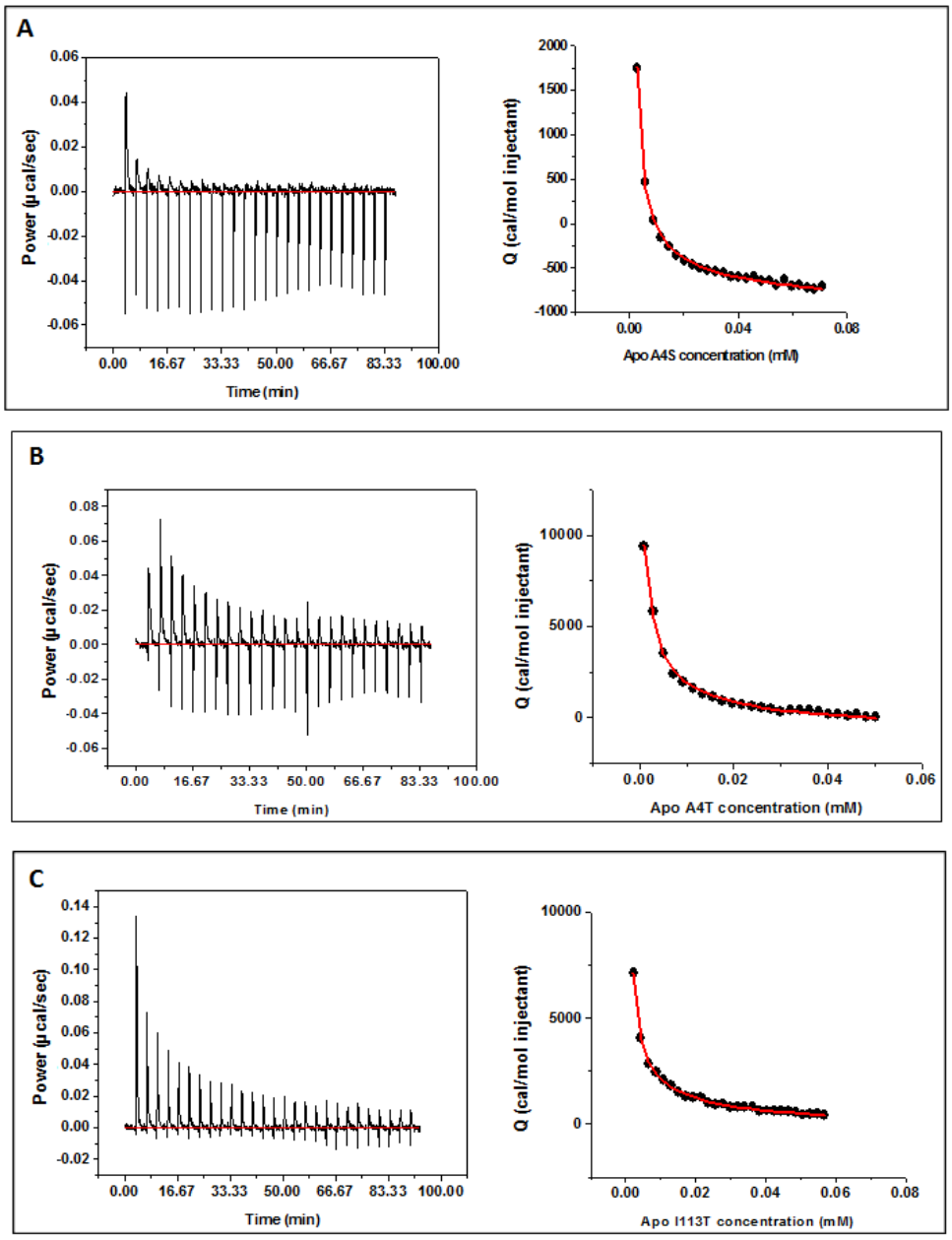

Figure 2.13. Raw ITC traces and integrated heats for A4T, A4S and I113T apo SODs at 37 °C. Raw ITC traces (power *versus* time) with the corresponding plots of heat (*Q*) *versus* concentration of protein after each injection (black closed circles) for the apo SOD dimer interface mutants (A) A4S, (B) A4T and (C) I113T. Each peak in the raw ITC trace (Left panel) represents a small volume injection (0.5 µM) of protein into the ITC cell. The heats (Right panel) is obtained by integrating peaks in the raw ITC trace. The temperature at which the experiments were carried out in all cases is 37°C. Fitting of the data (red solid lines) to a dimer dissociation model (Equation 2.71), yielded parameters presented in Table 2.6. Note that for apo A4T SOD, the first injection was a smaller volume (0.2µL) than subsequent injections, hence a smaller first peak in the raw ITC trace.

Table 2.7: Summary of thermodynamic parameters obtained from fitted parameters in Table 2.6

apo SOD	t (°C)	ΔH_d (kcal mol^{-1})	K_d (μM)	ΔS_d[d] (kcal mol^{-1}K^{-1})	ΔG_d[c] (kcal mol^{-1})
A4V[a]	25	13.0 ± 1.1	1.0 ± 0.2	0.016 ± 0.004	8.2 ± 0.1
A4V[a]	28	18.8 ± 1.3	2.1 ± 0.4	0.036 ± 0.004	7.8 ± 0.1
A4V[b]	30	24.1 ± 2.3	6.2 ± 1.3	0.056 ± 0.008	7.2 ± 0.1
A4V[a]	33	25.6 ± 0.6	5.3 ± 0.4	0.059 ± 0.002	7.4 ± 0.0
A4V[b]	37	32.4 ± 4.4	10.0 ± 3.1	0.08 ± 0.02	7.1 ± 0.2
A4S[b]	37	15.2 ± 3.0	1.6 ± 0.6	0.02 ± 0.01	8.2 ± 0.2
A4T[b]	37	30.9 ± 3.2	5.1 ± 1.2	0.08 ± 0.01	7.5 ± 0.1
I113T[b]	37	26.9 ± 3.0	3.9 ± 0.1	0.06 ± 0.01	7.7 ± 0.1
H46R[b]	37	14.7 ± 1.0	0.5 ± 0.2	0.02 ± 0.00	8.9 ± 0.2
H43R[b]	37	34.2 ± 3.3	0.7 ± 0.2	0.08 ± 0.01	8.8 ± 0.2
G93S[b]	37	30.7 ± 6.4	1.2 ± 0.3	0.07 ± 0.02	8.5 ± 0.2

[a]Values are from individual datasets in Table 6 with errors (±) in calculated thermodynamic parameters propagated using standard procedures (Taylor, 1982). [b]Values are derived from the average of multiple datasets presented in Table 5 with errors (±) calculated from the standard deviation. [c]Calculated from K_d as ΔG_d=-RTlnK_d, where R is the universal gas constant, and T is the temperature of the experiment in K. [d]calculated from (ΔG_d-ΔH_d)/T.

2.4 Discussion

2.4.1 Effects of fALS-associated mutations on apo SOD stability

Previously, the thermal unfolding mechanism and thermodynamic stability of apo mutants at only two locations in the SOD structure (G93 and E100) had been investigated. G93 is located in a tight turn and only this residue is well tolerated at this position, hence it is not surprising that all the known G93 fALS-associated mutations, G93A,D,R,S, and V destabilize SOD (Stathopulos, 2005; Stathopulos et al., 2006). The fALS mutant E100G, located in β strand 6 of the protein, was also found to be destabilizing, presumably due to removal of a salt bridge with K30 (Rumfeldt et al., 2006; Vassall et al., 2006). Despite mutations at both these sites being destabilizing, no evidence of intermediate formation was obtained, and the folding mechanism appeared to adhere, like the PWT control, to a 2-state dimer unfolding mechanism, albeit with high $\Delta H_{vH}/\Delta H_{cal}$ ratios indicating aggregation.

As shown in Figure 1.8, the mutants characterized here are distributed throughout the SOD structure, providing the potential to make more general conclusions regarding thermodynamic unfolding mechanism and stability. Before discussing the thermodynamic consequences of the mutations, it is worth considering their structural context and their predicted effects. H46R and G85R both have been shown to affect metal binding in SOD. In analyzing the structure of H46R SOD, one of the copper binding residues is replaced and as expected H46R has lower affinity for copper; additionally there is significant disorder in the zinc binding loop (Antonyuk et al., 2005). G85 is located in a β bulge of β strand 5 and is not directly involved in metal binding; however, replacement of G85 with R results in an alteration in the conformation of the zinc binding loop leading to reduced Zn binding affinity (Cao et al., 2008). Given that the zinc binding loop is known to be quite disordered in the apo PWT control (Strange et al., 2003),

both H46R and G85R could be expected to have a larger effect on the stability of holo SOD compared to apo SOD. The mutations A4V, T, S and I113T are located in the dimer interface of SOD and so they would be expected to negatively affect dimerization. The crystal structure of A4V reveals that this mutation results in the two SOD monomers in the dimer being twisted relative to each other, similar effects were also seen for I113T but to a lesser extent (Hough et al., 2004). Additionally, the mutation A4V disrupts the conserved residue L106, which is very important in stabilizing each monomer in the SOD homodimer, acting as a "plug" on one side of the β-barrel (Cardoso et al., 2002). Hence, in addition to having an effect on the dimer interface, A4V might also be expected to affect monomer stability. H43 and G37 are in an area of SOD structure where packing interactions are thought to be vitally important. Replacement of both residues with R introduces a more bulky residue that interferes with L38, which plugs the other side of the β-barrel, filling a cavity formed by several apoplar amino acids from different β strands (DiDonato et al., 2003; Hart et al., 1998). These mutations are expected to disrupt the three-dimensional structure of SOD and destabilize the protein. H43R also removes a hydrogen bond with the copper binding residue H120, while G37R significantly disrupts the orientation of the copper binding residues; however, there is little evidence that these mutations affect copper binding affinity (Borchelt et al., 1994; DiDonato et al., 2003; Hart et al., 1998). Based purely on these structural considerations, the mutations studied here can be preliminarily divided into 3 categories: mutations that are expected to affect predominantly metal binding (H46R, G85R); mutations that are expected to affect mainly dimerization (A4V, S, T, I113T); and mutations that affect 3D packing but not necessarily metal binding or dimerization (H43R, G37R).

2.4.1.1 Mutation-induced changes in stability and thermal unfolding mechanism of Apo SOD

When considering the structural contexts of the various SOD mutants, it would be expected that the mutations located far away from the dimer interface (H46R, H43R, G37R and G85R) would be the most likely to exhibit PWT-like behaviour and thermally unfold via a dimer 2-state unfolding mechanism. Conversely, it can be reasonably speculated that mutations occurring in the dimer interface (A4V, A4S, A4T and I113T) may be the most likely candidates for population of a monomeric intermediate due to a possible weakening of the homoaffinity of the two monomers. It was therefore somewhat surprising that two seemingly structurally unrelated mutants, A4V and H46R, populate a monomeric intermediate upon thermal unfolding, while all the other mutations, including the other two A4 mutants unfold via a 2-state mechanism. The results can be rationalized, however, by also taking into account the effects of mutations on monomer stability. A 2-state dimer unfolding mechanism will be observed when dimer dissociation occurs at a temperature where a folded or partially folded monomer is too unstable to be populated. This means that apparent 2-state unfolding will become likely if ΔG_1 is large relative to the total ΔG of unfolding, and/or ΔG_2 is low. This interplay between ΔG_1 and ΔG_2 is illustrated quite well when considering the stabilities of A4V and H46R. While both mutants populate a monomeric intermediate, H46R has a significantly higher ΔG_1, indicating that dimer dissociation will be less favourable. This higher ΔG_1 for H46R is compensated for by the significantly higher ΔG_2, which means that the monomer intermediate is much more stable and hence will remain folded at temperatures where the A4V intermediate will unfold. The fact that apo SOD can populate a monomeric intermediate is physically reasonable given that the dimer interface is not conserved across different organisms and *E. coli* SOD exists naturally as a monomer (Bordo et al., 1999; Bourne et al., 1996; Pesce et al., 1997). Also, a monomer variant of apo SOD has been engineered and shown to be folded, and apo SOD has be found to populate

a monomeric intermediate in kinetic folding studies (Banci et al., 2003; Lindberg et al., 2004; Svensson et al., 2006). Furthermore, disulfide-reduced apo SOD, which is monomeric, is thermally stable in calorimetry experiments (See Chapter 4).

The stability of the apo mutants relative to the PWT is presented in Table 2.5 as $\Delta\Delta G_s$ and indicates the order of stability of the apo mutants as: H46R> PWT>G85R> G37R> H43R> A4S> A4V> I113T> A4T. Previous estimates of stability of 5 of these apo mutants (H46R, G85R, H43R, A4V and I113T) were made by Oliveberg and co-workers based on folding kinetic measurements in urea; the $\Delta\Delta G_s$ are in a similar range to what is presented here, though the order of stability is different (Lindberg et al., 2005). Some discrepancies are expected, given that homodimer stability in that study was only indirectly determined using a combination of estimates of the rates of dimer dissociation and the folding and unfolding rates of the mutants in a monomeric PWT variant background containing charged residues in the dimer interface. The order of stability indicates that, consistent with the expectation that the metal binding mutants would have less of an effect on the apo protein, H46R and G85R are the two most stable mutants in this study. Also, the mutations that are located in the dimer interface appear to generally have a larger negative effect on the overall stability of SOD compared to the mutations that have been purported to affect β sheet packing such as H43R and G37R. Given that β sheet packing is expected to have greater effects on monomer stability than dimer interface strength, this implies that perturbations in the stability of the dimer interface may be the most important determinant in the overall stability of apo SOD.

It is interesting that all SOD mutants in this study increase entropy with compensatory increases in the enthalpy of unfolding; similar trends were previously reported for the apo G93 mutants (Stathopulos et al., 2006). Such entropy-enthalpy compensation is not uncommon in proteins and helps to explain why many protein mutations result in only modest changes in the

overall free energy (Liu et al., 2000; Sturtevant, 1994). It is not immediately apparent based on the structural context of the various SOD mutants why they all increase the enthalpy and entropy of unfolding. The result implies that perhaps the mutations, through altered packing of amino acids, introduce considerable strain in the SOD molecule. Whilst this strain may induce the formation of additional enthalpic contacts in the native state thereby increasing the enthalpy of unfolding, it may also compromise conformational freedom and decrease entropy in the native state leading to an increase in the entropy of unfolding. This idea is supported by molecular dynamic simulations on SOD mutants, which demonstrated that chemically and structurally diverse SOD mutants all cause a loss of dynamic coupling between the two SOD monomers resulting in a reduction of breathing motions (Khare and Dokholyan, 2006). Generally, however, it is difficult to make definitive conclusions on mutation induced changes in enthalpy and entropy due to complicated solvent effects, mainly related to the reorganization of water molecules as the protein changes conformation (Liu et al., 2000; Sturtevant, 1994).

2.4.1.2 Consequences of apo SOD mutations on dimer dissociation propensity

One disadvantage of differential scanning calorimetry is that relatively high protein concentrations are required for the experiments. Typically, it is only possible to obtain data at protein concentrations exceeding 0.05 mg/mL providing that the protein undergoes large changes in enthalpy upon unfolding. For a dimeric/oligomeric protein, a monomeric intermediate will be more populated (as a fraction of total protein) as protein concentration is decreased owing to mass action. Thus, the higher concentrations required for DSC experiments may preclude the identification of a monomeric intermediate, and result in apparent 2-state unfolding (see Figure 2.14). While this 2-state fitting will accurately report on the overall stability of the protein,

information about the dimer interface or monomer stability cannot be obtained. ITC dilution experiments can be advantageous in such cases, in that they can measure the dissociation of the dimer at very low protein concentrations, potentially allowing thermodynamic characterization of dimer dissociation. While ITC dilution experiments on apo PWT SOD did not produce analyzable results there were some small endothermic heats of dissociation observed for the initial injections, hinting that some dimer dissociation is occurring. Given that all the apo SOD mutants by contrast produced several more and much larger heats of dilution which led to analyzable results, it is clear that all the apo SOD mutants negatively affect the strength of the dimer interface. This is an interesting and particularly noteworthy observation, as it cannot be predicted based purely on consideration of the structural contexts of the various mutations studied. For example, G93S, H46R and H43R are all very far from the dimer interface and it is not obvious from inspection of the native structure how or why their effects would propagate to the dimer interface. When analyzing the K_ds and ΔG_d (Table 2.7), however, it is noticeable that the mutations that occur in the dimer interface do have a larger tendency to dissociate.

In considering the structural changes caused by the mutations, it is perhaps not surprising that A4V has the weakest dimer interface among the dimer interface mutants. It has been shown that the structural alterations in the dimer interface caused by A4V result from the addition of a bulkier sidechain and aberrant hydrophobic contacts involving the additional methyl groups (Hough et al., 2004). While A4T introduces a sidechain that is similar in size to V, it presumably cannot make the same incorrect hydrophobic contacts due to the polar nature of T. A4S also introduces a larger residue, however, it is smaller than both V and T. This perhaps explains why it has the least destabilized dimer interface of the A4 mutants, being just a little more destabilized than the non-dimer interface mutant, G93S. As mentioned earlier, the I113T mutant, in comparison to A4V, produces a similar but smaller change in the orientation of the

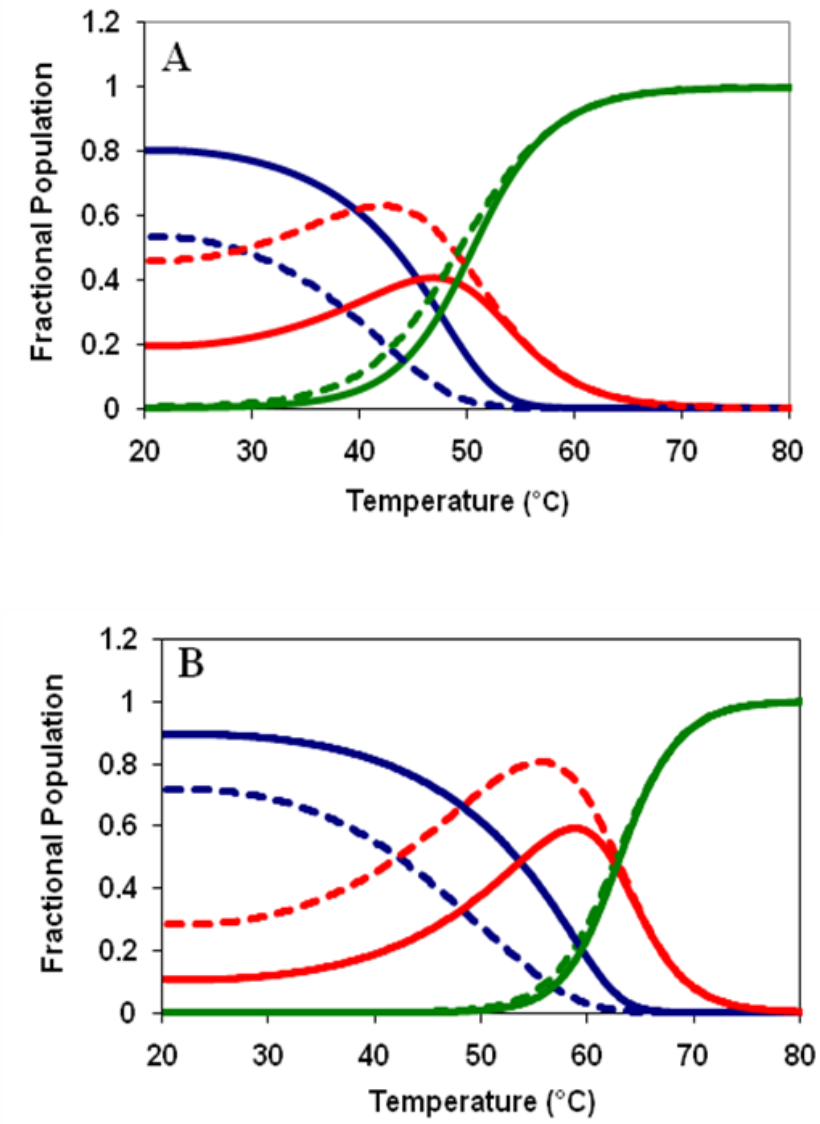

Figure 2.14. The populations of the different species present at equilibrium in thermal unfolding of A4V and H46R apo SODs. The Fractional populations of the native dimer (blue line), monomeric intermediate (red line) and unfolded monomer (green line) for (A) A4V and (B) H46R, determined from the thermodynamic parameters generated from data fitting to a dimer 3-state model with monomer intermediate. Broken lines represent the populations at the lowest concentrations of each mutant (0.2 mg/mL for A4V and 0.077mg/mL for H46R) while solid lines represent the highest concentrations (1.95mg/mL for A4V and 0.76 mg/mL for H46R). The intermediate becomes significantly populated as temperature increases reaching a maximal molar fraction exceeding 0.6 for both mutants at the lower concentrations. The population of intermediate increases as protein concentration decreases as would be expected with the population of a monomeric intermediate.

two monomers of the dimer pair (Hough et al., 2004) and hence the observation that it affects the dimer interface less than A4V is reasonable. Interestingly, previous ITC dimer dilution experiments conducted in 20 mM HEPES, pH 7.8 at 65 °C on holo PWT, holo A4V and holo I113T SODs indicated that while holo PWT SOD does not dissociate under these conditions, both of the mutants did, with holo A4V SOD dissociating more readily than I113T (Stathopulos, 2005). These results are similar to what is reported here for the apo protein at 37 °C and suggest that metal binding may not fully compensate for the effects on the dimer interface caused by these mutations.

Although the monomer stability (ΔG_{mon}) could not be directly determined in these experiments, it can be estimated from the total ΔG (ΔG_{tot}) extrapolated to 37 °C from DSC measurements and ΔG_d from ITC measurements: $\Delta G_{mon}=(\Delta G_{tot}-\Delta G_d)/2$. These estimated stabilities are shown in Figure 2.15. For H46R and A4V, the ΔG_2 from DSC fitting, which is equivalent to the monomer stability, is presented. Except for H46R, which has a monomer stability of 4.75 kcal mol^{-1}, in all cases, the monomer is only marginally stable with free energies generally being close to 1.5 kcal mol^{-1} for G93S and A4V and less than 1 kcal mol^{-1} for the other mutants. The overall order of monomer stability from this analysis is H46R>G93S>A4V>A4S>A4T>I113T>H43R. The particularly low monomer stabilities for the dimer interface mutations A4S, A4T and I113T help explain why, despite having K_d values higher than the non-dimer interface mutants, they do not populate an intermediate in DSC measurements.

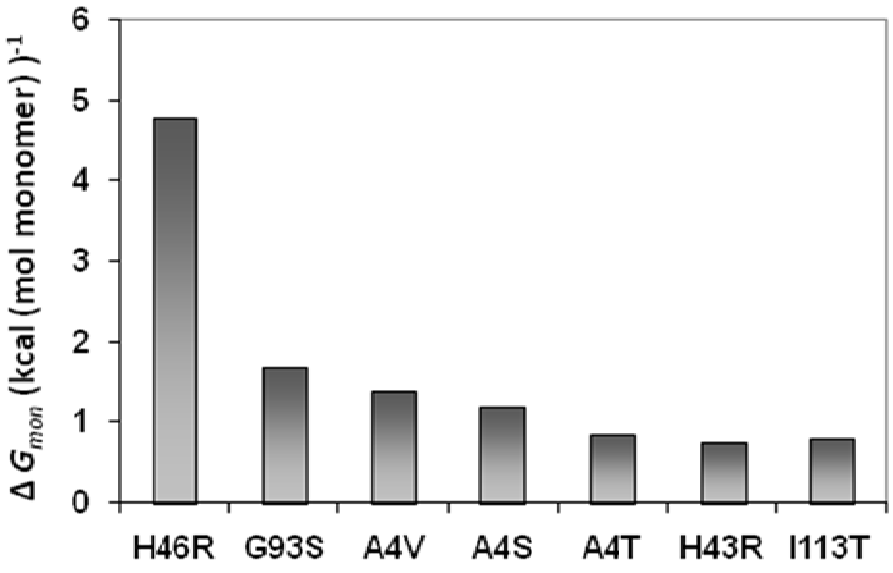

Figure 2.15. Estimation of monomer stability from DSC and ITC data for apo SOD mutants. Bar graph showing the estimated monomer stability (ΔG_{mon}) of fALS-associated SOD mutations calculated from the total stability (ΔG_{tot}) from DSC data and the dimer interface stability (ΔG_d) from ITC data at 37°C ($\Delta G_{mon}=(\Delta G_{tot}-\Delta G_d)/2$) (Table 2.4 and 2.7). For A4V and H46R, the monomer stability presented is the ΔG_2 obtained from data fitting DSC data to a 3-state monomer intermediate model.

2.4.2 Implications for SOD aggregation and ALS

Of central importance in combating SOD-mediated ALS is a deciphering of the mutation-driven mechanisms that can transform a benign molecule into a precursor of toxic cellular aggregates. Given that aggregation has been shown to be enhanced by loss of native structure (Chiti and Dobson, 2006), it is expected that SOD requires some conformational change prior to aggregation. Destabilization of the protein will make the transformation of the native structure to an aggregation-prone precursor more thermodynamically favorable. It is thus interesting and noteworthy that all holo fALS-associated SOD mutations studied to date have been found to be destabilizing (Rumfeldt et al., 2009; Rumfeldt et al., 2006; Stathopulos et al., 2006). However, despite this destabilization, holo SOD mutants are still highly stable, with temperatures of melting often greater than 85°C and stabilities generally exceeding 25 kcal mol^{-1} at 37 °C (Stathopulos et al., 2006). For this reason, attention has been focused on the less stable apo forms, which generally have melting temperatures up to 40°C lower and roughly half the ΔG of unfolding compared to the holo protein (Stathopulos et al., 2006). Furthermore, aggregation studies on SOD demonstrated that metal loss from the holo protein is a precursor to SOD aggregation, providing direct evidence that the apo form of the protein could be very important (Khare et al., 2004). Additionally, it has been shown that the apo protein, compared to the holo protein, shows a greater tendency to aggregate based on van't Hoff to calorimetric enthalpy ratios greater than 1 when thermal unfolding traces are fit to a 2-state dimer unfolding model (Stathopulos et al., 2006). High ratios were also seen here for several of the mutants studied. Unlike the holo protein however, it had been suggested through apparent melting temperatures but never before verified through thermodynamic equilibrium measurements that some metal binding mutations, including apo H46R, are not destabilized relative to apo WT (Rodriguez et al., 2005). The thermodynamic data presented here for H46R corroborates this suggestion and

implies that that an overall reduction in thermodynamic stability of the apo protein cannot be the only causative factor for SOD-associated fALS (Valentine et al., 2005). Indeed, it has been suggested that other factors such as alterations in protein net charge, local conformational fluctuations, and changes in β sheet propensity and hydrophobicity are also very important (Meiering, 2008; Sandelin et al., 2007; Shaw and Valentine, 2007; Wang et al., 2008).

In considering thermodynamic unfolding data, perhaps of greater importance than the overall stability of the protein is the thermodynamic stability of the dimer interface, which measures the ease of dimer dissociation. Several studies have suggested that monomerization is required as a precursor to SOD aggregation (Chattopadhyay et al., 2008; Khare et al., 2004; Rakhit et al., 2004). Furthermore, molecular dynamics simulations have identified residues at both SOD polypeptide chain termini as well as residues including 113-115 as having high aggregation propensity (Khare et al., 2005). These regions are sequestered when the protein is dimeric but become exposed upon dimer dissociation. Exposed dimer interfaces have been indentified in protein aggregates in fALS patients by antibody binding studies, which provides additional support for an important role of dimer dissociation (Rakhit et al., 2007). Dissociation of the SOD dimer, as shown here and in other studies, can liberate the monomer, which has low thermodynamic and kinetic stability (Lindberg et al., 2004; Svensson et al., 2006). The low stability might make the apo monomer more structurally malleable, enabling it to undergo the conformational changes required for aggregation. Structural studies on a monomeric variant of apo SOD have shown that the monomer is significantly less well structured than the apo homodimer (Banci et al., 2003). A loss of overall compactness in the apo monomer is also seen here when looking at the ΔC_p of dimer dissociation of apo A4V through Kirchoff analysis (Figure 2.11). The ΔC_p of 1.60 kcal $mol^{-1}K^{-1}$ for dimer dissociation is almost half of the previously determined total ΔC_p of unfolding for apo SOD, implying a significant increase in

solvent exposure upon dimer dissociation. Additionally and perhaps most importantly, the results presented here suggest that a decrease in the dimer interface stability could be a ubiquitous property of SOD mutants at least when in the apo form. Our results provide key experimental support for previous molecular dynamic simulations carried out on over 70 fALS-associated SOD mutations, which found that the dimer interface is destabilized in the vast majority of mutants (Khare et al., 2006). An aggregation mechanism that begins with the formation of monomer would not be unique to SOD. Another protein, the tetrameric transthyretin, which causes familial amyloid polyneuropathies through the formation of toxic aggregates, must dissociate to monomers prior to aggregation (Johnson et al., 2005). Perhaps one strategy that could be used to treat SOD-mediated ALS is to stabilize the SOD dimer by binding a molecule across the dimer interface (Ray and Lansbury, 2004). Such an approach is supported by the findings that both the introduction of an intermolecular disulfide bond in A4V and the binding of various molecules to the dimer interface of a limited number of fALS SOD mutants stabilized the protein and reduced or eliminated *in vitro* aggregation (Ray et al., 2005; Ray et al., 2004).

Chapter 3: Thermodynamic analysis of disulfide-intact apo superoxide dismutases using equilibrium GdmCl denaturation

This chapter is based largely on previously published work. As an author I have permission to reproduce the article in part or whole for a dissertation or thesis providing that the following be stated:

"Reproduced (or reproduced in part) with permission from Vassall, K.A., *et al.,* Equilibrium thermodynamic analysis of amyotrophic lateral sclerosis-associated mutant apo Cu,Zn superoxide dismutases. Biochemistry, 2006. **45**(23): p. 7366-79. Copyright, 2006, American Chemical Society."

Acknowledgements

I would like to thank Jarrod Johnson for measuring E100G chemical denaturation curves in the absence of sodium sulphate, and Colin Campbell for assistance with Matlab.

3.1 Introduction

In the previous chapter, the thermodynamic stability of a variety of mutant apo SODs was probed by measuring thermal unfolding using differential scanning calorimetry. While DSC is very useful for measuring thermodynamic parameters, its relative lack of sensitivity means that fairly high concentrations of apo SOD are required in these experiments. The use of high protein concentrations can mask the formation of a monomeric intermediate, preventing the characterization of a potentially important aggregation-prone intermediate. In this chapter,

thermodynamic analyses of apo PWT SOD and mutants are presented using equilibrium guanidinium chloride (GdmCl) denaturation curves monitored by circular dichrosim (CD) and fluorescence spectroscopy. The higher sensitivity of optical probes allows protein unfolding to be experimentally measurable at significantly lower protein concentrations, presenting an opportunity to thermodynamically characterize a potentially sparsely populated monomeric intermediate, which has been implied by ITC studies (Chapter 2) and prior kinetic studies (Lindberg et al., 2004). Additionally, this technique allows us to independently verify the results from DSC studies, and complements similar GdmCl denaturation experiments completed by others in this laboratory on holo PWT SOD and mutants (Rumfeldt et al., 2006).

3.1.1 CD and Fluorescence spectroscopy

Both CD and fluorescence spectroscopy have been used extensively to monitor protein folding for many different proteins. CD spectroscopy measures the differences in absorbance of left and right circularly polarized light by chiral molecules (Woody and Dunker, 1996). The far UV regions of CD spectra (< 250 nm) are sensitive to changes in protein secondary structure (Woody and Dunker, 1996). Monitoring changes in the near UV region gives information regarding aromatic side chains and disulfide bonds and is useful for observing changes in tertiary structure (Woody and Dunker, 1996). CD spectra of holo and apo SOD are very similar and both exhibit minima at ~ 210 nm (Silva et al., 1993) typical of β-sheet proteins. Importantly, there are key differences in the CD spectra depending on the conformation of SOD (Figure 3.1A). The characteristic minimum shifts to higher ellipticity values upon unfolding of the protein. Additionally, there are key changes at ~230 nm where there is a decrease in ellipticity as the protein unfolds.

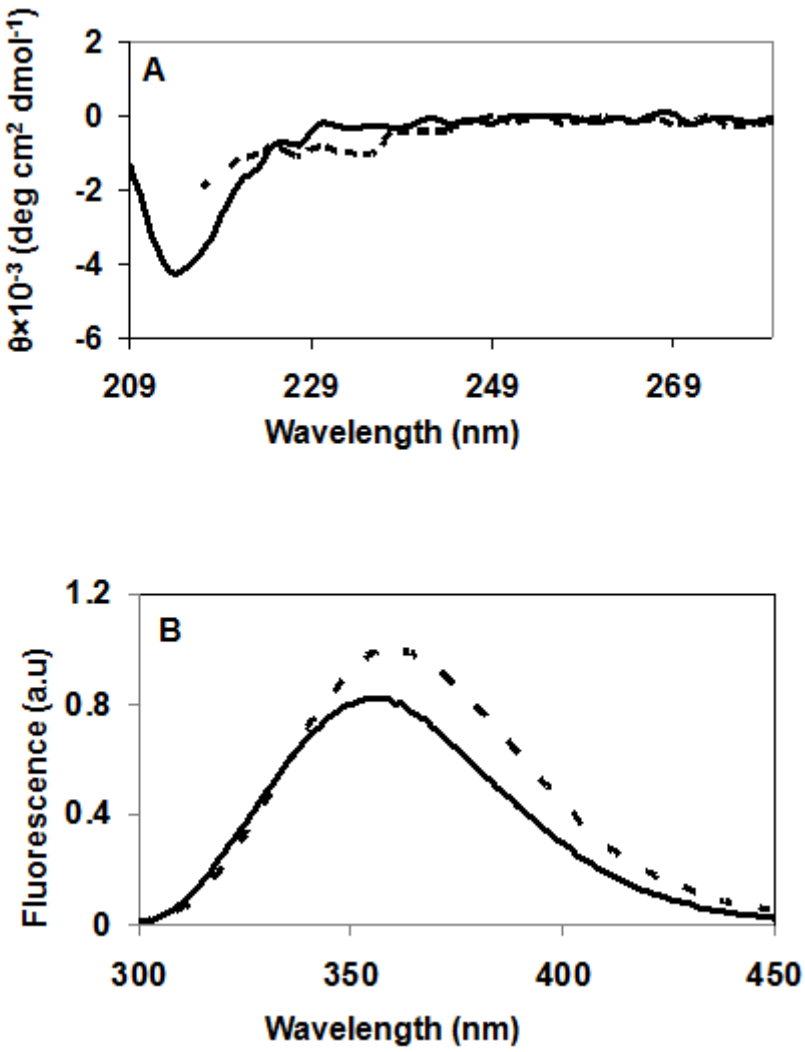

Figure 3.1. CD and fluorescence spectra of folded and unfolded apo SOD. Spectra of folded apo SOD (solid lines) were acquired in 20mM HEPES, pH 7.8 while spectra of unfolded protein (broken lines) were acquired in 4.5M GdmCl, 20 mM HEPES, pH 7.8. Both (A) CD and (B) fluorescence spectra were acquired at 25 °C with buffer spectra subtracted. CD data were collected on a Jasco J715 spectropolarimeter (JASCO Inc., Easton, MD) using a 0.1 cm pathlength cuvette and a 1 nm bandwith. Data for unfolded SOD could only be collected down to 214 nm due to saturation of the detector at lower wavelengths. Fluorescence data were collected on a Fluorolog 3-22 (Instruments SA, Edison NJ) with a 1 cm pathlength cuvette; slit widths for excitation and emission were 1 nm and 5 nm, respectively, and the excitation wavelength was 282 nm.

Electrons in an intrinsic chromophore within a protein can absorb radiation and be excited from the ground state to an excited state. Fluorescence spectroscopy measures the radiation emitted when these electrons fall to lower energy levels (Hof et al., 2005). Intrinsic chromophores in proteins are the aromatic amino acids tryptophan, phenylalanine and tyrosine. SOD contains 1 tryptophan and 4 phenylalanines per subunit; of these intrinsic chromophores, tryptophan makes the most predominant contribution to the emission fluorescence spectrum (Lakowicz, 2006). Intrinsic fluorescence spectra of apo SOD, acquired by exciting the protein at 282 nm and measuring fluorescence between 300 and 450 nm both in a folded and unfolded conformation are shown in Figure 3.1B. Upon unfolding, the wavelength of maximum Trp fluorescence signal is slightly red shifted from ~ 354nm to ~ 360nm and the maximum signal is increased.

3.1.2 Optically measured equilibrium denaturation curves

The changes in CD and fluorescence signal upon unfolding of apo SOD (described in the previous section) are convenient ways to monitor the progress of a protein unfolding reaction. Protein can be systematically denatured by altering conditions such as pH, heat, or by adding chemical denaturants such as urea or, as in the case of this study, guanidinium chloride (GdmCl).

A denaturation curve at is composed of three regions: a native or pre-transition baseline, an unfolded or post-transition baseline, and a transition region (Figure 3.2). The native and unfolded baselines are measures of the dependence of the optical signal of the fully folded protein and fully unfolded protein, respectively, on denaturant concentration. While

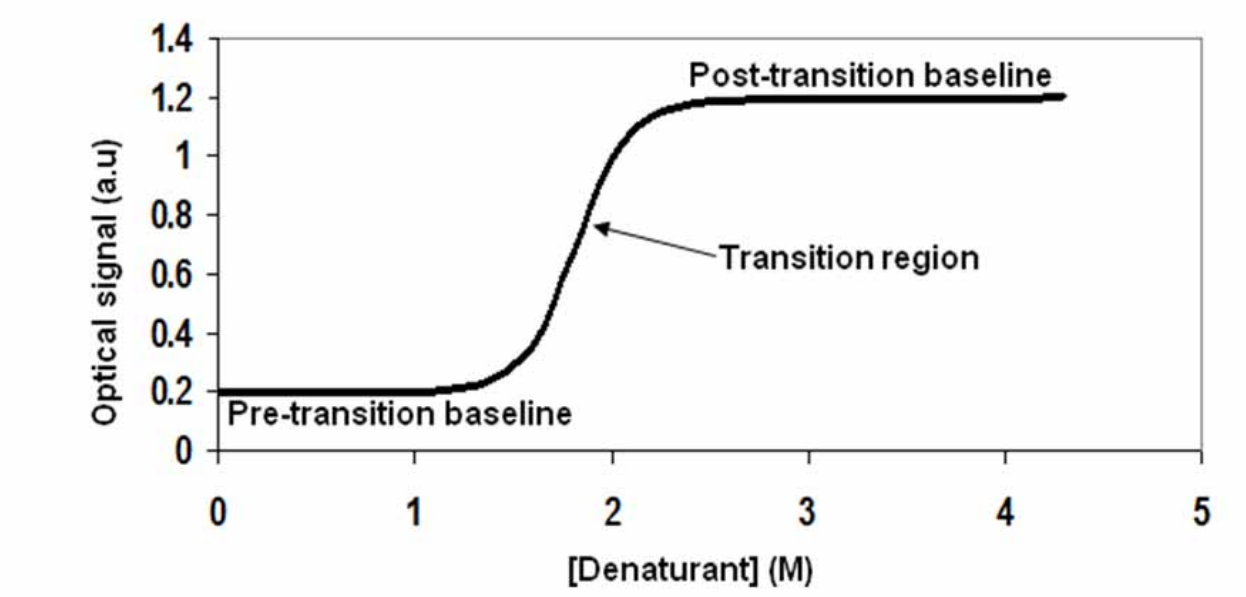

Figure 3.2. Typical features of a denaturation curve monitored by change in optical signal. In the region of the pre-transition baseline, the protein is in a native conformation. In the transition region, the denaturant concentration is sufficiently high that the protein begins to unfold while in the post-transition baseline region the protein is fully unfolded.

the baselines represent protein in either a fully folded or fully unfolded conformation, the transition region represents a mixture of the 2 conformations. At the beginning of the transition, the protein is still mostly native, however, relatively small increases of denaturant are needed to effect the transformation to fully unfolded protein. The sensitivity of the protein to increasing denaturant concentration in the transition region is an indication of the cooperativity of unfolding. A steeper transition region generally reflects more cooperative unfolding while the converse is true for a more shallow transition (Tanford, 1970)

3.1.2.1 Dimeric protein unfolding

As for measurement of thermal unfolding by DSC (Section 2.1.1), the nature of the folding mechanism of a dimeric protein may be elucidated by observing the changes in the shape of a denaturation curve as a function of protein concentration (Rumfeldt et al., 2008) (Figure 3.3). In the case of a strictly 2-state transition ($N_2 \leftrightarrow 2U$, where N_2 is native dimer and U the unfolded monomer), curves obtained at all concentrations will be identical in shape; the curves will be monophasic with only a single observable transition. However, there will be a systematic increase in the midpoint of unfolding (denaturant concentration at half unfolding) as protein concentration increases (Figure 3.3A).

For slightly more complex dimer unfolding mechanisms, involving the population of a dimeric ($N_2 \leftrightarrow I_2 \leftrightarrow 2U$) or monomeric ($N_2 \leftrightarrow 2I \leftrightarrow 2U$) intermediate ($I$), curves at some protein concentrations can exhibit biphasic character with two distinct transitions (Figures 3.3B and 3.3C). The first of these transitions describes the reaction whereby the protein goes from a native conformation to a partially unfolded intermediate conformation and the second describes the transition from intermediate to the unfolded protein. The two mechanisms have distinct

protein concentration dependence of denaturation curves. For the population of a monomeric intermediate, the first transition will be concentration-dependent because this step involves a change in molecularity of the protein, while for a dimeric intermediate, the second transition will be concentration dependent (Figure 3.3B and 3.3C). These distinctive differences in the character of denaturation curves due to the mechanism of unfolding were utilized in these studies by measuring denaturation curves as a function of concentration for both PWT and mutants.

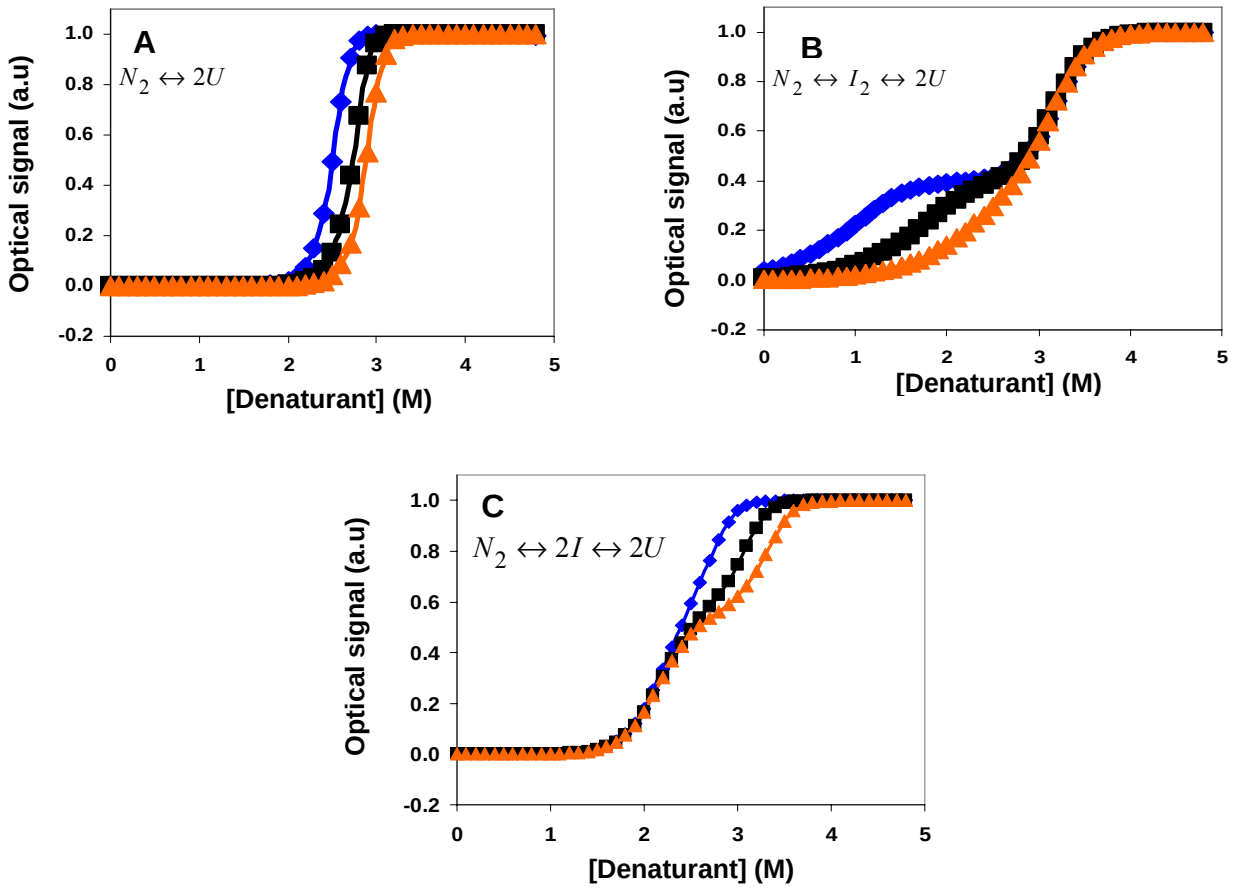

Figure 3.3. 2-state and 3-state equilibrium dimer unfolding models. Simulated concentration dependence of chemical denaturation for a dimeric protein. Protein concentrations used in the simulation are 0.2 μM (blue), 5 μM (black) and 50 μM (orange). (A) Concentration dependence for 2-state dimer unfolding. The curves are monophasic and the shape of the curves are independent of protein concentration. For the simulation, ΔG_{tot} was set to 30 kcal (mol dimer)$^{-1}$ while m was set to 8.5 kcal (mol dimer)$^{-1}$M^{-1}. (B) Concentration dependence for 3-state dimer unfolding with a monomeric intermediate. The curves are biphasic, particularly at lower protein concentration, indicating the two transitions corresponding to dimer dissociation followed by monomer unfolding. The first transition is protein concentration-dependent, because it involves a change in molecularity while the second transiton which does not involve a change in molecularity is protein concentration independent. For the simulation, parameters of ΔG_1 and ΔG_2 were set to 11 kcal (mol dimer)$^{-1}$ and 9.5 kcal (mol monomer)$^{-1}$ respectively while m_1 and m_2 were set to 2.5 kcal (mol dimer)$^{-1}$M^{-1} and 3 kcal (mol monomer)$^{-1}$M^{-1} respectively. (C) Concentration dependence for 3-state dimer unfolding with a dimeric folding intermediate. There is increasing biphasic character in the curves as protein concentration increases, indicating an increase in the population of intermediate at high protein concentration. The first transition corresponds to native dimer unfolding to a dimeric intermediate and is protein concentration-independent. The second transition corresponds to unfolding of the dimeric intermediate to 2 unfolded monomers and hence this step is protein concentration dependent. For the simulation ΔG_1 and ΔG_2 were set to 6.5 kcal (mol dimer)$^{-1}$ and 23.5 kcal (mol dimer)$^{-1}$ while m_1 and m_2 were set to 3 kcal (mol dimer)$^{-1}$ M^{-1} and 5.5 kcal (mol dimer)$^{-1}$ M^{-1} respectively.

3.2 Materials and Methods

3.2.1 Equilibrium Chemical Denaturation and Renaturation Curves.

Apo SOD was prepared and protein concentration was measured as described in Section 2.2.2 and 2.2.3 respectively. Equilibrium denaturation curves were obtained for apo PWT and mutants by diluting 10x concentrated stock protein into solutions containing HEPES and different concentrations of the denaturant GdmCl. The final concentration of HEPES was 20 mM, pH 7.8. For curves obtained in sodium sulphate, this was added to the mixture to a final concentration of 0.75 M. Samples were equilibrated at 25 °C by incubating in a temperature-controlled water bath. Renaturation curves were acquired using the same methodology, with the exception that the stock protein solution was first denatured in 4 M GdmCl before dilution into the appropriate solutions. Circular dichroism (CD) measurements at 216 and 231nm were carried out using a J715 CD spectropolarimeter (JASCO Inc., Easton, MD.) equipped with a Peltier temperature controlled cell holder. Steady state fluorescence measurements were made using a Fluorolog 3-22 (Instruments SA, Edison NJ) with a thermostated water-jacketed cuvette holder, with excitation and emission wavelengths of 282 nm and 360 nm, respectively.

3.2.2 GdmCl Curve Analysis

Chemical denaturation data were fit to equations for a dimer 2-state model and 3-state models with monomer or dimer intermediate (Park and Bedouelle, 1998; Rumfeldt et al., 2008).

3.2.2.1 Equations

The optical signal of each probe (CD or fluorescence) Y_o, is proportional to the intrinsic signal of each species *i* present at equilibrium such that:

$$Y_o = \sum X_i Y_i \tag{3.1}$$

where, X_i is the mole fraction of each species and Y_i is its spectroscopic signal. The signal of each species varies linearly with [GdmCl] such that:

$$Y_i = Y_{H_2O,i} + s_i[\text{GdmCl}] \tag{3.2}$$

where, $Y_{H_2O,i}$ is the signal of a particular species *i* at 0M GdmCl and s_i describes the dependence of the signal on [GdmCl]. From the mole fractions of each species *i*, the equilibrium constant of unfolding, *K* and hence ΔG can be determined at each [GdmCl]. The ΔG at 0M GdmCl can then be determined based on extrapolation, assuming a linear dependence of ΔG (Tanford, 1970) with [GdmCl] such that:

$$\Delta G = -RT\ln K = \Delta G_{H_2O} + m[\text{GdmCl}] \tag{3.3}$$

where ΔG_{H_2O} is the Gibbs free energy at 0M GdmCl, *m* describes the magnitude of the dependence of ΔG on [GdmCl], *R* is the universal gas constant and *T* is the absolute temperature in Kelvin.

In a dimer 2-state model, only the native (N_2) and the unfolded (U) states of the protein are populated at equilibrium ($N_2 \leftrightarrows 2U$). The equilibrium constant *K* for this process is defined as:

$$K = \frac{[U]^2}{[N_2]} \tag{3.4}$$

Equation 3.1 can be expressed with respect to equilibrium constant *K* and total protein concentration *P* (expressed as concentration of dimers in M):

$$Y_o = Y_n\left(1 - \left(\frac{\sqrt{K^2 + 16KP} - K}{8P}\right)\right) + Y_u\left(\frac{\sqrt{K^2 + 16KP} - K}{8P}\right) \tag{3.5}$$

where Y_n and Y_u are the spectroscopic signals for the native (N_2) and the unfolded (U) states, respectively.

In a 3-state model, either a monomer intermediate (I) or a dimer intermediate (I_2) are also populated at equilibrium. For the 3-state monomer intermediate model ($N_2 \leftrightarrows 2I \leftrightarrows 2U$), the 2 equilibrium constants K_1 and K_2 that define each unfolding step are given by :

$$K_1 = \frac{[I]^2}{[N_2]} \tag{3.6}$$

and

$$K_2 = \frac{[U]}{[I]} \tag{3.7}$$

Equation 3.1 is defined in terms of K_1, K_2 and P such that the final equation used for fitting is:

$$Y_o = \left(Y_n + \left(Y_j - Y_n + K_2\left(Y_u - Y_n\right)\right)\left(\frac{\sqrt{K_1{}^2(1+K_2)^2 + 16K_1P} - K_1(1+K_2)}{8P} \right) \right) \tag{3.8}$$

where the subscripts n, j and u indicate native dimer, intermediate and unfolded monomer, respectively.

In the 3-state model with dimer intermediate ($N_2 \leftrightarrows I_2 \leftrightarrows 2U$), the equilibrium constants K_1 and K_2 are given by:

$$K_1 = \frac{[I_2]}{[N_2]} \tag{3.9}$$

and

$$K_2 = \frac{[U]^2}{[I_2]} \tag{3.10}$$

Data were fit to:

$$Y_o = \left(Y_u + \left(Y_n - Y_u + K_1 \left(Y_j - Y_u \right) \right) \left(\frac{1 - \left(\frac{\sqrt{(K_1 K_2)^2 + 16(1 + K_1)(K_1 K_2)P} - K_1 K_2}{8P(1 + K_1)} \right)}{1 + K_1} \right) \right) \qquad (3.11)$$

3.2.2 Data Fitting

Fits to individual GdmCl curves were performed using MATLAB software, version 7.0.4 (The MathWorks Inc., Natick, MA.), while global fits for multiple curves were performed with Origin 5.0 SR2 (Microcal Inc., Northampton, MA.). Due to the many parameters inherent to these models, the fitting programs could not provide an accurate fit if all were allowed to vary. The following steps were taken to address this. The slope and intercept of the native and unfolded baselines were first fit using linear regression analysis and fixed in subsequent fitting. The native baseline is most pronounced and least scattered for the highest concentration curves. Hence, the slope and intercept for the native baseline of the highest concentration curves of each dataset were used for lower protein concentrations with appropriate scaling. CD data tended to be more scattered than fluorescence data, which made linear regression analysis of the native baseline less accurate. Hence, given that several high protein concentration CD curves (30μM) were acquired, the native baseline used in fitting was an average slope and intercept from all these curves.

Despite the above simplifications, fits of individual datasets to 3-state models were precluded due to large errors reported by the fitting programs. However, multiple datasets could be accurately fit simultaneously with ΔG and m values as globally shared parameters. CD and fluorescence datasets were considered separately for the global fits. In all 3-state monomer

intermediate fits, the slope of the intermediate was set to 0. For fluorescence data acquired in sodium sulphate, the signal of the intermediate was set to a value of 30% of the total amplitude (unfolded signal – native signal) of the transition. This value of 30% was determined by globally fitting the 1, 5, 10 and 30 μM fluorescence datasets of apo PWT SOD in 0.75 M Na_2SO_4, and systematically changing the magnitude of the intermediate signal from 10-80% of the total amplitude of the transition. The value of 30% corresponded to the lowest chi squared value for fitting. Due to the lower population of intermediate and the less pronounced native baselines of denaturation curves acquired in the absence of sodium sulphate, determination of the intermediate fluorescence value was less accurate. This was compounded by non-linear native baseline effects resulting from GdmCl (see section 3.3.2). Hence, the better defined intermediate fluorescence value of 30% obtained from fitting data collected in sodium sulphate was also used for data without sodium sulphate. For CD data, the intermediate is ill-defined likely due to the increased scatter of the data and the higher protein concentrations that were required (owing to the lower sensitivity of the probe). Varying the intermediate value from 20-80% produced little variation in m and ΔG (~10%). The value of 30% was therefore used for all 3-state monomer intermediate fits. It should be noted that the signal for the intermediate will not in general be the same when measured by different optical probes; however, the approach taken above is experimentally reasonable and has little effect on the fitted values.

For the determination of ΔGs (Table 3.1) for all probes using a 3-state monomer intermediate model, data obtained in 0.75M Na_2SO_4 were fit to a fixed m_1 (the dependence of the free energy of dimer dissociation, ΔG_1, on denaturant concentration) value of 1.4 kcal (mol dimer)$^{-1}$ M^{-1} and a fixed m_2 (the dependence of the free energy of intermediate unfolding, ΔG_2, on denaturant concentration) value of 3.5 kcal (mol monomer)$^{-1}$ M^{-1}. These m values were determined by globally fitting each apo SOD mutant and apo PWT SOD datasets from all 3

probes (fluorescence, CD 216nm and CD 231nm) and averaging the resulting *m* values. For the PWT datasets without sodium sulphate, the *m* values were best defined by the fluorescence results, thus the values of m_1 = 2.7 kcal (mol dimer)$^{-1}$ M^{-1} and m_2 = 2.6 kcal (mol monomer)$^{-1}$ M^{-1} obtained from the fluorescence global fit were also used for fitting CD datasets. Regardless of the intermediate and *m* values used in fitting, the 3-state model with dimer intermediate did not account well for the data across all 3 probes in this study.

3.3 Results

3.3.1 Denaturation of apo PWT is highly reversible

Chemical denaturation of apo PWT and mutant apo SODs by GdmCl in 20mM Hepes, pH 7.8, 25 °C is highly reversible as evident from the congruence of denaturation and renaturation curves (Figure 3.4). Denaturation curve samples typically required as little as 4hrs of incubation to reach equilibrium while renaturation took slightly longer, reaching equilibrium after 24 hrs (Figure 3.4). Similarly, chemical denaturation of holo SODs has been found previously to also be highly reversible under these conditions; however, the holo proteins take much longer (many days) to reach equilibrium (Rumfeldt et al., 2006). The shape of the apo SOD curves is similar to curves obtained for holo SOD, with a sigmoidal shape indicating cooperativity, but the former are shifted by >2 M to lower GdmCl concentrations indicating significant destabilization. As expected for a dimeric protein, the curves depend significantly on protein concentration, with transition midpoints shifting to higher GdmCl concentration with increasing protein concentration (Figures 3.5).

3.3.2 Apo mutants: G85R, E100G, G93R and I113T are destabilized

Similarly to apo PWT SOD, chemical denaturation curves were measured for the apo mutants G85R, E100G, G93R and I113T (Figure 3.6). The mutants are clearly destabilized as evident from significantly lower apparent midpoints of denaturation. Based on these midpoints, the order of stability is PWT>G85R=E00G>G93R>I113T. As a consequence of destabilization, the mutants have significantly shorter pre-transition (native) baselines which are largely ill-

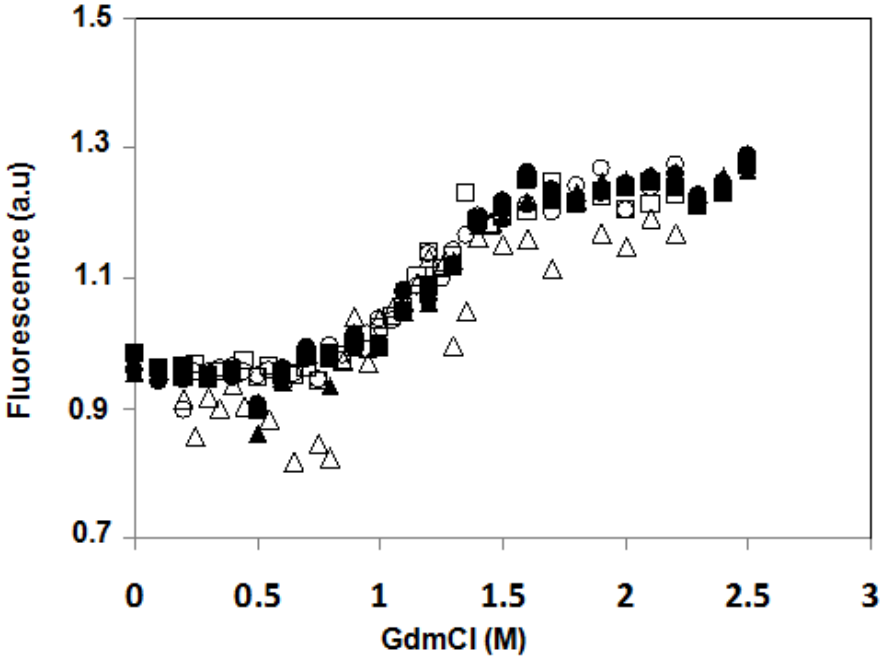

Figure 3.4. Apo PWT denaturation and renaturation curves measured by fluorescence as a function of time. Curves were measured at 4 (triangles), 24 (squares) and 48 (circles) hours after dilution. Denaturation and renaturation data are represented as closed and open symbols, respectively. Both denaturation and renaturation curves are highly coincident after 24 hrs indicating a highly reversible equilibrated system.

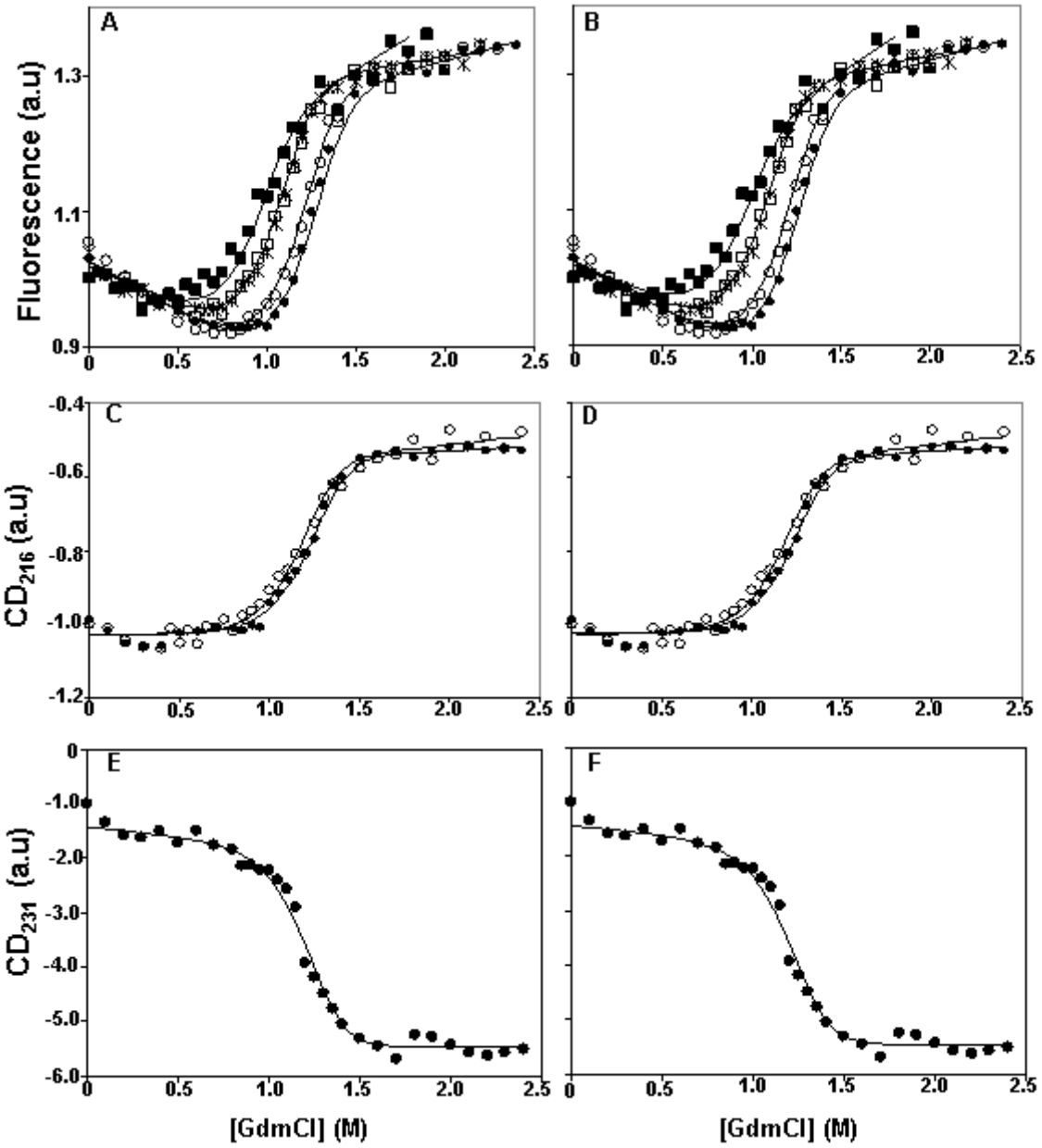

Figure 3.5. Protein concentration dependence of equilibrium denaturation curves for apo PWT, in 20 mM HEPES, pH 7.8, 25 °C. Samples were measured after a minimum of 48 hrs of incubation to ensure sufficient time for equilibrium. Protein concentrations are: 0.2 μM (■), 1 μM (∗), 5 μM (○) and 10 μM (●). A 1 μM renaturation curve (□) is also shown to illustrate the reversibility of unfolding. Data are scaled for differences in protein concentration to facilitate comparison. Curves were monitored by: (A,B) fluorescence; (C,D), CD at 216 nm; and (E,F) CD at 231 nm. The lines correspond to fits (Table 3.1) for each optical probe to a dimer 2-state model (A,C,E) and a 3-state model with monomer intermediate (B,D,F). Multiple datasets for each probe were fit globally.

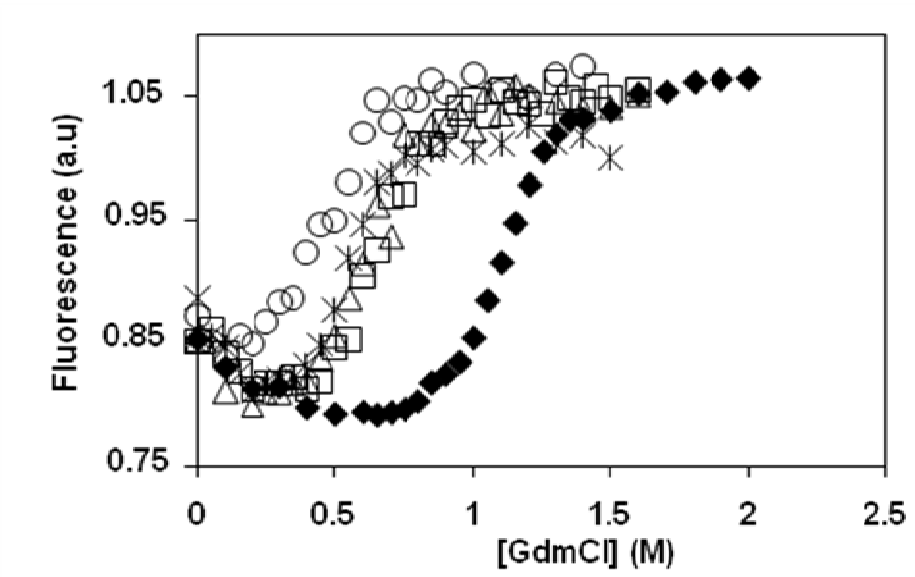

Figure 3.6. Equilibrium denaturation curves for apo PWT and mutant SODs. Curves were measured after a minimum of 24 hrs of incubation by fluorescence at 25 °C in 20mM HEPES, pH 7.8 at a protein concentration of 1μM for I113T (○), G93R (∗), G85R (Δ), E100G (□) and PWT (♦).

defined. Additionally, the native baselines appear to exhibit slight curvature; similar non-linear effects were also observed for fluorescence curves of the holo proteins at low [GdmCl] (>1 M), however, NMR analysis demonstrated that these changes in fluorescence do not correspond to a major structural transition (Rumfeldt et al., 2006). These non-linear effects could be related to protein sticking to the sides of the cuvette at low denaturant concentration.

3.3.3 Sodium Sulphate Markedly Stabilizes PWT and Mutant Apo SODs

Owing to the largely ill defined baselines of mutant apo SODs, which would complicate quantitative thermodynamic analysis, GdmCl denaturation curves for both PWT and mutants were also measured with the addition of the stabilizing agent, sodium sulphate. Similarly to data acquired in the absence of sodium sulphate (see section 3.3.1), denaturation of both PWT and mutant proteins is highly reversible in 0.75 M sodium sulphate, with equilibrium occurring within 48 hrs as evaluated by denaturation and renaturation curves being highly coincident (Figures 3.7 and 3.8). The addition of 0.75 M sodium sulphate increases the mid-point of chemical denaturation by ~1.9 M GdmCl (Figure 3.5 and 3.7). This results in a much better defined pre-transition baseline, enabling a more accurate thermodynamic analysis (see below). As is the case for curves in the absence of sodium sulphate (section 3.3.2), there are slight non-linear effects in the pre-transition baseline at low denaturant, with the effect being most apparent for the mutant I113T (Figures 3.7 and 3.8). These non-linear effects are more apparent for curves measured by fluorescence and are largely absent in CD curves (Figures 3.7, 3.8 and 3.9).

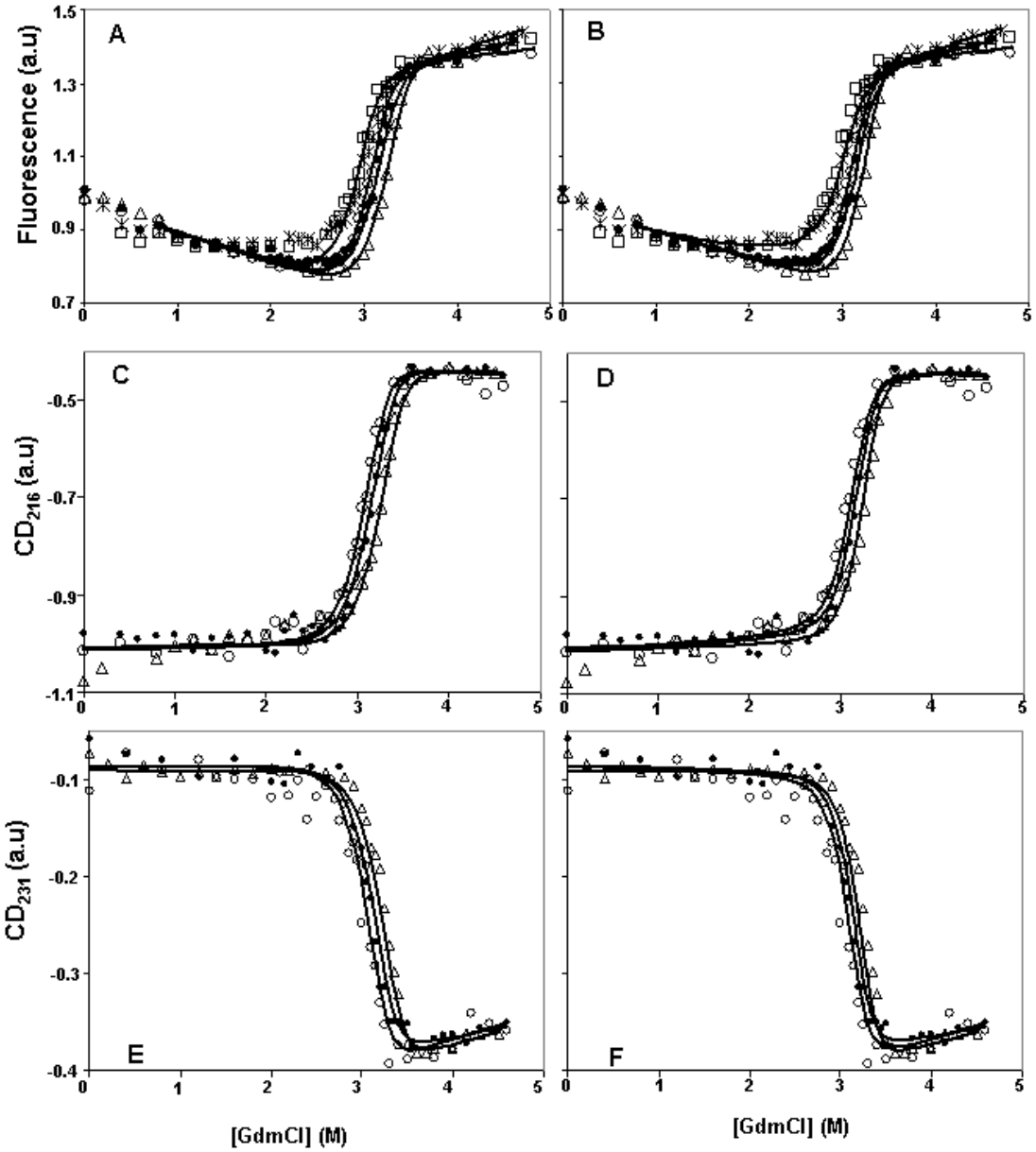

Figure 3.7. Protein concentration dependence of equilibrium denaturation curves of apo PWT SOD in 0.75M sodium sulphate, 20 mM HEPES, pH 7.8, 25 °C. Samples were measured after a minimum of 48 hrs of incubation to ensure sufficient time for equilibrium. Protein concentrations are 1μM (∗), 5μM (○), 10μM (●), and 30μM (Δ). A 1 μM renaturation curve (□) is also shown. Data are scaled for differences in protein concentration to facilitate comparison. Lines corresponding to global dimer 2-state (A,C,E) and 3-state monomer intermediate (B,D,F) fits for curves monitored by fluorescence (A,B), CD at 216nm (C,D) and 231nm (E,F) are also shown. Data below 0.8M GdmCl were not included in the fit due to non-linear optical effects at low denaturant (see Section 3.3.2 and 3.3.3). The fits demonstrate that data at high protein concentrations are well accounted for by the 2-state fits. At lower protein concentrations a monomer intermediate becomes increasingly populated leading to deviations from 2-state fits. This is most apparent for the 1 μM curve. Parameters for fits to a global 3-state model with a monomer intermediate as well as to a dimer 2-state model are given in Table 3.1.

Figure 3.8. Concentration dependence of equilibrium unfolding of apo PWT mutants measured by fluorescence. The apo mutants (A) E100G, (B) G85R, (C) I113T and (D) G93R are shown. Samples were measured after a minimum of 48 hrs of incubation to ensure sufficient time for equilibrium. Protein concentrations shown are: 1μM (∗), 3μM (◇), 5μM (○), 10μM (●) and 30μM (Δ). Measurements were performed at 25 °C, 20mM HEPES pH 7.8 with 0.75M sodium sulphate. Renaturation curves acquired at a protein concentration of 1uM (□) for G85R, I113T and G93R and 3uM (♦) for E100G are also shown. Data are scaled for protein concentration for ease of comparison. As was the case for PWT, data points below 0.8M GdmCl were not fit due to non-linear effects at low denaturant. The lines represent global fits of equilibrium unfolding data to a 3-state model with a monomer intermediate. Fitted values for Δ*G*s from fluorescence measurements agree well with values obtained from circular dichroism measurements at 216 and 231 nm (Table 3.1, Figure 3.9).

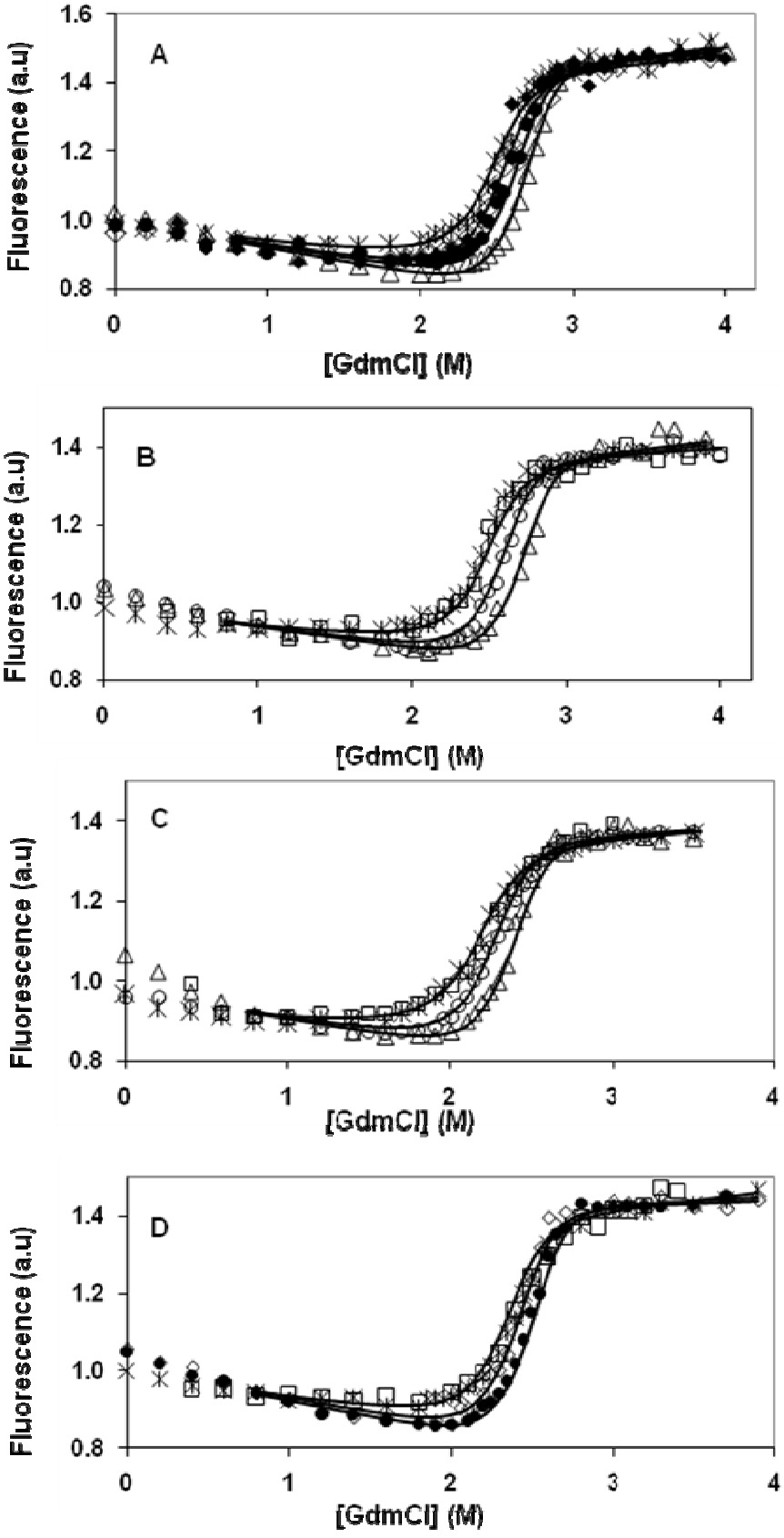
A
B
C
D
Fluorescence (a.u)
[GdmCl] (M)
1.6
1.4
1.2
1.0
0.8
0
1
2
3
4

Figure 3.9. Concentration dependence of equilibrium unfolding of apo PWT mutants measured by CD. Samples were measured after a minimum of 48 hrs of incubation to ensure sufficient time for equilibrium. Curves measured by CD at 216 nm are shown for (A) E100G, (C) G85R, (E) I113T and (G) G93R while curves measured by CD at 231nm are illustrated for (B) E100G, (D) G85R, (F) I113T and (H) G93R. Protein concentrations shown are: 3μM (◇), 5μM (○), 10μM (●) and 30μM (Δ). Measurements were performed at 25 °C, 20 mM HEPES pH 7.8 with 0.75M sodium sulphate. Data are normalized, and scaled for protein concentration for ease of comparison. The lines represent global fits of equilibrium unfolding data to a 3-state model with a monomer intermediate. Fitted values are presented in Table 3.1

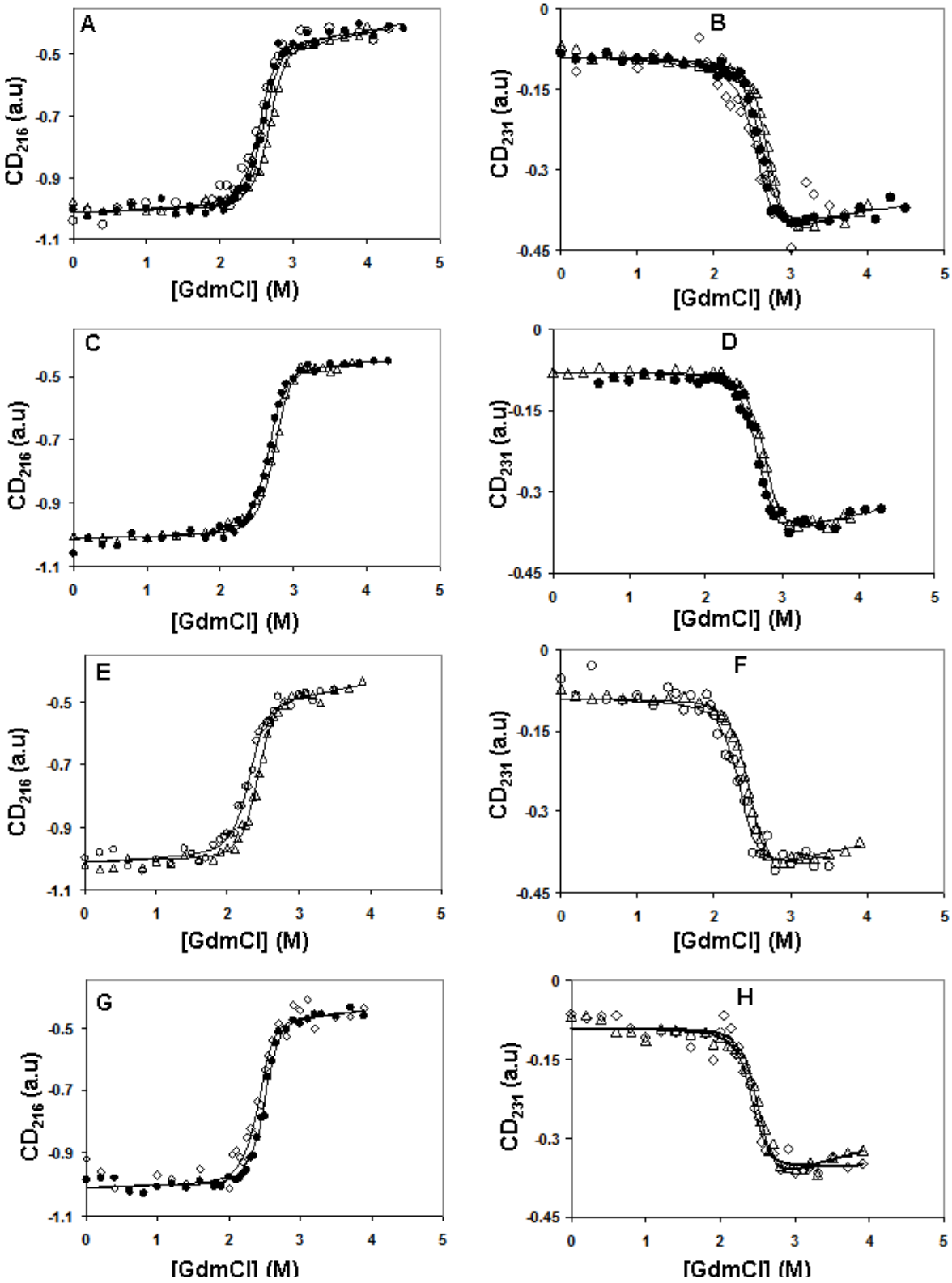
A
B
C
D
E
F
G
H
CD216 (a.u)
CD231 (a.u)
[GdmCl] (M)
-0.5
-0.7
-0.9
-1.1
-0.15
-0.3
-0.45
0
1
2
3
4
5

3.3.4 GdmCl denaturation curve analysis of apo SOD

3.3.4.1 Apo PWT SOD

Apo PWT SOD equilibrium chemical denaturation curves were acquired at different concentrations, monitored by fluorescence as well as CD at 216 and 231 nm, both with and without Na_2SO_4. These curves were initially fit to a dimer 2-state model for a transition between folded dimer (N_2) and unfolded monomer (U): $N_2 \leftrightarrows 2U$ (Equations 3.5, Figures 3.5, 3.7 and Table 3.1). Curves were fit individually as well as globally with ΔG_{tot} (change in Gibbs free energy of unfolding) and m_{tot} (dependence of ΔG_{tot} on denaturant concentration) as shared parameters (Table 3.1). Although the global 2-state fits for apo PWT SOD with 0 M Na_2SO_4 pass through the data points fairly well, analysis of the fitted parameters reveals that the lowest protein concentrations in individual data sets as well as the global fit m_{tot} and ΔG_{tot} values are somewhat lower than expected (Figure 3.5, Table 3.1 and below). Given that m_{tot} is proportional to the change in solvent accessible surface area (ΔASA), it can be estimated from the number of amino acids in the protein, assuming that SOD is a typically folded globular protein (Myers et al., 1995). For SOD which has 153 amino acids per monomer, the estimated m_{tot} value is ~9 kcal (mol dimer)$^{-1}$ M^{-1} (Geierhaas et al., 2007). However, the m_{tot} value obtained from fitting the data at the lowest protein concentration to a 2-state dimer unfolding model is only 5.5 ± 0.8 kcal (mol dimer)$^{-1}$ M^{-1} and the global fit m_{tot} value is 7.3±0.2 kcal (mol dimer)$^{-1}$ M^{-1}. In addition, both ΔG_{tot} and m_{tot} values for fits to individual curves systematically increase with increasing protein concentration (Table 3.1). Low and changing m and ΔG values are often indicative of the existence of an intermediate (Soulages, 1998; Spudich and Marqusee, 2000). The changes in values are more pronounced at lower protein concentrations and become smaller at higher protein concentrations. Similar results were also obtained for holo SODs, where

Table 3.1:Thermodynamic parameters from GdmCl curves of PWT and mutant apo SODs

				Dimer 2-State Model		Dimer 3-State with Monomer Intermediate[a]		
Protein	**$[Na_2SO_4]$ (M)**	**[Protein] (μM)**	**Probe**	**m_{tot}[c] (kcal(mol dimer)$^{-1}$M^{-1})**	**ΔG_{tot}[c] $(N_2 \leftrightarrows 2U)$ (kcal(mol dimer)$^{-1}$**	**ΔG_1[c] $(N_2 \leftrightarrows 2I)$ (kcal(mol dimer)$^{-1}$)**	**ΔG_2[c] $(I \leftrightarrows U)$ (kcal(mol monomer)$^{-1}$)**	**ΔG_{tot}[d,e] $(N_2 \leftrightarrows 2I \leftrightarrows 2U)$ (kcal(mol dimer)$^{-1}$)**
PWT	0	0.2	Fl	5.5±0.8	13.4±0.7			
PWT	0	1	Fl	7.4±0.5	15.6±0.5			
PWT	0	5	Fl	7.7±0.6	15.9±0.7			
PWT	0	10	Fl	8.5±0.7	16.7±0.8			
PWT	0	0.2,1,5,10[b]	Fl	7.3±0.2	15.3±0.2	12.4±0.7	1.8±0.4	16.0±0.9
PWT	0	5	CD_{216}	6.6±0.9	15±1			
PWT	0	10	CD_{216}	8.4±0.9	17±1			
PWT	0	5, 10[b]	CD_{216}	7.7±0.7	15.8±0.8	12.7±0.5	1.7±0.2	16.1±0.6
PWT	0	10	CD_{231}	9±1	17±2	13.3±0.6	1.3±0.3	15.9±0.7
PWT	0.75	1	Fl	4.4±0.5	21±1			
PWT	0.75	5	Fl	6.9±0.4	28±1			
PWT	0.75	10	Fl	6.4±0.5	26±1			
PWT	0.75	30	Fl	6.9±0.8	28±3			
PWT	0.75	1,10,5,30[b]	Fl	6.5±0.2	26.7±0.6	12.0±0.1	10.33±0.04	32.7±0.1
PWT	0.75	5	CD_{216}	6.1±0.7	25±2			
PWT	0.75	10	CD_{216}	7.8±0.8	29±2			
PWT	0.75	30	CD_{216}	6.3±0.9	26±3			
PWT	0.75	5,10,30[b]	CD_{216}	6.3±0.3	26±1	11.9±0.1	10.5±0.1	32.9±0.2
PWT	0.75	5	CD_{231}	7±1	30±3			
PWT	0.75	10	CD_{231}	8±1	30±3			
PWT	0.75	30	CD_{231}	7.8±0.5	31±2			
PWT	0.75	5,10,30[b]	CD_{231}	6.6±0.4	27±1	12.3±0.3	10.2±0.1	32.7±0.3
G85R	0.75	1	Fl	5.3±0.5	21±1			
G85R	0.75	5	Fl	7.5±0.5	26±1			
G85R	0.75	30	Fl	7.3±0.8	26±2			
G85R	0.75	1,5,30[b]	Fl	6.6±0.2	23.8±0.4	11.7±0.1	8.4±0.1	28.5±0.2
G85R	0.75	10	CD_{216}	7.2±0.6	26±2			
G85R	0.75	30	CD_{216}	6.0±0.6	22±2			
G85R	0.75	10,30[b]	CD_{216}	7.0±0.2	25.0±0.5	11.5±0.2	8.6±0.1	28.7±0.2
G85R	0.75	30	CD_{231}	7.6±0.6	27±2	11.7±0.3	8.6±0.2	28.9±0.4
E100G	0.75	1	Fl	5.2±0.6	20±1			
E100G	0.75	3	Fl	5.8±0.8	22±2			
E100G	0.75	10	Fl	6.5±0.5	23±1			
E100G	0.75	30	Fl	7.4±0.5	26±1			
E100G	0.75	1,3,10,30[b]	Fl	6.9±0.2	24.4±0.4	11.3±0.1	8.47±0.05	28.2±0.1
E100G	0.75	5	CD_{216}	6.2±0.9	22±2			
E100G	0.75	10	CD_{216}	7.7±0.8	26±1			
E100G	0.75	30	CD_{216}	6.5±0.8	23±2			
E100G	0.75	5,10,30[b]	CD_{216}	6.8±0.2	23.9±0.5	11.4±0.2	8.3±0.1	28.0±0.2
E100G	0.75	5	CD_{231}	5±1	20±3			
E100G	0.75	10	CD_{231}	7.8±0.8	27±2			
E100G	0.75	30	CD_{231}	7.3±0.6	25±2			
E100G	0.75	3,10,30[b]	CD_{231}	6.8±0.3	24.2±0.7	11.0±0.2	8.6±0.1	28.2±0.2
G93R	0.75	1	Fl	5.5±0.4	21±1			
G93R	0.75	3	Fl	7.5±0.6	25±1			
G93R	0.75	10	Fl	7.5±0.4	25±1			
G93R	0.75	1,3,10[b]	Fl	7.9±0.2	26.1±0.5	11.7±0.1	7.8±0.1	27.3±0.2
G93R	0.75	3	CD_{216}	7±1	23±3			
G93R	0.75	10	CD_{216}	9.0±0.9	29±2			
G93R	0.75	3,10[b]	CD_{216}	7.5±0.3	25.2±0.8	12.0±0.5	7.7±0.2	27.4±0.6
G93R	0.75	3	CD_{231}	9±2	28±5			
G93R	0.75	10	CD_{231}	6.3±0.7	22±1			
G93R	0.75	3,10[b]	CD_{231}	9.4±0.3	30.2±0.7	11.8±0.5	7.8±0.3	27.4±0.7
I113T	0.75	1	Fl	4.4±0.3	17.1±0.7			
I113T	0.75	5	Fl	5.8±0.2	19.8±0.5			
I113T	0.75	30	Fl	7.8±0.8	24±2			
I113T	0.75	1,5,30[b]	Fl	7.1±0.3	22.7±0.6	10.6±0.1	7.56±0.04	25.7±0.1
I113T	0.75	5	CD_{216}	5.9±0.7	20±2			
I113T	0.75	30	CD_{216}	7.2±0.6	23±2			
I113T	0.75	5,30[b]	CD_{216}	6.8±0.3	22.3±0.6	10.8±0.2	7.6±0.1	26.0±0.2
I113T	0.75	5	CD_{231}	6±1	21±3			
I113T	0.75	30	CD_{231}	7.1±0.3	23.1±0.8			
I113T	0.75	5,30[b]	CD_{231}	7.4±0.3	23.8±0.8	10.9±0.3	7.7±0.1	26.3±0.3

[a] For data with 0M Na_2SO_4, m_1 and m_2 were fixed to 2.7 kcal (mol dimer)$^{-1}$ M^{-1} and 2.6 kcal (mol monomer)$^{-1}$ M^{-1}, respectively, while with 0.75M Na_2SO_4, m_1 and m_2 were fixed to 1.4 kcal (mol dimer)$^{-1}$ M^{-1} and 3.5 kcal (mol monomer)$^{-1}$ M^{-1} respectively.[b] Data were fit globally with *m*s and **Δ***G*s as shared parameters.[c] Errors are from the fitting program.[d] $\Delta G_{tot} = \Delta G_1 + 2\Delta G_2$. [e]Errors were propogated using standard procedures (Taylor, 1982).

unfolding is close to 2-state at high protein concentration but a folded monomer intermediate becomes significantly populated at low protein concentration (Rumfeldt et al., 2006). Deviation from a 2-state global fit at low protein concentration is more apparent for data acquired in 0.75 M Na_2SO_4 (Figure 3.7, Table 3.1).

Due to the deviations for the 2-state fits, the data were also fit to 3-state models with monomer (*I*) or dimer intermediate (I_2). The data without and with sodium sulphate are not well fit by the dimer intermediate model ($N_2 \leftrightarrows I_2 \leftrightarrows 2U$), but are well fit by the monomer intermediate model ($N_2 \leftrightarrows 2I \leftrightarrows 2U$) over the full protein concentration range (Figures 3.5 and 3.7), enabling determination of both ΔG_1 (Gibbs free energy of dimer dissociation) and ΔG_2 (Gibbs free energy of monomer intermediate unfolding) (Table 3.1). The resulting fitted values are consistent across all structural probes (Table 3.1). For data in the absence of sodium sulphate, ΔG_1 and ΔG_2 values of 12.8 ±0.5 kcal (mol dimer)$^{-1}$ and 1.6±0.3 kcal (mol monomer)$^{-1}$, respectively, averaged across all three probes, were obtained from fitting to the 3-state model with monomeric intermediate. Considering that the free energy of dimer dissociation of apo SOD has been previously estimated to be >10.9 kcal (mol dimer)$^{-1}$ at 20 °C from analytical ultracentrifugation experiments (Doucette et al., 2004), the value presented here for ΔG_1 is in the expected range. However, ΔG_2 of 1.6 kcal (mol monomer)$^{-1}$ is somewhat lower than expected, given that kinetic and equilibrium analysis of a monomeric variant of apo SOD, containing charged residues in the dimer interface to prevent dimerization, gave values between 3 and 4 kcal (mol monomer)$^{-1}$ (Lindberg et al., 2005; Svensson et al., 2006). The high ΔG_1 combined with the marginal stability of the SOD monomeric intermediate results in a very low population of intermediate, which could lead to errors in thermodynamic characterization. Additionally, the marginal stability of the apo monomer means that small absolute errors could lead to large relative errors. Nevertheless, despite potential errors in accurately determining the ΔG of the monomeric

intermediate, the total ΔG of unfolding, calculated from $\Delta G_{tot} = \Delta G_1 + 2 \times \Delta G_2$ to be 16.0±0.1 kcal (mol dimer)$^{-1}$ is close to the previously obtained DSC derived value of 17.4 ± 2.4 kcal (mol dimer)$^{-1}$ (Stathopulos et al., 2006) . Oliveberg and coworkers have reported a similar value for ΔG_{tot} determined by urea denaturation, but did not to show any equilibrium data in their primarily kinetic study (Lindberg et al., 2004).

Fits of the data obtained with sodium sulphate give a ΔG_{tot} of 32.8±0.1 kcal (mol dimer)$^{-1}$, indicating a significant stabilizing effect of sodium sulphate, comparable to effects observed for other proteins (Ferguson et al., 1999; Timasheff, 1998); this stabilization may well be biologically relevant (see Discussion). Interestingly, the values of ΔG_1 without and with sodium sulphate are quite similar at 12.8±0.5 and 12.1±0.2 kcal (mol dimer)$^{-1}$, respectively. In contrast, ΔG_2 increases from 1.6±0.3 kcal (mol monomer)$^{-1}$ to 10.3±0.2 kcal (mol monomer)$^{-1}$. Thus, the overall stabilizing effect of sodium sulphate is dominated by the effect on the monomer intermediate. As a consequence, there is a significant increase in the population of the monomer intermediate in sodium sulphate (Figure 3.10). The values of m_{tot} ($m_{tot} = m_1 + 2m_2$; where m_1 and m_2 are the denaturant dependence of ΔG_1 and ΔG_2, respectively) are similar without and with sodium sulphate, 7.9 kcal (mol dimer)$^{-1}$ M^{-1} and 8.4 kcal (mol dimer)$^{-1}$ M^{-1}, respectively. These values are close to the values calculated using empirical formulae (see above) and measured for holo SODs (Rumfeldt et al., 2006). Despite these similarities, m_1 decreases from 2.7 to 1.4 kcal (mol dimer)$^{-1}$ M^{-1} in sodium sulphate, while m_2 increases from 2.6 to 3.5 kcal (mol monomer)$^{-1}$ M^{-1}.

3.3.4.2 Mutant Apo SODs

The effects of mutations on folding mechanism and stability were investigated by obtaining GdmCl denaturation curves in sodium sulphate monitored by fluorescence and CD as a

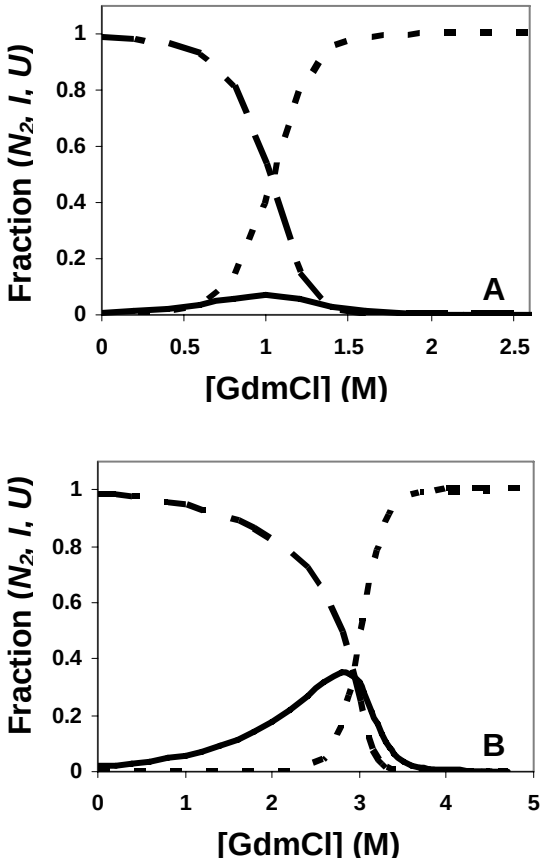

Figure 3.10. Fractions of the native dimer (— — —), monomer intermediate (——), and denatured monomer (----) as a function of GdmCl concentration for 1μM apo PWT SOD. Comparison of the fractions of these various protein conformations in (A) 0M sodium sulphate and (B) 0.75M sodium sulphate demonstrate that the monomer intermediate is much more populated in sodium sulphate as evidenced by the maximal fraction of intermediate increasing from (0.07) without sodium sulphate to (0.35) in sodium sulphate.

function of protein concentration for apo G85R, E100G, G93R and I113T (Figures 3.8, 3.9 and Table 3.1). As for PWT, the mutant data are best fit by the monomer intermediate model. The changes in total Gibbs free energy of unfolding from native dimer to unfolded monomers, $\Delta\Delta G_{tot}$, ($\Delta\Delta G_{tot} = \Delta G_{tot}^{mutant} - \Delta G_{tot}^{PWT}$) show that all the mutants are destabilized relative to the apo PWT SOD (Table 3.2), as expected based on the decreased midpoints of unfolding (Figures 3.7 and 3.8). The order of stability, from most stable to least stable, is PWT>G85R>E100G>G93R>I113T. The order of stability of the mutants measured by chemical denaturation is the same as in DSC experiments (Table 3.2). The magnitudes of the destabilization ($\Delta\Delta G_{tot}$) of the mutants are slightly smaller, however, when measured by DSC; this is likely due to the effects of sodium sulphate which is present only for the chemical denaturation experiments (see Section 3.4.2).

Both dimer dissociation (ΔG_1) and monomer stability (ΔG_2) are negatively affected by the mutations, with the destabilization of the monomer being the greater contributor to the decrease in overall stability (Table 3.2). Despite the smaller impact on ΔG_1, these differences in stability significantly increase the relative population of intermediate (Figure 3.11). For example, for G93R, although ΔG_1 is decreased just 0.3 kcal (mol dimer)$^{-1}$, the ratio of monomer intermediate concentration of mutant relative to PWT is ~1.3 (i.e. 30% increase in intermediate concentration). G85R, E100G and I113T have larger effects on ΔG_1 and the ratio of intermediate concentration is increased to ~ 1.5, 2 and 3, respectively. The mutations cause even larger effects on the populations of unfolded monomers. For the G93R mutation the ratio of concentration of unfolded monomers of mutant relative to PWT is 85 (i.e. the concentration of unfolded monomers is increased 85-fold, or 8500%), while the ratios for G85R, E100G and I113T are ~30, 40 and 280, respectively.

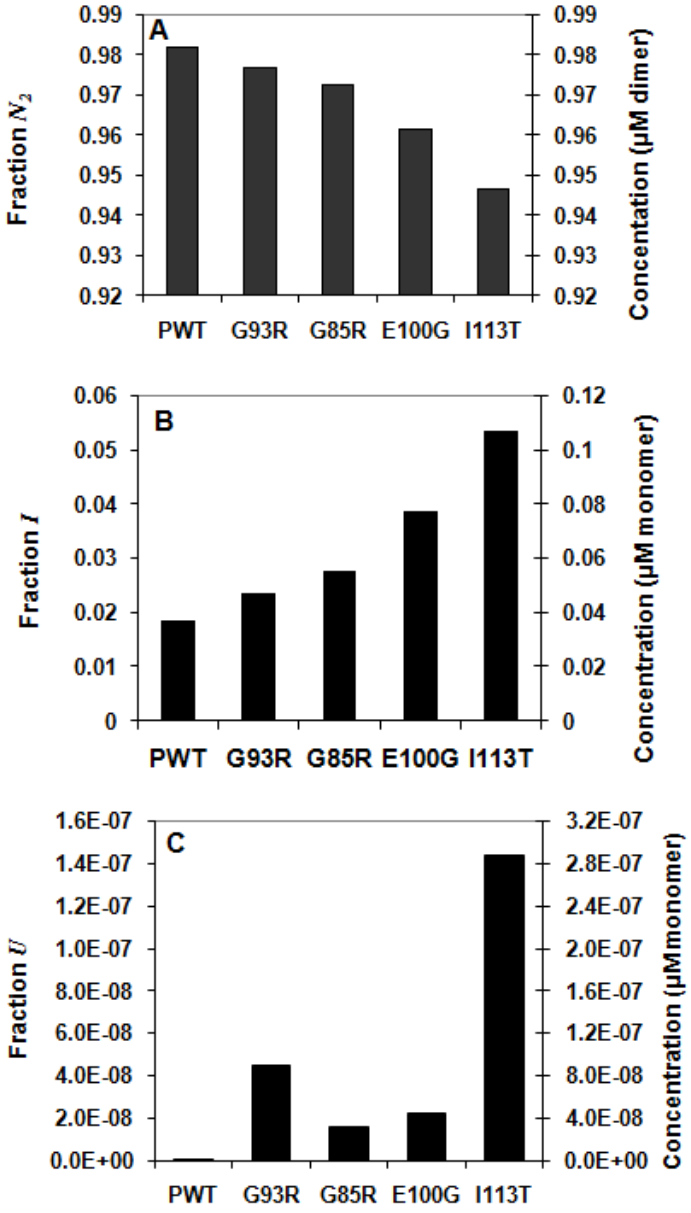

Figure 3.11. Relative fractions and concentrations of the different species present at equilibrium for 1 μM apo PWT and mutants in 0.75 M sodium sulphate and 0M GdmCl. Mutations in SOD result in a decrease in the fraction and concentration of (A) the native state with corresponding increases in (B) the folded monomer intermediate and larger increases in (C) the unfolded monomer.

Table 3.2: Summary of thermodynamic parameters of PWT and Mutant apo SODs by GdmCl curve analysis

Protein	ΔG_1[a] (kcal (mol dimer)$^{-1}$)	ΔG_2[a] (kcal (mol monomer)$^{-1}$)	ΔG_{tot}[b] (kcal (mol dimer)$^{-1}$)	$\Delta\Delta G_1$[c] (kcal (mol dimer)$^{-1}$)	$\Delta\Delta G_2$[d] (kcal (mol monomer)$^{-}$	$\Delta\Delta G_{tot}$[e] (kcal (mol dimer)$^{-1}$)	$\Delta\Delta G(_{tot}, t_{avg}$[f]) (kcal (mol dimer)$^{-1}$)
PWT	12.1±0.2	10.3±0.2	32.8±0.1	n/a	n/a	n/a	n/a
G85R	11.6±0.1	8.5±0.1	28.7±0.2	-0.5	-1.8	-4.1	-1.6
E100G	11.2±0.2	8.5±0.2	28.2±0.1	-0.9	-1.8	-4.6	-3.6
G93R	11.8±0.2	7.8±0.1	27.4±0.1	-0.3	-2.5	-5.4	-4.1
I113T	10.8±0.2	7.6±0.1	26.0±0.3	-1.3	-2.7	-6.8	-4.7

n/a, not applicable. t_{avg} = 51.8 ˚C is the average of the $t_{0.5}$ values of PWT and mutant datasets from Table 2.1

[a] ΔG_1 and ΔG_2 are derived from 3-state monomer intermediate global fitting of GdmCl curves in 0.75 M Na_2SO_4 (Table 3.1). Values are an average of fitted values from 3 probes (CD 216 nm, CD 231 nm and fluorescence). Errors (±) are standard deviations from averaging the 3 probes. [b] $\Delta G_{tot} = \Delta G_1 + 2\Delta G_2$. Errors (±) are standard deviations from averaging the 3 probes. [c] $\Delta\Delta G_1 = {}_{\Delta G_1}^{mu\tan t} - {}_{\Delta G_1}^{PWT}$. [d] $\Delta\Delta G_2 = {}_{\Delta G_2}^{mu\tan t} - {}_{\Delta G_2}^{PWT}$. [e] $\Delta\Delta G_{tot} = \Delta G^{mutant} - \Delta G^{PWT}$. Values were derived from 3-state monomer intermediate fits of GdmCl denaturation curves, negative value indicates that the mutant SOD is destabilized relative to the PWT. [f] ${}_{\Delta\Delta G_{tot(tavg)}} = {}_{\Delta G_{tot(tavg)}}^{mu\tan t} - {}_{\Delta G_{tot(tavg)}}^{PWT}$. Values derived from DSC analysis of data using ΔGs calculated at the t_{avg}. The DSC scans were obtained in 20 mM HEPES, pH 7.8 in the absence of sodium sulphate. Values calculated at the t_{avg} are more accurate than values calculated at significantly higher or lower temperatures due to shorter extrapolation of fitted parameters (see section 2.3.3). Values for PWT, G85R and I113T are taken from Table 2.4 while values for G93R and E100G are calculated from fitted parameters presented in Stathopulus, *et. al*. 2006 and Vassall, *et al*. 2006 respectively.

3.4 Discussion

3.4.1 Mechanism of unfolding of apo PWT SOD.

This chapter focuses on the quantitative equilibrium thermodynamic analysis of apo SOD unfolding using GdmCl denaturation curves and thereby complements DSC thermal unfolding studies (Chapter 2). It was demonstrated that apo PWT SOD undergoes reversible denaturation in GdmCl, which is well fit by a 3-state model with monomer intermediate (Figures 3.5). The intermediate is increasingly populated with decreasing protein concentration, as evidenced by increasingly biphasic character in the GdmCl curves, whereas the transition approaches a monophasic 2-state transition at high protein concentration (Figures 3.5 and Table 3.1). Interestingly, a 3-state transition with a monomer intermediate was also reported for GdmCl denaturation studies of holo PWT SOD (Rumfeldt et al., 2006) and copper-depleted wild-type SOD (Stroppolo et al., 2000), indicating that loss of metal does not alter the folding mechanism of SOD. The observation of the monomer intermediate for apo SOD is not entirely unexpected, given that kinetic studies have suggested that monomer folding precedes dimerization (Lindberg, 2004; Svensson et al., 2006). Additionally, as reported in chapter 2, two apo mutants namely, H46R and A4V, populate a monomeric intermediate in DSC studies, illustrating that this protein can in fact populate a monomer at equilibrium under similar conditions to those used in this study. It should be noted however that DSC thermal unfolding data for apo PWT SOD are well fit to a 2-state dimer unfolding model indicating that no intermediate is significantly populated (see chapter 2 and (Stathopulos et al., 2006)). The apparent difference in thermal unfolding and chemical unfolding mechanisms is likely due to the protein concentration range surveyed by each technique. In DSC, as indicated in chapter 2, the lowest working concentration is close to

0.05 mg/mL or ~1.6 μM dimer. This concentration might be too high to significantly populate a monomeric intermediate. This is illustrated in Figure 3.10, which demonstrates that the maximal population of monomeric intermediate in PWT chemical denaturation is less than 10% at 1 μM and will only decrease with increasing protein concentration. This limitation of DSC means that only ΔG_{tot} of unfolding can be measured, while equilibrium chemical denaturation allows stability to be deconvoluted into individual contributions of ΔG_1 (dimer dissociation) and ΔG_2 (monomer unfolding).

An interesting finding of this study is that the ΔG_1 for apo PWT SOD at 12.8 kcal (mol dimer) $^{-1}$ is very similar to the value obtained for the holo protein, which has been determined to be ~13 kcal (mol dimer)$^{-1}$ from analysis of GdmCl denaturation curves under identical conditions as those used in this study (Rumfeldt et al., 2006). Additionally a value of ~12.5 kcal (mol dimer)$^{-1}$ has been reported from GdmCl denaturation curve analysis of copper free WT SOD at 20 °C pH 7.4 (Stroppolo et al., 2000). By contrast, the stability of the monomer intermediate reported in these studies is substantially higher than what is seen for the apo protein with a reported value of ~11 kcal (mol monomer)$^{-1}$ for holo PWT SOD (assuming no metal dissociation from the monomer when the protein unfolds) and ~4 kcal (mol monomer)$^{-1}$ for WT copper depleted SOD. This indicates that the metals exert most of their effects on the monomer and very little effect on the dimer interface.

3.4.2 Effects of Sodium Sulphate

Sodium sulphate is known to stabilize proteins *via* a mechanism of preferential exclusion of salt ions from the protein solvent sphere (Timasheff, 2002), and to enhance the population of kinetic folding intermediates (Ferguson et al., 1999; Rami and Udgaonkar, 2002; Sauder et al.,

1996). There is, however, little quantitative data on the effects of sodium sulphate on the stability of equilibrium intermediates. The extent of sodium sulphate-mediated protein stabilization is related to solvent accessible surface area. Unfolding of the apo SOD monomer intermediate produces a larger change in surface area than does dimer dissociation, based on the higher *m* value for the former (Myers et al., 1995) and structural data (Strange et al., 2003). Consistent with these changes, sodium sulphate causes a relatively large stabilization of the monomer intermediate with little effect on dimerization. It is interesting that sodium sulphate causes a decrease in the m_1 value while increasing m_2 (see Section 3.3.4.1). This suggests that sodium sulphate also causes a compaction of the apo monomer intermediate; structural studies conducted on a monomeric variant of apo SOD have shown it to be less compact and more flexible than the holo protein (Banci et al., 2003). Compaction of poorly structured states by sodium sulphate has also been observed for other proteins (Cerasoli et al., 2003; Nishimura et al., 2001; Rami and Udgaonkar, 2002).

The experiments reported herein for apo SODs demonstrate that sodium sulphate can be used to facilitate measurements of the determinants of intermediate stability. The similarity of the changes in overall stability ($\Delta\Delta G$) measured by chemical denaturation in sodium sulphate and by DSC in the absence of sodium sulphate further validate the former approach, which may be useful for the study of intermediates in other systems. It is worth noting, however, that the changes in stability measured in sodium sulphate are slightly larger than those measured by DSC (Table 3.2). Similarly, trehalose also tended to increase the free energy changes caused by mutations (Chen et al., 2005). This leads to the interesting observation that small molecule stabilizers not only enhance net protein stability but also enhance the effects of individual amino acids on stability. It is also worth pointing out that the measurements of stability and stability changes made in the presence of stabilizing agents may actually be more biologically relevant

than measurements made in dilute buffers, since the cellular environment has high ionic strength and high concentrations of molecules which may increase protein stability (Bolen and Baskakov, 2001; Chamberlin and Strange, 1989; Somero, 1986).

3.4.3 Effects of Mutations

The apo SOD mutants studied here by chemical denaturation are chemically and structurally diverse and are located in different areas of SOD structure (Figure 1.8). The structural contexts of the mutations have been previously discussed in Section 2.4.1 and will only be briefly re-iterated here. The mutation G85R interferes with zinc binding due to its proximity to the zinc binding ligands, E100G disrupts a salt bridge with K30, G93R substitutes a less flexible residue in a type *i* +3 turn and I113T introduces a polar residue into the dimer interface resulting in a twisting of the monomers in the dimer (Cao et al., 2008; Hough et al., 2004; Rumfeldt et al., 2006; Stathopulos et al., 2006). All the apo SOD mutant proteins share the same basic folding mechanism as apo PWT SOD, populating a folded monomeric intermediate at equilibrium in addition to native dimer and unfolded monomer; however, the mutations are all destabilizing. Consistent with the postulate that metal binding mutations have less effect on the apo protein state than the holo protein state, G85R is the least destabilized of mutants studied here; however, it is nevertheless significantly destabilized. Further evidence of the differential effects of metal binding mutants on the holo and apo SOD forms can be obtained from a comparison of chemical denaturation studies presented here and holo SOD chemical denaturation studies reported previously (Rumfeldt et al., 2006). Chemical denaturation analysis of holo G85R and E100G SODs indicates that the latter is more stable, the reverse of what is seen here for the apo proteins (Rumfeldt et al., 2006).

Analysis of trends in $\Delta\Delta G_1$ and $\Delta\Delta G_2$ indicates that, as expected, the dimer interface apo SOD mutant I113T causes the largest decrease in dimer interface stability. Somewhat unexpectedly, however, the mutation also markedly decreases monomer intermediate stability, despite substituting a more polar residue at the monomer surface. Given that I113 is surrounded by hydrophobic residues, this destabilization may result from inefficient packing and hence increased exposure of these hydrophobic residues upon substitution with T. The other 3 mutations exhibit their destabilizing effects mainly through a decrease in apo SOD monomer stability ($-\Delta\Delta G_2$), indicating that the overall effects of the mutations are through their effects on the SOD β-barrel, which is predicted from the structural contexts described above. Interestingly, however, the mutations G85R, E100G and G93R, even though they are far from the dimer interface, also tend to enhance apo SOD dimer dissociation (ΔG_1). This study hence validates the conclusions from ITC dimer dissociation experiments (Section 2.4.1.2), providing further evidence that a common characteristic of apo SOD mutants could be destabilization of the dimer interface (Khare et al., 2006). Furthermore, the effects of E100G and G85R on ΔG_1 in the apo protein differ from those observed in chemical denaturation experiments on the holo protein, where these mutations had little or no effect on ΔG_1 (Rumfeldt et al., 2006). This suggests that the effects of mutations may tend to propagate more in the apo protein than in the holo protein. Compaction with concomitant increase in stability resulting from SOD metal binding may cause the effects of mutations to be more localized.

3.4.4 Disease Implication

It is particularly striking that all ALS-associated SOD mutations studied to date appear to decrease the stability of holo SOD, and usually also of apo SOD (Lindberg et al., 2005; Rodriguez et al., 2005; Rodriguez et al., 2002; Rumfeldt et al., 2006; Stathopulos et al., 2006;

Stathopulos et al., 2003). This suggests that decreased stability is a key factor in causing disease. Destabilizing mutations have been proposed to cause increased toxic aggregation not only in ALS but in many other protein misfolding diseases (Bendotti and Carri, 2004; Gregersen et al., 2005; Valentine et al., 2005). This emphasizes the need for accurate equilibrium stability measurements, not only for apo, but also for holo SODs, whose destabilization has also been implicated in toxic aggregation (Banci et al., 2005; Hough et al., 2004; Rodriguez et al., 2005; Rumfeldt et al., 2006). Stability data may also provide important information for understanding disease mechanism, such as elucidating which states of the protein may be aggregating. In general, aggregation is thought to arise from the increased population by mutant proteins of partially folded aggregation-prone species (Chow et al., 2004). In this regard, it is noteworthy that both the populations of the monomer intermediate and the unfolded monomer are increased for all the apo mutants (Figure 3.11). Either species could promote SOD aggregation in ALS. In fact, it has been shown directly that apo SOD aggregation can be induced if samples are incubated with agitation at 37 °C, pH 7.4 with the addition of 1M GdmCl (Chattopadhyay et al., 2008). Apo SOD under these conditions will mostly populate either fully or partially unfolded monomers and thus this result directly implicates one or both of these species as precursors to aggregation.

It is important to note that, since DSC endotherms of these mutants could only be analyzed using a 2-state mechanism, only information on the relative populations of the native and unfolded conformation could be obtained (see Chapter 2 and (Rumfeldt, 2006; Stathopulos et al., 2006)). Hence, the methodology introduced here expands our quantitative capabilities, enabling us to more fully evaluate the effects of mutations on potentially aggregation-prone species. This could be instrumental in finding common properties of the mutants that causes ALS.

Chapter 4: Folding and aggregation of disulfide-reduced apo SOD

Acknowledgments

I would like to thank Ryan Sobering, for working with me in collecting chemical denaturation data on PWT and H46R. I would also like to thank Lee-Ann Briere at the University of Western Ontario for running the analytical ultracentrifugation experiments and fitting the data as well as Professor Stanley Dunn at the University of Western Ontario for his assistance in analytical ultracentrifugation experimental design and analysis.

4.1 Introduction

In vivo SOD has a complex maturation process involving several steps before becoming a fully stable and functional protein. The most immature form of SOD existing after synthesis on the ribosome is the apo protein, which lacks the native intramolecular disulfide bond between C57 and C146. The post-translational formation of the disulfide bond is thought to be aided by the copper chaperone for SOD (CCS), which is also responsible for the addition of the catalytic Cu^{2+}, while Zn^{2+} binds by an unknown mechanism, possibly before CCS interacts with SOD (see Section 1.4.2.1) (Furukawa et al., 2004). Depending on whether any one of these post-translational modifications is present or absent and also considering monomer dimer equilibria, SOD can theoretically exist in 44 different microstates (Furukawa and O'Halloran, 2006), but it is not known which is/are the most important for SOD pathology. Recently, there has been heightened interest in the most immature, apo disulfide-reduced form of the protein. *In vitro* studies have shown that ALS-linked SOD mutants are more easily reduced than WT indicating that reduction of the disulfide bond might contribute to mutant SOD toxicity (Tiwari and Hayward, 2003). Furthermore, disulfide-reduced mutant demetallated SOD has been shown to

have a greater tendency to bind to hydrophobic matrices; hydrophobic patches on the surface of SOD could mediate aberrant intermolecular association in aggregation (Tiwari et al., 2005). Significantly, it has been found that extracts from the CNS of ALS-mice contain at least a sub-fraction of misfolded SOD that lacks the disulfide bond and is not fully metallated (Jonsson et al., 2006; Wang et al., 2009; Zetterstrom et al., 2007). There is evidence from *in vitro* aggregation studies that disulfide-reduced apo SOD protein aggregates can seed the aggregation of more mature forms (Chattopadhyay et al., 2008).

It has been speculated that the important structural role played by the disulfide bond in SOD makes the protein more susceptible to aggregation upon its removal. The lone disulfide bond serves to anchor loop 4 to the β sandwich in SOD (Tainer et al., 1982). Reduction of the disulfide bond dramatically influences the stability of the dimer interface. Analytical ultracentrifugation experiments (Doucette et al., 2004) as well as gel filtration studies suggest that the disulfide-reduced apo protein has increased tendency to monomerize and kinetic unfolding studies suggest marginal stability (Lindberg et al., 2004). The crystal structure of a mutant of SOD, which cannot form the disulfide bond due to replacement of all cysteines in the protein with alanine, (Hornberg et al., 2007) reveals that the liberation of loop 4 causes a re-orientation of the loop that extend it into the dimer interface, resulting in a displacement of the hydrophobic residues 52-54. These hydrophobic residues become unable to participate in crucial interactions across the dimer interface. Additionally dimer dissociation is thought to become more favourable due to the increased entropy of loop 4 in the resulting monomer (Hornberg et al., 2007).

Despite the fact that the majority of mutations destabilize both holo and apo disulfide-intact SOD, mutants are still predominantly folded in these forms and unfolded states are not highly populated at physiological temperature and pH (Rumfeldt et al., 2006; Stathopulos et al.,

2006; Vassall et al., 2006). In contrast, studies of thermal melting at physiological pH on disulfide-reduced apo SOD reveal that mutations in this background may significantly increase the population of partially or fully unfolded forms of SOD, which have been proposed to be important precursors for aggregation (Furukawa and O'Halloran, 2005; Rodriguez et al., 2005). Previous stability studies on disulfide-reduced apo SOD focused only on the apparent $t_{0.5}$s of a few mutants; no thermodynamic analysis was reported, presumably due to irreversibility of unfolding (Furukawa and O'Halloran, 2005; Rodriguez et al., 2005). Here, using similar techniques and protocols as outlined in the previous two chapters, data on additional mutants are presented in the first comprehensive thermodynamic analysis of disulfide-reduced apo SOD and fALS-associated mutants. This study provides a more thorough determination of the thermodynamic consequences of SOD maturation, which should help to illuminate which form of SOD is most important in ALS. Additionally, further evidence of the increased aggregation propensity of the mutants compared to PWT in this disulfide-reduced apo background is presented.

4.2 Materials and Methods

4.2.1 Preparation of disulfide-reduced apo SOD

Disulfide-reduced apo SOD was produced directly from the disulfide-intact apo SOD (prepared as described in Sections 2.2.2 and 2.2.3) using the reducing agent *tris*(2-carboxyethyl) phosphine (obtained as *tris*(2-carboxyethyl)phosphine hydrochloride from Pierce). The disulfide bond in SOD is in a hydrophobic environment and is not easily accessible to a charged reducing agent such as *tris*(2-carboxyethyl) phosphine (TCEP). In order to expose the disulfide bond to reducing agent, disulfide-intact apo SOD samples were first unfolded in 2 M GdmCl, 20 mM HEPES, pH 7.8, for 30 minutes at ambient temperature. This mixture was degassed before adding TCEP to a final concentration of 10 mM with reduction occurring in an anaerobic environment for 1 hr. The sample was then exchanged into buffer containing 1 mM TCEP, 20 mM HEPES pH 7.4 by doing 5 successive 5-fold dilutions and reconcentrations using a 3 kDa cutoff membrane nanosep concentration device (Pall Corporation, East Hills, NY). After exchanges were complete, protein concentration was re-checked by measuring absorbance at 280nm using a molar monomer extinction coefficient of 5400 $M^{-1}cm^{-1}$ (Lyons et al., 1996). Successful reduction was confirmed by the presence of a single peak in the DSC thermogram of the protein at a temperature lower than what would be expected for disulfide-intact protein (Figure 4.2). Reduction was also confirmed by performing SDS-PAGE gels on samples before and after DSC (Figure 4.1). Disulfide-reduced apo SOD migrates slightly slower on a denaturing gel due to being less compact than the disulfide-intact conformation. In order to prevent re-oxidation of the protein on the gel, free cysteines were modified with iodoacetamide (IA) as previously described (Furukawa and O'Halloran, 2005). Briefly, samples were precipitated by adding an equal volume of an aqueous solution containing 20% trichloroacetic acid and

incubating on ice for 20 minutes. Protein samples were then pelleted by centrifuging at 14,000 rpm and the supernatant was discarded. The pellet was then washed by re-suspending it in acetone followed by centrifuging at 14,000 rpm to recover the pellet and remove the acetone supernatant. The pellet was then further dried under vacuum. After drying, the pellet was re-dissolved in buffer containing 50 mM HEPES, 2.5% SDS, 1 mM bathocuproine disulfonate and 100 mM iodoacetamide, pH 7.2. After one hour of anaerobic incubation at 37 °C, the samples were loaded onto a SDS-PAGE gel and run at a constant voltage of 150V.

4.2.2 Differential scanning calorimetry

Excess specific heat as a function of temperature for the thermal unfolding of disulfide-reduced apo SOD was measured using a differential scanning calorimeter (LLP VP, Microcal Inc., Northampton MA). Protein concentrations ranged from 0.11-2.4 mg and samples were scanned in 1mM TCEP, 20mM HEPES, pH 7.4, unless otherwise specified. There is negligible scan rate dependence on the excess specific heat absorption of disulfide-reduced apo SOD for scan rates of 0.5 °C min^{-1} to 1.5 °C min^{-1}, and so the usual scan rate employed was 1 °C min^{-1}. Buffer *versus* buffer scans were conducted prior to protein *versus* buffer scans; these buffer *versus* buffer scans were subtracted from protein *versus* buffer scans before data analysis.

Data were fit to a 2-state monomer unfolding model and also, for comparison, to a 2-state dimer unfolding model, described in Section 2.2.4.1 (Equations 2.26 and 2.27). In addition to Equation 2.27, which describes a 2-state monomer model where pre-transition and post-transition baselines are fit, some scans were also fit to a 2-state monomer model in which baselines were subtracted prior to fitting (MN2-state model in Microcal Origin 5.0). In the latter approach, only the excess heat capacity ($C_{p\ ex}$) is fit; the final equation used for fitting is:

$$C_{p\,ex} = \frac{\gamma \Delta H(T)^2 \alpha(1-\alpha)}{RT^2} \tag{4.1}$$

where ΔH (T) is the fitted enthalpy of unfolding at temperature T (in K), α is the extent of the unfolding reaction, R is the universal gas constant and γ is the ratio of van't Hoff to calorimetric enthalpy ($\Delta H_{vH}/\Delta H_{cal}$). In contrast to fitting to Equation 2.27, where data were normalized to cal g^{-1} of protein, data were normalized to cal (mol monomer)$^{-1}$ prior to fitting Equation 4.1.

4.2.3 Chemical renaturation and denaturation

To prepare chemical renaturation curves of the disulfide-reduced apo SOD, a degassed denaturing mixture consisting of 10x concentrated disulfide-intact apo SOD, 3.5 M urea and 10mM TCEP was first incubated for 4hrs, under nitrogen. During this initial incubation, the disulfide bond is reduced by TCEP and the protein is fully unfolded by the urea in the mixture. Ten-fold dilutions of this incubated mixture were then made into different solutions containing HEPES and various concentrations of urea. This dilution protocol produced samples that contained the disulfide-reduced protein along with final concentrations of 1 mM TCEP, 20 mM HEPES, pH 7.4, and urea concentrations of 0.35 M to 3.5 M. The samples were then further incubated under nitrogen for 24 hrs at 25 °C to allow time for equilibration before their fluorescence was measured using a Fluorolog 3-22 (Instruments SA, Edison, NJ) with excitation at 282 nm and emission at 360 nm, and CD measurements at 216 and 231 nm using a J715 spectropolarimeter (Jasco Research Ltd.). Temperature was set at 25 °C and controlled during optical measurements using a circulating water bath for fluorescence and a Peltier cell for CD.

Denaturation was monitored by first preparing 10x concentrated disulfide-reduced apo protein in 10mM TCEP, 200mM HEPES, pH 7.4. This mixture was diluted 10-fold into solutions

containing different concentrations of urea. As for the renaturations curves, these samples were incubated for 24 hrs under nitrogen at 25 °C before making fluorescence and CD measurements.

4.2.3.1 Data fitting and analysis of denaturation and renaturation curves

Curves were fit to 2-state monomer unfolding model (Pace, 1986) in which the folded native protein, *N*, is in equilibrium with the unfolded protein, *U*:

$$N \xleftrightarrow{K_U} U \tag{4.2}$$

where K_U is the equilibrium constant of the process which can be expressed as,

$$K_U = \frac{[U]}{[N]} = \frac{f_U}{f_N} \tag{4.3}$$

where f_U and f_N are the fractions of unfolded and native protein, respectively. From the conservation of mass, f_N can be expressed as:

$$f_N = 1\text{-}f_u \tag{4.4}$$

and hence,

$$K_U = \frac{[U]}{[N]} = \frac{f_U}{1 - f_U} \tag{4.5}$$

Rearranging Equation 4.5, one obtains an expression for f_U in terms of K_U:

$$f_U = \frac{K_U}{1 + K_U} \tag{4.6}$$

K_U at any urea concentration is related to the ΔG_U (free energy of unfolding) by:

$$K_U = e^{-\frac{\Delta G_U}{RT}} \tag{4.7}$$

where R is the universal gas constant and T is the absolute temperature in K. Using the assumption that ΔG_U changes linearly with [urea] (Tanford, 1970) one obtains:

$$\Delta G_U = \Delta G_U^{H_2O} - m[\text{urea}] \quad (4.8)$$

where, $\Delta G_U^{H_2O}$ is the free energy of reaction in the absence of denaturant, and m is the dependence of ΔG_U on urea concentrations. From Equations 4.5 and 4.7, it can be seen that K_U =1 and hence ΔG_U=0 when the protein is half unfolded, which occurs at the concentration corresponding to the midpoint of the equilibrium curve (C_{mid}). Hence, $\Delta G_U^{H_2O}$ can also be expressed as:

$$\Delta G_U^{H_2O} = mC_{mid} \quad (4.9)$$

Substituting Equation 4.9 into 4.8 yields:

$$\Delta G_U = m(C_{mid} - [\text{urea}]) \quad (4.10)$$

The observed optical signal (Y_{obs}) is related to the fraction of unfolded protein by:

$$Y_{obs} = Y_N(1-f_U)+Y_U(f_U) \quad (4.11)$$

where Y_N and Y_U are the optical signals for the native species and the unfolded species, respectively. Values of Y_N and Y_U may vary with [urea] in a linear fashion such that:

$$Y_N = Y_N^0 + S_N[urea] \quad (4.12)$$

and

$$Y_U = Y_U^0 + S_U[urea] \quad (4.13)$$

where Y_N^0 and Y_U^0 are the native and unfolded signals in the absence of urea, and S_N and S_U describe the dependence of the native and unfolded signals with urea respectively. By combining Equations 4.6, 4.7, 4.10, and 4.11, the final equation used for fitting can be expressed as:

$$Y_{obs} = \frac{(Y_N - [Y_N - Y_U])e^{\frac{m([Urea]-C_{mid})}{RT}}}{1+e^{\frac{m([Urea]-C_{mid})}{RT}}} \quad (4.14)$$

Both denaturation and renaturation curves were fit individually as well as globally (for the different protein concentrations) with *m* and C_{mid} as shared parameters using the program Origin 5.0 (Microcal, Northampton MA)

4.2.4 Analytical ultracentrifugation sedimentation velocity and equilibrium studies

Disulfide-reduced apo protein samples were analyzed by sedimentation velocity and/or equilibrium analysis at the Biomolecular Interactions and Conformations Facility, University of Western Ontario, ON. Samples were equilibrated with reference buffer using a nanosep device (3 Kda cuttoff membrane, Pall Corporation, East Hills, NY); analysis was under the same solution conditions as DSC measurements (20 mM HEPES, 1 mM TCEP, pH 7.4). Experiments were carried out using an Optima XL-A Analytical Ultracentrifuge (Beckman Coulter Inc., Fullerton, CA) with an An60Ti rotor and 2/6-channel cells (for velocity/equilibrium experiments respectively) with Epon-charcoal centerpieces. To eliminate potential metal contamination, centerpieces were soaked prior to use in 10 mM EDTA/100 mM NaCl, followed by brief soaking in 20 mM HEPES buffer, 1 mM TCEP, pH 7.4. Centrifugation was carried out at 20 °C using absorbance detection at either 252 or 280 nm. Velocity data were acquired at 50,000 rpm with measurements (average of 3 readings) collected at radial step sizes of 0.003 cm; scans were taken at 10 minute intervals for a total of 30 scans. Equilibrium data were acquired for a range of rotor speeds (20,000 to 45, 000 rpm) with measurements collected in radial step sizes of 0.002 cm and averaged over 10 readings. Prior to the collection of equilibrium measurements, samples were spun at the various rotor speeds for 16 hours to allow time for equilibration; readings subsequent to this initial measurement were taken in 4 hour increments to ensure equilibrium was reached as

judged by no further change in readings. All disulfide-reduced apo SODs were found to reach equilibrium during the initial 16 hour period.

Sedimentation velocity data were analyzed using the method of van Holde and Weischet (van Holde, 1978) using the program Sedfit (Schuck, 2000). Sedimentation equilibrium data were fit to equations describing a single homogeneous species as well as to association models for monomer/dimer, monomer/trimer and monomer/tetramer equilibria (McRorie, 1993). Briefly, for a single homogeneous species model, sedimentation equilibrium data were fit to:

$$A = A_o \exp\left[\frac{\omega^2}{2RT} MW_{obs}(1-\bar{\upsilon}\rho)(x^2 - x_o{}^2)\right] + I_o \tag{4.15}$$

where A is the absorbance at radius x, A_o is the absorbance at reference radius x_o, ω is the angular velocity of the rotor, MW_{obs} is the fitted molecular weight of the protein, $\bar{\upsilon}$ is the partial specific volume of the protein, ρ is the density of the solvent, R is the ideal gas constant, T is the temperature in Kelvin, and I_o is the baseline offset. Both $\bar{\upsilon}$ and ρ were determined using the program SEDNTERP (Laue, 1992), the former estimated from the protein primary sequence. MW_{obs} was globally shared between datasets acquired at different rotor speeds. In fitting of equilibrium data to the various association models, a 2-state transition between the disulfide-reduced monomer and oligomer was assumed, such that:

$$n[M] \xleftrightarrow{K_A} [M_n] \tag{4.16}$$

where M is monomeric, disulfide-reduced apo SOD, and M_n is a disulfide-reduced apo SOD homo-oligomer with n number of subunits. The transition between M and M_n is described by the association constant K_A:

$$K_A = \frac{[M_n]}{[M]^n} \tag{4.17}$$

K_A can be found by fitting the data to:

$$A = \left\{ A_o \exp\left[\frac{\omega^2}{2RT} MW(1-\bar{\upsilon}\rho)(x^2 - {x_o}^2) \right] \right\} + \left\{ {A_o}^n K_{abs} \exp\left[\frac{\omega^2}{2RT} nMW(1-\bar{\upsilon}\rho)(x^2 - {x_o}^2) \right] \right\} + I_o \quad (4.18)$$

where MW is the molecular weight of the monomer and K_{abs} is the association constant in absorbance units which is related to K_A using the Beer-Lambert Law according to:

$$K_{abs} = \frac{A_n}{A^n} = \frac{n \bullet \varepsilon_{mon}[M_n]d}{(\varepsilon_{mon}[M_n]d)^n} = \frac{n}{\varepsilon_{mon} d} \frac{[M_n]}{[M]^n} = \frac{n}{\varepsilon_{mon} d} K_A \quad (4.19)$$

which can be arranged as,

$$K_A = \frac{K_{abs} \varepsilon_{mon} d}{n} \quad (4.20)$$

where A and A_n are the absorbances of monomer and oligomer, respectively, ε_{mon} is the extinction coefficient in monomer units and d is the pathlength of the optical detection system (1.2 cm). In fitting sedimentation equilibrium data to Equation 4.18, MW was fixed to 15750 which is the known molecular weight of the SOD monomer and K_{abs} was set as a globally shared parameter between datasets collected as different rotor speeds; data were fit using Graphpad Prism, version 5.0 (Graphpad Software Inc., La Jolla, CA).

4.3 Results

4.3.1 Thermal unfolding of disulfide-reduced apo PWT is highly reversible.

Disulfide-reduced apo SOD was analyzed by DSC in 20 mM HEPES, pH 7.4, 1mM TCEP. TCEP is an ideal reducing agent for calorimetry studies due to its high thermal stability, lack of experimental artifacts and low propensity to oxidize in air (Han and Han, 1994). This suitability to DSC studies is in contrast to the more commonly used reducing agent dithiothreitol (DTT), which can be problematic in DSC studies in general due to its higher tendency to oxidize, and its lower effectiveness at neutral pH (Han and Han, 1994; Schoppe et al., 1997). It was confirmed that the samples remained reduced throughout scanning by performing SDS-PAGE with iodoacetamide modification of free cysteines on samples before and after DSC experiments (Figure 4.1). Previously, holo and disulfide-intact apo PWT SOD themal unfolding was found to be highly reversible when conducted in 20 mM HEPES pH 7.8 (Stathopulos et al., 2006). Similarly, disulfide-reduced apo PWT SOD thermal unfolding is highly reversible as assessed by scanning the sample, followed by immediate cooling and re-scanning (Figure 4.2). Reversibility is typically 90-99% when scanning just to the end of the unfolding transition, based on the areas for the two unfolding endotherms. This reversibility is only slightly lower than the previously reported reversibility of disulfide-intact apo PWT SOD (Stathopulos et al., 2006). In addition, when comparing disulfide-intact apo PWT to disulfide-reduced apo PWT it is noticeable that the apparent $t_{0.5}$, the temperature at maximum peak height, is significantly lower for the reduced species indicating marked destabilization (59 *versus* 48 °C).

The apparent $t_{0.5}$ of 48 °C reported here for disulfide-reduced apo SOD is approximately 10 °C higher than what was seen in previous thermal unfolding studies conducted at pH 7.8 in

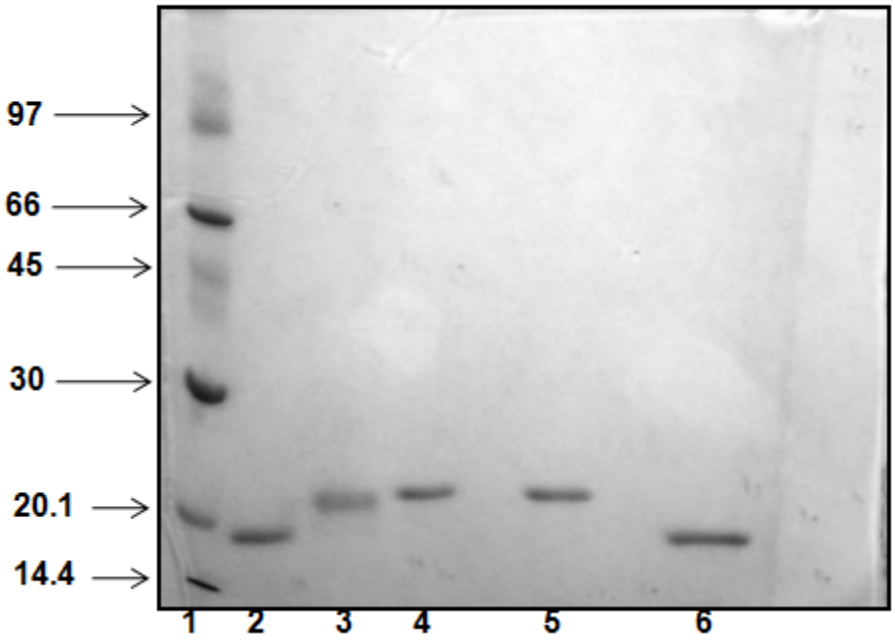

Figure 4.1. SDS-PAGE of disulfide-reduced apo SOD before and after DSC experiments. The gel contained 12% acrylamide and was visualized by staining with coomassie blue dye. Lane 1 is a low molecular weight marker with molecular weights as indicated. Lanes 2 and 6 are disulfide-intact apo SOD controls while lane 3 is apo SOD with disulfide reduced by β mercaptoethanol. Lanes 4 and 5 are disulfide-reduced apo SOD before and after DSC scanning respectively. Samples in lanes 4 and 5 were treated with iodoacetamide prior to loading on the gel in order to prevent free cysteines from being reoxidized on the gel. As can be clearly seen the DSC samples both before and after DSC scanning run much closer to the disulfide-reduced control in lane 3 than the oxidized controls in lanes 2 and 6, indicating that the samples were successfully reduced and remained reduced throughout the experiment.

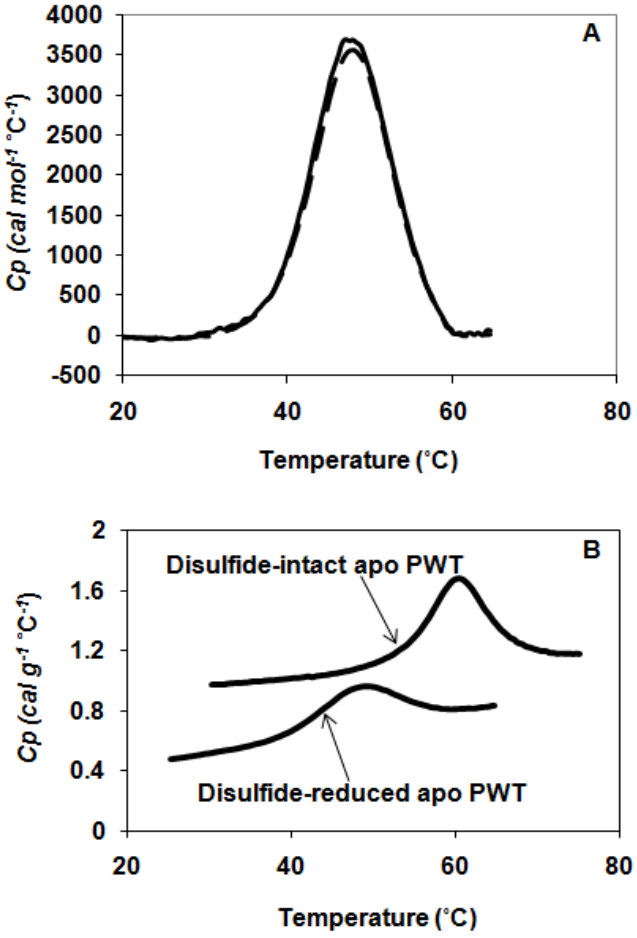

Figure 4.2. DSC scans of apo SOD in both disulfide-reduced and disulfide-intact forms. (A) Consecutive thermal unfolding traces of disulfide-reduced PWT apo SOD in which the sample was scanned (thermally unfolded), cooled and rescanned. The first (solid line) and second (broken line) scan are almost coincident. Calculation of the peak areas for both the first scan and the rescan after baseline subtraction indicates reversibility ~ 95%. (B) Comparison of disulfide-reduced apo PWT SOD and disulfide-intact apo PWT scanned in 20 mM HEPES, 1mM TCEP, pH 7.4 and 20 mM HEPES, pH 7.8 respectively. Disulfide reduction leads to a destabilization of apo SOD as evidenced by the apparent $t_{0.5}$ being reduced from ~59 to ~48 °C.

50 mM phosphate, 1 mM TCEP on a similar pseudo-WT construct (Furukawa and O'Halloran, 2005). This increased apparent $t_{0.5}$ is likely due to the use of HEPES buffer *versus* phosphate buffer and is also observed for the more mature disulfide-intact apo SOD (Rodriguez et al., 2005; Stathopulos et al., 2003). In addition, the reversibility of thermal unfolding is also greater in HEPES than in phosphate for the disulfide-reduced apo protein as well as the disulfide-intact apo and holo forms (Vassall, K.A., Stathopolus, P.B. and Meiering, E.M., Unpublished data).

4.3.2 Mechanism of thermal unfolding of disulfide-reduced apo PWT SOD

Given that reduction of the disulfide bond in apo SOD has been shown in previous studies to greatly weaken the dimer interface of SOD (Doucette et al., 2004; Lindberg, 2004), it has been suggested that disulfide-reduced apo SOD is monomeric at micromolar concentrations. Thermal unfolding of monomeric proteins do not exhibit a protein concentration dependence for the temperature of unfolding and hence evidence that disulfide-reduced apo SOD unfolds as a monomer can be obtained by investigating thermal unfolding over a large protein concentration range. Accordingly, the molecularity of thermal unfolding of disulfide-reduced apo PWT was probed by performing calorimetry scans over an ~ 20-fold protein concentration range (0.11-2.4 mg/mL). A protein concentration dependent shift to higher temperatures of unfolding would be expected if the protein unfolds as a dimer unit (Sturtevant, 1987). In contrast, no significant changes in the temperature of unfolding over the entire protein concentration range was observed (Figure 4.3A). The mechanism of thermal unfolding was further probed by fitting to a 2-state monomer unfolding model ($N \leftrightarrow U$, Equation 2.27, Table 4.1) as well as a 2-state dimer unfolding model ($N_2 \leftrightarrow 2U$, Equation 2.28). Data were only fit to the approximate end of the transition due to the presence of downward sloping post-transition baselines,

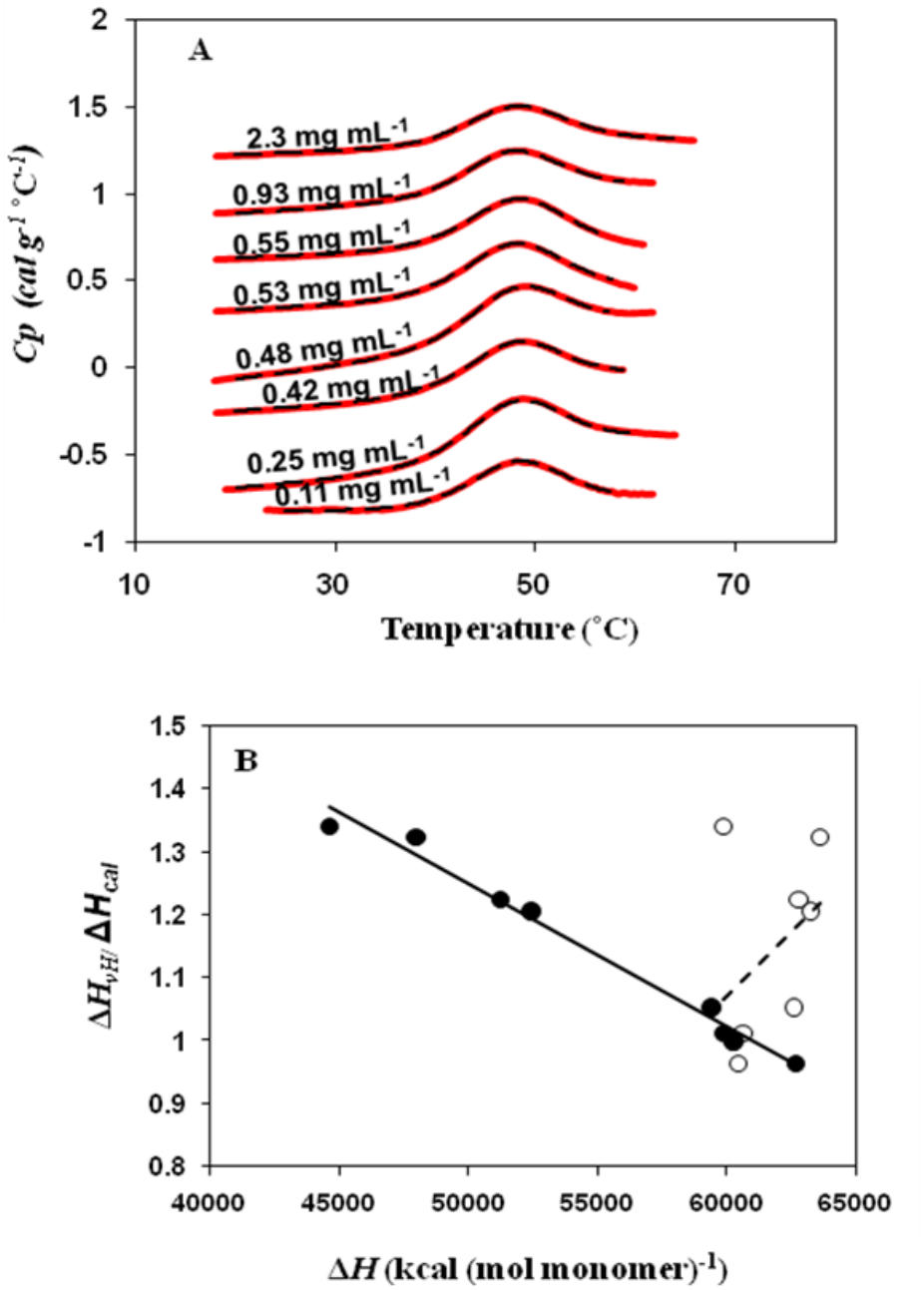

Figure 4.3. Fits of disulfide-reduced apo PWT to a 2-state monomer unfolding model. (A) DSC thermograms (red solid lines) at different protein concentrations as indicated. There is no concentration dependent shift to higher temperatures of unfolding as expected for a monomer. The data over the >20-fold concentration range is well fit (black broken lines) by a monomer 2-state unfolding model (Equation 2.27). Fitted parameters are given in Table 4.1. (B) Plots of $\Delta H_{vH}/\Delta H_{cal}$ *versus* ΔH_{vH} (closed circles) and $\Delta H_{vH}/\Delta H_{cal}$ *versus* ΔH_{cal} (open circles). There is an excellent linear correlation between $\Delta H_{vH}/\Delta H_{cal}$ and ΔH_{cal} (r= -0.992) while no good correlation is obtained between $\Delta H_{vH}/\Delta H_{cal}$ and ΔH_{vH}.

Table 4.1: DSC 2-state monomer unfolding fitted parameters for disulfide-reduced apo SOD

Apo SOD	[protein] (mg/ml)	$t_{0.5}$[a] (°C)	$\Delta C_p(t_{0.5})$[b] (kcal (mol monomer)$^{-1}$°C^{-1})	$\Delta H_{vH}(t_{0.5})$[c] (kcal (mol monomer)$^{-1}$)	$\Delta H_{cal}(t_{0.5})$[c] (kcal (mol monomer)$^{-1}$)	$\frac{\Delta H_{vH}}{\Delta H_{cal}}$
PWT	0.11	47.3±0.1	1.12	63.5±1.7	47.9±0.8	1.33
PWT	0.25	47.0±0.5	1.66	60.4±1.1	62.6±0.7	0.96
PWT	0.42	47.4±0.3	0.88	63.2±2.8	52.4±1.9	1.21
PWT	0.48	47.8±0.6	0.80	62.5±5.4	59.4±4.0	1.05
PWT	0.53	47.5±0.0	0.71	60.2±0.6	60.2±0.4	1.00
PWT	0.55	48.8±0.0	-0.27	60.6±0.7	59.8±0.4	1.01
PWT	0.93	47.7±0.3	0.27	62.7±3.2	51.2±1.9	1.22
PWT	2.30	47.5±0.1	0.61	59.8±1.7	44.6±0.8	1.34
AVG ± S.D[d]		47.6±0.5	0.7±0.6	61.6±1.5	54.8±6.6	1.1±0.2
H46R	0.33	52.3±0.1	-0.05	77.1±2.1	75.6±1.2	1.02
H46R	0.48	52.5±0.0	0.17	70.5±0.8	80.9±0.1	0.87
H46R	0.57	53.2±0.2	-1.39	70.5±2.9	73.2±1.6	0.96
AVG ± S.D[d]		52.6±0.5	-0.4±0.9	72.7±3.8	76.5±4.0	1.0±0.1
G85R	0.17	40.6±2.0	-0.46	52.2±13.9	74.3±13.2	0.70
G85R	0.38	40.4±0.6	0.22	50.9±3.8	47.1±2.5	1.08
G85R	1.42	41.2±0.2	-0.11	49.3±1.5	35.0±0.7	1.41
AVG ± S.D[d]		40.7±0.4	-0.11±0.33	50.8±1.5	52.3±20.2	1.1±0.4
E100G	0.43	35.0±0.1	0.32	42.2±1.0	32.8±0.4	1.24
E100G	0.49	32.7±1.1	0.87	45.5±6.8	37.9±4.8	1.20
E100G	0.75	33.0±0.1	0.89	43.4±1.3	32.3±0.7	1.34
E100G	0.80	32.1±0.1	1.07	42.1±1.2	32.6±0.5	1.29
AVG ± S.D[d]		33.2±1.2	0.79±0.32	43.3±1.4	34.3±2.6	1.3±0.1

[a]Errors (±) obtained from the fitting program. [b]Errors (±) from individual fits could not be reliably determined because they are based on uncertainties in five independent variables. [c]Errors (±) derived using standard procedures (Taylor, 1982) from errors in fitted $\Delta h_{cal}(t_{0.5})$ and β returned by the fitting program. [d]Average and standard deviation.

presumably due to exothermic aggregation of the unfolded protein at higher temperatures. Data fitting to the two models reveals that the data is better described by the 2-state monomer unfolding model (Figure 4.4). Analysis of the parameters returned from fitting to the 2-state monomer unfolding model reveals that the $t_{0.5}$ values are consistent across the entire protein concentration range as expected for monomer unfolding. Another measure of the appropriateness of a particular fitting model is a van't Hoff to calorimetric enthalpy ratio ($\Delta H_{vH}/\Delta H_{cal}$) at or close to unity (Sturtevant, 1987). While fits of disulfide-reduced apo PWT data to a 2-state dimer unfolding model gave ratios less than 1 (data not shown), fits to a 2-state monomer unfolding model gave an average $\Delta H_{vH}/\Delta H_{cal}$ of 1.1 ± 0.2 across all datasets (Table 4.1). As can be seen from Table 4.1, some datasets have increased $\Delta H_{vH}/\Delta H_{cal}$, which could in theory suggest that some slight dimerization may be occurring (Sturtevant, 1987). It is more likely in this case that increases in $\Delta H_{vH}/\Delta H_{cal}$ result from very slight random aggregation and not native dimerization. This is a reasonable conclusion for the following reasons: firstly, there is no systematic increase in $\Delta H_{vH}/\Delta H_{cal}$ with protein concentration as would be expected for a dimerizing system (Table 4.1); and secondly, the ΔH_{vH} is relatively constant across the protein concentration range. It was previously outlined in Section 2.3.2 but is worth reiterating here that an increase in the size of the molecular co-operative unfolding unit would be expected to cause high $\Delta H_{vH}/\Delta H_{cal}$ through increases in ΔH_{vH} (Sturtevant, 1987). It would appear that the high $\Delta H_{vH}/\Delta H_{cal}$ seen for some datasets of disulfide-reduced apo PWT is caused by decreases in ΔH_{cal}; changes in $\Delta H_{vH}/\Delta H_{cal}$ correlate very closely with ΔH_{cal} (r = -0.992), whereas no correlations are apparent between $\Delta H_{vH}/\Delta H_{cal}$ and ΔH_{vH} (Figure 4.3B). The decreases in ΔH_{cal} could be caused by the evolution of exothermic heat from aggregate formation, which would make the endotherm associated with unfolding appear smaller. Alternatively, decreases in ΔH_{cal} could result from the presence of pre-existing aggregates, quantified by the protein concentration assay but which does not unfold

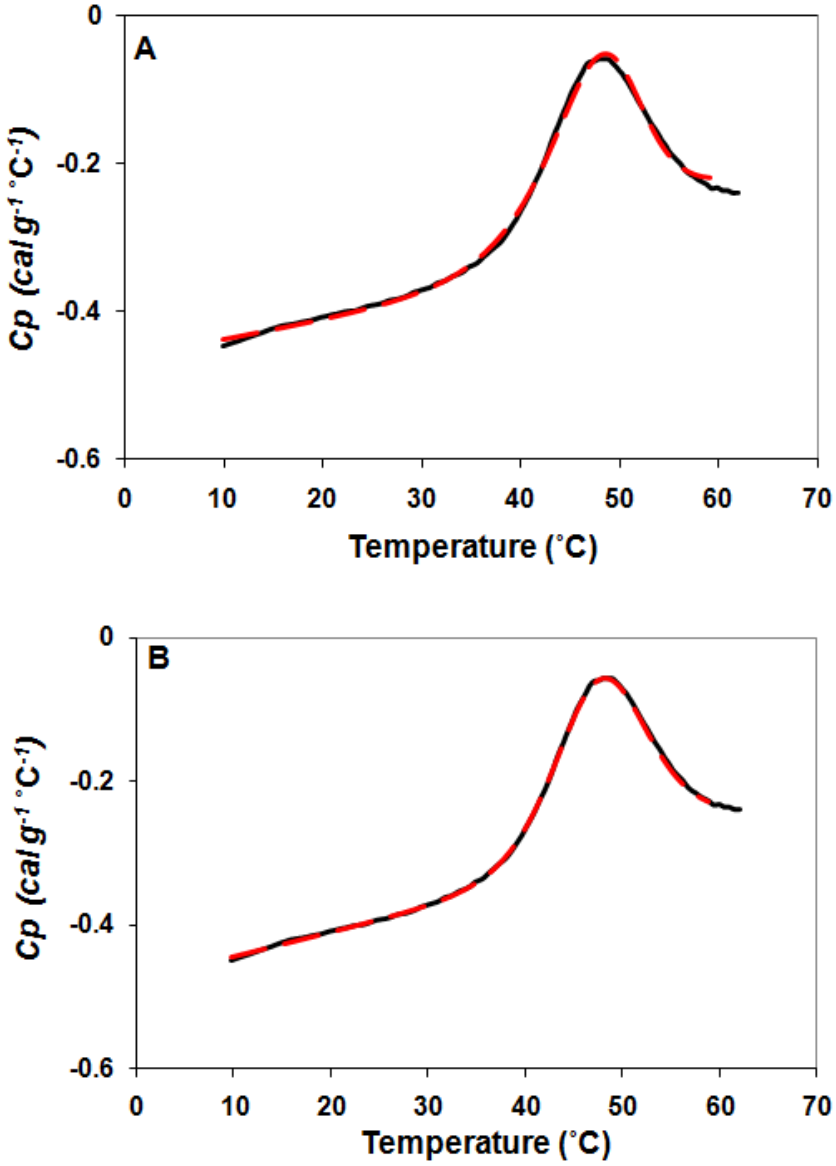

Figure 4.4. Comparison of 2-state monomer and 2-state dimer fits of apo disulfide-reduced PWT SOD. A thermal unfolding trace of 0.93 mg/mL apo disulfide-reduced PWT SOD is shown. Data (black solid lines) were fit (red broken lines) to models describing (A) 2-state dimer unfolding (Equation 2.28) and (B) 2-state monomer unfolding. (Equation 2.27). There are clear systematic deviations in the fit to the 2-state dimer unfolding model but not for the 2-state monomer unfolding model.

(see Section 2.3.2). Further evidence that the cooperative unfolding unit of disulfide-reduced apo PWT is a monomer at typical concentrations used in calorimetry studies was derived from analytical ultracentrifugation studies, which indicated only the presence of monomeric SOD (Section 4.3.7).

4.3.3 Determination of ΔC_p of unfolding of disulfide-reduced apo PWT SOD

As previously described, ΔC_p is a fundamental thermodynamic quantity that is required to evaluate the parameters ΔH, ΔG and ΔS at temperatures other than the $t_{0.5}$ (Equations 2.61-2.64). As outlined in Section 2.1.1, ΔC_p can be derived from fitting as the difference between the unfolded and folded baselines, and it is related to the increase in solvent accessible surface area upon unfolding (Myers et al., 1995). However, as previously noted, the ΔC_p value derived from data fitting is subject to very large errors due to the inherent uncertainty in determining an accurate slope and intercept of the post-transition baseline (Section 2.3.2). This further is compounded by fitting data only to the end of the unfolding transition. The average ΔC_p obtained from fitting disulfide-reduced apo PWT data is 0.7±0.6 kcal mol^{-1} °C^{-1} (Table 4.1); the large standard deviation is a testament to the unreliability of the ΔC_p obtained in this way. Additionally, it is apparent that higher concentrations of PWT generally tend to have lower ΔC_ps. Low ΔC_ps could result from an exothermic process such as intermolecular aggregation as the protein unfolds, which would lead to the post-transition baseline being decreased to just slightly above or even below the pre-transition baseline (Stathopulos et al., 2006). It does not appear that low or even negative ΔC_p dramatically affects the other fitted parameters as these seem to be fairly consistent across the protein concentration range as noted in the previous section (Table 4.1).

ΔC_p can alternatively be determined by performing DSC scans on successively destabilized protein samples, commonly achieved by performing scans at different pHs (Privalov, 1979). ΔC_p is then calculated through Kirchoff analysis (from the slope of plots of ΔH *versus* $t_{0.5}$) from the various datasets. This approach was attempted for disulfide-reduced apo PWT SOD; specifically, DSC scans were conducted in 1 mM TCEP, 20 mM sodium acetate at pHs 5 and 5.6. Thermal unfolding at these pHs is largely irreversible and hence the data are not suitable for thermodynamic analysis (Figure 4.5). This is in contrast to disulfide-intact apo PWT, which thermally unfolds reversibly in this buffer at a similar pH (Stathopulos, 2005). Another way the SOD protein can be destabilized is by using a chemical denaturant such as urea or GdmCl (Lindberg, 2004; Stathopulos et al., 2006). The use of a chemical denaturant can be an advantage, given that the extent of destabilization can be accurately controlled and the denaturant can often dissociate any aggregates that may form upon destabilization (Nölting, 2006). Urea is the weaker of the two denaturants and was chosen for this study, as it is a neutral molecule and thus does not alter the ionic strength of the sample. Thermal scans of disulfide-reduced protein samples in 1 mM TCEP, 20 mM HEPES, pH 7.4 were conducted at different urea concentrations ranging from 0-1.25 M, corresponding to reductions in apparent $t_{0.5}$s ranging from ~36 to 48 °C (Table 4.2, Figure 4.6). All scans in urea were highly reversible (data not shown). A significantly larger range of $t_{0.5}$s could not be achieved due to the instability of the disulfide-reduced protein and the general broadening of the DSC endotherm, which occurs as the protein is destabilized. Generally, the pre-transition baselines in urea were quite variable, with some scans demonstrating significant increases in the slope of the pre-transition baseline. This caused complications when data were fit to a 2-state monomer unfolding model using Equation 2.27 (in which both pre and post-transition baselines are included in data fitting).

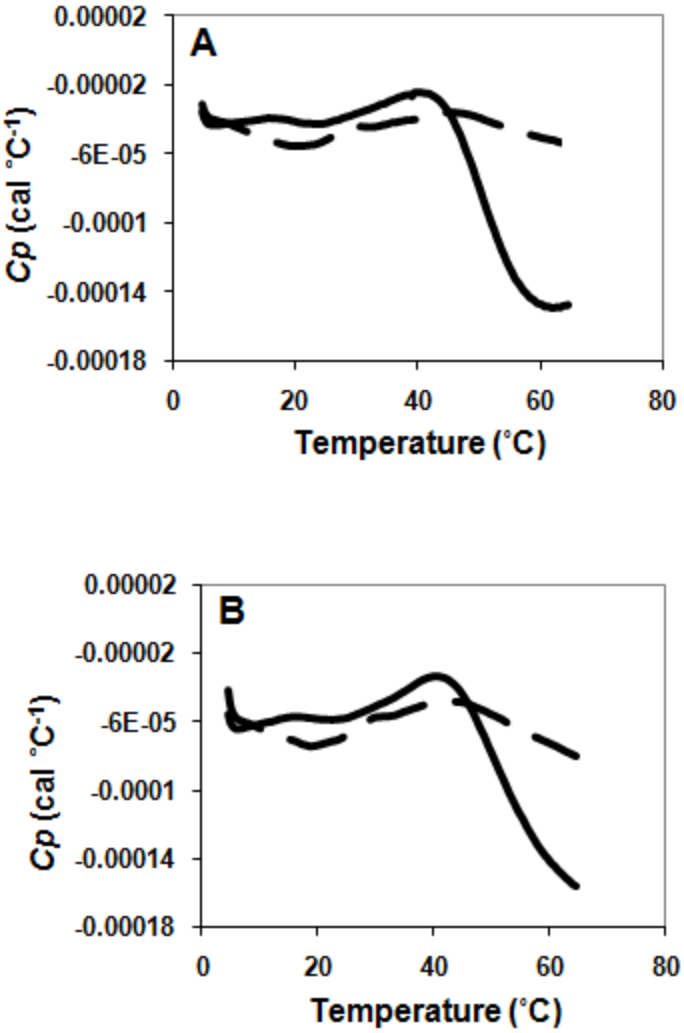

Figure 4.5. Disulfide-reduced apo PWT SOD DSC thermograms at lower pH. Data was collected in 20mM sodium acetate, 1mM TCEP, at (A) pH 5.0 and (B) pH 5.6. The first scans are represented by solid lines while the second scans acquired by cooling the sample after the first scan and immediately re-scanning are shown as broken lines. In contrast to scans conducted in 20mM HEPES, pH 7.4, the first and second scans are not coincident, indicating decreased reversibility under these conditions.

Table 4.2: 2-state monomer unfolding DSC fitted parameters for disulfide-reduced apo PWT SOD for data obtained in urea

[urea] (M)	$t_{0.5}$ (°C)	ΔH_{vH} (kcal (mol monomer)$^{-1}$)	ΔH_{cal} ($t_{0.5}$) (kcal (mol monomer)$^{-1}$)	$\frac{\Delta H_{vH}}{\Delta H_{cal}}$
0	47.6 ± 0.5	61.6 ± 1.5	54.8 ± 6.6	1.14
0.25	46.2 ± 0.0	58.0 ± 0.5	67.4 ± 0.5	0.86
0.50	43.4 ± 0.0	54.0 ± 0.4	50.5 ± 0.3	1.07
0.75	41.4 ± 0.0	52.8 ± 0.3	55.5 ± 0.2	0.95
0.88	40.6 ± 0.0	51.9 ± 0.4	46.8 ± 0.3	1.11
1.00	38.9 ± 0.0	51.6 ± 0.3	47.1 ± 0.3	1.10
1.25	36.8 ± 0.1	49.4 ±0.5	44.5 ± 0.4	1.11

All errors (±) obtained from the fitting program.

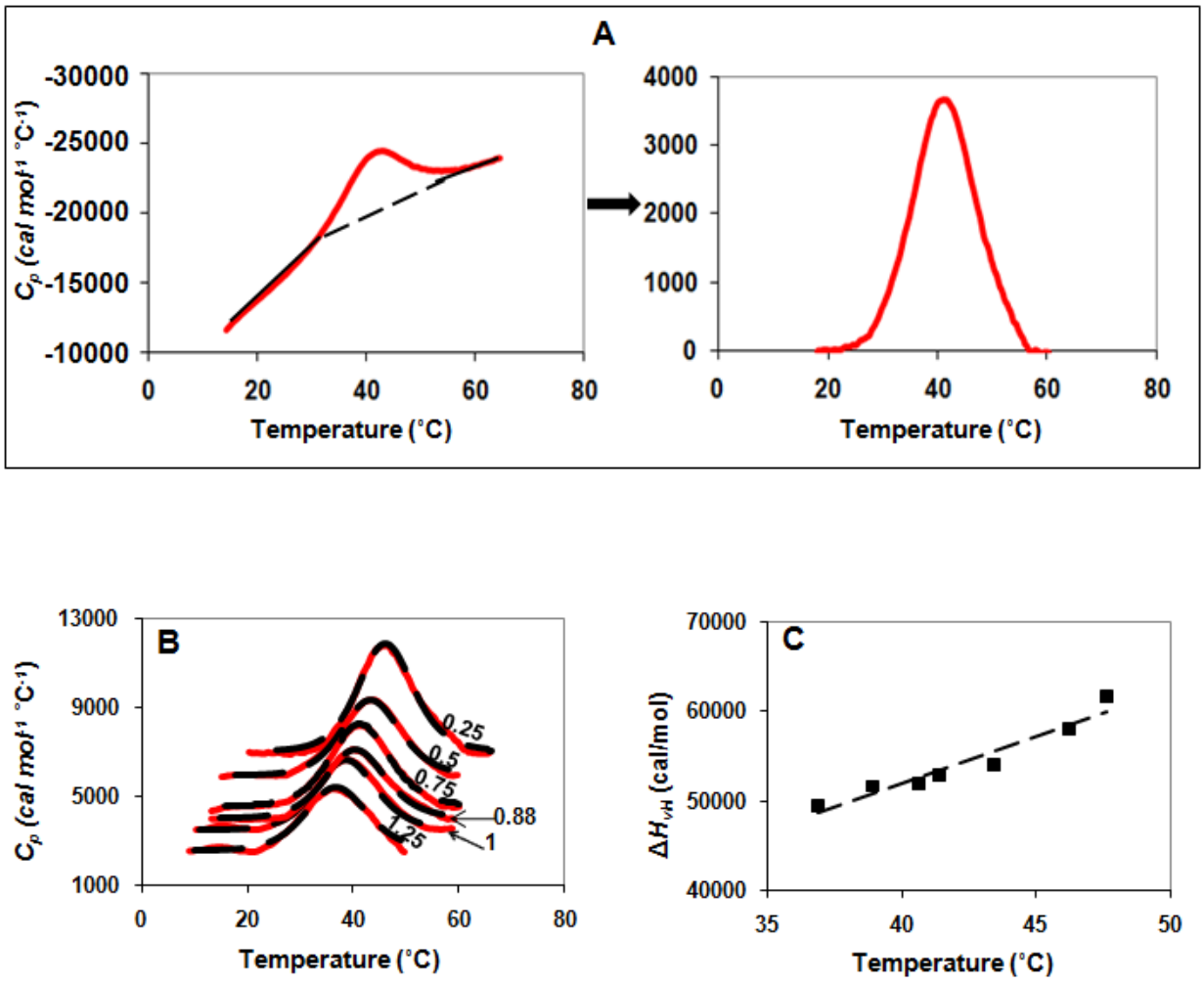

Figure 4.6. Data fitting of disulfide-reduced apo PWT DSC scans in urea. (A) Baseline subtraction of DSC data collected in urea using a linear connect method. Both pre and post-transition baselines are approximated by straight lines, which are linearly connected under the unfolding endotherm (Left panel). Subtraction of the baselines from the data results in the excess heat ($C_{p,ex,}$) as shown (Right panel). (B) 2-state monomer unfolding fits (Equation 4.1, black broken lines) of data (solid red lines) acquired in 0.25, 0.5, 0.75, 0.875, 1 and 1.25M urea (top to bottom). (C) Kirchoff plot (ΔH_{vH} vs. $t_{0.5}$) to determine ΔC_p of thermal unfolding of disulfide-reduced apo PWT SOD. The values for the plot were obtained from fits to a 2-state monomer unfolding model (panel B and Table 4.2) and is well approximated by a linear regression fit (r=0.967). The slope from this linear regression ($\Delta\Delta H_{vH}/\Delta t_{0.5}=\Delta C_p$) is 1.05 ±0.1 kcal mol^{-1} °C^{-1}.

For this reason, only the excess heat obtained after subtraction of the baselines were fit to a 2-state monomer unfolding model (Equation 4.1) as is commonly done in DSC analyses (Consalvi et al., 2000; Jha et al., 2004; McCrary et al., 1998; Yang et al., 2004). In the process of subtracting baselines, a linear connect method was utilized which effectively removes the influence of the baselines (Figure 4.6a). For the purpose of comparison, disulfide-reduced apo PWT SOD datasets acquired in the absence of urea were also subjected to the same analytical treatment as the urea scans and it was found that the fitted parameters change very little, thereby validating this approach (<10% for ΔH_{vH} and ΔH_{cal}; and <1% for $t_{0.5}$).

Fitting of the urea scans revealed a uniform decrease in ΔH with decreasing $t_{0.5}$ (Table 4.2, Figure 4.6B), as expected when a protein with a positive ΔC_p is destabilized (Sturtevant, 1987). Additionally, given that $\Delta H_{vH}/\Delta H_{cal}$ is very close to 1 across the various urea concentrations used (Table 4.2), it appears that urea does not change the folding mechanism of the protein nor is there significant aggregation upon urea-mediated destabilization. A plot of ΔH_{vH} *versus* $t_{0.5}$ is well fit to a linear residual with r = 0.965 yielding a ΔC_p from the slope of 1.05 kcal mol^{-1} °C $^{-1}$ (Figure 4.6C). The ΔC_p from the Kirchoff plot is ~ 30% larger than the average ΔC_p of 0.7 ± 0.6 kcal mol^{-1} °C $^{-1}$ obtained from 2-state fitting of the various PWT datasets (see above). It is, however, unclear if this difference is significant, given that 1.05 kcal mol^{-1}°C^{-1} is within the large errors of the value from the fits. The value of ΔC_p derived from the Kirchoff plot is in fact quite low. Given that ΔC_p is proportional to the change in solvent-accessible surface area upon unfolding, a protein with the number of amino acids in the SOD monomer is expected to have a ΔC_p on the order of 2 kcal mol^{-1} °C^{-1}(Geierhaas et al., 2007; Myers et al., 1995). An unusually low ΔC_p could indicate that the disulfide-reduced monomer is less well structured than a typical globular protein.

It should be noted that, although ΔC_p from the Kirchoff analysis appeared to be lower than expected, it might in fact even be an overestimation. Obtaining ΔC_p by scanning samples in denaturant can lead to artifactual increases in ΔC_p due to exothermic enthalpies of denaturant binding to the protein (Makhatadze and Privalov, 1992; Zweifel and Barrick, 2002). Given that low concentrations of urea were used here, the heats associated with urea binding are likely small and should not have a large affect on the ΔC_p determination. Furthermore, a similar strategy was adopted to measure the ΔC_p of holo SOD using a much larger range of denaturant concentration (GdmCl up to 2.4M), which yielded a similar ΔC_p to that determined by a Kirchoff plot with pH destabilization and in fairly good agreement with theoretically calculated values based on changes in solvent accessible surface area (Stathopulos et al., 2006).

4.3.4 Thermodynamic stability of disulfide-reduced apo PWT SOD

The ΔC_p from the Kirchoff plot was used to calculate ΔG, ΔS and ΔH of thermal unfolding of the disulfide-reduced PWT protein at temperatures away from the $t_{0.5}$ (Table 4.3). The ΔC_p was assumed to be temperature-independent, as is common for analyses of this type and is generally valid when the extrapolation range is small (Prabhu and Sharp, 2005). Similarly to data collected on the disulfide-intact apo protein (Section 2.3.3), ΔH_{vH} was used in calculations of thermodynamic parameters as it is less variable across datasets than ΔH_{cal} and seems to be relatively insensitive to aggregation. The ΔG of unfolding at 37 °C is 1.8 ± 0.1 kcal (mol monomer)$^{-1}$, while ΔH and ΔS are 50.5 ± 1.6 kcal (mol monomer)$^{-1}$and 0.157 ± 0.005 kcal (mol monomer)$^{-1}$K^{-1} respectively. Interestingly, the value of ΔG depends very little on the value of ΔC_p used.

Table 4.3: Summary of thermodynamic parameters for disulfide-reduced apo SOD mutant thermal unfolding analyzed by DSC

Protein	$t_{0.5}$ (°C)	$t_{0.5}$[a] (°C)	ΔG (25°C)[b,c] (kcal (mol of monomer)$^{-1}$)	ΔG (37°C)[b,c] (kcal (mol of monomer)$^{-1}$)	ΔH (37°C)[b,c] (kcal (mol of monomer)$^{-1}$)	ΔS (37°C)[b,c] (kcal (mol of monomer)$^{-1}$)K^{-1}	$\Delta\Delta G$ (37°C)[d] (kcal (mol of monomer)$^{-1}$)	$\Delta\Delta H$ (37°C)[d] (kcal (mol of monomer)$^{-1}$)	$\Delta\Delta S$ (37°C)[d] (kcal (mol of monomer)$^{-1}$) K^{-1}	ΔG (37°C)[e] (kcal (mol of dimer)$^{-1}$)
PWT	47.6 ± 0.5	n/a[f]	3.5 ± 0.1	1.8 ± 0.1	50.5 ± 1.6	0.157 ± 0.005	n/a	n/a	n/a	13.2 ± 1.3
H46R	52.6 ± 0.5	+5	4.9 ± 0.1	3.1 ± 0.1	56.1 ± 4.2	0.171 ± 0.013	+1.2	+5.6	+0.014	18.1 ± 0.3
G85R	40.7 ± 0.4	-6.9	2.1 ± 0.1	0.6 ± 0.0	46.9 ± 1.8	0.149 ± 0.006	-1.3	-3.7	-0.008	13.3 ± 0.4
E100G	33.2 ± 1.2	-14.4	1.0 ± 0.1	-0.6 ± 0.2	47.3 ± 2.0	0.155 ± 0.007	-2.4	-3.0	0.002	12.8 ± 0.8

[a]Calculated from $t_{0.5\ \text{mutant}} - t_{0.5\ \text{PWT}}$, negative values indicate destabilization. [b]Values calculated using Equations 2.61-2.64 using a temperature-independent ΔC_p value of 1.05 kcal (mol of monomer)$^{-1}$°C^{-1} derived from Kirchoff analysis (Figure 4.7). [c]Values shown are averages of the individual datasets from Table 4.1 while errors (±) are standard deviations. [d]$\Delta\Delta H = \Delta H_{(\text{mutant})} - \Delta H_{(\text{PWT})}$, $\Delta\Delta S_{(\text{mutant})} - \Delta S_{(\text{mutant})}$, $\Delta\Delta G = \Delta G_{(\text{mutant})} - \Delta G_{(\text{PWT})}$. [e]$\Delta G$ of the disulfide-intact apo protein at 37 °C. Values for PWT, H46R and G85R are reproduced from Table 2.4 while values for E100G were calculated from 2-state dimer unfolding fitted parameters presented in Vassall et al., 2006 using a temperature independent ΔC_p of 3.3 kcal (mol of dimer)$^{-1}$°C^{-1} (Equations 2.61-2.64). The error presented for E100G is from the standard deviation of 3 independent datasets. [f]n/a not applicable.

For example, an increase or decrease in ΔC_p of 50% only changes this value of ΔG by -0.1 and +0.1 kcal (mol monomer)$^{-1}$ respectively. Given that the ΔG of unfolding of disulfide-intact apo PWT SOD is 13.24 ± 1.24 kcal (mol dimer)$^{-1}$ (or 6.6 kcal (mol monomer)$^{-1}$) (Table 2.4), it is apparent that despite a relatively moderate reduction of ~10 °C in the $t_{0.5}$ of unfolding, there is a marked destabilization in the free energy of unfolding upon disulfide reduction.

4.3.5 Thermal unfolding of disulfide-reduced apoSOD mutants

In order to determine the effects of ALS-associated SOD mutations in a disulfide-reduced apo background, chemically and structurally diverse mutants were characterized: A4V, A4T, E100G, G93R, G93S, G37R, G85R, H43R and H46R. All of these mutants produced measurable unfolding endotherms (Figure 4.7). This is in contrast to previous investigations, where no measurable endotherms were obtained for two of the mutants, A4V and G93R (Rodriguez et al., 2005) and another where the stabilizing osmolyte glycerol was needed in order to obtain a measurable endotherm for A4V (Furukawa and O'Halloran, 2005). When looking at the apparent $t_{0.5}$ values, it is evident that all mutants, with the exception of H46R, are destabilized compared to PWT (Table 4.4). Some mutants are destabilized by as much as 17 °C. In fact, all of the disulfide-reduced apo SOD mutants except for H46R and G85R have $t_{0.5}$ values at or below 37 °C. This is in contrast to the more mature disulfide-intact holo and apo forms of SOD, which have considerably higher $t_{0.5}$ values (~90 °C and ~59 °C) respectively and so remain predominantly folded at 37 °C even when destabilized by mutations (Stathopulos et al., 2006; Vassall et al., 2006). The reversibility of unfolding of all the disulfide-reduced apo SOD mutations was evaluated, similarly to PWT, by scanning of the sample

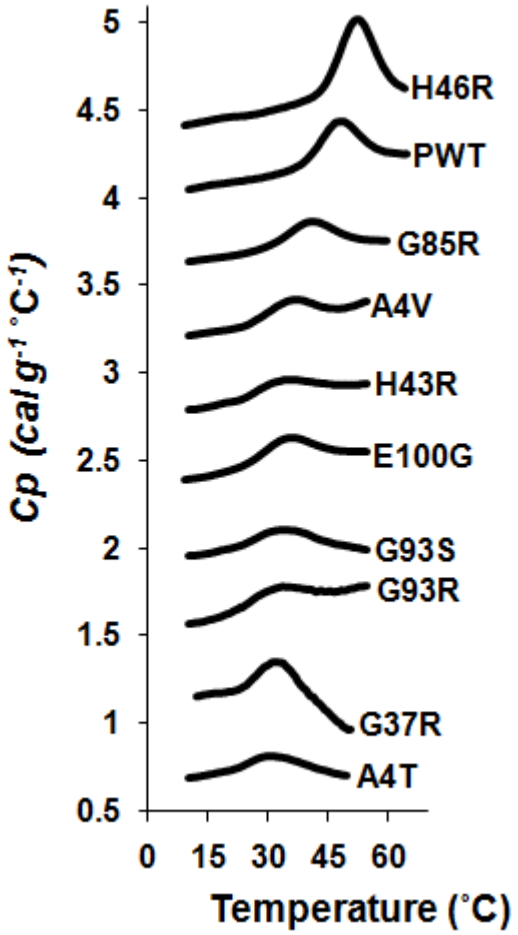

Figure 4.7. DSC thermograms for disulfide-reduced apo PWT and fALS-associated mutants. All the mutations with the exception of H46R are destabilized as demonstrated by the lower temperatures needed to unfold the proteins (Table 4.4). The thermograms are normalized and offset for ease of comparison.

Table 4.4: Summary of apparent $t_{0.5}$ values for disulfide-reduced apo SOD

Apo isoform	Apparent $t_{0.5}$ (disulfide-reduced)[a] (°C)	$t_{0.5}$ (disulfide-intact)[b] (°C)	$\Delta t_{0.5}$ (disulfide-reduced)[c] (°C)	$\Delta t_{0.5}$ (disulfide-intact)[c] (°C)	$t_{0.5\ (\text{disulfide -reduced})} - t_{0.5\ (\text{disulfide-intact})}$[d] (°C)
PWT	48.5 ± 0.3	59	n/a	n/a	-10.5
H46R	52.8 ± 0.4	62.7	+4.3	+3.7	-9.9
G85R	41.2 ± 0.3	54.5	-7.3	-4.5	-13.3
A4V	36.3 ± 0.2	48.9	-12.2	-10.1	-12.6
H43R	35.4 ± 0.4	48.5	-13.1	-10.5	-13.1
E100G	35.3 ± 0.7	51.3	-13.2	-7.7	-16.0
G93S	33.8 ± 1.2	50.7	-14.7	-8.3	-16.9
G93R	35.4 ± 1.8	48.9	-13.1	-10.1	-13.5
G37R	33.5 ± 1.2	50.1	-15	-8.9	-16.6
A4T	30.9 ± 0.3	44.5	-17.6	-14.5	-13.6

[a]Values are the temperature at maximum C_p (Figure 4.7) and are an average of at least 3 independent scans except for G93R, G37R and A4T which are an average of 2 independent scans. Errors (±) are the standard deviation. [b]Values of $t_{0.5}$ for the apo disulfide –intact protein for PWT, H46R, G85R, A4V, A4T, G37R, and H43R are reproduced from $t_{0.5}$ values presented in Table 2.4. These values were determined at 0.5 mg/mL from average stability plots. For H46R and A4V, the $t_{0.5}$ of the second transition (monomer unfolding is presented; see Table 2.4). Values for G93R and G93S were obtained from (Stathopulos et al., 2006) while the value for E100G was obtained from Vassall et al, 2006 and were determined at 0.5 mg/mL from average stability plots. [c]Calculated from $t_{0.5\ \text{mutant}} - t_{0.5\ \text{PWT}}$, negative values indicate destabilization. [d]The extent of reduction in $t_{0.5}$ for each mutant when the disulfide bond in reduced.

followed by immediate cooling and rescanning. Most mutants thermally unfold with low reversibility (less than 50%); however relatively high reversibility, comparable to what was seen for disulfide-reduced apo PWT, was seen for three of the mutants: H46R, E100G and G85R (Figure 4.8). Hence, while only estimates of stability may be obtained for the mutants that unfold with low reversibility, more extensive thermodynamic analysis is possible for the mutants which unfold with high reversibility. The disulfide-reduced apo SOD mutants H46R, E100G and G85R were all fit, similarly to PWT, to a 2-state monomer unfolding model (Equation 2.27, Figure 4.9 and Table 4.1). Despite the high reversibility of the mutants, there is some evidence of increased aggregation from the fitted parameters. H46R and G85R have very low, mostly negative ΔC_p values with the average being -0.42 and -0.11 kcal mol^{-1} °C^{-1} respectively. This is in contrast to PWT, which despite some high concentration datasets having low ΔC_p values, all but one is positive. E100G does not display unusually low ΔC_p values, however, its $\Delta H_{vH}/\Delta H_{cal}$ is higher than 1 at 1.28 which can be indicative of aggregates being present (Privalov and Potekhin, 1986). High ratios were also obtained for this mutant in the disulfide-intact apo protein (Rumfeldt, 2006; Vassall et al., 2006). Similarly to what was seen for disulfide-reduced apo PWT SOD, ΔH_{vH} is very consistent across the disulfide-reduced apo SOD mutant datasets, much more so than $\Delta H_{cal,}$ and hence again it was used for the calculation of thermodynamic parameters (Table 4.3). These parameters were also determined at 37 °C for these mutants using the ΔC_p determined from the Kirchoff plot (Figure 4.6c). When looking at the $\Delta\Delta Gs$ (ΔG_{mut}-ΔG_{pwt}) of the disulfide-reduced apo SOD mutants, it is apparent that H46R is slightly stabilizing (+1.2 kcal mol^{-1}) while G85R is slightly destabilizing (-1.3 kcal mol^{-1}). E100G is also destabilizing (-2.4 kcal mol^{-1}) and significantly the ΔG at 37 °C is negative indicating that there is a higher population of unfolded than folded conformation at physiological temperature. Analysis of the $\Delta\Delta H$ and $\Delta\Delta S$ values, defined as the difference between ΔH (or ΔS) between disulfide-reduced

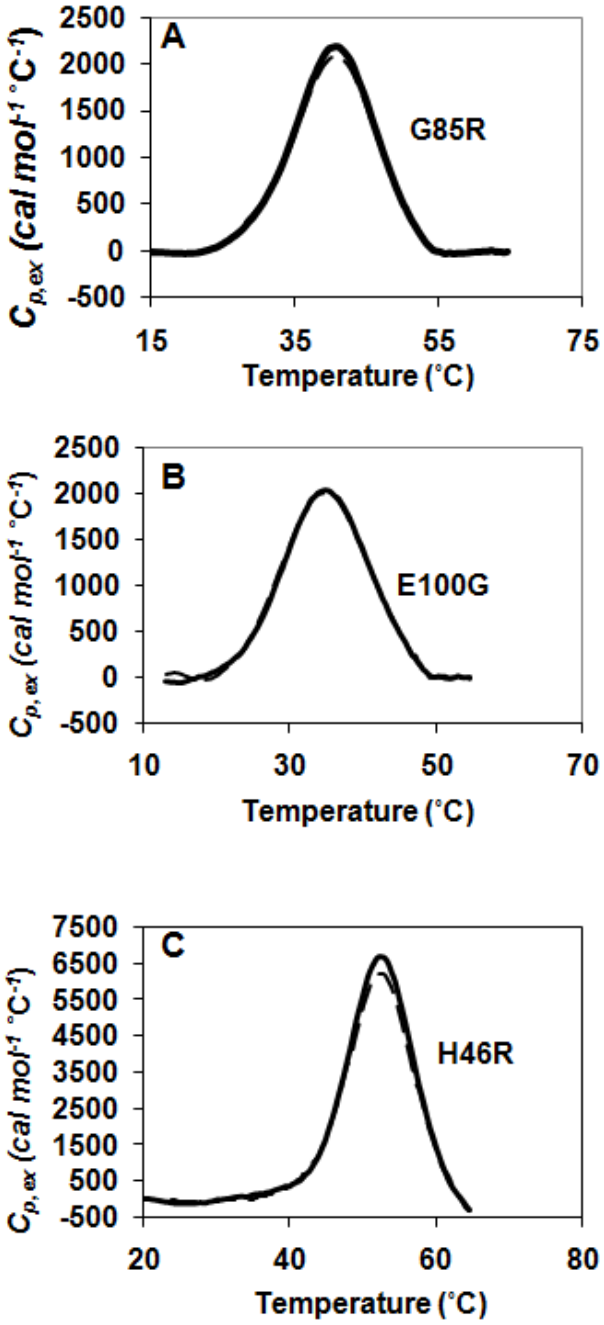

Figure 4.8. Consecutive thermal unfolding traces of disulfide-reduced apo SOD mutants G85R, E100G and H46R. Two consecutive scans were obtained to determine reversibility with the second scan (broken lines) obtained immediately after cooling the sample upon completion of the first scan (solid line). The extent of reversibility was determined by assessing the area under the unfolding endotherm after subtraction of baselines and was found to exceed 90% for all mutants.

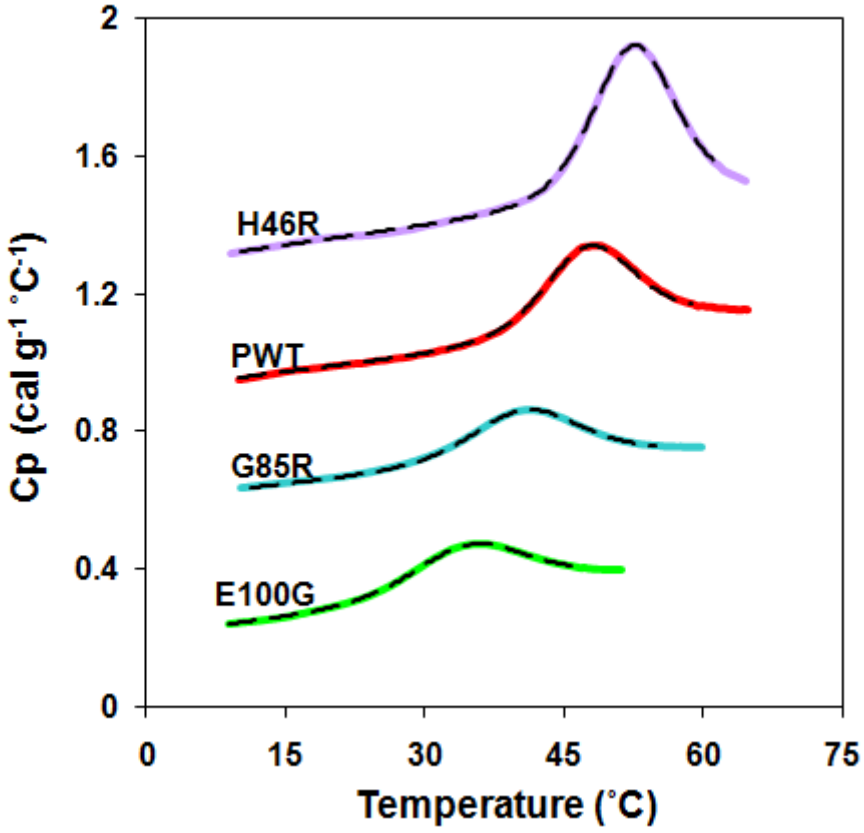

Figure 4.9. DSC data fitted to the 2-state monomer unfolded model for disulfide-reduced apo PWT and apo mutants. Typical thermograms (solid lines) with corresponding 2-state monomer fits (Equation 2.27, broken lines) are shown. Datasets are offset for clarity. The mutants E100G and G85R are destabilized as evidenced by the downward shifts in temperatures of unfolding compared to PWT while H46R is slightly more stable. Parameters obtained from the fits are displayed in Table 4.1.

apo mutant and PWT SOD, reveals that H46R is enthalpically stabilized while G85R and E100G are enthalpically destabilized.

4.3.6 Chemical denaturation and renaturation of disulfide-reduced apo SOD

Equilibrium urea chemical denaturation and renaturation curves were obtained with the protein in 1 mM TCEP, 20 mM HEPES pH 7.4 at 25 °C for the disulfide-reduced PWT as well as the mutant H46R in order to independently measure ΔG of unfolding for comparison to the calorimetry results. The curves were measured by Trp fluorescence as well as by CD at 216 and 231 nm. The fluorescence curves are very scattered and as a result impossible to interpret, as they did not have the expected sigmoidal shape (data not shown). However, the CD curves, especially curves measured at 231 nm are much less scattered and have a much better defined transition that lends itself to accurate analysis (Figure 4.10). Urea renaturation curve protein samples were incubated for 24 hrs before being measured and are highly reversible as judged by the congruence of denaturation and renaturation curves (Figure 4.10). Global fits to a 2-state monomer unfolding model of datasets at 216 and 231 nm for disulfide-reduced apo PWT and H46R SODs yield similar m values with the average being 2.49 ± 0.30 kcal mol^{-1}, while the midpoint of denaturation (C_{mid}) for PWT is ~ 1.6 M and for H46R is ~ 0.4 M higher (Table 4.5). The fact that both m and C_{mid} values (especially considering the scatter in curves measured at 216 nm) are similar for data measured at both wavelengths is indicative that the 2-state monomer unfolding model used is appropriate. The higher C_{mid} for H46R suggests greater stability for this mutant, which is consistent with DSC results (Table 4.5). It is interesting that, while ΔC_p obtained from DSC analysis is lower than expected for a protein of this size, the m value, which is also related to change in solvent accessible surface upon unfolding is close to what is expected (Geierhaas et al., 2007; Myers et al., 1995). Such discrepancies between m and ΔC_p have also

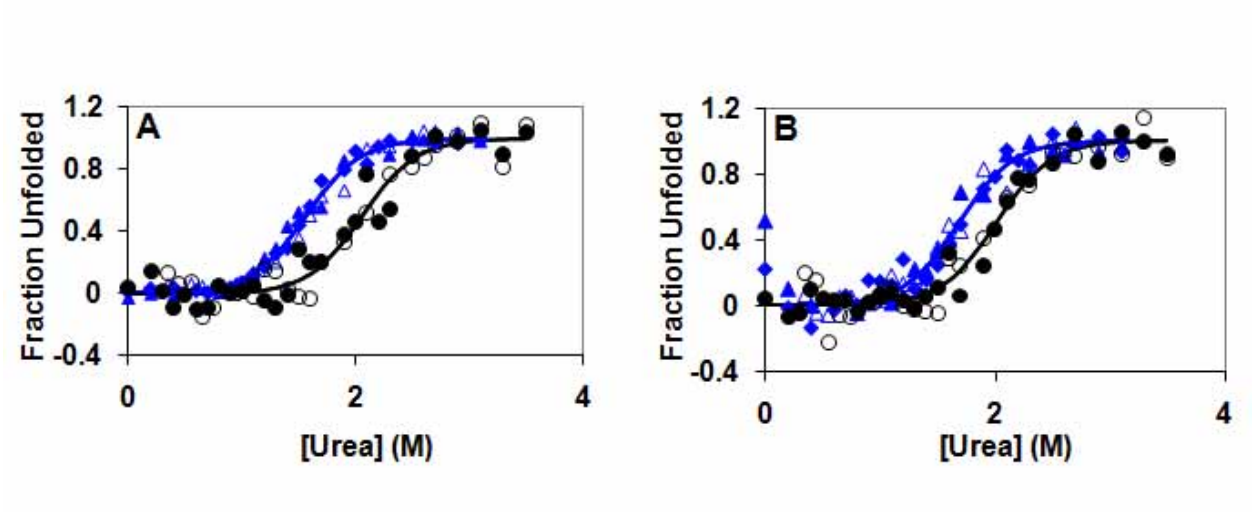

Figure 4.10. Urea renaturation and denaturation curves of disulfide-reduced apo SOD at 25 °C. Data for PWT is shown in blue while data for H46R is shown in black. Protein concentrations for the curves are 14 μM (triangles), 24 μM (diamonds) and 8.5 μM (circles). Denaturation data are plotted as closed symbols while renaturation data are plotted as open symbols. Data for each protein acquired at (A) CD 216 nm and (B) CD 231 nm were fit globally to a 2-state monomer unfolding model (Equation 4.14) with C_{mid} and m as shared parameters (Table 4.5).

Table 4.5: Summary of 2-state monomer unfolding fitted parameters from urea denaturation and renaturation curve analysis of disulfide-reduced apo SOD

Apo SOD	[protein] (μM)	Probe	m[b] (kcal (mol of monomer)$^{-1}$M^{-1})	C_{mid}[b] (M)	ΔG[c] (kcal (mol of monomer)$^{-1}$)
PWT	14, 14, 24[a]	CD 216 nm	2.5 ± 0.3	1.69 ± 0.03	4.2 ± 0.4
PWT	14, 14, 24[d]	CD 216 nm	2.49	1.68 ± 0.03	4.2 ± 0.1
PWT	14, 14, 24[a]	CD 231 nm	2.4 ± 0.1	1.57 ± 0.02	3.7 ± 0.2
PWT	14, 14, 24[d]	CD 231 nm	2.49	1.57 ± 0.02	3.9 ± 0.0
PWT	14, 14, 24	Average (CD 216nm and 231nm)		1.6 ± 0.1[e]	4.0 ± 0.2[e]
H46R	8.5,8.5[a]	CD 216 nm	2.9 ± 0.4	2.00 ± 0.03	5.8 ± 0.9
H46R	8.5,8.5[d]	CD 216 nm	2.49	2.01 ± 0.04	5.0 ± 0.1
H46R	8.5,8.5[a]	CD 231 nm	2.2 ± 0.4	2.07 ± 0.05	4.6 ± 0.7
H46R	8.5,8.5[d]	CD 231 nm	2.49	2.06 ± 0.04	5.1 ± 0.1
H46R	8.5,8.5	Average (CD 216nm and 231nm)		2.04 ± 0.03[e]	5.1 ± 0.1[e]

[a]Data were globally fit with m and C_{mid} as shared parameters. [b]Errors (±) derived from the fitting program. [c]ΔG calculated from the product of C_{mid} and m (Equation 4.9), errors (±) were propagated using standard methods (Taylor, 1982). [d]Data were globally fit to a fixed average m value of 2.49 kcal (mol of monomer)$^{-1}$M^{-1} derived from averaging the m values from fits to PWT and H46R. [e]Values are an average from data where m was fixed to a value of 2.49 kcal (mol of monomer)$^{-1}$M^{-1} in fitting, errors (±) were propagated using standard methods (Taylor, 1982).

been seen in other studies (Baskakov and Bolen, 1999); and could be related to differences in residual structure of the thermally denatured *versus* the chemically denatured protein.

In order to more accurately compare the stability of PWT and H46R, datasets were re-fit to a fixed average *m* value of 2.49 kcal $mol^{-1}M^{-1}$ (see above and Table 4.5). Δ*G*s were calculated from the product of C_{mid} and *m* and are very similar at both wavelengths, with the average being 4.0 ± 0.2 and 5.1 ± 0.1 kcal mol^{-1} for PWT and H46R respectively. The Δ*G* for PWT obtained here at 25 °C is higher than the Δ*G* of 2.9 ± 0.3 kcal mol^{-1} obtained by Oliveberg and co-workers through urea denaturation of reduced apo wild-type SOD at the same temperature (Lindberg et al., 2004). However, this is not surprising, given that Oliveberg used a pH of 6.3 *versus* 7.4 used here. The Δ*G* values from the urea curves measured here were also compared to the Δ*G* values obtained from the DSC scans by extrapolating from the $t_{0.5}$ to 25 °C using the ΔC_p determined from the Kirchoff plot. Overall, the Δ*G* values of 3.5 ± 0.1 and 4.9 ± 0.1 kcal mol^{-1} for PWT and H46R respectively, calculated at 25 °C from the DSC data compare quite well to the urea curve values. This validates the applicability of the DSC analysis and the accuracy of our experimentally determined ΔC_p.

4.3.7 Aggregation studies on disulfide-reduced apo SODs by analytical ultracentrifugation.

Analytical ultracentrifugation experiments were conducted for disulfide-reduced apo PWT and mutant SOD samples under the same conditions as DSC measurements in order to further investigate and quantify aggregation implied by the calorimetry results. It is important to note that some non-ideality is possible in ultracentrifugation experiments under these low salt conditions which, can complicate quantitative analysis; however, a comparative analysis of the sedimentation behaviour between the PWT and the mutant proteins can still be instructive.

Sedimentation velocity experiments were performed at 20 °C on disulfide-reduced PWT SOD and the disulfide-reduced mutant H43R at concentrations of 0.6 and 0.8mg/mL respectively. The results were analyzed using the van Holde and Weischet method and are presented as plots of boundary fraction *versus* sedimentation coefficient, S (Figure 4.11) (van Holde, 1978). This method eliminates the contributions of boundary spreading due to diffusion, and is a very sensitive indicator of sample homogeneity (Cole, 1999). PWT was found to have a sedimentation coefficient of ~1.8 S. Sedimentation coefficients of ~2.6 S, 1.8 S and 1.4 S were measured previously in 100 mM acetate, pH 5.5, for the folded apo WT SOD dimer, folded apo monomer and GdmCl induced unfolded monomer, respectively (Doucette et al., 2004). Hence, the sedimentation coefficient obtained here is comparable to the previously determined coefficient for disulfide-intact folded monomeric SOD and is consistent with disulfide-reduced apo SOD existing as a folded monomer in solution, consistent with DSC and chemical denaturant data. The H43R mutant has a somewhat lower sedimentation coefficient of ~1.6 S, indicating a possible expansion of the structure for this mutant at 20 °C, despite the apparent $t_{0.5}$ being 35.4 °C (Figure 4.11). Although there is a positive slope in the boundary fractions *versus* s plots, which could be indicative of sample heterogeneity in both PWT and mutant (Hansen et al., 1994), the effect is quite small and the samples appear to be mostly homogenous.

While sedimentation velocity experiments are useful for providing information regarding sample heterogeneity and protein conformational changes, they are generally less accurate than sedimentation equilibrium experiments for determining the average molecular mass, which can be useful in determining if a protein is aggregating. Hence, sedimentation equilibrium (SE) experiments were also performed under the same solution conditions as the velocity measurements. In addition to PWT and H43R, the SE behaviour of 2 additional mutants E100G

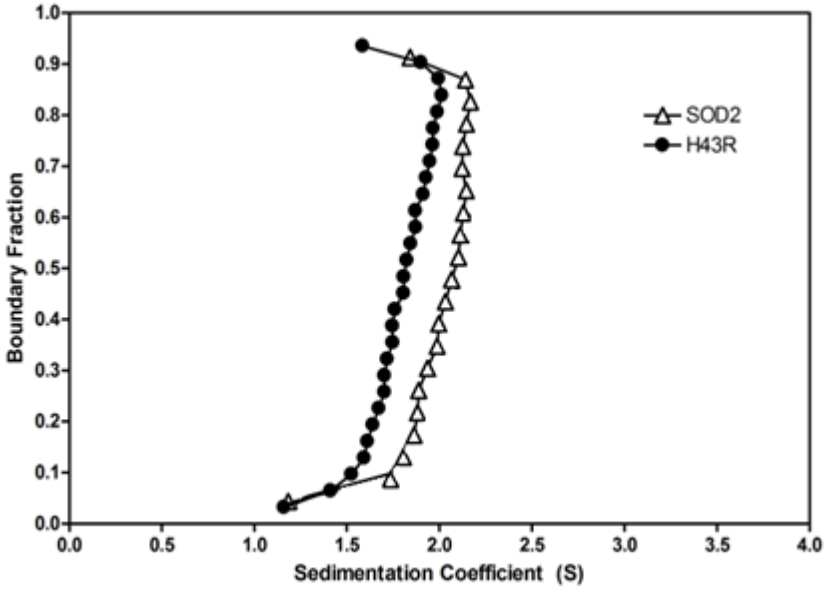

Figure 4.11. Van Holde-Weischet analysis of sedimentation velocity analytical ultracentrifugation experiments for disulfide-reduced apo PWT and H43R SOD. The protein concentrations measured were 0.6 mg/mL and 0.8 mg/mL respectively. Experiments were conducted at 20 °C, pH 7.4. The S value for PWT is ~1.8 while for H46R it is ~1.6.

and A4V were investigated to illuminate possible differences. SE experiments were carried out at 2 different rotor speeds for H43R: 15,000 and 25,000 rpm and 4 different rotor speeds for PWT, A4V and E100G: 20,000, 25,000, 30,000, and 35,000 rpm. Three datasets for each of the disulfide-reduced apo SODs were collected at each rotor speed fit to a single species model with molecular weight apparent (MW) as a globally shared parameter across the 3 datasets collected at a particular rotor speed (Figure 4.12A). In analyzing the results of these fits, it is immediately apparent that there is a decrease in MW with increasing rotor speed. For PWT, this decrease is small: from 15.2 kDa at 20,000 rpm to 13.5 kDa at 35,000 rpm. This systematic decrease in molecular weight with increasing rotor speed is an indicator of non-ideal behaviour and could be caused by reversible association/aggregation (Briere and Dunn, 2006; Fairman et al., 1999). The molecular mass expected for monomeric reduced SOD is ~15.75 kDa, however, the molecular mass for PWT at the highest rotor speed is ~13.5 kDa. This unexpectedly low measured molecular mass could be a consequence of the low ionic strength of the sample, which can result in charge repulsion effects and an artificially low MW (Ralston, 1993). The decrease in molecular mass with rotor speed is significantly more pronounced for the mutants. For example, A4V molecular weights ranged from 24.2 kDa to 16.5 kDa at 20,000 to 35,000 rpm, respectively. Furthermore, at all rotor speeds, the molecular weight obtained for the mutants is greater than that for PWT, indicating that there is likely more aggregation for the mutants compared to PWT. In addition to fitting datasets at each rotor speed, data were also globally fit for each mutant across all rotor speeds, which gave a single best fit average apparent MW for each mutant across all speeds (Figure 4.12 B, C, and D). The global fits give an indication of some non-ideal behaviour of both PWT and mutants through non randomness of residuals. The overall higher global MW for all the disulfide-reduced apo SOD mutants

Figure 4.12. Analysis of sedimentation equilibrium analytical ultracentrifugation data for disulfide-reduced apo PWT and mutant SODs. (A) Molecular weights as a function of rotor speed obtained from fitting data to a single homogeneous species model (Equation 4.15). As displayed in both the bar chart and inset table, the molecular weights decrease with increased rotor speed far more for the mutants. (B) Molecular weights obtained from single homogeneous species model global fitting of data across all rotor speeds. These values hence represent an average molecular weight for species present in the sample. Typical examples of sedimentation equilibrium data collected at different rotor speeds are shown for (C) PWT and (D) A4V. Data are represented as circles with each of the different colours representing data collected at each rotor speed: 20,000 rpm (black), 25,000 rpm (red), 30,000 rpm (blue) and 35,000 rpm (green). The data for both PWT and A4V were globally fit to a single ideal species model (solid lines) across all rotor speeds with the monomer molecular weight as a shared parameter (see panel B) with the residuals for the fits as indicated (upper panels in C and D).

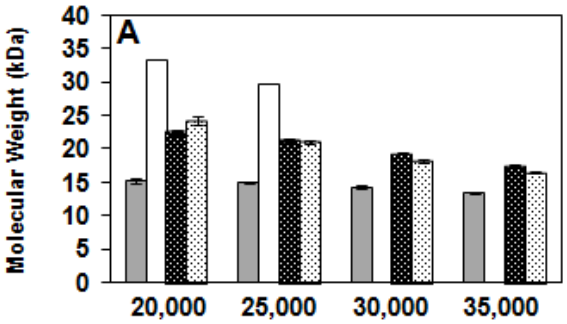

PWT	15.2	15.0	14.3	13.5
H43R	33.4	29.6		
E100G	22.5	21.3	19.3	17.5
A4V	24.2	21.1	18.2	16.5

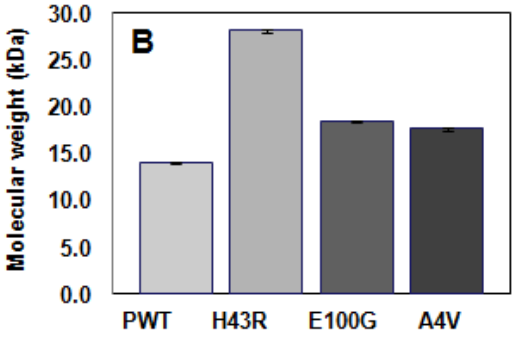

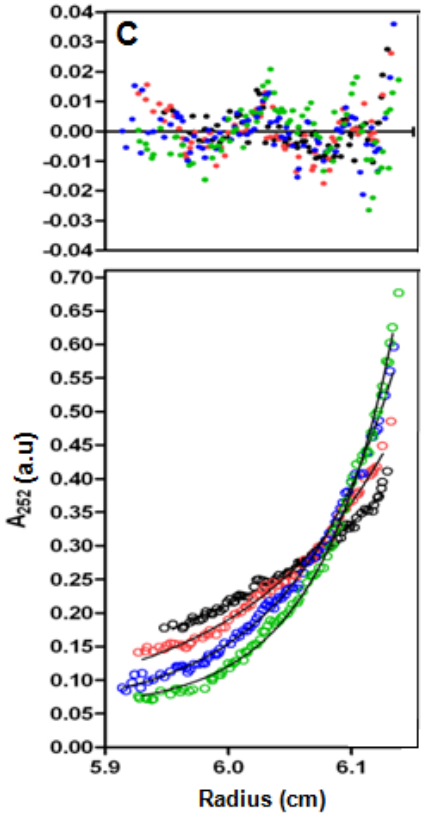

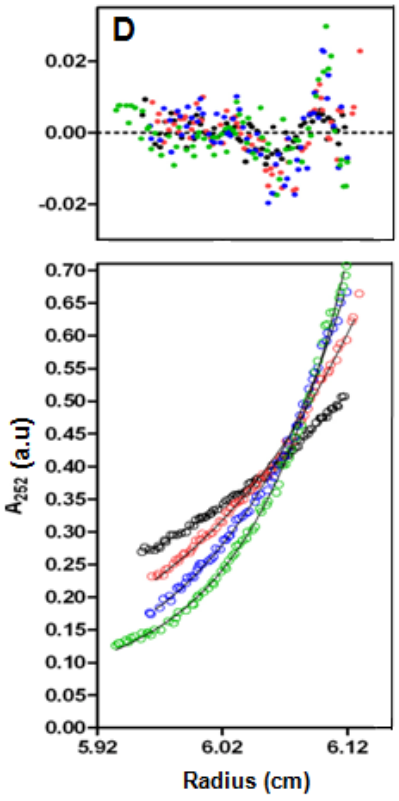

compared to PWT is again an indication that the mutants have an increased propensity to aggregate.

Due to the relatively long time required to complete sedimentation equilibrium experiments (typically 24 hrs or greater), there was concern that re-oxidation of the protein could occur, despite the presence of 1 mM TCEP in all samples. It should be noted that the reformation of the native disulfide bond would result in a large increase in the propensity for dimerization. Additionally, formation of non-native intermolecular disulfide bonds could result in the formation of covalently linked oligomers. Since both events can influence the outcome of our SE experiments, samples before and after SE experiments were routinely checked for oxidized product. This was done using the SDS-PAGE protocol with modification of free cysteines by IA as was used for DSC samples (see Figure 4.1). These experiments clearly showed that, similarly to DSC experiments, there is little if any reformation of the native disulfide bond or formation of high molecular oligomers due to aberrant disulfide cross-linking.

Given that the molecular weights for the mutants obtained from single species fitting tended to be larger than would be expected for a monomer, mutant and PWT data were also fit to association models describing a monomer/dimer, monomer/trimer and monomer/tetramer equilibrium with association constant K_a as a shared parameter for all datasets across all rotor speeds (Equations 4.16-4.20). There is significant non-randomness in the residuals for all 3 models, although the fits to the monomer/dimer model are best and fits become successively worse when fitting to monomer/trimer and monomer/tetramer (fits not shown). A more thorough analysis of SOD aggregation is likely needed to decipher the mechanism, including performing SE experiments over large concentration ranges (Schuck, 2007) as well as utilizing additional techniques such as dynamic light scattering and atomic force microscopy; such experiments are

ongoing in the Meiering group (see Section 5.6.6). It seems likely, however, that aggregates formed by disulfide-reduced apo mutants are smaller oligomers rather than large fibrils.

4.4 Discussion

4.4.1 Role of the disulfide bond in apo SOD

The mechanism and thermodynamic stability of unfolding of SOD with the disulfide bond intact, both in the holo and apo states have been studied extensively (Rumfeldt et al., 2006; Stathopulos et al., 2006; Vassall et al., 2006). Here the results of a similar study on the disulfide-reduced apo protein are reported. Thermal unfolding of disulfide-intact holo and apo PWT SODs is generally well described by a 2-state dimer unfolding model while chemical denaturation for both states is best described by a dimer 3-state unfolding model with a monomeric intermediate (Chapter 3). Removal of metals does not have a major impact on the dimerization propensity of disulfide-intact SOD; both apo and holo SOD have a K_d <10^{-8} M at 20 °C (Doucette et al., 2004). It is thus significant that disulfide reduction results in such a weakening of quaternary structure that the reduced apo protein unfolds as a monomer even up to the highest concentration used in DSC analysis (2.4 mg/mL or 0.15 mM). An apo SOD variant which lacks cysteines and hence cannot form the disulfide bond has been shown to dimerize at concentrations between 10 and 18 mg/mL (0.6-1.14 mM), hence it would appear that elimination of the disulfide bond in the apo protein leads to an increase in K_d from a picomolar to a micromolar concentration (Hornberg et al., 2007). Given that the disulfide-intact apo protein derives most of its stability from a strong dimer interface (Chapter 3), it is no surprise that disulfide-bond reduction has such dramatic thermodynamic consequences, reducing the ΔG at 37 °C from 6.6 kcal mol^{-1} monomer to only 1.8 kcal mol^{-1} monomer (see Table 4.3).

Despite the strong destabilizing effect that disulfide bond elimination has on the apo protein, it does not affect the ability of the protein to fold reversibly. This is not entirely

unexpected, given that *E. coli* apo SOD, which is monomeric and has a similar fold to the human enzyme but contains no disulfide, has been shown to also thermally unfold with high reversibility (Battistoni et al., 1998). Interestingly, the aforementioned thermal unfolding study of *E. coli* SOD also reported a $t_{0.5}$ value for unfolding of the apo protein of 53.6 °C and a ΔH of unfolding of 61 kcal mol^{-1}, which are remarkably similar to the properties of the human disulfide-reduced apo enzyme which has a $t_{0.5}$ of 48 °C and a ΔH_{vH} of 62 kcal mol^{-1}. This is likely reflective of the evolutionary relationship between the various Cu Zn SODs which share significant structural homology at the level of tertiary structure but differ at the quaternary structural level (Bourne et al., 1996; Getzoff et al., 1989).

It has been proposed that stabilization arising from disulfide formation occurs generally through a reduction in the entropy of the unfolded state (Pace et al., 1988). However, comparing the disulfide-reduced apo monomer with the disulfide-intact apo monomer, it appears that the disulfide bond in SOD has little stabilizing effect. A ΔG of unfolding of 3.7 ± 0.4 kcal mol^{-1} at pH 6.3, 25 °C was calculated from chemical denaturation studies on a monomeric variant of PWT SOD, in which the introduction of the F50E/G51E mutations into the dimer interface prevents dimerization (Lindberg et al., 2004). This value is quite similar to 3.5 ± 0.1 kcal mol^{-1} obtained from DSC measurements on the disulfide-reduced protein at pH 7.4, 25 °C. This is consistent with molecular dynamic simulations, which predicted that disulfide formation has little effect on the stability of the free apo monomer (Ding and Dokholyan, 2008). Hence, it would appear that the primary function of the disulfide bond in apo SOD is not to increase the global stability of the monomer but rather simply to reduce the conformational freedom of loop 4 in the SOD structure (Figure 1.3), such that it is in the correct orientation to make vital contacts in the dimer interface. It should be noted that this function of the disulfide bond can be at least partially fulfilled by binding Zn^{2+} to the disulfide-reduced apo monomer. Zn^{2+} ligands in SOD

are also located in loop 4 and it has been shown that Zn^{2+} binding can help to re-orient loop 4 and restore the ability of SOD to dimerize (Arnesano et al., 2004; Banci et al., 2002; Banci et al., 2003; Hornberg et al., 2007). Hence, it would appear that the disulfide bond is of potentially greater importance in maintaining the structural efficacy of SOD in mutants that have compromised Zn^{2+} binding, such as the mutant G85R.

4.4.2 Effects of mutations on disulfide-reduced apo SOD stability

As stated previously, it is unclear which state of SOD is responsible for causing ALS. Hence, it is important to study the effects of mutations in all the different states. Most studies to date have focused on the effects of mutations in the disulfide-intact apo and holo states. In reviewing the available data, it is clear that despite the fact that all holo SOD mutants studied to date are destabilizing, all mutants retain high thermal unfolding reversibility and are still significantly stable with ΔG typically exceeding 20 kcal mol^{-1} at 25 °C and $t_{0.5}$ exceeding 80 °C (Rumfeldt et al., 2006; Stathopulos et al., 2006). Additionally, it has been found that at least some mutations do not have significant effects on the structure of the holo protein (Banci et al., 2007; Hart et al., 1998; Hough et al., 2004). Disulfide-intact apo SOD is of course significantly less stable than holo SOD, but even proteins with the most destabilizing mutations still unfold reversibly and greatly favor a folded conformation at physiological temperature (Chapter 2). The PWT disulfide-reduced apo SOD has only marginal stability, much lower than either the disulfide-intact apo or holo states. It is thus worth considering further how mutations affect reversibility, temperature and thermodynamics of unfolding in this background and to compare these trends to those for the disulfide-intact apo state.

4.4.2.1 Temperature of unfolding

Of the 9 disulfide-reduced apo SOD mutants studied here, all but 2 (G85R and H46R) have apparent $t_{0.5}$ of unfolding lower than 37 °C. An apparent $t_{0.5}$ of 37 °C means that these mutants are ~ 50% unfolded at this temperature. In comparing the apparent $t_{0.5}$ values of all the disulfide-reduced proteins studied here with the $t_{0.5}$ values for the same mutants in a disulfide-intact apo background, it is interesting that the decrease in apparent $t_{0.5}$ caused by disulfide reduction is greater for the mutants than PWT in all cases with the exception of H46R (Table 4.4). For example, reduction of the disulfide bond of the E100G mutant reduces the apparent $t_{0.5}$ by ~ 16 °C, while reduction of the PWT disulfide results in only an ~ 10.5 °C decrease in $t_{0.5}$. This could indicate that the destabilized mutants are generally more reliant on the disulfide bond for structural integrity compared to PWT. Additionally, the $\Delta t_{0.5}$, defined as the difference between the $t_{0.5}$ of the mutant protein and the PWT protein, is larger in magnitude for all destabilizing mutations in the disulfide-reduced background when compared to the disulfide-intact background (Table 4.4). Similar findings were reported in a more limited study that looked at 2 mutants: A4V and G93A, scanned in 20% glycerol (Furukawa and O'Halloran, 2005). This suggests that the looser structure of the disulfide-reduced apo SOD is more easily perturbed by mutations. It is unclear how general this trend is, however, as another thermal melting study found that the destabilizing mutant H48Q has a greater effect on $t_{0.5}$ in the disulfide-intact state while D101N (which like H46R is not destabilizing) did not show a difference (Rodriguez et al., 2005).

4.4.2.2 Reversibility

It is not entirely clear why only three apo disulfide-reduced apo SOD mutants included in this study, namely: H46R, G85R and E100G, thermally unfold highly reversibly, in contrast to the more mature apo disulfide-intact state where all mutants unfold highly reversibly (Chapter 2). H46R and G85R both predominantly affect metal binding in SOD and have already been shown to have less of an effect on stability in the apo disulfide-intact conformation compared to all the other mutants (Chapter 2). These mutations also have higher temperatures of unfolding in the disulfide-reduced apo conformation than all the other mutations studied here, and this thermal stability might protect them from irreversible aggregation. However, the other mutant that was found to unfold highly reversibly here, E100G, is only slightly more stable than the much less reversible mutants in the disulfide-intact apo state and has a comparable apparent $t_{0.5}$ of unfolding in the disulfide-reduced apo state (Table 4.4). The mutation E100G disrupts a salt-bridge with K30 and is also thought to further destabilize SOD through an increase in the entropy of the unfolded state due to the addition of an extra glycine (Rumfeldt et al., 2006). If aggregation proceeds *via* an unfolded or partially folded state, it is possible that this increased entropy also makes aggregate formation slightly less favourable for this mutant compared to other mutants of similar stability. Nevertheless, it is likely that other factors beyond simple thermodynamic stability or temperature of unfolding determine whether mutant disulfide-reduced SOD thermally unfolds reversibly. These could include differences in protein dynamics and local conformational changes.

4.4.2.3 Thermodynamic stability

Some interesting trends are seen when the thermodynamic effects of PWT, H46R, G85R, and E100G in the apo disulfide-reduced background *versus* the disulfide-intact background are compared. The mutants G85R and E100G both have very similar entropy to PWT ($\Delta\Delta S$ small in magnitude) in the apo disulfide-reduced state. However, both mutants clearly have lower enthalpy ($-\Delta\Delta H$) and are hence enthalpically destabilized (Table 4.3). This is in contrast to the disulfide-intact apo state, in which both these mutants are entropically destabilized (Table 2.5). The trends in entropy and enthalpy for disulfide-reduced H46R, however, in contrast to E100G and G85R do mirror what is seen in the apo disulfide-intact state in that this mutant has higher unfolding entropy than PWT ($+\Delta\Delta S$) which is more than compensated by increases in unfolding enthalpy ($+\Delta\Delta H$). As discussed previously in chapter 2, it is very difficult to rationalize mutation-induced changes in ΔS and ΔH. However, given that disulfide-reduced apo SOD is generally more structurally open and dynamic compared to disulfide-intact apo SOD (Ding and Dokholyan, 2008; Hornberg et al., 2007; Shaw et al., 2006), it is not surprising that some differences would be observed. Additionally, a more open structure might allow for more direct interaction of the solvent with individual residues; these interactions will likely contribute greatly to the observed trends in entropy and enthalpy (Brady and Sharp, 1997; Sturtevant, 1994).

In addition to entropy and enthalpy, the overall free energy change upon unfolding (ΔG) along with the relative changes in free energy ($\Delta\Delta G$, where $\Delta\Delta G = \Delta G_{mut} - \Delta G_{pwt}$) at 25 and 37 °C are summarised in Table 4.3. Inspection of these values shows that like PWT, the 3 disulfide-reduced apo SOD mutants are only marginally stable at 25 °C. At 37 °C, PWT, H46R and G85R are still predominantly folded with a positive ΔG, however E100G is more unfolded than folded as indicated by a negative ΔG. It should be noted that a negative ΔG does not necessarily indicate that all the protein is unfolded but rather that the overall population of protein is more

than half unfolded since ΔG at $t_{0.5}$ is equal to 0 (Figure 4.13). $\Delta\Delta G$ values at 37 °C indicate that the mutations have only moderate effects on the overall stability of disulfide-reduced apo protein with the $\Delta\Delta Gs$ of H46R, G85R and E100G being +1.2, -1.3 and -2.4 kcal (mol monomer)$^{-1}$. Similarly to PWT, the stability of all the mutants decreases quite markedly upon disulfide reduction with stability decreasing by ~ 5-6 kcal (mol monomer)$^{-1}$ (See Table 4.3). These large decreases in stability, resulting from disulfide reduction, lead to very large increases in the fraction of unfolded protein at 37 °C. PWT and all the disulfide-reduced apo SOD mutants have a significant population of unfolded protein with the fraction of unfolded protein being 4.7% for PWT, 0.6% for H46R, 28% for G85R and 71% for E100G (Figure 4.13). By comparison, the fraction of unfolded protein present at 37 °C at 0.5mg/mL protein (calculated from thermodynamic parameters in Table 2.4 and from Rumfeldt, 2006) for disulfide-intact apo SOD is 0.3%, 0.01%, 0.3%, and 0.5% for PWT, H46R, G85R and E100G, respectively. Hence, disulfide reduction increases the population of unfolded protein in all cases with these increases being particularly significant for the destabilized mutants G85R and E100G where the population of unfolded protein increases 93- and 142-fold. These striking increases in the fraction of unfolded protein underscore the importance of the disulfide bond in stabilizing apo SOD.

4.4.3 Misfolding and aggregation propensity of disulfide-reduced apo SOD

4.4.3.1 Increase in partially folded or unfolded states

One key finding of this study is that SOD has evolved so that even the most immature form is stable with a ΔG of 1.8 kcal mol^{-1} at 37 °C, pH 7.4 and a $t_{0.5}$ of ~48 °C. This stability is likely important to avoid aggregation and degradation mechanisms in the cell. Given the

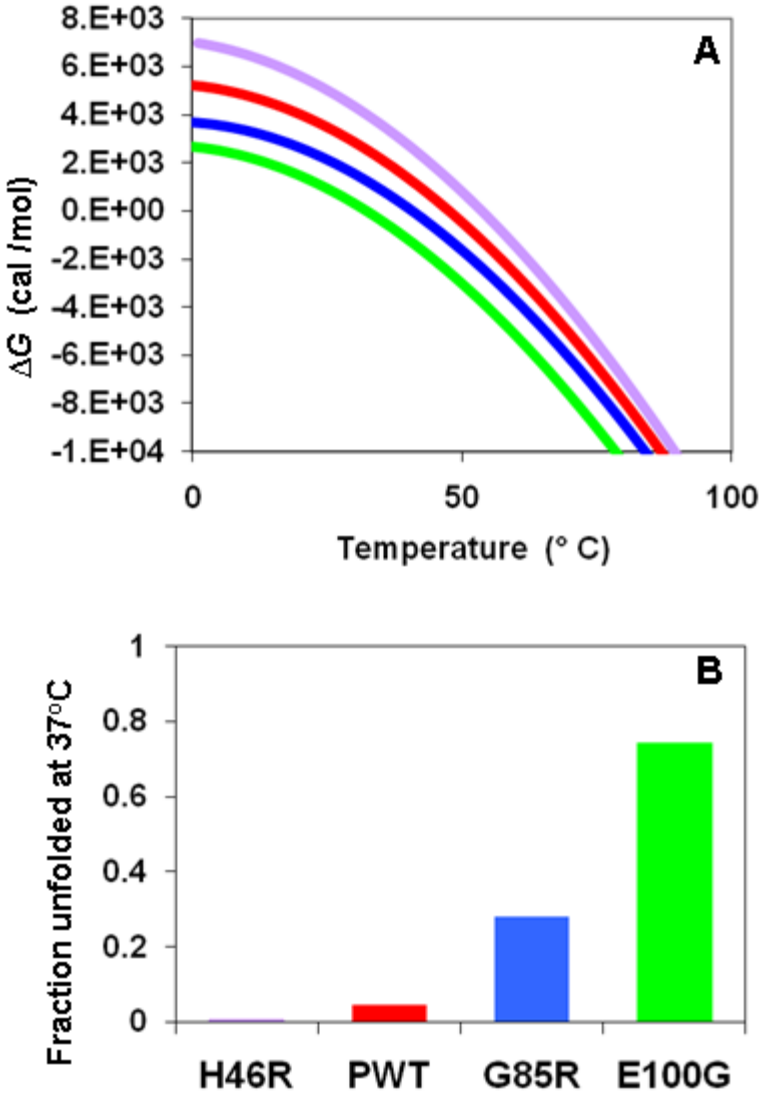

Figure 4.13 Stability analysis and population of unfolded protein of disulfide-reduced apo SOD at 37 °C. (A) A plot of Δ*G* vs. temperature for PWT (red) and the mutants H46R (purple), G85R (blue) and E100G (green). The Δ*G* s were calculated using values generated from 2-state monomer fitting of DSC scans and extrapolated from $t_{0.5}$ using a temperature independent ΔC_p of 1.05 kcal mol^{-1} $°C^{-1}$. B) Fraction of unfolded protein present at 37 °C for different apo disulfide-reduced apo SODs.

marginal stability of disulfide-reduced apo SOD, even relatively slight decreases in stability caused by ALS-associated point mutations are sufficient to greatly increase the population of potentially aggregation prone, misfolded or unfolded species (Figure 4.13).

In addition to increasing the population of unfolded forms of the protein, point mutations can result in an expanded native structure as was demonstrated for H43R in sedimentation velocity experiments at 20 °C, pH 7.4 (Figure 4.11) and by amide exchange experiments on A4V in other studies (Rodriguez et al., 2005). A less compact structure with more conformational freedom could expose hydrophobic patches which could be important for SOD self-aggregation or aggregation with other proteins. Such aggregation has been seen *in vivo* with the deletion mutant SOD1Leu126delTT, which cannot form the intramolecular disulfide-bond due to a pre-mature stop codon. This monomeric mutant has been shown to aggregate promiscuously with a large variety of other proteins (Watanabe et al., 2008).

4.4.3.2 Interruption of maturation

An additional potential complication of mutation-induced destabilization of the disulfide-reduced apo state is that it is unclear if loosely folded or unfolded forms of the apo disulfide-reduced protein can undergo the SOD maturation process efficiently. It has been proposed that zinc binding to the disulfide-reduced apo protein increases the ability of CCS to recognize SOD, which as previously mentioned aids in the formation of the disulfide bond (Furukawa et al., 2004). These post-translational modifications are critical, because either binding of Zn^{2+} or formation of the disulfide bond would result in dimerization and ameliorate many of the locally unfolded regions seen in disulfide-reduced apo SOD (Ding and Dokholyan, 2008). However, zinc will bind with lower affinity to the unfolded disulfide-reduced protein compared to the

folded protein. This is in fact seen in the disulfide-intact apo SOD, where the K_d of Zn^{2+} binding is in the nanomolar range with the folded monomer but only in the micromolar range with the unfolded protein (Kayatekin et al., 2008; Potter et al., 2007). This may also help to explain why H46R despite being more stable than PWT in both disulfide-intact and disulfide-reduced apo conformations, still causes ALS, albeit with milder symptoms and longer duration (Aoki et al., 1993). H46R has been unambiguously shown to be deficient in Cu binding, but it has also been suggested that it binds Zn less efficiently (Antonyuk et al., 2005; Hayward et al., 2002). Additionally, *in vivo* experiments have demonstrated that H46R in a CCS-independent mechanism spontaneously forms the disulfide bond at a slower rate compared to other mutants and WT (Bruns and Kopito, 2007). Hence, although H46R has a greater stability in the disulfide-reduced apo state, there may be an overall larger pool of this species in the cell. Given that misfolding events are much more likely to occur from the apo disulfide-reduced state than for more mature and stable states (Stathopulos et al., 2003), this larger pool may result in an overall net increase in toxic aggregation-prone precursors compared to WT. In fact, it has been proposed that any mutation-mediated interruption of SOD maturation that traps the protein in less stable states could be a key pathological feature in SOD-mediated fALS (Furukawa and O'Halloran, 2006).

4.4.3.3 Mutation-mediated increases in aggregation

Previous studies have yielded contradictory evidence regarding an enhanced ability of disulfide-reduced apo mutants to aggregate relative to controls. Gel filtration studies conducted on WT and the mutants G93A and A4V suggested the presence of oligomers for the mutants, while mostly monomer was observed for WT (Furukawa and O'Halloran, 2005). However, other

studies in which aggregation was monitored by increased thioflavin T fluorescence did not indicate significant differences in the aggregation tendency of mutant SODs compared to controls (Chattopadhyay et al., 2008; Furukawa et al., 2008). This difference could be due to the different experimental conditions that were used which included agitation of the sample during or prior to measurements. Significant aggregation tendency is not apparent for PWT disulfide-reduced apo SOD in this study; thermal unfolding had comparable reversibility with the apo disulfide-intact form. This is in marked contrast to many of the mutants, however, which despite unfolding quite reversibly when thermally unfolded with the disulfide bond intact, exhibit low reversibility once the disulfide bond is reduced. Even E100G, H46R and G85R, which are quite reversible, show evidence of aggregation through negative ΔC_p values or slightly high van't Hoff to calorimetric enthalpy ratios. Further evidence of increased tendency of mutants to aggregate was obtained from sedimentation equilibrium experiments on PWT, H43R, E100G and A4V. SE data when fit to a single species model suggest that the mutants have a greater tendency to aggregate compared to PWT based on their higher molecular weights at all rotor speeds (Figure 4.12). The decrease in MW as rotor speed increases also suggests formation of weakly associated/reversible aggregates. The reversible nature of the aggregates seen in sedimentation equilibrium experiments could indicate that they are structurally different from aggregates formed during thermal unfolding studies, which appear to be irreversible for most mutants. Aggregation in thermal unfolding studies likely occurs at high temperature when the protein is in an unfolded conformation, while the protein is mostly folded under the conditions used in sedimentation equilibrium experiments. Hence, in contrast to aggregates formed during thermal unfolding, it is likely that partially unfolded conformations of disulfide-reduced apo SOD are precursors to reversible aggregates.

4.4.3.4 Role of intermolecular disulfide cross-linking

There has been much debate about the role of disulfide cross-linking in the aggregation of disulfide-reduced apo SOD (Banci et al., 2009; Banci et al., 2008; Deng et al., 2006; Karch and Borchelt, 2008; Karch et al., 2009; Niwa et al., 2007). Analysis of aggregated SOD extracted from the spinal cord of ALS mice indicated the presence of disulfide cross-links (Deng et al., 2006; Furukawa et al., 2006). However, studies in which the cysteines of SOD were systematically mutated suggest that such cross-linking is not necessary for aggregation (Karch and Borchelt, 2008; Karch et al., 2009). Given that aggregates seen here in SE experiments appear to be reversible, it is very unlikely that cross-linking played a mechanistic role in their formation. Furthermore, SDS-PAGE analysis of samples after SE measurements, with free cysteines modified by IA did not indicate appreciable amounts of disulfide cross-linked species.

It is important to note that even though disulfide cross-linking might not be vital to the initiation or elongation phases of aggregation, there is an emerging consensus that it could be important in stabilizing large aggregates, protecting them from degradation (Furukawa and O'Halloran, 2006; Karch et al., 2009; Wang et al., 2006). Such a mechanism involves the initial formation of small soluble oligomers, which may later congregate and cross-link due to the close proximity of free cysteines. It is possible that the small soluble oligimers seen in SE experiments can serve as nuclei for these much larger aggregates. These small soluble oligomers could serve as promising pharmacological targets in the alleviation of SOD-mediated fALS. A promising strategy could be to design small molecules, which could bind to the oligomers prior to their assembly into larger insoluble aggregates.

Chapter 5: Summary and Future work

5.1 DSC and equilibrium chemical denaturation analysis of disulfide-intact apo SODs

Various fALS-associated mutations were investigated by DSC (Chapter 2) as well as by equilibrium chemical denaturation analysis (Chapter 3) (in 20 mM HEPES, pH 7.8). Both thermal unfolding monitored by DSC and chemical denaturation monitored by CD and fluorescence spectroscopy are highly reversible enabling a full equilibrium thermodynamic analysis of the effects of mutations on the stability of SOD apoprotein. Of the 8 mutants, namely: A4V, A4T, A4S, I113T, G85R, G37R, H43R and H46R, investigated by DSC, thermal unfolding of all except A4V and H46R was found to be well described by a 2-state dimer unfolding model, similarly to PWT. Some mutants, however, show evidence of aggregation through increased ratios of $\Delta H_{vH}/\Delta H_{cal}$ (see Section 5.4). In contrast to PWT, the mutants A4V and H46R are best described by a 3-state dimer unfolding model with a monomeric intermediate, populated at equilibrium, in addition to the folded dimer and fully unfolded monomer. The stability of the mutants and PWT ranges from ~9 to ~18 kcal mol^{-1} at 37 °C and all the mutants are destabilized with the exception of H46R which is slightly more stable (Table 2.4).

Chemical denaturation experiments with GdmCl were carried out on apo PWT and the mutants G85R, G93R, E100G and I113T in the presence and absence of 0.75 M of the stabilizing agent sodium sulphate at 25 °C. As expected from DSC studies presented in Chapter 2 and in studies conducted by others in the Meiering research group (Rumfeldt, 2006; Stathopulos et al., 2006), all mutants were found to be destabilized relative to the PWT as evidenced by the lower concentration of GdmCl needed to denature the mutants. Data for PWT collected both in the presence and absence of sodium sulphate was thermodynamically analyzed while only data

collected in sodium sulphate for the mutants could be analyzed owing to the lower stability of the mutants which consequently had ill defined pre-transition baselines. Similarly to chemical denaturation curves of the holoprotein (Rumfeldt et al., 2006), curves for apo PWT both with and without sodium sulphate are best fit to a 3-state dimer unfolding model with a monomer intermediate. This is in contrast to equilibrium thermal unfolding measured by DSC, which is well described by a 2-state unfolding model. This difference between chemical denaturation monitored by CD and fluorescence *versus* thermal denaturation measured by DSC is likely due to the protein concentration range surveyed in each technique. Due to the increased sensitivity of the spectroscopic techniques, lower protein concentrations can be used that favour the population of a monomeric intermediate, enabling the intermediate to be thermodynamically characterized. Hence, the use of chemical denaturation enables us to determine the stability of both the dimer interface (ΔG_1) and the monomer intermediate (ΔG_2) for PWT, while only the total ΔG of unfolding could be obtained from DSC measurements. The fact that the total ΔG of unfolding at 25 °C for PWT is very similar by DSC and by chemical denaturation at 17.4 kcal (mol dimer)$^{-1}$ and 16 kcal (mol dimer)$^{-1}$, respectively, validates the accuracy of both methods in determining the stability of SOD. The measured stability of apo SOD compares to a ΔG of ~32 kcal (mol dimer)$^{-1}$ for the holo protein under the same conditions (Rumfeldt et al., 2006; Stathopulos et al., 2006) indicating significant destabilization upon removal of metals.

Disulfide-intact apo SOD derives most of its stability from a strong dimer interface, while the monomer is only marginally stable. In fact, when comparing the disulfide-intact apo and holo (Rumfeldt et al., 2006) states of the protein, the stability of the dimer interface is very similar at ~ 12 kcal(mol dimer)$^{-1}$. This is consistent with analytical ultracentrifugation studies which estimated the K_d of both the holo and apo SOD at $<10^{-8}$ at 20 °C, pH 5.5 corresponding to

a $\Delta G>10.9$ kcal (mol dimer)$^{-1}$ (Doucette et al., 2004). Hence the results indicate that that the major destabilizing effect of metal loss is derived almost entirely from reductions in monomer stability. Three state fitting of curves measured in the presence of sodium sulphate reveals that the addition of sodium sulphate does not significantly alter the stability of the dimer interface, but the stability of the monomer is markedly increased leading to increased population of the monomer intermediate. The overall stabilizing effect of sodium sulphate is quite dramatic, increasing the total ΔG of unfolding of apo PWT from 16 to ~33 kcal (mol dimer)$^{-1}$.

Data derived from equilibrium GdmCl denaturation of all the apo mutants, analogous to that of PWT, is also best fit to a 3-state model with a monomeric intermediate. Destabilization of the mutants occurs mostly due to reductions in the stability of the monomer intermediate. Somewhat surprisingly, although only one mutation (I113T) is close to the dimer interface, all the mutants also tend to weaken the dimer interface. This result is in contrast to GdmCl curve analysis of the holo protein, where mutants are essentially entirely destabilized exclusively due to a reduction in monomer intermediate stability (Rumfeldt et al., 2006). This suggests that the effects of the mutations might propagate across the dimer interface more readily in the more loosely structured apo protein. Due to the reduction in both ΔG_1 and ΔG_2 of the mutants, the equilibrium populations of both monomeric intermediate and unfolded monomers are markedly increased; this is noteworthy since aggregation has been proposed to occur more readily from unfolded or partially folded states (Chiti and Dobson, 2006).

5.2 Dimer interface stability of disulfide-intact apo SOD probed by ITC

The thermodynamics of dimer dissociation of disulfide-intact apo SOD were investigated by isothermal titration calorimetry (Chapter 2). The heat of dissociation of the SOD dimer to two monomers was recorded for each injection with the data fit to a dimer dissociation model to

yield K_d and ΔH_d (and from which the other thermodynamic quantities ΔG_d and ΔS_d was calculated). There is very little heat of dissociation associated with the dilution of disulfide-intact apo PWT SOD at 37°C, indicating a very tight dimer under these conditions (K_d <10^{-8}M). The result for PWT is in contrast to the dimer interface mutations A4V, A4T, A4S and I113T, which all have significantly higher heats of dilution, enabling a full thermodynamic analysis. The K_d for these dimer interface mutants range from 2μM to 10μM with the order from largest K_d to smallest K_d being: A4V>A4T>I113T>A4S. Somewhat surprisingly, mutants that are located far from the dimer interface: G93S, H46R and H43R, also produce much larger heats of dissociation when diluted compared to PWT, although the fitted K_d of these mutants is up to an order of magnitude lower than for the dimer interface mutants. It had been suggested previously from molecular dynamic simulations that a common characteristic of fALS-associated mutants may be an increased tendency to dissociate to free monomers (Khare et al., 2006). The results presented here are the first systematic experimental analysis of the effect of fALS-associated mutants on the dimer interface of SOD and provides experimental verification of the computational results. In addition, these experimental results are in accord with results from chemical denaturation measurement, which also suggests that mutations tend to lower the stability of the dimer interface (see Section 5.1). Dissociation to free, marginally stable apo monomers could be an important precursor to aggregation of the protein (see Section 5.4).

5.3 Stability of disulfide-reduced apo SOD

Similar to experiments on the disulfide-intact SOD, the stability of the disulfide-reduced apo PWT and mutants was probed using DSC thermal unfolding experiments (Chapter 4). Previous stability studies of the apo disulfide-reduced protein provided only estimates of stability

through apparent melting temperatures on a few mutants (Furukawa and O'Halloran, 2005; Rodriguez et al., 2005). Several mutants were considered in this study namely: H46R, G85R, G37R, E100G, H43R, A4V, A4S, A4T, G93R and G93S, with each mutant producing measurable endotherms under these conditions. The fact that DSC endotherms were obtained for the mutants G93R and A4V is in contrast to other studies where no endotherms were obtainable for these mutants when thermal unfolding was analyzed by DSC under similar conditions to those used here (Furukawa and O'Halloran, 2005; Rodriguez et al., 2005). Similarly to the disulfide-intact apo state, PWT thermal unfolding is highly reversible, even though the apparent $t_{0.5}$ decreases from ~59 °C to ~48°C. In contrast to PWT, several of the mutants studied here have poor reversiblity when thermally unfolded. However, three mutants: H46R, G85R and E100G do unfold highly reversibly, similarly to PWT, and are amenable to quantitative thermodynamic analysis. Hence, results reported here represent the first systematic thermodynamic stability analysis of disulfide-reduced apo mutants.

Previously, it had been shown that reduction of the intermolecular disulfide bond in apo SOD results in monomerization of the protein (Hornberg et al., 2007; Lindberg, 2004). Removal of the disulfide bond severely affects the dimer interface of apo SOD, creating greater disorder in loop 4 and resulting in the displacement of hydrophobic residues that are crucial in making contacts across the interface (Hornberg et al., 2007). Consistent with this, thermal unfolding of disulfide-reduced apo PWT is well fit to a 2-state monomer unfolding model. Calculation of the ΔG of unfolding demonstrated that disulfide-reduced apo PWT has only a marginal stability of 1.8 kcal (mol monomer)$^{-1}$ at 37 °C (Table 4.3). Given that the ΔG of unfolding of the disulfide-intact apo protein is 13.4 kcal (mol dimer)$^{-1}$ or 6.7 kcal (mol monomer)$^{-1}$ (Table 2.4), it is immediately apparent that disulfide reduction results in a marked decrease in the stability of apo SOD as predicted by the lower apparent $t_{0.5}$.

Similarly to disulfide-reduced apo PWT, thermal unfolding endotherms of the highly reversible disulfide-reduced apo mutants H46R, G85R and E100G were fit to a 2-state monomer unfolding model to yield thermodynamic parameters (Table 4.3). Both G85R and E100G were found to be slightly destabilized relative to PWT with ΔGs at 37°C of 0.6 and -0.6 kcal (mol monomer)$^{-1}$ respectively ; this destabilization leads to a marked increase in the population of unfolded protein at physiological temperature for these mutants. The mutant H46R however is slightly stabilizing with a ΔG of 3.1 kcal (mol monomer)$^{-1}$ at 37°C. In order to verify the results from calorimetry measurements, PWT as well as H46R stability was also analyzed by equilibrium urea denaturation curves. Chemical denaturation of PWT as well as H46R is highly reversible and like thermal unfolding, data are well fit to a 2-state monomer unfolding model, yielding ΔG values very close to those obtained by DSC (Table 4.3, 4.5).

Despite not being able to do a full thermodynamic analysis on the other disulfide-reduced apo mutants due to insufficient reversibility of unfolding, indications of the stability of these mutants were obtained from their apparent $t_{0.5}$s of unfolding. All of these mutants have lower apparent $t_{0.5}$s compared to PWT, suggestive of destabilization (Table 4.4). Significantly, the apparent $t_{0.5}$s are all close to or lower than 37°C, indicating that these mutants are likely 50% or more unfolded at this temperature. This is in contrast to the disulfide-intact apo state, which is well folded at 37°C even when fALS-associated point mutations are introduced (Table 2.4). Additionally, in all cases destabilizing point mutations reduce the apparent $t_{0.5}$ of SOD more in the disulfide-reduced apo state than in the disulfide-intact apo state (Table 4.4). This implies that the mutations exert a larger effect on the less mature disulfide-reduced state.

5.4 SOD Aggregation

5.4.1 Aggregation of disulfide-intact apo SOD

An advantage of DSC analysis is that in addition to obtaining information on stability, it can also provide at least a qualititative measure of the aggregation tendency of proteins through analysis of ratios of $\Delta H_{vH}/\Delta H_{cal}$. It had been demonstrated previously by others in the Meiering group that numerous disulfide-intact apo SOD mutants have increased tendency to aggregate based on the observation that $\Delta H_{vH}/\Delta H_{cal}$ was greater than unity when data were fit to a 2-state dimer unfolding model (Stathopulos et al., 2006). Similarly, several of the mutants investigated here have markedly high ratios (A4S, A4T, G37R and G85R) while the ratio for H43R is slightly higher than 1 (Table 2.1). However, the mutant I113T has ratios that are relatively close to 1 when considering all datasets, though there is some evidence for increased ratios at higher protein concentrations (Table 2.1). It should be noted that enthalpy ratios could not be evaluated for the mutants H46R and A4V, which unfolded *via* a 3-state mechanism because the van't Hoff and calorimetric enthalpies had to be set to be equal in order to reduce the number of fitting parameters.

5.4.2 Aggregation of disulfide-reduced apo SOD

Similarly to the disulfide-intact mutant apo SODs, results from DSC studies, and more directly through analytical ultracentrifugation results, illustrated enhanced tendency of disulfide-reduced mutant SODs to aggregate relative to the PWT control. DSC endotherms for the disulfide-reduced apo SOD mutants revealed that while PWT can thermally unfold and refold with reversibility comparable to that of the apo disulfide-intact state, many of the mutants have

significantly lower reversibility in the disulfide-reduced state compared to the disulfide-intact state, despite being scanned to lower temperature. This suggests that these mutants have an increased tendency to aggregate when the disulfide-bond is reduced. For the three mutants that thermally unfold highly reversibly (H46R, E100G and G85R) analysis of the fitted parameters provided evidence for an increased tendency to aggregate relative to the disulfide-reduced apo PWT based on low or negative $\Delta C_{p,unf}$ and/or high van`t Hoff to calorimetric enthalpy ratios (Table 4.1). Analytical ultracentrifugation sedimentation equilibrium experiments demonstrated that the mutants H43R, E100G and A4V form soluble reversible aggregates while very little aggregation was apparent for PWT. Increased tendency of apo reduced mutants to aggregate could be related to expansion of the structure of the mutants. Evidence for this was obtained from analytical ultracentrifugation sedimentation velocity experiments on apo disulfide-reduced PWT and H43R in which it was found that H43R had lower sedimentation coefficient indicating a less compact shape. It should be noted that previous *in vitro* aggregation studies on apo SOD without the disulfide bond have yielded contradictory evidence regarding increased tendency of mutants to aggregate compared to controls (Chattopadhyay et al., 2008; Furukawa et al., 2008; Furukawa and O'Halloran, 2005). Differences are likely related to how the samples are handled; generally, control protein has only been shown to aggregate when the sample has been agitated (Chattopadhyay et al., 2008; Furukawa et al., 2008).

There has been much focus and debate in the literature regarding the role of intermolecular disulfide cross-linking in SOD aggregation (Banci et al., 2009; Banci et al., 2008; Deng et al., 2006; Karch and Borchelt, 2008; Karch et al., 2009; Niwa et al., 2007). An aggregation mechanism involving disulfide cross-linking would produce irreversible aggregates. Given that sedimentation equilibrium results presented here indicate that aggregates are reversible and a reducing environment was maintained at all times in these experiments it is very

unlikely that aberrant disulfide cross-linking played a role in observed aggregation. These results are consistent with *in vivo* studies reported by Borchelt and collegues (Karch and Borchelt, 2008; Karch et al., 2009) which indicated that disulfide cross-linking is not essential in initiating aggregation but may play a secondary role, possibly stabilizing larger aggregates.

5.5 Disease implications

Analyses of protein folding mechanisms and thermodynamic stabilities are valuable in detecting and quantifying populations of potentially aggregation-prone species. These species may be viable pharmacological targets for the treatment of fALS. Folding and stability studies presented here on disulfide-intact apo SOD have revealed the presence of a monomeric intermediate, which is far less stable than the corresponding holo monomer intermediate. Monomeric disulfide-intact apo SOD has been shown in previous studies to be prone to aggregation (Chattopadhyay et al., 2008; Khare et al., 2004) and so this species could be critical in fALS. The population of this monomer intermediate at equilibrium is primarily governed by the stability of the dimer interface. Both ITC results and GdmCl denaturation analysis suggest that all the mutations studied here decrease the stability of the dimer interface; hence, the population of this marginally stable intermediate will be increased by the mutations. It should be noted that the population of unfolded monomers also increases in the case of destabilized mutants but this is not a universal property of fALS-associated SOD apo mutants, since H46R is more stable than PWT. One proposed pharmacological strategy is to stabilize the dimer interface of mutant SOD by binding small molecules across it (Ray and Lansbury, 2004). This could reduce the tendency of SOD to dissociate to potentially aggregation-prone monomeric forms. A similar strategy has been proposed in the treatment of the disease familial amyloid

polyneuropathy, where dissociation of the tetrameric TTR is implicated as a precursor to disease (Johnson et al., 2005).

In addition to monomeric apo SOD with the disulfide bond intact, disulfide-reduced apo SOD monomers have been shown to have high aggregation tendency (Chattopadhyay et al., 2008). Significantly, disulfide-reduced apo SOD aggregates have been shown to seed aggregation of more mature SOD states (Chattopadhyay et al., 2008). Results presented here suggest increased aggregation tendency of mutants in the disulfide-reduced apo state possibly through an expansion of the native structure. Hence, an obvious pharmacological strategy could be to stabilize the monomeric disulfide-reduced apo SOD and prevent aggregation and ultimately disease. This could be done by designing antibodies that could bind the SOD monomer. Similarly, antibodies designed to bind to mutants of lysozyme, which causes hereditary non-neuropathic systemic amyloidosis, have been shown to stabilize the native structure and eliminate aggregation (Dumoulin et al., 2006). Another strategy that could be used to stabilize the disulfide-reduced apo protein is enhancement of the SOD maturation process, which includes binding of zinc and/or binding of copper and formation of the disulfide bond. Thus, possible therapeutic strategies could include administration of zinc or stimulation of CCS activity or protein expression levels which could aid in the formation of the native disulfide bond in addition to promoting copper binding(Furukawa and O'Halloran, 2006).

5.6 Future work

Much has been learned about the stability and aggregation of both disulfide-reduced and disulfide-intact apo SOD in this study; however, there are several future avenues for research. These future studies should ideally be focused on probing the dynamics and local conformational

changes of the protein and investigating the role of metals by investigating the Zn bound state of the protein and the holo form. Additionally, it would be desirable to investigate in more detail the mechanism of aggregation of the apo protein. Further details of these proposed future experiments are described below.

5.6.1 Analyzing local conformational changes in apo SOD

As an alternative strategy to the use of optical probes which give information only on global protein conformational changes. It would be interesting to investigate hydrogen deuterium amide exchange using nuclear magnetic resonance spectroscopy, which could provide information on local protein conformational changes and dynamics. Alternatively, mass spectrometry can be utilized (Englander, 2006). In these mass spectrometry experiments, deuterated protein, both folded and unfolded, is labelled with protons over various time intervals. The labelled protein is then subjected to proteolytic digestion followed by analysis of the resulting fragments by mass spectrometry. This will provide information on important sequence-specific protection, allowing a more localized description of partially folded states that may be important precursors of aggregation.

5.6.2 Thermodynamic analysis of disulfide-intact holo SOD

Thermodynamic analyses of the stabilities of several chemically and structurally diverse disulfide-intact apo mutants have been presented in this thesis. In future, it would be informative to also analyze the same mutants in the holo state, as has been done previously for the G93 mutations (Stathopulos et al., 2006). These studies would enable us to better understand the thermodynamic implications of SOD maturation and how SOD maturation is affected by

mutations. Such studies on the dimer interface mutants A4V, A4T, A4S and I113T as well as other holo mutants are currently underway in the Meiering laboratory using differential scanning calorimetry.

5.6.3 Thermodynamics of Zn binding to the reduced protein

Spontaneous zinc binding to the reduced apo protein has been proposed to be the first step in the maturation of SOD (Furukawa et al., 2004). It has been shown that Zn binding increases the stability of the disulfide-reduced protein (Furukawa and O'Halloran, 2005) and restores its dimerization affinity (Hornberg et al., 2007). However, little is known about the thermodynamics of Zn binding and how Zn binding might be affected by mutations. It seems likely that Zn affinity for many would be reduced, as has been demonstrated for several disulfide-intact apo mutants (Crow et al., 1997). Mutation-induced reduced affinity for zinc under physiological conditions could trap the protein in an unstable immature state which is likely more prone to aggregate. Important insights could be gained by investigating the thermodynamics of zinc binding using isothermal titration calorimetry for the various mutants. Additionally, the thermodynamics of unfolding of this zinc bound apo reduced state could be studied by DSC and chemical denaturation. Preliminary DSC experiments have focused on thermally unfolding disulfide-reduced apo protein that has been incubated with an equimolar amount of free zinc (Figure 5.1). There is clearly an increase in the apparent $t_{0.5}$ upon incubation with zinc, however the width of the endotherm suggests that a mixture of species are present and additional optimization is required.

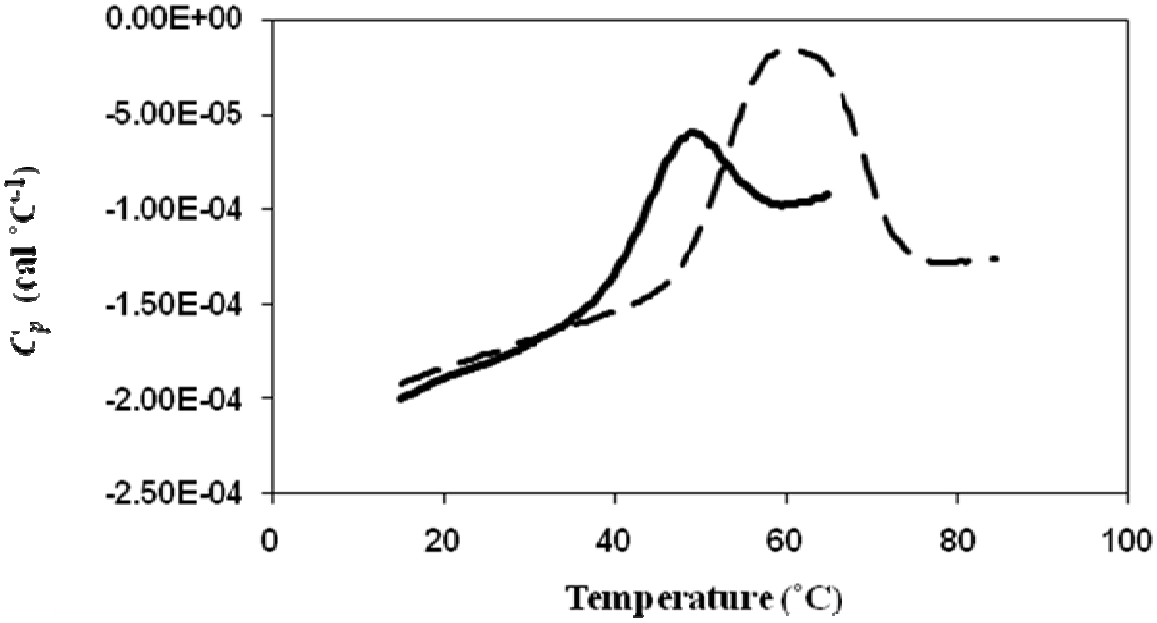

Figure 5.1. DSC scans of disulfide-reduced apo PWT both with and without Zn^{2+}. Both scans were conducted in 20 mM HEPES, pH 7.4 with 1 mM TCEP. Apo disulfide-reduced apo PWT scanned in the absence of Zn^{2+} is shown as a solid line while the sample scanned after incubation with 1 equivalent of Zn^{2+} for 24 hrs is shown as a broken line. There is clearly an increase in the temperature of unfolding upon incubation in Zn^{2+}; however the endotherm is quite broad indicating the presence of multiple species.

5.6.4 Thermal melting of disulfide-reduced apo SOD monitored by light scattering

Light scattering can be a powerful tool for detecting aggregate formation. Given that there is ample evidence of aggregate formation during thermal unfolding of some disulfide-reduced apo mutants monitored by DSC, light scattering could be a useful technique in directly detecting aggregates as a protein sample is heated. Preliminary light scattering experiments on disulfide-reduced apo PWT as well as the mutants H43R and G85R have been performed at protein concentrations close to 1 mg/mL (Figure 5.2). While no significant aggregation was seen for PWT and G85R as temperature is increased as evidenced by modest changes in scattering intensity with temperature, significant changes in H43R were observed. This result is consistent with thermal unfolding of H43R measured by DSC which is far more irreversible than either PWT or G85R and sedimentation equilibrium studies indicate a greater tendency for H43R to aggregate compared to PWT. Further experiments on additional mutants are currently ongoing.

5.6.6 Mechanism of aggregation of apo disulfide-reduced SOD

Analytical ultracentrifugation sedimentation equilibrium experiments presented in Chapter 2 illustrate the presence of reversible aggregates in samples of mutant proteins. However, there is currently insufficient data to characterize the mechanism of formation of these aggregates. Additional experiments could include collecting sedimentation equilibrium data over a large protein concentration range and over a variety of rotor speeds (Schuck, 2007).

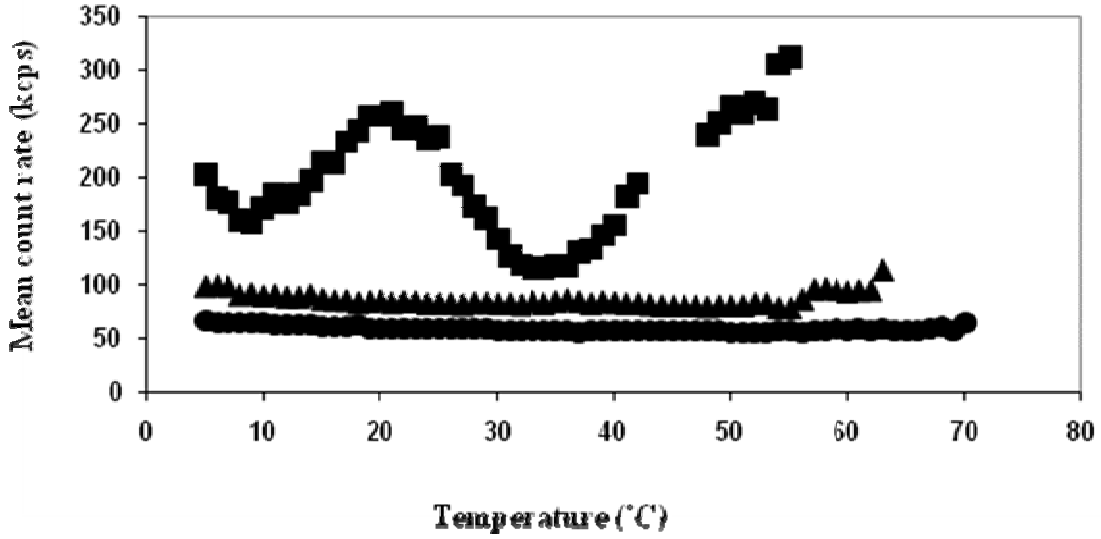

Figure 5.2. Thermal melting of disulfide-reduced apo SODs monitored by light scattering. Filtered samples at a protein concentration of ~ 1 mg/mL were scanned at a rate of ~ 1 °C/min in 1 mM TCEP, 20 mM HEPES, pH 7.4. Scattering intensity, as measured by mean count rate (kilo counts per second) of scattered photons is initially much higher for H43R (squares) when compared to PWT (circles) and G85R (triangles) and changes considerably with temperature. By contrast, both PWT and G85R scattering intensity changes very little with temperature. Experiments were conducted on a Zetasizer Nano-ZS instrument (Malvern).

Global fitting of this data to various 2-state and 3-state association models could yield information not only on the mechanism of aggregation but also the ΔG of aggregate formation. These experiments can be complemented by light scattering experiments in which increases in scattering intensity associated with protein aggregation would be followed with time and at different protein concentrations. Additional experiments could include atomic force microscopy which could be useful in determining the morphology of aggregates as well as transmission electron microscopy.

Bibliography

Agorogiannis, E. I., Agorogiannis, G. I., Papadimitriou, A. and Hadjigeorgiou, G. M. (2004) Protein misfolding in neurodegenerative diseases. *Neuropathol Appl Neurobiol* **30,** 215-24.

Andersen, P. M., Nilsson, P., Ala-Hurula, V., Keranen, M. L., Tarvainen, I., Haltia, T., Nilsson, L., Binzer, M., Forsgren, L. and Marklund, S. L. (1995) Amyotrophic lateral sclerosis associated with homozygosity for an Asp90Ala mutation in CuZn-superoxide dismutase. *Nat Genet* **10,** 61-6.

Anfinsen, C. B. (1973) Principles that govern the folding of protein chains. *Science* **181,** 223-30.

Antonyuk, S., Elam, J. S., Hough, M. A., Strange, R. W., Doucette, P. A., Rodriguez, J. A., Hayward, L. J., Valentine, J. S., Hart, P. J. and Hasnain, S. S. (2005) Structural consequences of the familial amyotrophic lateral sclerosis SOD1 mutant His46Arg. *Protein Sci* **14,** 1201-13.

Aoki, M., Ogasawara, M., Matsubara, Y., Narisawa, K., Nakamura, S., Itoyama, Y. and Abe, K. (1993) Mild ALS in Japan associated with novel SOD mutation. *Nat Genet* **5,** 323-4.

Apetri, A. C., Surewicz, K. and Surewicz, W. K. (2004) The effect of disease-associated mutations on the folding pathway of human prion protein. *J Biol Chem* **279,** 18008-14.

Arnesano, F., Banci, L., Bertini, I., Martinelli, M., Furukawa, Y. and O'Halloran T, V. (2004) The Unusually Stable Quaternary Structure of Human Cu,Zn-Superoxide Dismutase 1 Is Controlled by Both Metal Occupancy and Disulfide Status. *J Biol Chem* **279,** 47998-48003.

Baldwin, R. L. (2007) Energetics of protein folding. *J Mol Biol* **371,** 283-301.

Banci, L., Benedetto, M., Bertini, I., Del Conte, R., Piccioli, M. and Viezzoli, M. S. (1998) Solution structure of reduced monomeric Q133M2 copper, zinc superoxide dismutase (SOD). Why is SOD a dimeric enzyme? *Biochemistry* **37,** 11780-91.

Banci, L., Bertini, I., Boca, M., Calderone, V., Cantini, F., Girotto, S. and Vieru, M. (2009) Structural and dynamic aspects related to oligomerization of apo SOD1 and its mutants. *Proc Natl Acad Sci U S A* **106,** 6980-5.

Banci, L., Bertini, I., Boca, M., Girotto, S., Martinelli, M., Valentine, J. S. and Vieru, M. (2008) SOD1 and amyotrophic lateral sclerosis: mutations and oligomerization. *PLoS ONE* **3,** e1677.

Banci, L., Bertini, I., Cramaro, F., Del Conte, R. and Viezzoli, M. S. (2002) The solution structure of reduced dimeric copper zinc superoxide dismutase. The structural effects of dimerization. *Eur J Biochem* **269,** 1905-15.

Banci, L., Bertini, I., Cramaro, F., Del Conte, R. and Viezzoli, M. S. (2003) Solution structure of Apo Cu,Zn superoxide dismutase: role of metal ions in protein folding. *Biochemistry* **42,** 9543-53.

Banci, L., Bertini, I., D'Amelio, N., Gaggelli, E., Libralesso, E., Matecko, I., Turano, P. and Valentine, J. S. (2005) Fully metallated S134N Cu,Zn-superoxide dismutase displays abnormal mobility and intermolecular contacts in solution. *J Biol Chem.* **280,** 35815-21. Epub 2005 Aug 16.

Banci, L., Bertini, I., D'Amelio, N., Libralesso, E., Turano, P. and Valentine, J. S. (2007) Metalation of the amyotrophic lateral sclerosis mutant glycine 37 to arginine superoxide

dismutase (SOD1) apoprotein restores its structural and dynamical properties in solution to those of metalated wild-type SOD1. *Biochemistry* **46,** 9953-62.
Barber, S. C., Mead, R. J. and Shaw, P. J. (2006) Oxidative stress in ALS: a mechanism of neurodegeneration and a therapeutic target. *Biochim Biophys Acta* **1762,** 1051-67.
Baskakov, I. V. and Bolen, D. W. (1999) The paradox between m values and deltaCp's for denaturation of ribonuclease T1 with disulfide bonds intact and broken. *Protein Sci* **8,** 1314-9.
Battistoni, A., Folcarelli, S., Cervoni, L., Polizio, F., Desideri, A., Giartosio, A. and Rotilio, G. (1998) Role of the dimeric structure in Cu,Zn superoxide dismutase. pH-dependent, reversible denaturation of the monomeric enzyme from Escherichia coli. *J Biol Chem* **273,** 5655-61.
Beal, M. F., Ferrante, R. J., Browne, S. E., Matthews, R. T., Kowall, N. W. and Brown, R. H., Jr. (1997) Increased 3-nitrotyrosine in both sporadic and familial amyotrophic lateral sclerosis. *Ann Neurol* **42,** 644-54.
Beckman, J. S., Carson, M., Smith, C. D. and Koppenol, W. H. (1993) ALS, SOD and peroxynitrite. *Nature* **364,** 584.
Bello, M., Perez-Hernandez, G., Fernandez-Velasco, D. A., Arreguin-Espinosa, R. and Garcia-Hernandez, E. (2008) Energetics of protein homodimerization: effects of water sequestering on the formation of beta-lactoglobulin dimer. *Proteins* **70,** 1475-87.
Bendotti, C. and Carri, M. T. (2004) Lessons from models of SOD1-linked familial ALS. *Trends Mol Med* **10,** 393-400.
Bertini, I., Mangani, S., and Viezzoli, M. S. (1998) Structure and properties of copper/zinc superoxide dismutases. In *In Advanced Inorganic Chemistry*, (ed. S. AG), pp. 127-250, Academic Press, San Diego, CA, USA.
Bjelic, S. and Jelesarov, I. (2008) A survey of the year 2007 literature on applications of isothermal titration calorimetry. *J Mol Recognit* **21,** 289-312.
Bolen, D. W. and Baskakov, I. V. (2001) The osmophobic effect: natural selection of a thermodynamic force in protein folding. *J Mol Biol* **310,** 955-63.
Borchelt, D. R., Lee, M. K., Slunt, H. S., Guarnieri, M., Xu, Z. S., Wong, P. C., Brown, R. H., Jr., Price, D. L., Sisodia, S. S. and Cleveland, D. W. (1994) Superoxide dismutase 1 with mutations linked to familial amyotrophic lateral sclerosis possesses significant activity. *Proc Natl Acad Sci U S A* **91,** 8292-6.
Bordo, D., Djinovic, K. and Bolognesi, M. (1994) Conserved patterns in the Cu,Zn superoxide dismutase family. *J Mol Biol* **238,** 366-86.
Bordo, D., Matak, D., Djinovic-Carugo, K., Rosano, C., Pesce, A., Bolognesi, M., Stroppolo, M. E., Falconi, M., Battistoni, A. and Desideri, A. (1999) Evolutionary constraints for dimer formation in prokaryotic Cu,Zn superoxide dismutase. *J Mol Biol* **285,** 283-96.
Bourne, Y., Redford, S. M., Steinman, H. M., Lepock, J. R., Tainer, J. A. and Getzoff, E. D. (1996) Novel dimeric interface and electrostatic recognition in bacterial Cu,Zn superoxide dismutase. *Proc Natl Acad Sci U S A* **93,** 12774-9.
Brady, G. P. and Sharp, K. A. (1997) Entropy in protein folding and in protein-protein interactions. *Curr Opin Struct Biol* **7,** 215-21.
Briere, L. K. and Dunn, S. D. (2006) The periplasmic domains of Escherichia coli HflKC oligomerize through right-handed coiled-coil interactions. *Biochemistry* **45,** 8607-16.
Bruijn, L. I., Miller, T. M. and Cleveland, D. W. (2004) Unraveling the mechanisms involved in motor neuron degeneration in ALS. *Annu Rev Neurosci* **27,** 723-49.

Bruns, C. K. and Kopito, R. R. (2007) Impaired post-translational folding of familial ALS-linked Cu, Zn superoxide dismutase mutants. *Embo J* **26,** 855-66.
Burgos, I., Dassie, S. A. and Fidelio, G. D. (2008) Thermodynamic model for the analysis of calorimetric data of oligomeric proteins. *J Phys Chem B* **112,** 14325-33.
Burrows, S. D., Doyle, M. L., Murphy, K. P., Franklin, S. G., White, J. R., Brooks, I., McNulty, D. E., Scott, M. O., Knutson, J. R., Porter, D. and et al. (1994) Determination of the monomer-dimer equilibrium of interleukin-8 reveals it is a monomer at physiological concentrations. *Biochemistry* **33,** 12741-5.
Canet, D., Last, A. M., Tito, P., Sunde, M., Spencer, A., Archer, D. B., Redfield, C., Robinson, C. V. and Dobson, C. M. (2002) Local cooperativity in the unfolding of an amyloidogenic variant of human lysozyme. *Nat Struct Biol* **9,** 308-15.
Cao, X., Antonyuk, S. V., Seetharaman, S. V., Whitson, L. J., Taylor, A. B., Holloway, S. P., Strange, R. W., Doucette, P. A., Valentine, J. S., Tiwari, A., Hayward, L. J., Padua, S., Cohlberg, J. A., Hasnain, S. S. and Hart, P. J. (2008) Structures of the G85R variant of SOD1 in familial amyotrophic lateral sclerosis. *J Biol Chem* **283,** 16169-77.
Cardoso, R. M., Thayer, M. M., DiDonato, M., Lo, T. P., Bruns, C. K., Getzoff, E. D. and Tainer, J. A. (2002) Insights into Lou Gehrig's disease from the structure and instability of the A4V mutant of human Cu,Zn superoxide dismutase. *J Mol Biol* **324,** 247-56.
Carlioz, A. and Touati, D. (1986) Isolation of superoxide dismutase mutants in Escherichia coli: is superoxide dismutase necessary for aerobic life? *Embo J* **5,** 623-30.
Carrell, R. W. and Lomas, D. A. (1997) Conformational disease. *Lancet* **350,** 134-8.
Carroll, M. C., Girouard, J. B., Ulloa, J. L., Subramaniam, J. R., Wong, P. C., Valentine, J. S. and Culotta, V. C. (2004) Mechanisms for activating Cu- and Zn-containing superoxide dismutase in the absence of the CCS Cu chaperone. *Proc Natl Acad Sci U S A* **101,** 5964-9.
Cerasoli, E., Kelly, S. M., Coggins, J. R., Lapthorn, A. J., Clarke, D. T. and Price, N. C. (2003) Effects of salts on the function and conformational stability of shikimate kinase. *Biochim Biophys Acta* **1648,** 43-54.
Chamberlin, M. E. and Strange, K. (1989) Anisosmotic cell volume regulation: a comparative view. *Am J Physiol* **257,** C159-73.
Chattopadhyay, M., Durazo, A., Sohn, S. H., Strong, C. D., Gralla, E. B., Whitelegge, J. P. and Valentine, J. S. (2008) Initiation and elongation in fibrillation of ALS-linked superoxide dismutase. *Proc Natl Acad Sci U S A* **105,** 18663-8.
Chen, L., Cabrita, G. J., Otzen, D. E. and Melo, E. P. (2005) Stabilization of the ribosomal protein S6 by trehalose is counterbalanced by the formation of a putative off-pathway species. *J Mol Biol.* **351,** 402-16.
Chiti, F. and Dobson, C. M. (2006) Protein misfolding, functional amyloid, and human disease. *Annu Rev Biochem* **75,** 333-66.
Chiti, F., Stefani, M., Taddei, N., Ramponi, G. and Dobson, C. M. (2003) Rationalization of the effects of mutations on peptide and protein aggregation rates. *Nature* **424,** 805-8.
Chow, M. K., Lomas, D. A. and Bottomley, S. P. (2004) Promiscuous beta-strand interactions and the conformational diseases. *Curr Med Chem* **11,** 491-9.
Chrunyk, B. A. and Wetzel, R. (1993) Breakdown in the relationship between thermal and thermodynamic stability in an interleukin-1 beta point mutant modified in a surface loop. *Protein Eng.* **6,** 733-8.
Cleveland, D. W. (1999) From Charcot to SOD1: mechanisms of selective motor neuron death in ALS. *Neuron* **24,** 515-20.

Cole, J. L., Hansen, J.C. (1999) Analytical ultracentrifugation as a contemporary biomolecular research tool. *Journal of Biomolecular Techniques* **10,** 163-176.

Consalvi, V., Chiaraluce, R., Giangiacomo, L., Scandurra, R., Christova, P., Karshikoff, A., Knapp, S. and Ladenstein, R. (2000) Thermal unfolding and conformational stability of the recombinant domain II of glutamate dehydrogenase from the hyperthermophile Thermotoga maritima. *Protein Eng* **13,** 501-7.

Crow, J. P., Sampson, J. B., Zhuang, Y., Thompson, J. A. and Beckman, J. S. (1997) Decreased zinc affinity of amyotrophic lateral sclerosis-associated superoxide dismutase mutants leads to enhanced catalysis of tyrosine nitration by peroxynitrite. *J Neurochem* **69,** 1936-44.

Cudd, A. and Fridovich, I. (1982) Electrostatic interactions in the reaction mechanism of bovine erythrocyte superoxide dismutase. *J Biol Chem* **257,** 11443-7.

Culotta, V. C., Klomp, L. W., Strain, J., Casareno, R. L., Krems, B. and Gitlin, J. D. (1997) The copper chaperone for superoxide dismutase. *J Biol Chem* **272,** 23469-72.

Daggett, V. and Fersht, A. R. (2003) Is there a unifying mechanism for protein folding? *Trends Biochem Sci* **28,** 18-25.

Deng, H. X., Hentati, A., Tainer, J. A., Iqbal, Z., Cayabyab, A., Hung, W. Y., Getzoff, E. D., Hu, P., Herzfeldt, B., Roos, R. P. and et al. (1993) Amyotrophic lateral sclerosis and structural defects in Cu,Zn superoxide dismutase. *Science* **261,** 1047-51.

Deng, H. X., Shi, Y., Furukawa, Y., Zhai, H., Fu, R., Liu, E., Gorrie, G. H., Khan, M. S., Hung, W. Y., Bigio, E. H., Lukas, T., Dal Canto, M. C., O'Halloran, T. V. and Siddique, T. (2006) Conversion to the amyotrophic lateral sclerosis phenotype is associated with intermolecular linked insoluble aggregates of SOD1 in mitochondria. *Proc Natl Acad Sci U S A* **103,** 7142-7.

DiDonato, M., Craig, L., Huff, M. E., Thayer, M. M., Cardoso, R. M., Kassmann, C. J., Lo, T. P., Bruns, C. K., Powers, E. T., Kelly, J. W., Getzoff, E. D. and Tainer, J. A. (2003) ALS mutants of human superoxide dismutase form fibrous aggregates via framework destabilization. *J Mol Biol* **332,** 601-15.

Dill, K. A., Ozkan, S. B., Weikl, T. R., Chodera, J. D. and Voelz, V. A. (2007) The protein folding problem: when will it be solved? *Curr Opin Struct Biol* **17,** 342-6.

Dill, K. A., Truskett, T. M., Vlachy, V. and Hribar-Lee, B. (2005) Modeling water, the hydrophobic effect, and ion solvation. *Annu Rev Biophys Biomol Struct* **34,** 173-99.

Ding, F. and Dokholyan, N. V. (2008) Dynamical roles of metal ions and the disulfide bond in Cu, Zn superoxide dismutase folding and aggregation. *Proc Natl Acad Sci U S A* **105,** 19696-701.

Doucette, P. A., Whitson, L. J., Cao, X., Schirf, V., Demeler, B., Valentine, J. S., Hansen, J. C. and Hart, P. J. (2004) Dissociation of human copper-zinc superoxide dismutase dimers using chaotrope and reductant. Insights into the molecular basis for dimer stability. *J Biol Chem.* **279,** 54558-66. Epub 2004 Oct 12.

Dumoulin, M., Kumita, J. R. and Dobson, C. M. (2006) Normal and aberrant biological self-assembly: Insights from studies of human lysozyme and its amyloidogenic variants. *Acc Chem Res* **39,** 603-10.

Durham, H. D., Roy, J., Dong, L. and Figlewicz, D. A. (1997) Aggregation of mutant Cu/Zn superoxide dismutase proteins in a culture model of ALS. *J Neuropathol Exp Neurol* **56,** 523-30.

Ecroyd, H. and Carver, J. A. (2008) Unraveling the mysteries of protein folding and misfolding. *IUBMB Life* **60,** 769-74.

Eisen, A. (2009) Amyotrophic lateral sclerosis: A 40-year personal perspective. *J Clin Neurosci* **16,** 505-12.
Englander, S. W. (2006) Hydrogen exchange and mass spectrometry: A historical perspective. *J Am Soc Mass Spectrom* **17,** 1481-9.
Englander, S. W., Mayne, L. and Krishna, M. M. (2007) Protein folding and misfolding: mechanism and principles. *Q Rev Biophys* **40,** 287-326.
Fairman, R., Fenderson, W., Hail, M. E., Wu, Y. and Shaw, S. Y. (1999) Molecular weights of CTLA-4 and CD80 by sedimentation equilibrium ultracentrifugation. *Anal Biochem* **270,** 286-95.
Ferguson, N., Capaldi, A. P., James, R., Kleanthous, C. and Radford, S. E. (1999) Rapid folding with and without populated intermediates in the homologous four-helix proteins Im7 and Im9. *J Mol Biol.* **286,** 1597-608.
Forman, H. J. and Fridovich, I. (1973) On the stability of bovine superoxide dismutase. The effects of metals. *J Biol Chem* **248,** 2645-9.
Frank, H. S., Evans, M.W. (1945) Free volume and entropy in condensed systems. III. Entropyin binary liquid mixtures; partial molalentropy in dilute solutions; structure and thermodynamics in aqueous electrolytes. *J Chem Phys* **13,** 507-532.
Freire, E. (1995) Differential scanning calorimetry. *Methods Mol Biol* **40,** 191-218.
Fridovich, I. (1986) Superoxide dismutases. In *Advances in Enzymology, Vol. 58*, (ed. A. Meister), pp. 61, Interscience.
Furukawa, Y., Fu, R., Deng, H. X., Siddique, T. and O'Halloran, T. V. (2006) Disulfide cross-linked protein represents a significant fraction of ALS-associated Cu, Zn-superoxide dismutase aggregates in spinal cords of model mice. *Proc Natl Acad Sci U S A* **103,** 7148-53.
Furukawa, Y., Kaneko, K., Yamanaka, K., O'Halloran, T. V. and Nukina, N. (2008) Complete loss of post-translational modifications triggers fibrillar aggregation of SOD1 in the familial form of amyotrophic lateral sclerosis. *J Biol Chem* **283,** 24167-76.
Furukawa, Y. and O'Halloran, T. V. (2005) Amyotrophic lateral sclerosis mutations have the greatest destabilizing effect on the apo- and reduced form of SOD1, leading to unfolding and oxidative aggregation. *J Biol Chem* **280,** 17266-74.
Furukawa, Y. and O'Halloran, T. V. (2006) Posttranslational modifications in Cu,Zn-superoxide dismutase and mutations associated with amyotrophic lateral sclerosis. *Antioxid Redox Signal* **8,** 847-67.
Furukawa, Y., Torres, A. S. and O'Halloran, T. V. (2004) Oxygen-induced maturation of SOD1: a key role for disulfide formation by the copper chaperone CCS. *Embo J* **23,** 2872-81.
Galvagnion, C., Smith, M. T., Broom, A., Vassall, K. A., Meglei, G., Gaspar, J. A., Stathopulos, P. B., Cheyne, B. and Meiering, E. M. (2009) Folding and Association of Thermophilic Dimeric and Trimeric DsrEFH Proteins: Tm0979 and Mth1491 (dagger). *Biochemistry* **48,** 2891-906.
Geierhaas, C. D., Nickson, A. A., Lindorff-Larsen, K., Clarke, J. and Vendruscolo, M. (2007) BPPred: a Web-based computational tool for predicting biophysical parameters of proteins. *Protein Sci* **16,** 125-34.
Getzoff, E. D., Cabelli, D. E., Fisher, C. L., Parge, H. E., Viezzoli, M. S., Banci, L. and Hallewell, R. A. (1992) Faster superoxide dismutase mutants designed by enhancing electrostatic guidance. *Nature* **358,** 347-51.
Getzoff, E. D., Tainer, J. A. and Olson, A. J. (1986) Recognition and interactions controlling the assemblies of beta barrel domains. *Biophys J* **49,** 191-206.

Getzoff, E. D., Tainer, J. A., Stempien, M. M., Bell, G. I. and Hallewell, R. A. (1989) Evolution of CuZn superoxide dismutase and the Greek key beta-barrel structural motif. *Proteins* **5,** 322-36.

Getzoff, E. D., Tainer, J. A., Weiner, P. K., Kollman, P. A., Richardson, J. S. and Richardson, D. C. (1983) Electrostatic recognition between superoxide and copper, zinc superoxide dismutase. *Nature* **306,** 287-90.

Gomez, J., Hilser, V. J., Xie, D. and Freire, E. (1995) The heat capacity of proteins. *Proteins* **22,** 404-12.

Goodall, E. F. and Morrison, K. E. (2006) Amyotrophic lateral sclerosis (motor neuron disease): proposed mechanisms and pathways to treatment. *Expert Rev Mol Med* **8,** 1-22.

Gregersen, N. (2006) Protein misfolding disorders: pathogenesis and intervention. *J Inherit Metab Dis* **29,** 456-70.

Gregersen, N., Bolund, L. and Bross, P. (2005) Protein misfolding, aggregation, and degradation in disease. *Mol Biotechnol.* **31,** 141-50.

Guegan, C. and Przedborski, S. (2003) Programmed cell death in amyotrophic lateral sclerosis. *J Clin Invest* **111,** 153-61.

Hallewell, R. A., Imlay, K. C., Lee, P., Fong, N. M., Gallegos, C., Getzoff, E. D., Tainer, J. A., Cabelli, D. E., Tekamp-Olson, P., Mullenbach, G. T. and et al. (1991) Thermostabilization of recombinant human and bovine CuZn superoxide dismutases by replacement of free cysteines. *Biochem Biophys Res Commun* **181,** 474-80.

Hammarstrom, P., Jiang, X., Hurshman, A. R., Powers, E. T. and Kelly, J. W. (2002) Sequence-dependent denaturation energetics: A major determinant in amyloid disease diversity. *Proc Natl Acad Sci U S A* **99 Suppl 4,** 16427-32.

Han, J. C. and Han, G. Y. (1994) A procedure for quantitative determination of tris(2-carboxyethyl)phosphine, an odorless reducing agent more stable and effective than dithiothreitol. *Anal Biochem* **220,** 5-10.

Hand, C. K. and Rouleau, G. A. (2002) Familial amyotrophic lateral sclerosis. *Muscle Nerve* **25,** 135-59.

Hansen, J. C., Lebowitz, J. and Demeler, B. (1994) Analytical ultracentrifugation of complex macromolecular systems. *Biochemistry* **33,** 13155-63.

Hart, P. J., Balbirnie, M. M., Ogihara, N. L., Nersissian, A. M., Weiss, M. S., Valentine, J. S. and Eisenberg, D. (1999) A structure-based mechanism for copper-zinc superoxide dismutase. *Biochemistry* **38,** 2167-78.

Hart, P. J., Liu, H., Pellegrini, M., Nersissian, A. M., Gralla, E. B., Valentine, J. S. and Eisenberg, D. (1998) Subunit asymmetry in the three-dimensional structure of a human CuZnSOD mutant found in familial amyotrophic lateral sclerosis. *Protein Sci* **7,** 545-55.

Hayward, L. J., Rodriguez, J. A., Kim, J. W., Tiwari, A., Goto, J. J., Cabelli, D. E., Valentine, J. S. and Brown, R. H., Jr. (2002) Decreased metallation and activity in subsets of mutant superoxide dismutases associated with familial amyotrophic lateral sclerosis. *J Biol Chem* **277,** 15923-31.

Hof, M., Fidler, V. and Hutterer, R. (2005) Basics of Fluorescence Spectroscopy in Biosciences. Methods and Applications. In *Fluorescence Spectroscopy in Biology. Advanced Methods and their Applications to Membranes, Proteins, DNA, and Cells Vol. 3*, (eds. M. Hof, R. Hutterer and V. Fidler), Springer Berlin Heidelberg.

Hornberg, A., Logan, D. T., Marklund, S. L. and Oliveberg, M. (2007) The coupling between disulphide status, metallation and dimer interface strength in Cu/Zn superoxide dismutase. *J Mol Biol* **365,** 333-42.

Hough, M. A., Grossmann, J. G., Antonyuk, S. V., Strange, R. W., Doucette, P. A., Rodriguez, J. A., Whitson, L. J., Hart, P. J., Hayward, L. J., Valentine, J. S. and Hasnain, S. S. (2004) Dimer destabilization in superoxide dismutase may result in disease-causing properties: structures of motor neuron disease mutants. *Proc Natl Acad Sci U S A.* **101,** 5976-81. Epub 2004 Mar 31.

Jahn, T. R. and Radford, S. E. (2008) Folding versus aggregation: polypeptide conformations on competing pathways. *Arch Biochem Biophys* **469,** 100-17.

Jha, B. K., Mitra, N., Rana, R., Surolia, A., Salunke, D. M. and Datta, K. (2004) pH and cation-induced thermodynamic stability of human hyaluronan binding protein 1 regulates its hyaluronan affinity. *J Biol Chem* **279,** 23061-72.

Johnson, C. M. and Fersht, A. R. (1995) Protein stability as a function of denaturant concentration: ther thermal stability of barnase in the presence of urea. *Biochemistry* **34,** 6795-804.

Johnson, S. M., Wiseman, R. L., Sekijima, Y., Green, N. S., Adamski-Werner, S. L. and Kelly, J. W. (2005) Native state kinetic stabilization as a strategy to ameliorate protein misfolding diseases: a focus on the transthyretin amyloidoses. *Acc Chem Res* **38,** 911-21.

Johnston, J. A., Dalton, M. J., Gurney, M. E. and Kopito, R. R. (2000) Formation of high molecular weight complexes of mutant Cu, Zn-superoxide dismutase in a mouse model for familial amyotrophic lateral sclerosis. *Proc Natl Acad Sci U S A* **97,** 12571-6.

Jonsson, P. A., Graffmo, K. S., Andersen, P. M., Brannstrom, T., Lindberg, M., Oliveberg, M. and Marklund, S. L. (2006) Disulphide-reduced superoxide dismutase-1 in CNS of transgenic amyotrophic lateral sclerosis models. *Brain* **129,** 451-64.

Julien, J. P. and Kriz, J. (2006) Transgenic mouse models of amyotrophic lateral sclerosis. *Biochim Biophys Acta* **1762,** 1013-24.

Karch, C. M. and Borchelt, D. R. (2008) A limited role for disulfide cross-linking in the aggregation of mutant SOD1 linked to familial amyotrophic lateral sclerosis. *J Biol Chem* **283,** 13528-37.

Karch, C. M., Prudencio, M., Winkler, D. D., Hart, P. J. and Borchelt, D. R. (2009) Role of mutant SOD1 disulfide oxidation and aggregation in the pathogenesis of familial ALS. *Proc Natl Acad Sci U S A* **106,** 7774-9.

Kayatekin, C., Zitzewitz, J. A. and Matthews, C. R. (2008) Zinc binding modulates the entire folding free energy surface of human Cu,Zn superoxide dismutase. *J Mol Biol* **384,** 540-55.

Khare, S. D., Caplow, M. and Dokholyan, N. V. (2004) The rate and equilibrium constants for a multistep reaction sequence for the aggregation of superoxide dismutase in amyotrophic lateral sclerosis. *Proc Natl Acad Sci U S A* **101,** 15094-9.

Khare, S. D., Caplow, M. and Dokholyan, N. V. (2006) FALS mutations in Cu, Zn superoxide dismutase destabilize the dimer and increase dimer dissociation propensity: a large-scale thermodynamic analysis. *Amyloid* **13,** 226-35.

Khare, S. D. and Dokholyan, N. V. (2006) Common dynamical signatures of familial amyotrophic lateral sclerosis-associated structurally diverse Cu, Zn superoxide dismutase mutants. *Proc Natl Acad Sci U S A* **103,** 3147-52.

Khare, S. D., Wilcox, K. C., Gong, P. and Dokholyan, N. V. (2005) Sequence and structural determinants of Cu, Zn superoxide dismutase aggregation. *Proteins* **61,** 617-32.

Klug, D., Rabani, J. and Fridovich, I. (1972) A direct demonstration of the catalytic action of superoxide dismutase through the use of pulse radiolysis. *J Biol Chem* **247,** 4839-42.

Koide, T., Igarashi, S., Kikugawa, K., Nakano, R., Inuzuka, T., Yamada, M., Takahashi, H. and Tsuji, S. (1998) Formation of granular cytoplasmic aggregates in COS7 cells expressing mutant Cu/Zn superoxide dismutase associated with familial amyotrophic lateral sclerosis. *Neurosci Lett* **257,** 29-32.
Koshland, D. and Botstein, D. (1980) Secretion of beta-lactamase requires the carboxy end of the protein. *Cell* **20,** 749-60.
Kumar, M. D., Bava, K. A., Gromiha, M. M., Prabakaran, P., Kitajima, K., Uedaira, H. and Sarai, A. (2006) ProTherm and ProNIT: thermodynamic databases for proteins and protein-nucleic acid interactions. *Nucleic Acids Res* **34,** D204-6.
Laemmli, U. K. (1970) Cleavage of structural proteins during the assembly of the head of bacteriophage T4. *Nature* **227,** 680-5.
Lakowicz, J. R. (2006) Principles of Fluorescence Spectroscopy, Springer.
Laue, T. M., Shah,B.D., Ridgeway, T.M., Pelletier, S.L. (1992) Computer-aided interpretation of analytical sedimentation data for proteins. In *Analytical Ultracentrifugation in Biochemistry and Polymer Science*, (ed. S. Harding, Rowe, A.), pp. 90-125, Royal Society of Chemistry, Cambridge, UK.
Leavitt, S. and Freire, E. (2001) Direct measurement of protein binding energetics by isothermal titration calorimetry. *Curr Opin Struct Biol* **11,** 560-6.
Lepock, J. R., Frey, H. E. and Hallewell, R. A. (1990) Contribution of conformational stability and reversibility of unfolding to the increased thermostability of human and bovine superoxide dismutase mutated at free cysteines. *J Biol Chem* **265,** 21612-8.
Leventhal, C. (1969) How to fold graciously. *In Mossbauer Spectroscopy in Biological systems In Proceeding of a Meeting held at Allerton House (Monticello, I.L., ed), University of Illinois Press***,** 22-24.
Liberek, K., Lewandowska, A. and Zietkiewicz, S. (2008) Chaperones in control of protein disaggregation. *Embo J* **27,** 328-35.
Lindberg, M. (2004) Protein folding studies of human superoxide dismutase and ALS associated mutants. In *Department of Biochemistry*, Umea University, Umea.
Lindberg, M. J., Bystrom, R., Boknas, N., Andersen, P. M. and Oliveberg, M. (2005) Systematically perturbed folding patterns of amyotrophic lateral sclerosis (ALS)-associated SOD1 mutants. *Proc Natl Acad Sci U S A* **102,** 9754-9.
Lindberg, M. J., Normark, J., Holmgren, A. and Oliveberg, M. (2004) Folding of human superoxide dismutase: disulfide reduction prevents dimerization and produces marginally stable monomers. *Proc Natl Acad Sci U S A* **101,** 15893-8.
Lindberg, M. J., Tibell, L. and Oliveberg, M. (2002) Common denominator of Cu/Zn superoxide dismutase mutants associated with amyotrophic lateral sclerosis: decreased stability of the apo state. *Proc Natl Acad Sci U S A* **99,** 16607-12.
Lindberg, M. O. and Oliveberg, M. (2007) Malleability of protein folding pathways: a simple reason for complex behaviour. *Curr Opin Struct Biol* **17,** 21-9.
Lins, L. and Brasseur, R. (1995) The hydrophobic effect in protein folding. *Faseb J* **9,** 535-40.
Liu, C., Chu, D., Wideman, R. D., Houliston, R. S., Wong, H. J. and Meiering, E. M. (2001) Thermodynamics of denaturation of hisactophilin, a beta-trefoil protein. *Biochemistry* **40,** 3817-27.
Liu, L., Yang, C. and Guo, Q. X. (2000) A study on the enthalpy-entropy compensation in protein unfolding. *Biophys Chem* **84,** 239-51.

Liu, Y. and Sturtevant, J. M. (1996) The observed change in heat capacity accompanying the thermal unfolding of proteins depends on the composition of the solution and on the method employed to change the temperature of unfolding. *Biochemistry* **35,** 3059-62.
Lovatt, M., Cooper, A. and Camilleri, P. (1996) Energetics of cyclodextrin-induced dissociation of insulin. *Eur Biophys J* **24,** 354-7.
Lowry, O. H., Rosenbrough, N. J., Farr, L. A. and Randal, R. J. (1951) Protein measurement with the folin phenol reagent. *J Biol Chem* **193,** 265-75.
Luke, K., Apiyo, D. and Wittung-Stafshede, P. (2005) Dissecting homo-heptamer thermodynamics by isothermal titration calorimetry: entropy-driven assembly of co-chaperonin protein 10. *Biophys J* **89,** 3332-6.
Lyons, T. J., Liu, H., Goto, J. J., Nersissian, A., Roe, J. A., Graden, J. A., Cafe, C., Ellerby, L. M., Bredesen, D. E., Gralla, E. B. and Valentine, J. S. (1996) Mutations in copper-zinc superoxide dismutase that cause amyotrophic lateral sclerosis alter the zinc binding site and the redox behavior of the protein. *Proc Natl Acad Sci U S A* **93,** 12240-4.
Majoor-Krakauer, D., Willems, P. J. and Hofman, A. (2003) Genetic epidemiology of amyotrophic lateral sclerosis. *Clin Genet* **63,** 83-101.
Makhatadze, G. I. and Privalov, P. L. (1992) Protein interactions with urea and guanidinium chloride. A calorimetric study. *J Mol Biol* **226,** 491-505.
Makhatadze, G. I., Privalov, P.L. (1995) Energetics of Protein structure. In *Advances in protein chemistry, Vol. 47*, Academic Press, Inc.
Margerum, D. W., Cayley, G.R., Weatherburn, D.C., Pagenkopf, G.K. (1978) Coordination Chemistry*, Vol. 2*, (ed. A. E. Martell), pp. 1-220, American Chemical Society, Washingtion DC.
Marklund, S. and Marklund, G. (1974) Involvement of the superoxide anion radical in the autoxidation of pyrogallol and a convenient assay for superoxide dismutase. *Eur J Biochem* **47,** 469-74.
Matsumoto, S., Kusaka, H., Ito, H., Shibata, N., Asayama, T. and Imai, T. (1996) Sporadic amyotrophic lateral sclerosis with dementia and Cu/Zn superoxide dismutase-positive Lewy body-like inclusions. *Clin Neuropathol* **15,** 41-6.
McCord, J. M. and Fridovich, I. (1969) Superoxide dismutase. An enzymic function for erythrocuprein (hemocuprein). *J Biol Chem* **244,** 6049-55.
McCord, J. M., Keele, B. B., Jr. and Fridovich, I. (1971) An enzyme-based theory of obligate anaerobiosis: the physiological function of superoxide dismutase. *Proc Natl Acad Sci U S A* **68,** 1024-7.
McCrary, B. S., Bedell, J., Edmondson, S. P. and Shriver, J. W. (1998) Linkage of protonation and anion binding to the folding of Sac7d. *J Mol Biol* **276,** 203-24.
McCrary, B. S., Edmondson, S. P. and Shriver, J. W. (1996) Hyperthermophile protein folding thermodynamics: differential scanning calorimetry and chemical denaturation of Sac7d. *J Mol Biol* **264,** 784-805.
McRee, D. E., Redford, S. M., Getzoff, E. D., Lepock, J. R., Hallewell, R. A. and Tainer, J. A. (1990) Changes in crystallographic structure and thermostability of a Cu,Zn superoxide dismutase mutant resulting from the removal of a buried cysteine. *J Biol Chem* **265,** 14234-41.
McRorie, D. K., Voelker, P.J. (1993) Self-Associating Systems in the Analytical Ultracentrifuge, Beckman Intruments Inc., Palo Alto, CA.
Meiering, E. M. (2008) The threat of instability: neurodegeneration predicted by protein destabilization and aggregation propensity. *PLoS Biol* **6,** e193.

Miller, A. F. (2004) Superoxide dismutases: active sites that save, but a protein that kills. *Curr Opin Chem Biol* **8,** 162-8.
Miller, E. M. and Nickoloff, J. A. (1995) Escherichia coli electrotransformation. *Methods Mol Biol* **47,** 105-13.
Miller, J. F. (1994) Bacterial transformation by electroporation. *Methods Enzymol* **235,** 375-85.
Mitchell, J. D. and Borasio, G. D. (2007) Amyotrophic lateral sclerosis. *Lancet* **369,** 2031-41.
Murphy, R. M. and Kendrick, B. S. (2007) Protein misfolding and aggregation. *Biotechnol Prog* **23,** 548-52.
Myers, J. K., Pace, C. N. and Scholtz, J. M. (1995) Denaturant m values and heat capacity changes: relation to changes in accessible surface areas of protein unfolding. *Protein Sci* **4,** 2138-48.
Natvig, D. O., Imlay, K., Touati, D. and Hallewell, R. A. (1987) Human copper-zinc superoxide dismutase complements superoxide dismutase-deficient Escherichia coli mutants. *J Biol Chem* **262,** 14697-701.
Nishimura, C., Uversky, V. N. and Fink, A. L. (2001) Effect of salts on the stability and folding of staphylococcal nuclease. *Biochemistry* **40,** 2113-28.
Niwa, J., Yamada, S., Ishigaki, S., Sone, J., Takahashi, M., Katsuno, M., Tanaka, F., Doyu, M. and Sobue, G. (2007) Disulfide bond mediates aggregation, toxicity, and ubiquitylation of familial amyotrophic lateral sclerosis-linked mutant SOD1. *J Biol Chem* **282,** 28087-95.
Nölting, B. (2006) Protein folding kinetics: biophysical methods, Springer.
Okhrimenko, O. and Jelesarov, I. (2008) A survey of the year 2006 literature on applications of isothermal titration calorimetry. *J Mol Recognit* **21,** 1-19.
Orrell, R., de Belleroche, J., Marklund, S., Bowe, F. and Hallewell, R. (1995) A novel SOD mutant and ALS. *Nature* **374,** 504-5.
Pace, C. N. (1986) Determination and analysis of urea and guanidine hydrochloride denaturation curves. *Methods Enzymol* **131,** 266-80.
Pace, C. N., Grimsley, G. R., Thomson, J. A. and Barnett, B. J. (1988) Conformational stability and activity of ribonuclease T1 with zero, one, and two intact disulfide bonds. *J Biol Chem* **263,** 11820-5.
Pace, C. N., Shirley, B. A., McNutt, M. and Gajiwala, K. (1996) Forces contributing to the conformational stability of proteins. *Faseb J* **10,** 75-83.
Parge, H. E., Hallewell, R. A. and Tainer, J. A. (1992) Atomic structures of wild-type and thermostable mutant recombinant human Cu,Zn superoxide dismutase. *Proc Natl Acad Sci U S A* **89,** 6109-13.
Park, Y. C. and Bedouelle, H. (1998) Dimeric tyrosyl-tRNA synthetase from Bacillus stearothermophilus unfolds through a monomeric intermediate. A quantitative analysis under equilibrium conditions. *J Biol Chem* **273,** 18052-9.
Pesce, A., Capasso, C., Battistoni, A., Folcarelli, S., Rotilio, G., Desideri, A. and Bolognesi, M. (1997) Unique structural features of the monomeric Cu,Zn superoxide dismutase from Escherichia coli, revealed by X-ray crystallography. *J Mol Biol* **274,** 408-20.
Potter, S. Z., Zhu, H., Shaw, B. F., Rodriguez, J. A., Doucette, P. A., Sohn, S. H., Durazo, A., Faull, K. F., Gralla, E. B., Nersissian, A. M. and Valentine, J. S. (2007) Binding of a single zinc ion to one subunit of copper-zinc superoxide dismutase apoprotein substantially influences the structure and stability of the entire homodimeric protein. *J Am Chem Soc* **129,** 4575-83.

Prabhu, N. V. and Sharp, K. A. (2005) Heat capacity in proteins. *Annu Rev Phys Chem* **56,** 521-48.
Privalov, P. L. (1979) Stability of proteins: small globular proteins. *Adv Protein Chem* **33,** 167-241.
Privalov, P. L. and Makhatadze, G. I. (1990) Heat capacity of proteins. II. Partial molar heat capacity of the unfolded polypeptide chain of proteins: protein unfolding effects. *J Mol Biol* **213,** 385-91.
Privalov, P. L. and Potekhin, S. A. (1986) Scanning microcalorimetry in studying temperature-induced changes in proteins. *Methods Enzymol* **131,** 4-51.
Rae, T. D., Schmidt, P. J., Pufahl, R. A., Culotta, V. C. and O'Halloran, T. V. (1999) Undetectable intracellular free copper: the requirement of a copper chaperone for superoxide dismutase. *Science* **284,** 805-8.
Rakhit, R., Crow, J. P., Lepock, J. R., Kondejewski, L. H., Cashman, N. R. and Chakrabartty, A. (2004) Monomeric Cu,Zn-superoxide dismutase is a common misfolding intermediate in the oxidation models of sporadic and familial amyotrophic lateral sclerosis. *J Biol Chem* **279,** 15499-504.
Rakhit, R., Robertson, J., Vande Velde, C., Horne, P., Ruth, D. M., Griffin, J., Cleveland, D. W., Cashman, N. R. and Chakrabartty, A. (2007) An immunological epitope selective for pathological monomer-misfolded SOD1 in ALS. *Nat Med* **13,** 754-9.
Ralston, G. (1993) Introduction to Analytical Ultracentrifugation, Beckman Instruments Fullerton, CA.
Rami, B. R. and Udgaonkar, J. B. (2002) Mechanism of formation of a productive molten globule form of barstar. *Biochemistry.* **41,** 1710-6.
Ray, S. S. and Lansbury, P. T., Jr. (2004) A possible therapeutic target for Lou Gehrig's disease. *Proc Natl Acad Sci U S A* **101,** 5701-2.
Ray, S. S., Nowak, R. J., Brown, R. H., Jr. and Lansbury, P. T., Jr. (2005) Small-molecule-mediated stabilization of familial amyotrophic lateral sclerosis-linked superoxide dismutase mutants against unfolding and aggregation. *Proc Natl Acad Sci U S A* **102,** 3639-44.
Ray, S. S., Nowak, R. J., Strokovich, K., Brown, R. H., Jr., Walz, T. and Lansbury, P. T., Jr. (2004) An intersubunit disulfide bond prevents in vitro aggregation of a superoxide dismutase-1 mutant linked to familial amytrophic lateral sclerosis. *Biochemistry* **43,** 4899-905.
Reaume, A. G., Elliott, J. L., Hoffman, E. K., Kowall, N. W., Ferrante, R. J., Siwek, D. F., Wilcox, H. M., Flood, D. G., Beal, M. F., Brown, R. H., Jr., Scott, R. W. and Snider, W. D. (1996) Motor neurons in Cu/Zn superoxide dismutase-deficient mice develop normally but exhibit enhanced cell death after axonal injury. *Nat Genet* **13,** 43-7.
Richardson, J., Thomas, K. A., Rubin, B. H. and Richardson, D. C. (1975) Crystal structure of bovine Cu,Zn superoxide dismutase at 3 A resolution: chain tracing and metal ligands. *Proc Natl Acad Sci U S A* **72,** 1349-53.
Ripps, M. E., Huntley, G. W., Hof, P. R., Morrison, J. H. and Gordon, J. W. (1995) Transgenic mice expressing an altered murine superoxide dismutase gene provide an animal model of amyotrophic lateral sclerosis. *Proc Natl Acad Sci U S A* **92,** 689-93.
Robinson, C. R., Liu, Y., O'Brien, R., Sligar, S. G. and Sturtevant, J. M. (1998) A differential scanning calorimetric study of the thermal unfolding of apo- and holo-cytochrome b562. *Protein Sci* **7,** 961-5.

Rodriguez, J. A., Shaw, B. F., Durazo, A., Sohn, S. H., Doucette, P. A., Nersissian, A. M., Faull, K. F., Eggers, D. K., Tiwari, A., Hayward, L. J. and Valentine, J. S. (2005) Destabilization of apoprotein is insufficient to explain Cu,Zn-superoxide dismutase-linked ALS pathogenesis. *Proc Natl Acad Sci U S A.* **102,** 10516-21. Epub 2005 Jul 14.

Rodriguez, J. A., Valentine, J. S., Eggers, D. K., Roe, J. A., Tiwari, A., Brown, R. H., Jr. and Hayward, L. J. (2002) Familial amyotrophic lateral sclerosis-associated mutations decrease the thermal stability of distinctly metallated species of human copper/zinc superoxide dismutase. *J Biol Chem* **277,** 15932-7.

Rose, G. D., Fleming, P. J., Banavar, J. R. and Maritan, A. (2006) A backbone-based theory of protein folding. *Proc Natl Acad Sci U S A* **103,** 16623-33.

Rosen, D. R., Siddique, T., Patterson, D., Figlewicz, D. A., Sapp, P., Hentati, A., Donaldson, D., Goto, J., O'Regan, J. P., Deng, H. X. and et al. (1993) Mutations in Cu/Zn superoxide dismutase gene are associated with familial amyotrophic lateral sclerosis [published erratum appears in Nature 1993 Jul 22;364(6435):362] [see comments]. *Nature* **362,** 59-62.

Rothstein, J. D. (2009) Current hypotheses for the underlying biology of amyotrophic lateral sclerosis. *Ann Neurol* **65 Suppl 1,** S3-9.

Rowland, L. P. and Shneider, N. A. (2001) Amyotrophic lateral sclerosis. *N Engl J Med* **344,** 1688-700.

Rumfeldt, J. A., Galvagnion, C., Vassall, K. A. and Meiering, E. M. (2008) Conformational stability and folding mechanisms of dimeric proteins. *Prog Biophys Mol Biol* **98,** 61-84.

Rumfeldt, J. A., Lepock, J. R. and Meiering, E. M. (2009) Unfolding and folding kinetics of amyotrophic lateral sclerosis-associated mutant Cu,Zn superoxide dismutases. *J Mol Biol* **385,** 278-98.

Rumfeldt, J. A., Stathopulos, P. B., Chakrabarrty, A., Lepock, J. R. and Meiering, E. M. (2006) Mechanism and Thermodynamics of Guanidinium Chloride-induced Denaturation of ALS-associated Mutant Cu,Zn Superoxide Dismutases. *J Mol Biol* **355,** 106-23.

Rumfeldt, J. A. O. (2006) Thermodynamics, kinetics and structural dynamics of amyotrophic lateral sclerosis-associated mutant copper-zinc superoxide dismutases. In *Chemistry, Vol. Ph.D*, pp. 299, University of Waterloo, Waterloo.

Sandelin, E., Nordlund, A., Andersen, P. M., Marklund, S. S. and Oliveberg, M. (2007) Amyotrophic lateral sclerosis-associated copper/zinc superoxide dismutase mutations preferentially reduce the repulsive charge of the proteins. *J Biol Chem* **282,** 21230-6.

Sauder, J. M., MacKenzie, N. E. and Roder, H. (1996) Kinetic mechanism of folding and unfolding of Rhodobacter capsulatus cytochrome c2. *Biochemistry.* **35,** 16852-62.

Schoppe, A., Hinz, H. J., Agashe, V. R., Ramachandran, S. and Udgaonkar, J. B. (1997) DSC studies of the conformational stability of barstar wild-type. *Protein Sci* **6,** 2196-202.

Schuck, P. (2000) Size-distribution analysis of macromolecules by sedimentation velocity ultracentrifugation and lamm equation modeling. *Biophys J* **78,** 1606-19.

Schuck, P. (2007) Sedimentation equilibrium analytical ultracentrifugation for multicomponent protein interactions. In *Protein Interactions: Biophysical approaches for the study of complex reversible systems, Vol. 5*, (ed. M. Z. Atassi), pp. 289-316, Springer.

Schwartz, A. L. and Ciechanover, A. (2009) Targeting proteins for destruction by the ubiquitin system: implications for human pathobiology. *Annu Rev Pharmacol Toxicol* **49,** 73-96.

Shaw, B. F., Durazo, A., Nersissian, A. M., Whitelegge, J. P., Faull, K. F. and Valentine, J. S. (2006) Local unfolding in a destabilized, pathogenic variant of superoxide dismutase 1 observed with H/D exchange and mass spectrometry. *J Biol Chem* **281,** 18167-76.

Shaw, B. F. and Valentine, J. S. (2007) How do ALS-associated mutations in superoxide dismutase 1 promote aggregation of the protein? *Trends Biochem Sci* **32,** 78-85.
Shibata, N., Asayama, K., Hirano, A. and Kobayashi, M. (1996) Immunohistochemical study on superoxide dismutases in spinal cords from autopsied patients with amyotrophic lateral sclerosis. *Dev Neurosci* **18,** 492-8.
Shibata, N., Hirano, A., Kobayashi, M., Sasaki, S., Kato, T., Matsumoto, S., Shiozawa, Z., Komori, T., Ikemoto, A., Umahara, T. and et al. (1994) Cu/Zn superoxide dismutase-like immunoreactivity in Lewy body-like inclusions of sporadic amyotrophic lateral sclerosis. *Neurosci Lett* **179,** 149-52.
Siddique, T. and Deng, H. X. (1996) Genetics of amyotrophic lateral sclerosis. *Hum Mol Genet* **5 Spec No,** 1465-70.
Silva, N., Jr., Gratton, E., Mei, G., Rosato, N., Rusch, R. and Finazzi-Agro, A. (1993) Molten globule monomers in human superoxide dismutase. *Biophys Chem* **48,** 171-82.
Somero, G. N. (1986) Protons, osmolytes, and fitness of internal milieu for protein function. *Am J Physiol* **251,** R197-213.
Soto, C. (2003) Unfolding the role of protein misfolding in neurodegenerative diseases. *Nat Rev Neurosci* **4,** 49-60.
Soulages, J. L. (1998) Chemical denaturation: potential impact of undetected intermediates in the free energy of unfolding and m-values obtained from a two-state assumption. *Biophys J* **75,** 484-92.
Spudich, G. and Marqusee, S. (2000) A change in the apparent m value reveals a populated intermediate under equilibrium conditions in Escherichia coli ribonuclease HI. *Biochemistry* **39,** 11677-83.
Stathopulos, P. B. (2005) Stability and aggregation of amyotrophic lateral sclerosis-associated mutant copper, zinc superoxide dismutases. In *Biology, Vol. Ph.D*, pp. 377, University of Waterloo, Waterloo.
Stathopulos, P. B., Rumfeldt, J. A., Karbassi, F., Siddall, C. A., Lepock, J. R. and Meiering, E. M. (2006) Calorimetric analysis of thermodynamic stability and aggregation for apo and holo amyotrophic lateral sclerosis-associated Gly-93 mutants of superoxide dismutase. *J Biol Chem* **281,** 6184-93.
Stathopulos, P. B., Rumfeldt, J. A., Scholz, G. A., Irani, R. A., Frey, H. E., Hallewell, R. A., Lepock, J. R. and Meiering, E. M. (2003) Cu/Zn superoxide dismutase mutants associated with amyotrophic lateral sclerosis show enhanced formation of aggregates in vitro. *Proc Natl Acad Sci U S A* **100,** 7021-6.
Stefani, M. and Dobson, C. M. (2003) Protein aggregation and aggregate toxicity: new insights into protein folding, misfolding diseases and biological evolution. *J Mol Med* **81,** 678-99. Epub 2003 Aug 27.
Strange, R. W., Antonyuk, S., Hough, M. A., Doucette, P. A., Rodriguez, J. A., Hart, P. J., Hayward, L. J., Valentine, J. S. and Hasnain, S. S. (2003) The structure of holo and metal-deficient wild-type human Cu, Zn superoxide dismutase and its relevance to familial amyotrophic lateral sclerosis. *J Mol Biol* **328,** 877-91.
Strong, M. J., Kesavapany, S. and Pant, H. C. (2005) The pathobiology of amyotrophic lateral sclerosis: a proteinopathy? *J Neuropathol Exp Neurol* **64,** 649-64.
Stroppolo, M. E., Malvezzi-Campeggi, F., Mei, G., Rosato, N. and Desideri, A. (2000) Role of the tertiary and quaternary structures in the stability of dimeric copper, zinc superoxide dismutases. *Arch Biochem Biophys* **377,** 215-8.

Sturtevant, J. M. (1987) Biochemical applications of differential scanning calorimetry. *Ann Rev Phys Chem* **38,** 463-88.
Sturtevant, J. M. (1994) The thermodynamic effects of protein mutations. *Current Opinion in Structural Biology* **4,** 69-78.
Subramaniam, J. R., Lyons, W. E., Liu, J., Bartnikas, T. B., Rothstein, J., Price, D. L., Cleveland, D. W., Gitlin, J. D. and Wong, P. C. (2002) Mutant SOD1 causes motor neuron disease independent of copper chaperone-mediated copper loading. *Nat Neurosci* **5,** 301-7.
Svensson, A. K., Bilsel, O., Kondrashkina, E., Zitzewitz, J. A. and Matthews, C. R. (2006) Mapping the folding free energy surface for metal-free human Cu,Zn superoxide dismutase. *J Mol Biol* **364,** 1084-102.
Tai, H. C. and Schuman, E. M. (2008) Ubiquitin, the proteasome and protein degradation in neuronal function and dysfunction. *Nat Rev Neurosci* **9,** 826-38.
Tainer, J. A., Getzoff, E. D., Beem, K. M., Richardson, J. S. and Richardson, D. C. (1982) Determination and analysis of the 2 A-structure of copper, zinc superoxide dismutase. *J Mol Biol* **160,** 181-217.
Tainer, J. A., Getzoff, E. D., Richardson, J. S. and Richardson, D. C. (1983) Structure and mechanism of copper, zinc superoxide dismutase. *Nature* **306,** 284-7.
Tamura, A., Kojima, S., Miura, K. and Sturtevant, J. M. (1994) Effect of an intersubunit disulfide bond on the stability of Streptomyces subtilisin inhibitor. *Biochemistry* **33,** 14512-20.
Tamura, A., Kojima, S., Miura, K. and Sturtevant, J. M. (1995) A thermodynamic study of mutant forms of Streptomyces subtilisin inhibitor. II. Replacements at the interface of dimer formation, Val13. *J Mol Biol* **249,** 636-45.
Tamura, A. and Sturtevant, J. M. (1995) A thermodynamic study of mutant forms of Streptomyces subtilisin inhibitor. I. Hydrophobic replacements at the position of Met103. *J Mol Biol* **249,** 625-35.
Tanford, C. (1970) Protein denaturation. C. Theoretical models for the mechanism of denaturation. *Adv Protein Chem* **24,** 1-95.
Taylor, J. R. (1982) An Introduction to Error Analysis. In *A Series of Books in Physics*, (ed. E. D. Commins), University Science Books, Mill Valey, CA.
Timasheff, S. N. (1998) Control of protein stability and reactions by weakly interacting cosolvents: the simplicity of the complicated. *Adv Protein Chem.* **51,** 355-432.
Timasheff, S. N. (2002) Protein hydration, thermodynamic binding, and preferential hydration. *Biochemistry* **41,** 13473-82.
Tiwari, A. and Hayward, L. J. (2003) Familial amyotrophic lateral sclerosis mutants of copper/zinc superoxide dismutase are susceptible to disulfide reduction. *J Biol Chem* **278,** 5984-92.
Tiwari, A., Xu, Z. and Hayward, L. J. (2005) Aberrantly increased hydrophobicity shared by mutants of Cu,Zn-superoxide dismutase in familial amyotrophic lateral sclerosis. *J Biol Chem* **280,** 29771-9.
Travaglini-Allocatelli, C., Ivarsson, Y., Jemth, P. and Gianni, S. (2009) Folding and stability of globular proteins and implications for function. *Curr Opin Struct Biol* **19,** 3-7.
Valentine, J. S., Doucette, P. A. and Potter, S. Z. (2005) Copper-Zinc Superoxide Dismutase and Amyotrophic Lateral Sclerosis. *Annu Rev Biochem* **74,** 563-593.
Valentine, J. S. and Hart, P. J. (2003) Misfolded CuZnSOD and amyotrophic lateral sclerosis. *Proc Natl Acad Sci U S A* **100,** 3617-22.

van Holde, K. E., Weischet, W.O. . (1978) Boundary analysis of sedimentation velocity experiments with monodisperse and paucidisperse solutes. *Biopolymers***,** 1387-1403.
Vassall, K. A., Stathopulos, P. B., Rumfeldt, J. A., Lepock, J. R. and Meiering, E. M. (2006) Equilibrium thermodynamic analysis of amyotrophic lateral sclerosis-associated mutant apo Cu,Zn superoxide dismutases. *Biochemistry* **45,** 7366-79.
Velazquez-Campoy, A., Leavitt, S. A. and Freire, E. (2004) Characterization of protein-protein interactions by isothermal titration calorimetry. *Methods Mol Biol* **261,** 35-54.
Wang, J., Farr, G. W., Zeiss, C. J., Rodriguez-Gil, D. J., Wilson, J. H., Furtak, K., Rutkowski, D. T., Kaufman, R. J., Ruse, C. I., Yates, J. R., 3rd, Perrin, S., Feany, M. B. and Horwich, A. L. (2009) Progressive aggregation despite chaperone associations of a mutant SOD1-YFP in transgenic mice that develop ALS. *Proc Natl Acad Sci U S A* **106,** 1392-7.
Wang, J., Xu, G. and Borchelt, D. R. (2006) Mapping superoxide dismutase 1 domains of non-native interaction: roles of intra- and intermolecular disulfide bonding in aggregation. *J Neurochem* **96,** 1277-88.
Wang, J., Xu, G., Gonzales, V., Coonfield, M., Fromholt, D., Copeland, N. G., Jenkins, N. A. and Borchelt, D. R. (2002) Fibrillar inclusions and motor neuron degeneration in transgenic mice expressing superoxide dismutase 1 with a disrupted copper-binding site. *Neurobiol Dis* **10,** 128-38.
Wang, Q., Johnson, J. L., Agar, N. Y. and Agar, J. N. (2008) Protein aggregation and protein instability govern familial amyotrophic lateral sclerosis patient survival. *PLoS Biol* **6,** e170.
Watanabe, Y., Morita, E., Fukada, Y., Doi, K., Yasui, K., Kitayama, M., Nakano, T. and Nakashima, K. (2008) Adherent monomer-misfolded SOD1. *PLoS ONE* **3,** e3497.
Weisiger, R. A. and Fridovich, I. (1973) Superoxide dismutase. Organelle specificity. *J Biol Chem* **248,** 3582-92.
Wetlaufer, D. B. (1973) Nucleation, rapid folding, and globular intrachain regions in proteins. *Proc Natl Acad Sci U S A* **70,** 697-701.
Williams, P. D., Pollock, D. D. and Goldstein, R. A. (2006) Functionality and the evolution of marginal stability in proteins: Inferences from lattice simulations. *Evol Bioinform Online* **2,** 91-101.
Woody, R. and Dunker, K. (1996) Circular dichroism and the conformational analysis of biomolecules, (ed. G. D. Fasman), pp. 25-69, 109-159, Plenum Press, New York and London.
Yang, Z. W., Tendian, S. W., Carson, W. M., Brouillette, W. J., Delucas, L. J. and Brouillette, C. G. (2004) Dimethyl sulfoxide at 2.5% (v/v) alters the structural cooperativity and unfolding mechanism of dimeric bacterial NAD+ synthetase. *Protein Sci* **13,** 830-41.
Youn, H. D., Kim, E. J., Roe, J. H., Hah, Y. C. and Kang, S. O. (1996) A novel nickel-containing superoxide dismutase from Streptomyces spp. *Biochem J* **318 (Pt 3),** 889-96.
Zetterstrom, P., Stewart, H. G., Bergemalm, D., Jonsson, P. A., Graffmo, K. S., Andersen, P. M., Brannstrom, T., Oliveberg, M. and Marklund, S. L. (2007) Soluble misfolded subfractions of mutant superoxide dismutase-1s are enriched in spinal cords throughout life in murine ALS models. *Proc Natl Acad Sci U S A* **104,** 14157-62.
Zweifel, M. E. and Barrick, D. (2002) Relationships between the temperature dependence of solvent denaturation and the denaturant dependence of protein stability curves. *Biophys Chem* **101-102,** 221-37.